# FUNCTIONAL ELASTOMERIC SCAFFOLD DEVELOPMENT FOR TISSUE ENGINEERING

by

**John Joseph Stankus**

BA, Washington & Jefferson College, 2000

Submitted to the Graduate Faculty of

School of Engineering in partial fulfillment

of the requirements for the degree of

Doctor of Philosophy

University of Pittsburgh

2006

UNIVERSITY OF PITTSBURGH

SCHOOL OF ENGINEERING

This dissertation was presented

by

John Joseph Stankus

It was defended on

April 5, 2006

and approved by

Eric J. Beckman, PhD, Professor, Chemical Engineering

Alan J. Russell, PhD, Professor, Bioengineering, Chemical Engineering and Surgery

Michael S. Sacks, PhD, Professor, Bioengineering

Dissertation Director: William R. Wagner, PhD, Associate Professor, Bioengineering, Chemical Engineering and Surgery

**FUNCTIONAL ELASTOMERIC SCAFFOLD DEVELOPMENT FOR TISSUE ENGINEERING**

John J. Stankus, PhD

University of Pittsburgh, 2006

Scaffolds for engineering soft tissue would ideally be mechanically compliant and anisotropic while possessing inherent bioactivity and enzyme sensitivity similar to the native extracellular matrix. Biodegradable elastomers, such as cytocompatible poly(ester urethane)ureas, represent attractive alternatives to more common biodegradable polyesters utilized in tissue engineering. These materials can be processed by electrospinning into scaffolds suitable for *in vivo* placement and support of cellular adhesion and growth. This process, where an electric field overcomes surface tension to generate and draw nanoscale fibers, can create scaffolds with extracellular matrix-like morphologies that retain mechanical strength and flexibility while also permitting protein incorporation into spun fibers to impart bioactivity.

Poly(ester urethane)urea (PEUU) was blended with collagen or urinary bladder matrix and processed with electrospinning into nanofibrous scaffolds. Protein incorporation into the matrices resulted in increased cellular adhesion and scaffold degradation rate. PEUU scaffolds were fabricated with various degrees of fiber alignment to more closely mimic soft tissue anisotropy such as that of the native pulmonary valve. The fabrication of mechanically anisotropic scaffolds is desired due to their ability to direct cell growth during tissue remodeling.

PEUU elastomeric matrices could serve as mechanical support scaffolds for cell adhesion and growth but can require long seeding and culture times to achieve high density cellular in-growth. Therefore, a microintegration technique was developed where the elastomeric fibers are spun concurrently with electrospraying of cells. This process produced viable, high cell density constructs and lessened the time necessary for scaffold fabrication and seeding.

The functionality of electrospun PEUU was evaluated for its ability to release bioactive basic fibroblast growth factor or the antibiotic tetracycline. These controlled release elastomeric matrices might be appropriate for application in wound repair or management. Electrospun PEUU was also evaluated in fabricating a functional tissue engineered blood vessel. Small diameter electrospun PEUU tubular conduits were implanted as rat aorta replacements and demonstrated patency and tissue remodeling at 2 wks. In addition, the cellular microintegration technology was extended as a means to incorporate cells into electrospun small diameter tubes *in vitro*. These materials possessed mechanical compliance similar to native vessels and demonstrated great potential for tissue engineering.

## TABLE OF CONTENTS

**ABSTRACT……...…iv**

**TABLE OF CONTENTS…….....vi**

**LIST OF TABLES……...…xiii**

**LIST OF FIGURES…….....xiv**

**ACKNOWLEDGEMENTS…….....xx**

**NOMENCLATURE……..xxii**

**1.0 INTRODUCTION……...…1**

**1.1 TISSUE ENGINEERING……1**

**1.1.1 Clinical relevance…….3**

**1.1.2 Functional tissue engineering…….…….4**

**1.2 SCAFFOLD MATERIALS.…….8**

**1.2.1 Extracellular matrix based materials……...…….9**

**1.2.1.1 Collagen……..10**

**1.2.1.2 Elastin……..…….11**

**1.2.1.3 Decellularized ECM matrices……...14**

**1.2.2 Biodegradable polyesters……..16**

**1.2.2.1 Polyglycolide, polylactide, poly(ε-caprolactone) and their copolymers……..18**

**1.2.2.2 Poly(trimethylene carbonate) copolymers……...19**

**1.2.2.3 Poly(glycerol sebacate)……..20**

**1.2.3 Biodegradable polyurethanes ……..21**

**1.3 SCAFFOLD PROCESSING.……30**

**1.3.1 Particulate leaching……...31**

**1.3.2 Thermally induced phase separation……...32**

**1.3.3 Rapid prototyping……..32**

**1.3.4 Electrospinning……..33**

**1.4 SPECIFIC AIMS.……...35**

**2.0 SYNTHESIS AND ELECTROSPINNING OF BIODEGRADABLE POLYURETHANES…….....38**

**2.1 INTRODUCTION..…….38**

**2.2 METHODS..……40**

**2.2.1 Synthesis of biodegradable poly(ester urethane)urea (PEUU)……..40**

**2.2.2 Synthesis of biodegradable poly(ether ester urethane)urea (PEEUU)….41**

**2.2.3 Polymer characterization…….…….43**

**2.2.4 Surface modification…….…….44**

**2.2.5 Electrospinning……..45**

**2.2.6 Scaffold characterization…….……..47**

**2.2.7 Endothelial cell adhesion and growth……..47**

**2.2.8 Statistics…….….48**

**2.3 RESULTS..……..48**

**2.3.1 Polymer characterization……..48**

**2.3.1.1 PEUU characterization……..48**

**2.3.1.2 PEEUU characterization…….……...……...49**

**2.3.2 Electrospinning and scaffold characterization……50**

**2.3.3 Endothelial cell adhesion and proliferation…….53**

**2.4 DISCUSSION……..……56**

**3.0 ELECTROSPINNING OF COLLAGEN BASED ELASTOMERIC SCAFFOLDS.…59**

**3.1 INTRODUCTION..…….59**

**3.2 METHODS..……60**

**3.2.1 PEUU/collagen scaffold fabrication…….60**

**3.2.2 Scaffold characterization……..61**

**3.2.3 Cell adhesion on PEUU/collagen scaffolds……..62**

**3.2.4 Statistics…….…….…...….63**

**3.3 RESULTS...……...…….63**

**3.3.1 Scaffold characterization…….…….....63**

**3.3.2 Circular dichroism spectroscopy…….....67**

**3.3.3 Mechanical properties…….…..69**

**3.3.4 Degradation……71**

**3.3.5 Cell adhesion on PEUU/collagen scaffolds……..73**

**3.4 DISCUSSION..……77**

**4.0 ELECTROSPINNING OF URINARY BLADDER MATRIX BASED ELASTOMERIC SCAFFOLDS……..81**

**4.1 INTRODUCTION..…….81**

**4.2 METHODS..……82**

**4.2.1 Electrospinning UBM/PEUU scaffolds……82**

**4.2.2 Electrospun UBM/PEUU scaffold characterization……..……..83**

**4.3 RESULTS AND DISCUSSION..……..……..……..84**

**4.3.1 Electrospun UBM scaffolds……...84**

**4.3.2 Electrospun UBM/PEUU scaffolds……...…86**

**4.3.3 Electrospun UBM/PEUU scaffold characterization and cytocompatibility……87**

**5.0 ELECTROSPINNING OF BIOMIMETIC ALIGNED NANOFIBER MATRICES….89**

**5.1 INTRODUCTION..…….89**

**5.2 METHODS…..……..……91**

**5.2.1 Aligned scaffold fabrication…..……..…….91**

**5.2.2 Aligned scaffold characterization…….92**

**5.2.3 Smooth muscle cell growth and morphology……...94**

**5.3 RESULTS…...……..94**

**5.3.1 Aligned scaffold fabrication and analysis……..……94**

**5.3.2 Biaxial mechanical properties……...98**

**5.3.3 Smooth muscle cell growth and morphology…….100**

**5.4 DISCUSSION...……..102**

**6.0 CELLULAR MICROINTEGRATION……..……104**

**6.1 INTRODUCTION..……...104**

**6.2 MATERIALS AND METHODS.……..…….107**

**6.2.1 Polymer synthesis and characterization……..……107**

**6.2.2 Electrospinning…….……107**

**6.2.3 SMC spraying / electrospraying…….108**

**6.2.4 SMC Microintegration……108**

**6.2.5 Muscle derived stem cell microintegration……111**

**6.2.6 Endothelial progenitor cell microintegration……111**

**6.2.7 Scaffold / cell culture……...…112**

**6.2.8 Characterization……..113**

**6.2.9 Statistics……115**

**6.3 RESULTS AND DISCUSSION.....…….…….115**

**6.3.1 Polymer characterization……115**

**6.3.2 SMC spraying / electrospraying…….115**

**6.3.3 Microintegration……..117**

**6.3.4 SMC growth and morphology……119**

**6.3.5 Mechanical properties…….128**

**6.3.6 MDSC microintegration, culture and characterization……...129**

**6.3.7 EPC microintegration, culture and characterization…….……..131**

**7.0 CONTROLLED RELEASE NANOFIBER MATRICES FOR FASCIA AND ABDOMINAL REPAIR…..……133**

**7.1 INTRODUCTION..……...133**

**7.2 BASIC FIBROBLAST GROWTH FACTOR DELIVERY FROM NANOFIBER MATRICES.....…….....135**

**7.2.1 Methods……..…135**

**7.2.1.1 bFGF loading and scaffold fabrication…….….135**

**7.2.1.2 bFGF release and mitogenicity…….…..136**

**7.2.1.3 Rat hindlimb implantation…….…….137**

**7.2.2 Results……...138**

**7.2.2.1 Scaffold characterization…….……138**

**7.2.2.2 bFGF release and mitogenicity…….……..139**

**7.2.2.3 Scaffold explantation and histology……..…..…….….142**

**7.2.3 Discussion…….…….145**

**7.3 TETRACYCLINE DELIVERY FROM NANOFIBER MATRICES……..147**

**7.3.1 Methods……...……..147**

**7.3.1.1 Tetracycline loading and scaffold fabrication……...147**

**7.3.1.2 Tetracycline release measurement…….148**

**7.3.1.3 Bacteria culture and antimicrobial activity assays……...148**

**7.3.2 Results……...149**

**7.3.2.1 Tetracycline loaded scaffold fabrication……149**

**7.3.2.2 Bacteria culture and antimicrobial activity assays……...151**

**7.3.3 Discussion…….153**

**8.0 ELECTROSPUN TUBULAR CONSTRUCTS FOR BLOOD VESSEL TISSUE ENGINEERING…….…….156**

**8.1 INTRODUCTION..…….……..156**

**8.2 ELECTROSPUN POLYURETHANE TUBULAR CONDUITS..…….……..157**

**8.2.1 Methods…….……157**

**8.2.1.1 Tubular electrospinning and scaffold fabrication……...…….157**

**8.2.1.2 Surface seeding of conduit lumen…….……..159**

**8.2.1.3 *In vivo* implantation as a rat aorta replacement…….……..159**

**8.2.2 Results…….……..160**

**8.2.2.1 Scaffold morphology and mechanical characterization…..……..160**

**8.2.2.2 Surface seeding of conduit lumen…….…..….162**

**8.2.2.3 Graft function and explant histology in a rat model……163**

**8.3 SMC MICROINTEGRATED POLYURETHANE CONDUITS…….……...165**

**8.3.1 Methods……165**

**8.3.1.1 Conduit microintegration technique……165**

**8.3.1.2 Conduit characterization……166**

**8.3.2 Results……167**

**8.3.2.1 Scaffold structure……167**

**8.3.2.2 Cell growth and histology……168**

**8.3.2.3 Mechanical properties……169**

**8.3.3 Discussion……173**

**9.0 CONCLUSIONS AND FUTURE WORK……177**

**9.1 CONCLUSIONS……177**

**9.2 FUTURE WORK……180**

**9.2.1 Multi-nozzle electospinning for elastomeric synthetic ECM development……180**

**9.2.2 Coaxial electrospinning for controlled drug release……180**

**9.2.3 Co-microintegration for development of functional vascularized tissue……182**

**APPENDIX A……183**

**APPENDIX B……184**

**APPENDIX C……185**

**APPENDIX D……186**

**APPENDIX E……187**

**APPENDIX F……188**

**APPENDIX G……189**

**BIBLIOGRAPHY……191**

## LIST OF TABLES

**Table 1-1.** Patency of various graft types [5]…….6

**Table 1-2**. Physical properties of some soft biodegradable polymers……..17

**Table 1-3**. Composition and physical properties of linear biodegradable polyurethanes and polyurethane ureas…….25

**Table 2-1.** Physical property summary of PEUU and PEEUU…….……...49

**Table 3-1.** Comparison of ellipticities of ππ* (minima) and nπ* (maxima) transitions between type I collagen control and collagen processed into ePEUU/Col scaffolds……...69

**Table 3-2.** Tensile properties of electrospun scaffolds compared with cast PEUU…….....70

**Table 3-3.** Summary of 8 wks *in vitro* degradation for electrospun PEUU/collagen……..73

**Table 3-4**. SMC adhesion on biohybrid scaffolds……75

**Table 4-1.** Electrospun UBM/PEUU scaffold properties…….88

**Table 5-1.** Summary of aligned scaffold properties and morphologies……...…97

**Table 6-1**. Tensile properties of SMC microintegrated PEUU and PEUU/collagen blends…..129

## LIST OF FIGURES

**Figure 1-1.** Tissue engineering approach where cells are seeded onto scaffolds which are then implanted *in vivo*. A scaffold is necessary because normal cells cannot grow into three dimensional shapes *in vitro* without sufficient vascularization. Reproduced from [4]…….2

**Figure 1-2.** Tissue engineered blood vessel cultured under pulsatile flow from smooth muscle cell sheets. Reproduced from [3]……....7

**Figure 1-3.** Sample chemical structures of biodegradable polyesters for tissue engineering…..17

**Figure 1.4.** Two step reaction to form polyurethane or polyurethane ureas [1]……..22

**Figure 1-5.** Chemical structures of diisocyanates used as monomers in biodegradable polyurethanes [1].....23

**Figure 2-1.** Poly(ester urethane)urea (PEUU) synthesis……..41

**Figure 2-2.** Poly(ether-ester urethane)urea (PEEUU) synthesis……..43

**Figure 2-3.** Radio frequency glow discharge with ammonia gas, followed by RGDS attachment with a BDI spacer……..……..45

**Figure 2-4.** Electrospinning setup consisting of a syringe pump to feed polymer solution along with a combination of 3 high-voltage generators and a steel mesh screen to control the area of fiber deposition……..46

**Figure 2-5.** FTIR spectrum of PEUU. The spectrum for PEEUU exhibited similar functionalities……..…50

**Figure 2-6.** Scanning electron micrographs of electrospun PEUU as a function of polymer concentration in HFIP (scale bars = 1μm)…….51

**Figure 2-7.** Electrospun fiber diameter as a function of PEUU concentration in the feed solution ($r$ = 0.90; $p$ < 0.05)……....51

**Figure 2-8.** SEMs demonstrating fibrous scaffold morphology of electrospun PEEUU…..……52

**Figure 2-9.** Typical stress-strain curves of PEUU cast film, electrospun PEUU scaffold, and TIPS PEUU scaffold……..53

**Figure 2-10.** 24 h HUVEC adhesion to PEUU and RGDS modified PEUU relative to TCPS...54

**Figure 2-11.** HUVEC growth on TCPS, PEUU cast film, RGDS modified cast PEUU film and electrospun PEUU…….…….55

**Figure 3-1.** Scanning electron micrographs of electrospun scaffolds composed of varying ratios of PEUU and type I collagen…….....64

**Figure 3-2.** Water-in-air contact angle of PEUU/collagen blends as a function of collagen concentration…….…….65

**Figure 3-3.** FTIR spectra of (a) blend of 50/50 PEUU/collagen, (b) PEUU, and (c) difference spectrum resulting from subtraction of (b) from (a). Peaks attributable to collagen are noted in the difference spectrum…….…….65

**Figure 3-4.** Picrosirius red staining of electrospun PEUU/collagen blends: (a) optical micrograph of 50/50 PEUU/collagen, polarized light micrographs of (b) collagen (c) 50/50 electrospun PEUU/collagen, and (d) 0/100 electrospun PEUU/collagen…….…….66

**Figure 3-5.** Absorbance normalized to scaffold mass as a function of collagen concentration for picrosirius red stain removed by NaOH…….……...66

**Figure 3-6.** CD spectra of 1mg/mL collagen removed from scaffolds in 0.1*M* acetic acid compared with spectra of type I collagen control and thermally denatured type I collagen…….68

**Figure 3-7.** Typical stress-strain curves of PEUU cast film, electrospun PEUU scaffold, and electrospun PEUU/collagen (50/50)……..70

**Figure 3-8.** Mass remaining of electrospun biohybrid scaffolds as result of incubation time in buffer with or without collagenase. (% PEUU / % collagen; + indicates with collagenase)……72

**Figure 3-9.** HUVEC adhesion on electrospun PEUU/collagen scaffolds compared with cast PEUU film. Data are normalized to TCPS. ($p < 0.05$)…….……74

**Figure 3-10.** Representative HUVEC morphology on electrospun PEUU…….…..……74

**Figure 3-11.** Representative SMC morphology on electrospun PEUU……..…….76

**Figure 4-1.** Morphologies of electrospun UBM at 9wt% (a), 10wt% (b), 12wt% (c), and 15wt% (d)…….…….…….85

**Figure 4-2.** SEMs of continuous fiber morphologies of electrospun UBM/PEUU at 25, 50, and 75% UBM…….…….……86

**Figure 4-3**. Confocal micrograph of SMCs cultured on electrospun UBM / PEUU (50/50) after 10 days. (red = f-actin, blue = nuclei)……...87

**Figure 5-1.** Rotating aluminum barrel target (4.5″ diameter) utilized to produce anisotropic electrospun PEUU scaffolds at speeds from 0 to 2300 rpm……..91

**Figure 5-2.** Schematic of biaxial mechanical testing device (left panel) and sample preparation (right panel). Reproduced from Sacks et al. [2]……93

**Figure 5-3.** Fiber morphologies of PEUU electrospun onto a mandrel rotating at 0 to 2300 rpm (linear velocities of 0 to 13.8 m/s) as imaged by SEM…….….95

**Figure 5-4.** Fiber alignment as a function of mandrel linear velocity from 0 to 13.8 m/s using custom analysis program. (Data courtesy of T. Courtney)…….……..96

**Figure 5-5.** XRD spectra of PEUU electrospun at various rpm speeds…….…..97

**Figure 5-6.** Biaxial mechanical properties of electrospun PEUU scaffolds as a function of fiber direction and mandrel velocity. (Data courtesy of T. Courtney)……...99

**Figure 5-7.** Comparison of biaxial tensile properties of aligned electrospun PEUU (13.8 m/s) versus a bioprosthetic heart valve. (Data courtesy of T.Courtney)……99

**Figure 5-8.** Smooth muscle cell growth on random and aligned electrospun PEUU compared with TCPS……100

**Figure 5-9.** Morphologies of random (top) and aligned (bottom) electrospun PEUU before (left panels) and after (right panels) cell culture…….…….101

**Figure 6-1.** Approaches to cellular microintegration. (a) Microintegration using a side-by-side capillary configuration for electrospinning polymer and electrospraying cells onto a flat target moving on an x-y stage. (b) Microintegration using a perpendicular capillary configuration for electrospinning polymer and electrospraying cells onto a rotating mandrel moving on a linear stage to result in the construct shown in (c)…….……110

**Figure 6-2.** Schematic of the perfusion bioreactor employed with microintegrated constructs. 13-mm diameter construct discs (a) were placed between O-rings (b) and a support screen (c) of in-line filter holders (d) followed by perfusion at 0.5 mL/min with a multi-channel peristaltic pump (e). Each construct was placed in its own loop consisting of a 32mL media bag (f), silicone tubing gas exchanger (g) and syringes for media exchange……...…113

**Figure 6-3.** Trypan blue staining results for SMC viability after various processing treatments. (Spraying = SMCs sprayed from spray nozzle, Spraying -15 kV = SMCs sprayed from spray nozzle onto -15 kV charged target, Spraying -15 kV + e-PEUU = SMCs sprayed from spray nozzle onto -15 kV charged target during PEUU electrospinning, Electrospraying -15kV = SMCs electrosprayed at 10kV onto -15 kV charged target, Electrospraying -15 kV + e-PEUU = SMCs electrosprayed SMCs electrosprayed at 10kV onto -15kV charged target during PEUU electrospinning…….118

**Figure 6-4.** Cell growth in thin SMC microintegrated e-PEUU constructs fabricated on a flat target versus TCPS over 1 week in static culture. (* $p < 0.05$ increase from 1 day to 1 week)..119

**Figure 6-5.** Confocal imaging of SMC integrated thin PEUU constructs immediately after fabrication (left panel) and 1 day after static culture (right panel). (red = f-actin, blue = nuclei, and green = apoptotic cells)…….120

**Figure 6-6.** Representative electron micrographs of thin flat sheet SMC microintegrated samples after 1 wk of static culture…….121

**Figure 6-7**. (a) Initial cellular uniformity in SMC microintegrated e-PEUU fabricated on a mandrel target. (b) Cell growth in thick SMC microintegrated e-PEUU constructs with static versus perfusion culture. Perfusion was initiated after 1 day in static culture. (* $p < 0.05$ increase with perfusion versus static culture). ……124

**Figure 6-8.** Fluorescent micrographs of SMC microintegrated e-PEUU constructs after one day of static culture (a), day 4 of perfusion culture (b), day 4 of perfusion culture (c), day 7 of perfusion culture (d), day 4 of static culture (e), high cell number surface image of day 4 of static culture (f), day 7 of static culture (g), and day 7 of static culture (h). (scale bar = 40 μm, red = f-actin and e-PEUU, blue = nuclei)……125

**Figure 6-9.** Hematoxylin and eosin stained sections of SMC microintegrated e-PEUU constructs after one day of static culture (a, c), day 4 of static culture (b, e), and day 4 of perfusion culture (c, f)…….126

**Figure 6-10.** H&E staining or SEM of SMC microintegrated PEUU/collagen (75/25). (a) SMCs are aligned into the plane of the sample after 1 day of static culture. (b) SEM illustrates SMC alignment near the surface of PEUU/collagen after 13 days of perfusion culture (scale bar = 10 μm). (c) H&E stain after 13 days of perfusion culture indicating cells aligned into the plane of the image. (d) H&E stain after 13 days of perfusion culture indicating high density cell alignment. Note that perfusion was initiated at 0.5 mL/min after 1 day of static culture……..127

**Figure 6-11.** MTT data for MDSC microintegrated PEUU after 6 days of culture. Samples were cultured statically for 1 day and then subjected to either perfusion (0.5 mL/min) or static culture for an additional 5 days……130

**Figure 6-12.** (Left panel) Confocal micrograph of MDSC microintegrated PEUU demonstrating high density of aligned cells (red = f-actin, blue = nuclei, scale bar = 40 μm). (Right panel) Masson's Trichrome stained MDSC sample indicating collagen production. Both samples are after 5 days of perfusion culture at 0.5 mL/min……...131

**Figure 6-13.** Microintegrated EPC viability. (a) MTT results after 3 days of static or perfusion culture. (b) Confocal micrograph of day 4 static culture sample. (c) Confocal micrograph of day 4 perfusion sample. (red = f-actin, blue = nuclei)…….132

**Figure 7-1.** SEMs of bFGF loaded electrospun PEUU. No beads visible as a result of protein incorporation. (left scale bar = 10 μm, right scale bar = 1 μm)……..139

**Figure 7-2.** Release profile of I-125 radiolabelled bFGF from electrospun PEUU……...140

**Figure 7-3.** bFGF release profile for bFGF loaded electrospun PEUU scaffold degradation media as measured by ELISA……..…...140

**Figure 7-4.** Released bFGF bioactivity at 1 wk using a SMC mitogenic assay with comparison to a 1 ng/mL bFGF control (left) and SMC adhesion on PEUU loaded with bFGF (*$p < 0.05$ vs. medium control, #$p < 0.05$ greater than PEUU control)……..141

**Figure 7-5.** Appearance of electrospun patch explants at 12 wks after implantation. (left panels = PEUU control, right panels = bFGF loaded specimen)……...….143

**Figure 7-6.** Representative histology of electrospun patch explants at 12 wks. (a) H&E stain of electrospun PEUU control exhibiting fibrous encapsulation. (b) H&E stain showing more apparent degradation and patch fragmentation of bFGF loaded PEUU. (c) Immunostaining of PEUU control indicating sparse capillary development. (d) Immunostaining of bFGF loaded PEUU with evidence of several capillaries in patch periphery. (green = SMC α-actin, blue = nuclei, and red = CD31, data courtesy of K.Fujimoto)……144

**Figure 7-7.** Chemical structure of tetracycline hydrochloride……...……147

**Figure 7-8.** Scaffold morphologies of tetracycline loaded scaffolds at 1% (a, d), 5% (b, e) and 10% (c, f) of PEUU by weight as imaged with SEM. (scale bars = 10 μm (a, b, c) or 100 μm (d, e, f))……...……...150

**Figure 7-9.** Tetracycline release from electrospun PEUU scaffolds into buffer as measured at 350 nm…….151

**Figure 7-10.** Antibacterial activity of degradation solutions from 10% tetracycline loaded electrospun PEUU (PEUU/tet) and controls of PEUU alone and tetracycline……...152

**Figure 7-11.** Inhibition zone diameters for 6-mm electrospun scaffold discs plated on agar growths of *E.coli* and *S.aureus* as measured at 24 h. (* $p < 0.05$)…….153

**Figure 8-1.** Target used to electrospin 1.3 mm inner diameter porous conduits for blood vessel tissue engineering. The mandrel is rotated at 250 rpm and charged at -3 kV…….……...158

**Figure 8-2.** Macroscale appearance of electrospun tube. (bottom = higher magnification).…160

**Figure 8-3.** SEMs of PEUU electrospun tubes. Bottom left image displays tube exterior (scale bar = 10 μm). Bottom right image displays tube cross-section (scale bar = 10 μm)…..……161

**Figure 8-4.** Fluorescent micrograph of MDSCs lining the interior of an electrospun tubular conduit. (Left panel) Nuclear (blue, Dapi) and f-actin (green, rhodamine phalloidin) staining indicating cell attachment on polymer lumen (red, autofluorescence) after 24 h of static culture. (Right panel) Confocal image stack demonstrating nuclear (blue, draq5) and f-actin (red, rhodamine phalloidin) staining of the PEUU lumen (Data courtesy of L.Soletti)…...……....162

**Figure 8-5.** Image of electrospun vascular graft immediately after implantation to replace a section of the rat aorta. (Data courtesy of A. Nieponice)……163

**Figure 8-6.** H&E / Trichrome stains of 2 wk explants of electrospun vascular grafts. Notice the presence of collagenous capsule and neovessels in graft exterior (bottom) and luminal cell growth (top). (Data courtesy of A. Nieponice)……164

**Figure 8-7.** Images of SMC microintegrated PEUU conduit (left) prepared for insertion into perfusion bioreactor (right)…….....166

**Figure 8-8.** Gross appearance of SMC microintegrated tubular constructs after removal from the fabrication mandrel……..168

**Figure 8-9.** MTT SMC viability data for microintegrated conduits of either PEUU or PEUU/collagen. Perfusion was initiated after 1 day of static culture for cell attachment……..169

**Figure 8-10.** Uniform SMC placement after 1 day of static culture for microintegrated PEUU conduit…….…….170

**Figure 8-11.** Averaged stress-strain curve for ring test of SMC microintegrated 4.7mm electrospun PEUU tube. (Data courtesy of L.Soletti)……..171

**Figure 8-12.** Pressure / diameter relationship comparison between porcine mammary artery (pMA) and SMC microintegrated PEUU tubular constructs (μSMC-PEUU). (Data courtesy of L.Soletti)……..……172

**Figure 9-1.** Coaxial electrospinning feed chamber consisting of concentric polymer solution chambers……..181

**Figure 9-2.** Sequential integration of ECs and SMCs during electrospinning of a synthetic extracellular matrix conduit…….182

## ACKNOWLEDGEMENTS

The work completed in this dissertation would not have been possible without the assistance, advice, encouragement, and patience of many individuals. First and foremost, I would like to express my utmost gratitude to my advisor, Dr. William Wagner, for his expert guidance scientific reasoning, and commitment to my projects. He has served as a great role model for me in my pursuit of a successful research career in biomaterials science and engineering and has always made himself available to offer professional and courteous advice on important matters.

I would also like to thank the other members of my dissertation committee, Drs. Beckman, Russell, and Sacks, for lending their valuable expertise and time during this important process. In addition, I thank Drs. Ataai, Badylak, Federspiel, and Vorp for their time and guidance in helping me make my graduate study successful and challenging.

I would like to acknowledge every member of the Wagner Laboratory for their support of this work. Most of all, I would like to sincerely thank Dr. Jianjun Guan for his expert advice and friendship during my time here. I treasure the time we have spent working together on many exciting tissue engineering projects. His polymer science expertise enabled me to better conduct many experiments and his company will be greatly missed.

I would also like to express gratitude for the surgical expertise of Drs. Kazuro Fujimoto and Alejandro Nieponice without which much of this work would not have been possible. I wish

to thank some of my fellow graduate students, collaborators, and friends such as Todd Courtney, Lorenzo Soletti, Donald Freytes, Lorenza Draghi, Bin Li, David Merryman, and Joel Kaar, for their dedication and patience in helping me pursue these projects. Furthermore, a number of undergraduates have assisted on many of these projects including Daquian Wu, Mike Strahota, Mike Callahan, Jim Culhane, Hann-Chung E. Wong, and Mihoko Hashimoto.

Special thanks go to Dan McKeel for his time and friendship in helping me put to task many ideas in the machine shop. I also acknowledge the staff at the Center for Biologic Imaging at the University of Pittsburgh for their assistance and patience. I would like to recognize my funding support including grants from the National Institutes of Health, (#HL069368), the National Tissue Engineering Center (NTEC), and the Commonwealth of Pennsylvania.

Lastly I would like to thank my family for their continued support during my education. My father has always been there for me to help me achieve my goals. I thank my wife, Michele, and daughter, Taylor, for putting up with me for so long during this time consuming and difficult process. In the time I have spent pursuing my Ph.D. my wife has been extremely successful in a number of roles such as obtaining a law degree, starting a career, making our home a great place, and raising our daughter. Thank you so much for your love and support.

## NOMENCLATURE

| | |
|---|---|
| ANOVA | Analysis of variance |
| BDI | 1,4-butanediisocyanatobutane |
| BDO | 1,4-butanediol |
| bFGF | Basic fibroblast growth factor |
| BSA | Bovine serum albumin |
| C | Dynamic compliance |
| CD | Circular dichroism |
| CFU | Colony forming units |
| circ | Circumferential |
| CL | ε-caprolactone |
| col | Collagen |
| $D_d$ | Diameter during diastole |
| $D_s$ | Diameter during systole |
| DCL | Damage control laparotomy |
| DSC | Differential scanning calorimetry |
| DMEM | Dulbecco's Modified Eagle Medium |
| DMF | N,N-dimethyl formamide |
| DMSO | Dimethyl sulfoxide |
| ECM | Extracellular matrix |
| ELISA | Enzyme-linked immunosorbent assay |
| e | Electrospun scaffold |
| ePTFE | Expanded polytetrafluoroethlyene |
| e-PEUU | Electrospun poly(ester urethane)urea |
| FDM | Fused deposition modeling |
| FTIR | Fourier transform infrared spectroscopy |
| h | Hour |
| H&E | Hematoxylin and Eosin |
| HEMA | 2-hydroxyethyl methacrylate |
| HDI | 1,6-hexanediisocyanate |
| HFIP | Hexafluoroisopropanol |
| HGF | Hepatocyte growth factor |
| HUVEC | Human umbilical vein endothelial cell |
| kV | Kilovolt |
| LDI | Lysine diisocyanate |
| MDA | Methylene diphenyl diamine |
| MDI | Methylene diphenyl diisocyanate |
| MDSC | Muscle-derived stem cell |

| | |
|---|---|
| mdeg | Millidegree |
| min | Minute |
| MPa | Megapascal |
| MTT | (3-(4,5-dimethylthiazolyl-2)-2, 5-diphenyltetrazolium bromide) |
| NMP | 1-methyl-2-pyrrolidione |
| NMR | Nuclear magnetic resonance |
| $P_d$ | Pressure during diastole |
| $P_s$ | Pressure during systole |
| PBS | Phosphate-buffered saline |
| PCL | Poly(ε-caprolactone) |
| PD | Preferred direction of aligned scaffolds |
| PDGF | Platelet derived growth factor |
| PDX | Poly(dioxanone) |
| PGA | Polyglycolide |
| PGCL | Poly(glycolide-*co*-ε-caprolactone) |
| PGS | Poly(glycerol sebacate) |
| PLA | Polylactide |
| PLCL | Poly(lactide-*co*-ε-caprolactone) |
| PLGA | Poly(lactide-*co*-glycolide) |
| PEEUU | Poly(ether ester urethane)urea |
| PEG | Poly(ethylene glycol) |
| PEUU | Poly(ester urethane)urea |
| PHB | Poly(3-R-hydroxybutyrate) |
| PHV | Poly(3-R-hydroxyvalerate) |
| ppm | Parts per million |
| PTMC | Polytrimethylene carbonate |
| P(TMC-LA) | Poly(trimethylene carbonate-*co*-lactide) |
| PU | Polyurethane |
| PV | Pulmonary valve |
| rpm | Revolutions per minute |
| s | Seconds |
| SEM | Scanning electron microscopy |
| SIS | Small intestinal submucosa |
| SMC | Smooth muscle cell |
| $T_g$ | Glass transition temperature |
| $T_m$ | Melting temperature |
| TCPS | Tissue culture polystyrene |
| TDA | 2,4-toluene diamine |
| TDI | 2,4-toluene diisocyanate |
| TEBV | Tissue engineered blood vessel |
| tet | Tetracycline |
| TGF-β | Transforming growth factor |
| TIPS | Thermally induced phase separation |
| TMDI | 2,2,4-trimethyl-1,6-diisocyanate |
| UBS | Urinary bladder submucosa |
| UBM | Urinary bladder matrix |

| | |
|---|---|
| UV | Ultraviolet |
| VEGF | Vascular endothelial growth factor |
| wk | Week |
| wt% | Weight percent |
| XD | Cross-preferred direction of aligned scaffolds |
| XRD | X-ray diffraction |

# 1.0 INTRODUCTION

## 1.1 TISSUE ENGINEERING

Tissue engineering holds great promise for repair of damaged or diseased tissues and organs. Tissue engineering can be defined as "an interdisciplinary field that applies the principles and methods of engineering and the life sciences toward the development of biological substitutes to restore, maintain, or improve, tissue function [6]." A goal of tissue engineering is to "restore function through the delivery of living elements which become integrated into the patient [6]." The three main approaches of this field include implantation of engineered scaffolds alone, injection of cells alone, or implantation of engineered scaffolds seeded and cultured with appropriate cells. The theory behind the latter mode of tissue replacement (as shown in **Figure 1-1**) is that the scaffold will provide a structural framework on which the seeded cells can adhere and proliferate while allowing for adequate nutrient exchange. The scaffold will support the initial mechanical loads and stresses until the tissue is suitably developed. The stress will later be transferred to support by the biological component and the scaffolding material ultimately degraded. Hence, the scaffold supports the desired structure of the developing tissue and the seeded cells induce the biological response.

Appropriate cells for seeding on scaffolds can be derived from primary tissue or continuous cell lines. Cells can be allogenic, xenogenic (different species), or autologous. They should be proliferative, easy to obtain, and not induce immunogenic responses [6]. In the ideal

case, a patient's own cells would be harvested, expanded and cultured in developing tissue replacements. However, most adult cell types possess limited capabilities for expansion and regeneration. Therefore, the isolation of human adult or embryonic stem cells is seen as a possible solution to this problem since they can possess the ability to be expanded without limit providing a potential clinical cell source. Stem cells are also attractive to the tissue engineer since they can possess the ability to differentiate into the cell type of choice.

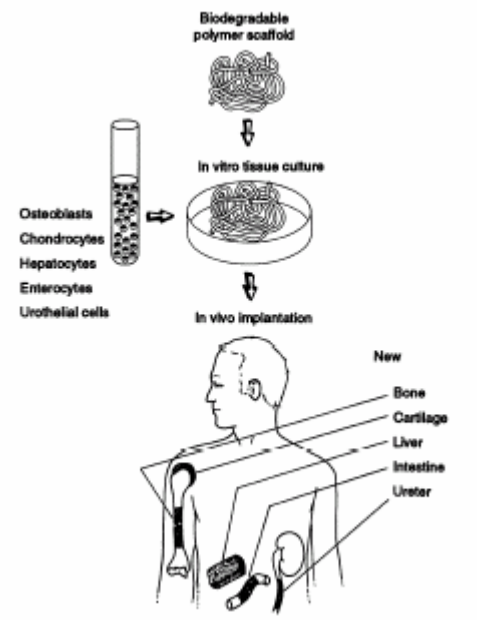


**Figure 1-1.** Tissue engineering approach where cells are seeded onto scaffolds which are then implanted *in vivo*. A scaffold is necessary because normal cells cannot grow into three dimensional shapes *in vitro* without sufficient vascularization. Reproduced from [4].

### 1.1.1 Clinical relevance

Tissue engineering offers a potential solution to many current clinical problems. Heart disease is a leading cause of death in the United States attributing to over 700,000 deaths each year which amounts to 30% of the total death rate in the US [7]. Cardiac cells possess a limited capability to regenerate such that the injured heart cannot mend itself. Patients can benefit from heart or tissue transplants but the number of available organs are limited. Even with transplants, lost heart function is not always recovered [8]. Instead, patients may benefit more from repair of specific non-functional structures such as the area of necrotic cardiac tissue, clogged or damaged vessels, or defective valves [8]. Therefore, a large clinical need exists for more specific treatment to repair the damaged heart after congestive heart failure or myocardial infarction.

Myocardial infarction is caused by ischemia from clogged arteries resulting in areas of necrotic cardiac tissue that do not function properly. This chronic disease of the arteries, arteriosclerosis, consists of a narrowing of the bore of arteries due to intimal hyperplasia. The primary surgical intervention is coronary artery bypass surgery and approximately 600,000 bypass surgeries are performed annually in the US alone [7]. This surgery consists of bypassing the injured area with a synthetic graft or autologous vessel. Success with autologous vessel replacements has been promising but supply is limited and use can lead to donor site morbidities. Synthetic grafts such as ePTFE or Dacron (polyester) are much more readily available and have been successful in treating arteries larger than 6-mm in internal diameter due to a low-level thromboembolic risk and the inability of thrombus formation to impede the larger blood flow.

While small beds of capillaries can be treated using molecular level therapies such as delivery of growth factors, treatment of smaller diameter vessels (< 6 mm inner diameter) has not

been successful using synthetic grafts with thrombosis rates higher than 40% after 6 months [9]. Autologous vessel replacements mainly using saphenous vein or internal mammary artery have done well with patency rates generally ranging between 50 and 70%. This success is probably due to the existence of endothelial cells on the inner surface of the grafts. Thrombosis and neointimal hyperplasia are the most common causes of failure. A limitation is that many patients do not possess suitable vessels because of disease or previous surgeries leading to a large clinical demand for developing a better treatment.

Tissue engineering represents a viable treatment for cardiovascular disease and other tissue ailments. While tissue engineering strategy has been widely applied for the engineering of both hard and soft tissues, the effort to develop soft tissues such as cardiovascular tissue is perhaps the most demanding and challenging application in tissue engineering. Cardiovascular tissue such as myocardium and blood vessels often possess large volumes, high cell densities and can be very mechanically demanding having to undergo large numbers of cyclic loading with little deformation.

### 1.1.2 Functional tissue engineering

As a result of the difficulties associated with replacement of tissue that functions in a biomechanical role, a new sub-discipline entitled “functional tissue engineering” was formed [10]. This field seeks to address issues such as measurement of *in vivo* stresses and which mechanical properties are the most important to mimic in engineering functional tissue. For example, is it most important for the tissue engineered construct to match only the failure properties of native tissue or its viscoelastic behavior as well [10]? Is proper anisotropy necessary to mimic tissue function? These are just some of the properties that must be addressed

in engineering functional tissue. These problems have led to increased consideration of tissue biomechanics in scaffold design and culture conditions in order to engineer functional tissue replacements.

For example, a critical requirement of blood vessel replacements is accurate replication of the original vessel compliance. Compliance is defined as the quality of yielding to pressure without disruption. Compliance mismatch is very complicated because it involves the host artery, anastomosis, and the graft itself [5]. Blood flow can be disturbed causing turbulence and low shear stress that favors platelet deposition. These complications can lead to myointimal hyperplasia and graft failure. Therefore, in developing an ideal vascular graft, it is deemed necessary to closely replicate the elastic properties of the vessel wall. The function of the vessel wall in systole (increase circumference) and diastole (contraction) is due to a combination of viscous and elastic time dependent properties exhibiting viscoelasticity. "Vessel compliance, the reciprocal value of Young's elastic modulus, is defined as the ratio in diameter change divided by the blood pressure change given by equation (1) where *D* and *P* represent diameter and pressure and *d* and *s* represent diastole and systole respectively [5],"

$$Compliance = \frac{(D_s - D_d)}{(D_d)(P_s - P_d)} x10^4 \qquad (1\text{-}1).$$

**Table 1-1** displays data from various groups that shows compliance of biological vessels to be greater than that for synthetic materials [5]. Graft patency decreases with an increase in compliance mismatch.

**Table 1-1:** Patency of various graft types [5].

| Graft Type | Compliance (mmHg) | Patency % |
|---|---|---|
| Host artery | 590 +/- 50 | - |
| Saphenous vein | 440 +/- 80 | 75 |
| Umbilical vein | 370 +/- 50 | 60 |
| Bovine heterograft | 260 +/- 30 | 59 |
| Dacron | 190 +/- 30 | 50 |
| ePTFE | 160 +/- 20 | 40 |

To function *in vivo*, constructed vessels will most likely need a burst pressure of approximately 2000 mmHg, a stress-strain curve similar to the physiological curve with stiffening at the higher pressure region, and possess correct cell phenotypes. In developing the ideal blood vessel replacement, not only must the biological requirement of an anti-thrombogenic surface (endothelial cells produce the only anti-thrombogenic surface known) be adhered to but also compliance must be closely matched to that of the native vessel.

Another facet of functional tissue engineering concerns the roles of *in vitro* mechanical stresses and strain. Results suggest that scaffolds should be designed to more effectively convey mechanical signals to the cells in the construct in developing tissue in a dynamic *in vitro* or *in vivo* environment [11]. It was shown by Kim et al. that cyclical straining upregulated extracellular matrix production in smooth muscle cells leading to increased construct mechanical properties [12]. Also for longer culture periods under cyclic strain, a more flexible scaffold material than PLLA-bonded PGA fibers would be required [13]. Increased matrix production and mechanical strength have been found in tissue engineered cardiac patches having undergone mechanical stimulation [14]. More histologically relevant vessels were fabricated after dynamic culture under pulsatile flow compared with those cultured under non-pulsed conditions [9].

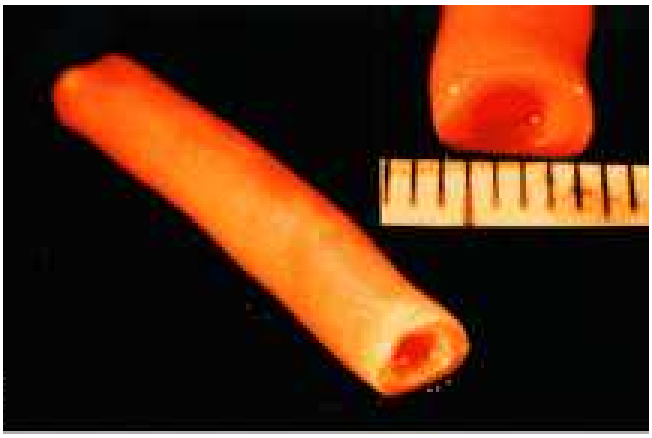

**Figure 1-2:** Tissue engineered blood vessel cultured under pulsatile flow from smooth muscle cell sheets. Reproduced from [3].

The problem of low burst strength of grafts was also alleviated by the work of L'Heureux et. al. who produced a small diameter tissue engineered blood vessel based exclusively on wrapped sheets of cultured smooth muscle cells and fibroblasts [3]. The vessel constructs, shown in **Figure 1-2**, featured a well-defined, three-layered organization and numerous extracellular matrix proteins including elastin. While a short-term grafting experiment in a canine model demonstrated only a 50% patency rate at 1 week, the burst strengths of the vessels (> 2000 mmHg) were comparable to those of native vessels. A limitation was that long culture times (> 13 wk) under mechanical stimulation were necessary to achieve those mechanical properties [3].

## 1.2 SCAFFOLD MATERIALS

Tissue scaffolding acts as a three dimensional structural support for cells during tissue development. Most scaffolds for tissue engineering are designed to be biodegradable and biocompatible and to produce a desired biological response. Complete scaffold resorption is ideal for eliminating the necessity of post-implant surgery. A well-defined biodegradation rate is also ideal so that host tissue can replace the scaffold and that stress can be transferred from the support scaffold to the new tissue. Scaffolds not only serve as a structural support, but can play an important role in facilitating cell adhesion, growth, and vascularization throughout the scaffold both during *in vitro* and *in vivo* tissue regeneration.

Scaffolds may be produced from natural or synthetic materials. Natural materials have the advantage of closely resembling the bioactivity of the native biological environment with the disadvantage of resulting in more frequent immunogenic responses compared with synthetic grafts. The advantage of synthetic polymers is better control over physical properties such as tensile strength, breaking strain, degradation rate, porosity, morphology, and surface chemistry. Modification of surface properties can lead to improved cell attachment and growth on synthetic materials. Among the limitations and concerns with synthetic materials are the potential toxicity of degradation products or remnant synthetic byproducts, material stimulation of inflammatory processes, and extra processing or manipulation that is necessary to impart bioactivity.

The following text will consist of a brief review of natural materials, synthetic polyesters, and biodegradable polyurethanes utilized in tissue engineering scaffold fabrication with an emphasis on biodegradable elastomers. Biodegradable elastomers represent more appropriate scaffolding materials since they offer attractive mechanical properties for many soft-tissue

engineering applications where non-flexible polyesters are currently utilized. As expected, several researchers are aggressively pursuing the development of novel biodegradable elastomers for use in biomedical applications [10, 15-21]. A class of novel biodegradable poly(ester urethane)ureas has been developed in our laboratory since these thermoplastic elastomers allow for great freedom in functionality through the incorporation of various hard and soft segments [15, 16].

### 1.2.1 Extracellular matrix based materials

A major limitation of synthetic biomaterials is the difficulty to mimic the resident bioactivity of the native extracellular matrix (ECM). ECM is an acellular component of tissue and organs that consists of structural and functional proteins and carbohydrates secreted by native cells. ECM provides a framework support for cells with attachment sites and cell signaling factors. The bioactive properties of ECM make it attractive for use as tissue scaffolding. The major ECM proteins utilized in soft tissue engineering include a load bearing structural constituent, collagen, and an elastic structural component, elastin. These will be reviewed in more detail along with decellularized ECM.

Proteins degrade by non-specific hydrolysis of the peptide bond, by thermal denaturation, and most importantly *in vivo*, through enzymatic action. Enzymatic degradation can be extremely specific, with a high dependence on the flanking peptide sequence and local protein conformation, or it can be more promiscuous with a large array of cleavage sites on numerous proteins that can interact with the active region of the enzyme. The enzymatic activity that a peptide-based polymer will face *in vivo* can vary greatly depending upon the tissue into which it is placed and the inflammatory status following implantation. In an environment with a high

concentration of activated phagocytes, the enzymatic degradation processes may be greatly accelerated. The free radicals and low pH that result from active inflammatory processes can also accelerate local degradation of peptide based polymers.

#### 1.2.1.1 Collagen

Collagen is the primary component of the ECM and amounts to approximately 30% of the body's protein content. It is located in bone, skin, tendon, and most tissue and organs. To date, at least 19 types of collagen have been discovered. Types I, II, III, and V possess rod-like molecules of 300 kDa with a unique triple helix structure consisting of three polypeptides wrapped around one another that further associate into fibrils. Type I collagen is by far the most common type and can be found in bone, skin, cornea, vascular tissue, cartilage and tendon. Collagen's unique tight left-handed α-helical structure primarily results from hydrogen bonding between glycine and other amino acid residues [22]. Fibrils of collagen occur when collagen molecules are aligned and the N-terminus and C-terminus of adjacent strands covalently crosslink. The fibril packing results in a 67-nm banding pattern due to end-to-end separations [23].

Collagen is a very useful ECM material for biomaterials applications due to its many inherent advantages. Since it is present in large quantities it can be readily isolated from animal sources. In general, collagen exhibits good biocompatibility and low antigenicity since its amino acid structure is conserved among animal species. Structurally intact collagen is a primary load bearing protein and hence possesses a large tensile strength at low elongations. Collagen also has been shown to be beneficial for cell adhesion, wound healing and can act as a haemostatic agent by promoting blood coagulation [24, 25]. Relative to other proteins, collagen is more

stable due to its tight triple helical structure. Yet, collagen is still enzyme degradable particularly to collagenases.

Collagen can be dissolved in dilute acids and processed by various methods into sponges and gels for tissue engineering. A disadvantage of processed collagen is that significant mechanical strength and stability are lost. Porous collagen sponges are typically mechanically weak and degrade relatively fast *in vitro* or *in vivo* [26]. Therefore, efforts to stabilize the collagen sponge have utilized chemical crosslinkers such as glutaraldehyde, carbodiimide, amines, and diisocyanates [26]. Physical stabilization methods include UV irradiation and thermal methods. While these methods may increase the material's resistance to degradation, they can also increase the toxicity due to the presence of residual crosslinkers and also mask some of the original collagen structure that is attractive for cell adhesion, cell infiltration, and wound healing.

Collagen scaffolds have found various applications for drug delivery and tissue engineering applications. Some tissue types investigated include cardiovascular, skin, and nervous tissue. For example, L'Heurex et al. investigated the use of collagen to construct a tissue engineered blood vessel [27]. Others have investigated its use in fabrication of a myocardium patch for replacement of necrotic myocardium [28, 29].

#### 1.2.1.2 Elastin

Proteins can perform many roles and functions while exhibiting diverse mechanical properties. The mechanical properties of elastic proteins include high breaking strains, low stiffness, and high resilience defined as the ability of a material to quickly return to its original shape after being deformed. Examples of some biopolymers that exhibit elastic properties

include silk, resilin, and elastin [30]. Spiders spin silk for both movement and trapping their prey. Resilin exists in specific areas of insects such as the junctions between the wings and the body. The presence of the protein elastin in ECM of human tissues such as blood vessels, lungs, skin, sphincter, ligaments and tendons gives these tissues the ability to recover after cyclic and non-cyclic deformation.

Elastin is an insoluble protein composed of a highly crosslinked network of amino acids. This protein is secreted as 70 kD single peptide chains termed tropoelastin which assemble with other microfibrillar components to form the elastic fibers of the ECM. This protein consists of approximately 750 residues with glycine, alanine, valine, proline and lysine being common amino acids present. Tropoelastin is for the most part separated into two phases. One phase is very hydrophobic and contains high levels of glycine, valine, proline, and alanine frequently occurring in the sequences GVGVP, GGVP, and GVGVAP. The other phase of tropoelastin is hydrophilic and rich in Lysine and Alanine frequently occurring as AAKAAKAA. In particular, the lysine residues in elastin are involved in highly interconnected networks of 4-way desmosine or isodesmosine crosslinks formed by the enzyme lysyl oxidase. These crosslinks permit strain recovery in the protein. Elastin from bovine ligament exhibits a modulus of 1.1 MPa, a tensile strength of 2 MPa, elongation at break of 150%, and a resilience of 90% [30].

Since elastin is composed of such a highly crosslinked network, it is difficult to solubilize for processing and application. Therefore, a number of research groups have synthesized elastin-like polypeptides [30-36]. The polypeptide poly(OrnGlyGlyOrnGly) was synthesized by replacing the valine residues in a typical sequence of elastin, -VGGVG-, to impart amine functionality into the protein backbone for cross-linking with glutaraldehyde [31]. The resulting polypeptides possessed similar structural morphologies to elastin.

An extensive study of the biocompatibility and potential of elastin-mimetic peptides with the repeating sequence, $(GVGVP)_x$, to alleviate stress urinary incontinence was conducted by Urry et al. [36]. Panitch et al. created an elastin-like peptide to support vascular endothelial cell adhesion for use in the repair or replacement of vascular tissue. This polymer was based on a repeating peptide sequence $(GVPGI)_x$, related to mammalian elastin, and a cell-binding domain derived from fibronectin [35]. Plates coated with polymer containing the sequence, MG[LD*CS5*$(GVPGI)_{20}]_5$LE, where *CS5* designates the sequence, -GEEIQIGHIPREDVDYHLYP- , were found to induce the attachment and spreading of plated human umbilical vein endothelial cells at a level similar to control fibronectin coated plates. Endothelial cell adhesion was attributed to the presence of the adhesive sequence REDV. In a subsequent study, the polymer design was extended by incorporating crosslinkable lysine residues near the termini of the previous protein to yield the sequence MMASMTGGQQMGRKTMG[LD*CS5*G$(VPGIG)_{20}$VP]$_x$LEKAAKLE , where x is 5, 3, or 1 [37]. The placement of the crosslinking residues near the termini of the polymer chains enabled control of the chain length between crosslinks and crosslink density. After glutaraldehyde crosslinking , the mechanical properties of these protein films were similar to those of native elastin with an elongation at break in the range of values reported by Abbott and Cambria, 100-200% [37, 38].

A recombinant 90 kDa protein containing the repeating sequence, $(VPGVG)_4$(VPGKG), in *E.coli* was produced [32]. This protein was processed by electrospinning into nanoscale fibers that mimic the size and shape of native elastin [39]. Subsequently, the elastin-mimetic protein, $(VPGVG)_4(VPGKG)_{39}$, was modified by incorporating methacrylate groups onto the chain ends [40]. These proteins were crosslinked by photoirradiation and fiber mats were found to have a

fiber diameter range of 300-1500 nm and an average pore size of 78 $\mu$m. Hydration substantially increased the elongation at break to 105 ± 8% for crosslinked samples which is comparable to the value for native elastin [40].

#### 1.2.1.3 Decellularized ECM matrices

As the ECM is a dynamic tissue composed of a myriad of structural and functional proteins, glycoproteins, and proteoglycans, present in a complex three dimensional structure, many believe it is ideal for scaffolding to mimic these properties as much as possible. Therefore, relatively unmodified and acellular ECM has been isolated and applied as tissue engineering scaffolding. These matrices are isolated and decellularized and are essentially unchanged from native ECM. In contrast to processed and crosslinked collagen and other ECM materials, these decellularized ECM matrices promote host responses that exhibit rapid tissue infiltration and remodeling for tissue repair and wound healing.

The primary feature of decellularized ECM that differentiates it from other ECM based materials is the natural diversity and morphology of bioactive and structural proteins present. Structural proteins include fibronectin, elastin, and collagen. In addition, growth factors found in these materials include vascular endothelial growth factor (VEGF), basic fibroblast growth factor (bFGF), transforming growth factor (TGF-β), hepatocyte growth factor (HGF), and plate derived growth factor (PDGF) [41]. These growth factors can have profound impacts on cell growth and behavior. For example, VEGF is a potent initiator of angiogenesis. While these factors can be isolated and loaded into natural or synthetic matrices, the relative concentrations and ratios necessary to mimic the *in vivo* structure is unknown. Decellularized ECM based materials have these proteins and factors already present in their *in vivo* states and quantities.

Sources for decellularized ECM can include skin dermis, small intestinal submucosa (SIS), urinary bladder submucosa (UBS), and liver [42]. These materials are isolated and not modified except for decellularization and sterilization. Decellularization usually involves some type of chemical or enzymatic procedures that minimize structural modification.

These matrices are very attractive for tissue engineering and have been studied in various applications. For example, porcine derived ECM has been studied for reconstruction of the urinary tract, dura matter, vascular tissue, and full thickness skin wounds [41]. The characteristic *in vivo* response to all of these materials typically involves intense cellular in-growth of leukocytes and mononuclear cells. After a few days up to two weeks the matrix becomes vascularized and degraded. At two weeks, the presence of parachymal cells such as smooth muscle cells, fibroblasts, skeletal muscle cells, and epithelial cells have been observed. There is also typically an absence of scar formation after wound healing with these materials [41].

ECM based materials as well as other materials that possess a biological basis, hold considerable potential for use as biomaterials. The chemical similarities or homology to native tissue components endow these materials with bioactivity that can enhance their overall performance. Enzymatic sensitivity allows these materials to be remodeled by natural mechanisms with a temporal and spatial variance dictated by the local tissue environment. These materials may also possess the capacity for interacting with cellular and molecular components of the host environment to facilitate integration. The binding of growth factors and other extracellular matrix components as well as the provision of cell-specific adhesive ligands exemplify this activity. Their degradation products would not appear to present any obvious toxicity concerns, although immunogenicity and unwanted bioactivity may be present and prove problematic. For example, degradation that is too susceptible to the enzymatic activity

associated with inflammatory processes may result in a very rapid mass loss and loss of mechanical properties. If chemical crosslinking is employed, toxicity concerns may be present due to the presence of residual crosslinker. Calcification often results *in vivo* with a variety of natural materials. In addition, protein-based materials present inherent challenges in processing due to their thermal lability and susceptibility to denaturation in organic solvents. Despite these potential disadvantages, there exists a wealth of possibilities in mimicking nature's materials.

### 1.2.2 Biodegradable polyesters

To date, biodegradable polyesters and hydrogels have been the most commonly studied synthetic materials in engineering scaffolds. Then again, these polyesters such as polyglycolide (PGA), polylactide (PLA), and their copolymers (PLGA), are relatively stiff, non-elastomeric polymers and are not ideally suited for engineering of soft flexible tissues operating under a mechanically demanding environment such as in cardiovascular tissue. Furthermore, hydrogels most often do not possess sufficient mechanical strength. Therefore, to better mimic the mechanical behavior of compliant soft tissues, synthetic biodegradable polyester based elastomers have been developed. These materials are designed to undergo multiple deformations during in vitro and in vivo tissue development. The following sections will review the various synthetic polyester based biodegradable elastomers and scaffold processing methods as applied for soft tissue engineering. A sample list of these biodegradable polymers is summarized in **Table 1-2** along with their representative properties and soft tissue applications. Chemical structures of the repeating units of these polymers are displayed in **Figure 1-3**.

**Table 1-2.** Physical properties of some soft biodegradable polymers.

| Polymer | Tg / °C | Tensile Strength (MPa) | Modulus (MPa) | Ultimate Elongation (%) | *In Vitro* Degradation % mass loss (time) | References |
|---|---|---|---|---|---|---|
| PLGA | 45-55 | 41.4-55.2 | 1400-1800 | 3-10 | varies | [43] |
| PCL | -64 | 20.7-34.5 | 0.21-.34 | 300-500 | varies | [43] |
| PGCL | -19.3 | 0.6* | - | 250* | 50% (8wks) | [44] |
| PLCL | -6.3 | 0.8* | - | 210* | 1.7% (8wks), 10.7% in-vivo (8wks) | [45, 46] |
| PTMC | -17 | 12 | 6 | 830 | negligible change in 2 years | [47] |
| P(TMC-CL) | -62 | 40 | 252 | 906 | negligible change in 1 year | [48] |
| P(TMC-LA) | 17 | 10 | 16 | 570 | 100% (1 year) | [47, 48] |
| PGS | - | 0.5 | 0.282 | 267 | 17% (8.5 wks), 100% in-vivo (8.5wks) | [49, 50] |
| PU (PCL, BDI, putrescine) | -53.2 | 29 | 78 | 660 | 10% (8 wks) | [15] |
| PU (PCL, BDI, lysine ethyl ester) | -54.3 | 13 | 38 | 841 | 50% (8wks) | [15] |
| PU (L-lactide / PCL, HDI, BDO) | -45 to 53 | .09 to 47 | 1.1-2100 | 3.7-1000 | 5% to 80% (10 wks) | [17] |
| PU (PCL-PEG, HDI, BDO) | -115.7 to -101.5 | 4-48.6 | 7.3-58.8 | 120-866 | 1.6% to 76% (1 year) | [51] |

* denotes porous scaffold properties

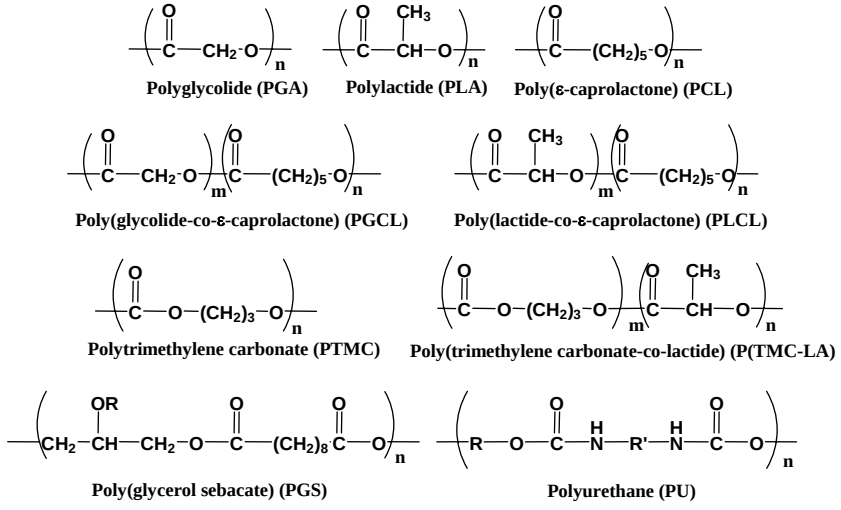


**Figure 1-3.** Sample chemical structures of biodegradable polyesters for tissue engineering.

#### 1.2.2.1 Polyglycolide, polylactide, poly(ε-caprolactone) and their copolymers

The most common synthetic materials studied to date in tissue engineering applications are aliphatic polyesters such as PGA, PLA, and their copolymers, PLGA. High molecular weight polymers are typically synthesized by ring opening of their respective lactones. These aliphatic esters degrade by hydrolysis of the ester moieties. These materials can be highly crystalline and stiff. PLGA has been extensively studied in scaffolds for engineering of most tissue types such as cardiovascular, esophagus, trachea, neural and musculoskeletal tissue such as bone, cartilage, and meniscus [43, 52]. The degradation rate of PLGA can be modified by varying the ratio of PLA and PGA in the polymer. A disadvantage to the use of PGA and PLA scaffolds is the generation of acidic degradation products leading to inflammatory responses *in vivo*. While PLGA is a softer material with tensile strengths and breaking strains appropriate for soft tissue engineering, the non-elastomeric character of PLGA does not allow for sufficient structure retention after mechanical stimulation during *in vitro* tissue development [13].

Poly(ε-caprolactone) (PCL) is an aliphatic polyester synthesized by ring opening polymerization of its respective lactone, ε-caprolactone. PCL is semicrystalline and exhibits a low $T_g$ of -64°C and low $T_m$ of 57°C so that it is soft at room temperature [43]. PCL exhibits a relatively slow degradation rate compared with PLGA on the order of months to years due to the larger number of methylene groups present. PCL has been copolymerized with PGA or PLA to result in softer materials. In some cases, microphase separated elastomeric poly(glycolide-co-ε-caprolactone) (PGCL) or poly(lactide-co-ε-caprolactone) (PLCL) have been synthesized by random copolymerization [53]. These materials consist of crystalline hard phases and amorphous soft phases. The elastomeric behavior is the result of physical crosslinks between the crystalline hard phases and flexibility from the soft phases.

The mechanical flexibility of PCL copolymers has led some groups to investigate these materials for soft tissue engineering applications. For example, high molecular weight amorphous PGCL (approximately 50:50) was synthesized for blood vessel and bladder tissue engineering [44]. This polymer possessed a $T_g$ of 19.3°C and exhibited rubber-like mechanical properties with scaffolds exhibiting elongations exceeding 250% and recoveries from deformation of more than 98%. This material degraded *in vitro* for a mass loss of 50% at 6 weeks [44].

A high molecular weight, elastomeric PLCL (50:50) was synthesized by Jeong et al. for vascular applications [54]. This material possessed a $T_g$ of -6.3°C and was flexible with elongations exceeding 200% and high recovery after deformation [54]. Degradation of this material was relatively slow with a mass loss of 1.7% *in vitro* and 10.7% *in vivo* at 8 weeks [45]. PLCL has also been seeded with vascular smooth muscle cells (SMCs) and cultured under pulsatile perfusion to result in aligned cells with a 2.5-fold upregulation of smooth muscle α-actin compared with static controls [55]. PLCL was surface modified with fibronectin and collagen and studied for esophageal tissue engineering as well [46].

#### 1.2.2.2 Poly(trimethylene carbonate) copolymers

High molecular weight poly(trimethylene carbonate) (PTMC) is an amorphous polymer that possesses high tensile strength and flexibility [48]. However, the very slow *in vitro* and *in vivo* degradation rates of PTMC have led to the necessity of copolymerization of with PLA or PCL [48, 56]. Random copolymerization of trimethylene carbonate and ε-caprolactone with a ε-caprolactone content higher than 70% resulted in elastomeric materials. For example, poly(trimethylene carbonate-co-ε-caprolactone) (P(TMC-CL)) (10:90) exhibited a tensile

strength of 40 MPa and an ultimate elongation of 906%. Yet, this material also suffered from relatively slow degradation with negligible *in vitro* mass loss up to 1 year [48]. P(TMC-CL) has been studied for fabrication of porous nerve guide conduits, with Schwann cells adhering and proliferating on the polymer *in vitro* [48, 57].

Poly(trimethylene carbonate-co-lactide) (P(TMC-LA)) (50:50) copolymers were also synthesized and found to exhibit elastomeric mechanical properties with a tensile strength of 10 MPa and an ultimate elongation of 570% [48]. This material exhibited a faster degradation rate with greater than 50% mass loss at 6 months and 100% at 12 months *in vitro*. These faster degradation rates were perhaps due to the greater hydrophilicity of the lactide segment compared with the more hydrophobic caprolactone. P(TMC-LA) has been fabricated into porous scaffolds for cardiomyocyte culture in engineering of myocardium [47].

#### 1.2.2.3 Poly(glycerol sebacate)

Polycondensation of the non toxic monomers, glycerol and sebacic acid, with a 1:1 molar ratio forms a transparent, lightly crosslinked elastomer termed poly(glycerol sebacate) (PGS) [50]. Glycerol is a building block for lipids and sebacic acid is a metabolic intermediate. Covalent crosslinks and hydrogen bonding between hydroxyl groups present on the polymer chain contribute to the elastomeric mechanical behavior of PGS. Tensile properties of PGS include a tensile strength of 0.5 MPa and an ultimate elongation of 267%. PGS is relatively hydrophilic due to its hydroxyl groups with a water-in-air contact angle of 32.0°. PGS is believed to degrade principally by surface erosion as evidenced by an approximately linear decrease in mechanical properties with degradation. PGS degraded *in vitro* to result in a 17% mass loss at 8.5 weeks and completely degraded subcutaneously *in vivo* during this time [50].

Before crosslinking, PGS can be processed in prepolymer form into porous scaffolds for soft tissue engineering. In vitro and in vivo cytocompatibility characterization of PGS has exhibited a good biocompatibility with support of cell growth such as endothelial cells, smooth muscle cells, cardiomyocytes, Schwann cells, and hepatocytes for applications in cardiovascular, neural, and liver tissue engineering [49].

### 1.2.3 Biodegradable polyurethanes

Polyurethanes are the most economically important elastomers for a variety of commercial applications. Therefore it is not surprising that this class of polymers has been the focus of many groups seeking to develop biodegradable elastomers for medical applications. Polyurethane and poly(urethane urea) thermoplastic elastomers derive their attractive mechanical properties from microphase separation between hard and soft segments. Selection of hard and soft segments and the complexity possible within these segments offers a multitude of options in achieving material design objectives. Although urethane and urea linkages are susceptible to degradation *in vivo*, efforts to make biodegradable polyurethanes have incorporated more labile bonds into the polymer backbone, usually by introducing polyester segments.

Polyurethanes are commonly synthesized by one of two methods. The first involves the reaction of bischloroformates with diamines. The second and more important method is the reaction of diisocyanates with dihydroxy compounds which has the advantage of no undesired byproducts. Diisocyanates can also react with diamines to form polyureas, with carboxylic acids to form polyamides and with water to form polyurea foam. Side reactions in polyurethane synthesis can occur when unreacted isocyanate groups react with the growing urethane or urea

chains to yield allophanate and biuret groups respectively. Biodegradable polyurethane elastomers can also consist of a network of chemically crosslinked chains. These elastomers can be synthesized by using monomers that are trifunctional or of higher functionalities compared with the difunctional monomers used in synthesizing linear (thermoplastic) polyurethanes [58-60]. Covalently crosslinked polyurethanes have the disadvantage of not being amenable to processing by thermal or solvent based techniques.

Polyurethane elastomers are usually constructed from long chain polyester or polyether diols and diisocyanates, with short chain diols or diamines utilized as chain extenders. The reaction is commonly carried out in two steps with the initial formation of a prepolymer of the polyester and diisocyanate that is subsequently chain extended to a high molecular weight **(Figure 1-4)**. Alternatively, the reaction can occur in one step (one-shot polymerization) when the monomers are mixed together at once. The longer chain polyester or polyether in the resulting polyurethane is referred to as the soft segment and the diisocyanate and chain extender

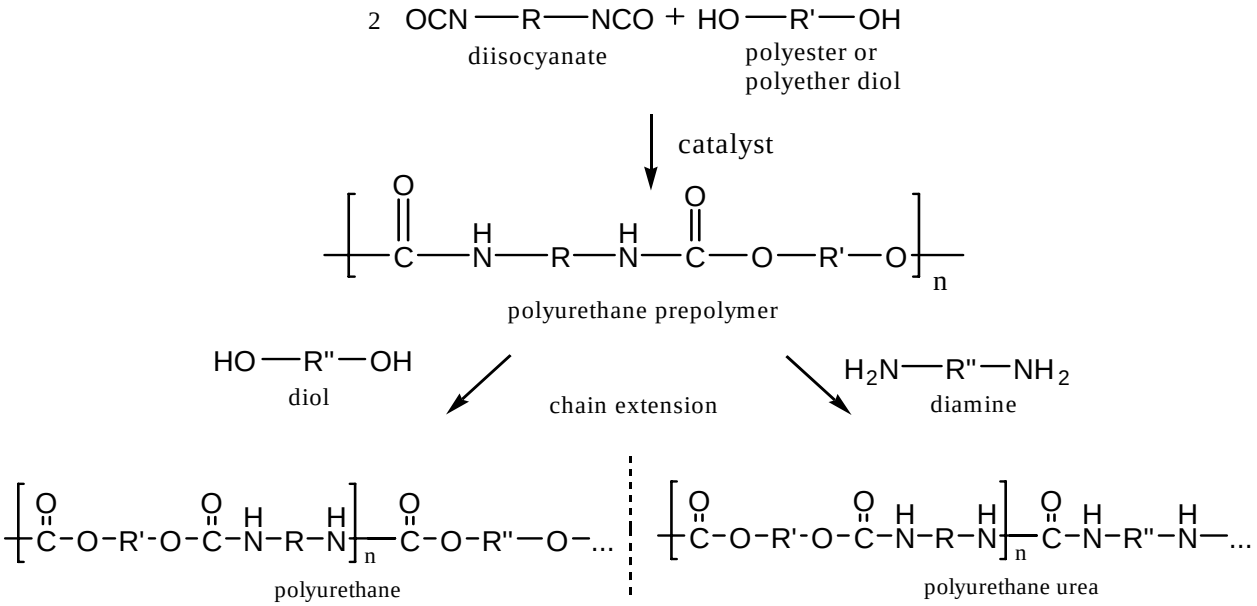


**Figure 1-4.** Two step reaction to form polyurethane or polyurethane ureas [1].

all of are referred to as the hard segment. Common polyester soft segments used in biodegradable polyurethanes include PCL [15, 21, 61], PLA [17], PGA [62], PEG [62], PEG-PCL copolymers [16, 63], PEG-PLA copolymers [64], and poly(hydroxybutyrate) (PHB) [62, 65]. Common diisocyanates used in constructing biodegradable polyurethanes are 1,6-hexamethylene diisocyanate (HDI) [51, 63], 1,4-butanediisocyanate (BDI) [15, 21, 61, 66], lysine diisocyanate (LDI) [67], isophorone diisocyanate, and 2,2,4-trimethyl-1,6-diisocyanate (TMDI) [68]. The use of aliphatic diisocyanates facilitates degradation and avoids use of potentially carcinogenic aromatic diisocyanates such as methylenediphenyl diisocyanate (MDI) and toluene diisocyanate (TDI), commonly employed industrial

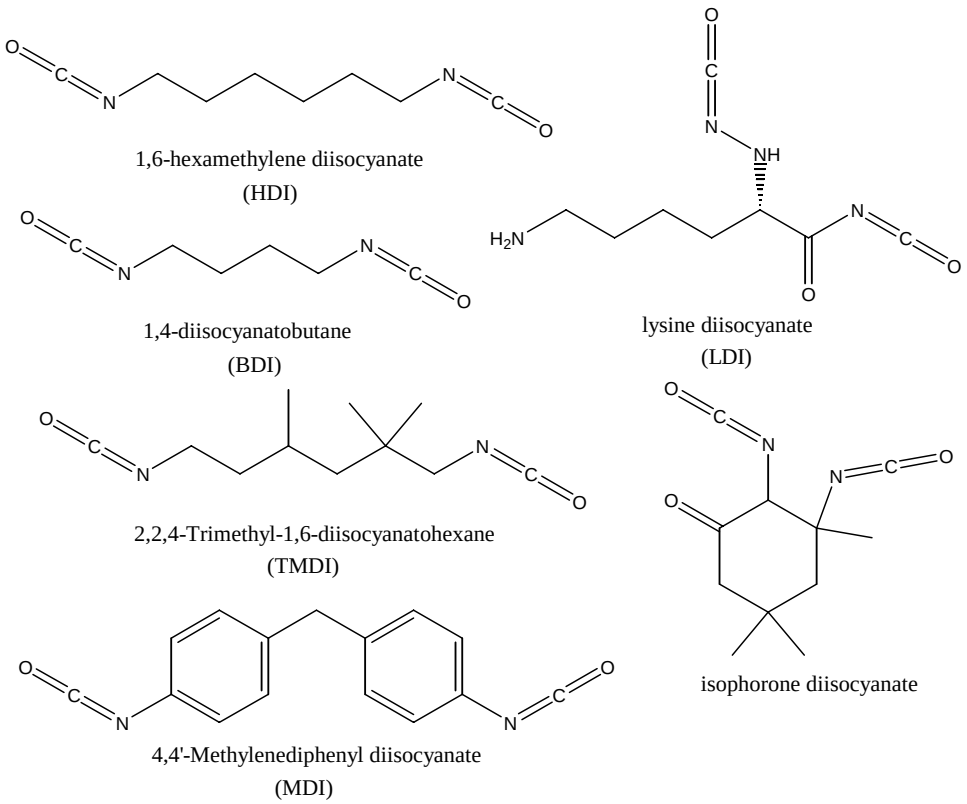


**Figure 1-5.** Chemical structures of diisocyanates used as monomers in biodegradable polyurethanes [1].

diisocyanates. There exists speculation that MDI and TDI degradation products, 4,4'-methylene aniline (MDA) and toluene diamine (TDA) are carcinogenic [69-71]. In contrast, LDI and BDI are attractive for tissue engineering applications since their primary degradation products, ethanol and L-lysine, and putrescine respectively, can be considered non-toxic. The chemical structures of these diisocyanates are shown in **Figure 1-5.**

The chemical and physical properties of polyurethanes can be varied by the choice of hard and soft segments. **Table 1-3** summarizes some different biodegradable polyurethanes that have been reported in the literature based on their soft and hard segment composition. The majority of these polymers contain PCL in the soft segment. Gorna et al. bulk polymerized PCL with aliphatic HDI and 1,4-butanediol (BDO) as a chain extender [51]. Other studies have introduced PEG along with PCL into the soft segment with or without BDO chain extenders [63, 72]. High molecular weight polyurethanes based on PCL soft segments with BDI were chain extended with BDO, BDO-b-BDI-b-BDO blocks, or BDI-b-BDO-b-BDI-b-BDO-b-BDI blocks [21, 61]. The larger chain extenders were used to prevent transesterification reactions from creating a large size distribution of hard segments. de Groot et al. synthesized a series of linear polyurethane ureas based on a PCL soft segment and hard segments consisting of either LDI, HDI or BDI that were chain extended with putrescine [73]. Similar poly(ester-urethane ureas) were synthesized by Guan et al. using putrescine and lysine ethyl ester as chain extenders [15].

**Table 1-3.** Composition and physical properties of linear biodegradable polyurethanes and polyurethane ureas.

| Soft Segment | Hard Segment Composition | | soft segment | Tensile Strength, | Modulus | Ultimate Elongation | |
|---|---|---|---|---|---|---|---|
| Composition | Diisocyanate | Chain Extender or Other | Tg / C | MPa | (MPa) | (%) | Reference |
| PCL* | HDI | BDO | -54.4 to -40.6 | 12-63 | 13-107 | 460-760 | [51] |
| PCL | LDI | putrescine | -45 | 17 | 40 | 800 | [67] |
| PCL | BDI | putrescine | -45 | 29 | 52 | 1042 | [67] |
| PCL | BDI | BDO | -54 | 23.1 | 23.2 | 843 | [21] |
| PCL | BDI | BDO.BDI.BDO | -54 | 44 | 70 | 560 | [61] |
| PCL | BDI | BDI.BDO.BDI.BDO.BDI | -60.4 | 35 | 105 | 650 | [61] |
| (50/50) L-lactide / PCL | BDI | BDO.BDI.BDO | -5 | 45 | 60 | 560 | [73] |
| PCL* | BDI | putrescine | -53.2 to -36.5 | 25-29 | 54-78 | 660-686 | [15] |
| PCL* | BDI | lysine ethyl ester | -54.3 to -39.7 | 9.2-13 | 14-38 | 841-895 | [15] |
| PCL* | LDI | p-alanine based diamine* | -51.9 to -6.2 | 12.5-30.8 | 6.6-81.9 | 618-676 | [20] |
| PCL-PEG* | HDI | BDO | -115.7 to -101.5 | 4-48.6 | 7.3-58.8 | 120-866 | [63] |
| PCL, PGA, PEG* | TMDI | PHB-*co*-PHV* | -44 to 2 | 2.6-15.9 | 50-500 | 50-1250 | [62] |
| PCL* | TMDI | poly(p-dioxanone)diol* | -51 to -39 | 17-25 | 34-90 | 540-1100 | [68] |

* Indicates series of polymers synthesized with different feed concentrations or monomer molecular weights.

Bioerodible polyurethanes have also been synthesized with L-lactide in the soft segment. Kylma and Seppala investigated co-monomers of lactic acid and caprolactone in poly(ester-urethanes) based on HDI [17]. Condensation copolymerization of lactide and ε-caprolactone at different feed ratios took place with stannous octoate as a catalyst. High molecular weight polyurethanes were produced by chain extending with HDI. Polyurethanes based on a 50/50 poly(L-lactide-co-ε-caprolactone) prepolymer with BDI were synthesized [73]. Because the lactide bond is susceptible to aminolysis, chain extension was not possible with putrescine. Furthermore, the use of BDO as a chain extender resulted in transesterification leading to poor mechanical properties. For these reasons, an isocyanate terminated chain extender, BDO-b-BDI-b-BDO, was used.

Several research groups have constructed biodegradable polyurethanes and polyurethane ureas by introducing biodegradable functionalities into the hard segment as well as the soft segment to facilitate hydrolytic degradation. Poly(ester-urethanes) consisting of crystallizable poly[(3-R-hydroxybutyrate)-*co*-(3-R-hydroxyvalerate)] (PHB-*co*-PHV) hard segments and amorphous segments from ε-caprolactone, diglycolide and ethylene glycol homopolymers or copolymers have been reported [62, 65]. Elastomeric polyurethanes have also been synthesized from poly(ε-caprolactone)diols and poly(*p*-dioxanone)diols (PDX) reacted with TMDI [62]. Skarja and Woodhouse synthesized novel polyurethane ureas with either PCL or PEG soft segments, HDI or LDI, and with an amino-acid based chain extender based on L-phenylalanine [18, 19].

The soft segments impart polyurethanes with softness, flexibility and low temperature properties while the hard segments reinforce or strengthen the soft segment to increase the hardness, modulus, tear strength, and high temperature properties of polyurethanes. The hard segments possess a high affinity for hydrogen bonding due to the large number of polar groups present. Urea groups provide even more opportunities for hydrogen bonding relative to urethane groups. The combination of crystallinity and hydrogen bonding in the phase separation of polyurethanes ties together the polymer chains in physical crosslinks. These physical crosslinks result in a network of polymer chains that display rubber-like elasticity.

Similar to multi-phase polyesters, the factors that affect mechanical properties of biodegradable polyurethanes include hard and soft segment composition, degree of crystallization of the hard segment and amount of microphase separation, and the molecular weight of the polymer. A summary of mechanical properties for different monomer compositions of biodegradable polyurethanes and polyurethane ureas is provided in **Table 1-3**. Gorna et al.

showed that the mechanical properties of polyurethanes with similar molecular weights were dependent on the hard segment content [51]. Tensile strength and modulus increased with increasing hard segment molecular weight or with shorter soft segments, while the breaking strain decreased. In an extensive study, the mechanical properties of polyurethanes based on L-lactide and ε-caprolactone copolymers were found to be highly dependent on the initial feed ratio of the monomers. Poly(ester-urethanes) containing a high ratio of L-lactide and ε-caprolactone were found to be rigid with tensile modulus of 1700-2100 MPa, tensile strengths of 36-47 MPa, and breaking strains of 4-7% [17]. Polymers with low L-lactide to ε-caprolactone ratios were found to be highly elastomeric with a maximum tensile strength of 9 MPa and breaking strain of greater than 1000%. These properties were found to be direct functions of the glass transition temperatures of the polymers. When the glass transition temperatures were above room temperature the soft segment was amorphous and mostly immobile which would contribute to higher tensile strengths and lower elongation [17].

Polyurethane biodegradation products and rates can be influenced by the choice of the soft and hard segment. Degradation is influenced by factors such as crystallinity and polymer molecular weight. Degradation of the common soft segment PCL usually occurs first by hydrolytic chain scission and then by bulk mass loss of subsequently lower chain lengths [74]. PCL alone has demonstrated some long degradation times that can extend to the order of years due to its hydrophobicity and tendency to crystallize at higher molecular weights. Since most studies are conducted over limited time periods, the time scales for complete resorption of most PCL based degradable polyurethanes both *in vitro* and *in vivo* are mostly unknown. Degradation of PCL based polyurethanes by Gorna et al. exhibited slow degradation times with a 1-2% mass loss at 48 weeks and a 1.1-3.8% mass loss at 76 weeks [63]. However, poly(ester

ether urethanes) composed of PCL-PEG diols exhibited levels of weight loss from 1.6-76% at 48 weeks and 1.6-96% at 76 weeks. The weight loss was found to increase with higher levels of the more hydrophilic PEG [63]. A similar *in vitro* degradation trend was observed for amino acid chain extended, PCL based polymers which exhibited little mass loss after 56 days compared with the PEG based polymers that exhibited high mass loss in this period [75].

The *in vitro* degradation of L-lactide / ε-caprolactone copolymer based polyurethanes was found to be highly dependent on the comonomer ratio. Polymers synthesized from high ratios of L-lactide to ε-caprolactone exhibited mass losses of more than 80% after 50 days compared with higher ε-caprolactone content polymers exhibiting less than 10 % weight losses after 50 days [17]. These degradation weights were related to the hydrophilicity of the monomers with lactic acid being more hydrophilic than PCL.

A very thorough investigation of the hydrolytic degradation of copoly(ester urethane)s with PHB-*co*-PHB hard blocks synthesized by Lendlein et al. has shown the degradation rate to be dependent on the amount and distribution of the glycolate ester bonds in the soft segments of the urethane [74]. Here, the polymer degradation began hydrolytically, decreasing the molecular weight and lowering the breaking strain. Next, weight loss decreased the sample size leaving the poly(PHB-PHV) hard segment as the principal remaining material. Due to the nature of the amorphous segment and crystalline segment of physically cross-linked polyurethanes, it is common for the soft segment to degrade at a much faster rate than the hard segment resulting in a non-linear degradation rate. However, a linear weight loss *in vitro* was demonstrated with a polyurethane based on PCL/PDX due to the high crystallinity of the polyesters [68]. The use of aliphatic diisocyanates in biodegradable polyurethanes facilitates degradation and avoids the potentially carcinogenic aromatic diisocyanates, MDI and TDI. The use of LDI and BDI as hard

segments is of interest because of their putative non-toxic degradation products, ethanol and L-lysine, and putrescine respectively.

Physical crosslinking is reversible with heat treatment or solvation, allowing polyurethanes to be processed by such methods as solvent casting, extrusion, and injection. Polyurethanes or polyurethane ureas consisting of physical crosslinks are referred to as linear or thermoplastic elastomers. Examples of some techniques to process polymers into porous scaffolds for cellular in-growth in tissue engineering applications include particulate leaching and phase separation. The BDO and BDI-b-BDO-b-BDI-b-BDO-b-BDI chain extended polyurethanes by Spaans et al. were processed into porous scaffolds by a combination of salt leaching and freeze drying in 1,4-dioxane solvent [21]. The scaffolds possessed interconnected pores ranging in size from 150-300 μm. This material showed a high compression modulus and was thought suitable for application as a meniscal prosthesis. Lendlein and Langer designed and characterized shape-memory thermoplastic polyurethanes to be used in minimally invasive surgical procedures [68]. The elastic polymers were melted and extruded into monofilaments to be used as sutures. The filaments were loosely sutured in dead rats and heated to 41°C. With the increase in temperature came shrinkage of the polymer resulting in a tighter wound closure.

Different compositions of polymers prepared from poly[glycolide-*co*-(ε-caprolactone)]-diol and crystalline poly[(*R*)-3-hydroxybutric acid-*co*-(*R*)-3-hydroxyvaleric acid]-diol with TMDI were melt extruded into thin hollow tubes for tissue engineering of nerve guidance channels [76]. Nerve guidance channels are polymers tubes onto which severed nerve endings can be grafted. Borkenhagen et al. studied nerve regeneration in rats at 4, 12, and 24 weeks. 23 out of 26 implants contained regenerated tissue cables composed of myelinated axons and Schwann cells within the lumen.

The number of research reports published in the area of biodegradable elastomers is rapidly rising as appreciation for the role of mechanical properties in tissue-biomaterial interactions grows. The negative effects of mechanical property mismatch between an implant (e.g. a stiff vascular graft) and the surrounding tissue have been documented and studied for some time. The importance of mechanical training in the appropriate development of tissue engineered constructs is more recently being recognized in several systems [10-13]. To create new biodegradable elastomeric materials that meet the needs for a variety of clinical applications, researchers are working toward solutions from naturally occurring materials or elastomers based on synthetic polymers widely utilized for non-medical applications. The synthetic approach advances as biomaterials engineers work from an increasingly assorted array of biocompatible starting materials and incorporate specific bioactivity. There is a trend towards convergence whereby materials would be created that possessed the processing and design flexibility of synthetic approaches and the inherent bioactivity and biocompatibility of natural materials.

## 1.3 SCAFFOLD PROCESSING

Synthetic elastomeric scaffolds utilized by the soft tissue engineer should ideally be designed to mimic the structure and function of the natural extracellular matrix. This structure is believed to be appropriate for functional tissue development since it may encourage correct cell spatial arrangement and growth as well as allow for sufficient nutrient and waste exchange. A highly porous microstructure is desired to produce a large surface area for cell attachment and to encourage effective diffusion. Also, for conventional *in vitro* cell scaffold seeding and culture

methods, pore sizes of at least 10 μm are believed necessary for adequate cellular in-growth and vascularization [77]. Scaffold fabrication methods for soft tissue engineering must also permit mechanical strength and flexibility retention since introduction of porosity can greatly reduce the mechanical strength relative to the non-porous material. Care must also be taken to avoid introduction of any toxic components and remove any traces of residual processing solvents. Some techniques used in fabricating porous scaffolds include solvent casting and particulate leaching, phase separation, rapid prototyping and electrospinning [78-80]. A summary of the benefits and limitations of these methods is presented below. In general, materials should not possess covalent crosslinking in order to be solubilized in suitable fabrication solvents or processed from the melt. Lightly crosslinked materials may be processable in their respective prepolymer forms.

### 1.3.1 Particulate leaching

The technique of solvent casting and particulate leaching involves dispersing a porogen such as sodium chloride into a polymer solution, casting the polymer and subsequently leaching out the porogen by dissolution in a polymer non-solvent. The resulting scaffolds can possess high crystallinities and high porosities greater than 90% and macropores greater than 100 μm [80]. Disadvantages to this method include the production of irregular pore shapes, surface irregularities dependent upon the casting method, and the potential for residual toxic solvents.

### 1.3.2 Thermally induced phase separation

Thermally induced phase separation (TIPS) can produce porous scaffolds by liquid-liquid phase extraction. Polymer is dissolved in a solvent, cooled, and then solvent is slowly extracted by freeze drying to obtain polymer-rich and polymer-poor phases. This method allows for processing of scaffolds of controlled pore size distributions and high porosities [81]. Scaffold macrostructure and microstructure can be manipulated by varying polymer concentration, quenching temperature and solvents [78]. Biodegradable polyurethane scaffolds fabricated using TIPS were found to have open interconnected pores with sizes ranging from a few micron to greater than 150 μm and porosities from 80-97%. These materials were flexible with tensile strengths of 1.0 MPa and elongations at break of 214% [81]. TIPS scaffolds have been shown to support cell growth and proliferation. This technique has the disadvantage of being relatively user and material sensitive.

### 1.3.3 Rapid prototyping

Rapid prototyping or solid freeform fabrication is a more recent technology applied to tissue engineering based on computer controlled scaffold fabrication. This technology has a distinct advantage of precise control of scaffold macrostructure and microstructure from computerized data. This control includes defined porosity, pore sizes and shapes to benefit cell in-growth and tissue development. Examples of rapid prototyping techniques applied for tissue engineering include stereolithography, selective laser sintering, fused deposition modeling (FDM), and three dimensional printing [82]. Some disadvantages of these methods include potential thermal

denaturation of proteins as well as limitations on process resolutions and applicable materials. In some instances materials must be specifically designed in order to be processed by these techniques. For instance, FDM requires exact sized filaments to be fed into a thermal extruder. FDM can produce honeycomb like scaffolds of precise structures through a computerized layer-by-layer extrusion processes onto a movable stage. PCL scaffolds have been fabricated using FDM with scaffold channel sizes ranging from 160-700 μm, filament diameters from 260-370 μm, and porosity from 48-77% [83]. Depending on scaffold structure, these materials possessed tensile strengths ranging from 0.4-3.6 MPa and elongations at break from 4-28% [83].

### 1.3.4 Electrospinning

Electrospinning is a method that can be used to process biodegradable elastomers into matrices that resemble in scale and architecture the native extracellular matrix. Briefly, electrospinning occurs when a polymer solution or melt is charged with a high voltage that generates an electrical force. When that force overcomes the surface tension of a hanging drop of polymer solution , it can form a conical shape called the Taylor cone and then eject a polymer jet [84]. This jet undergoes a complex bending and whipping process in conjunction with fiber splaying and rapid solvent evaporation. The result is a non-woven fabric composed of fibers of diameters that can range from a few nanometers to microns deposited on a charged or grounded surface. Processing variables include voltage magnitude, polymer feed rate, pendant drop-target distance, solution viscosity, solution concentration, polymer molecular weight, target geometry and target motion. These variables largely affect the resulting morphology and size of the electrospun fibers. The most significant phenomena is a transition from electrospraying (i.e. spraying drops

of polymer opposed to continuous nanofibers) to electrospinning upon increasing solution concentration and viscosity.

While this technique was initially developed in 1914 [85] and under patent by Formhals in the 1930's [86], it has found recent application in construction of scaffolds for tissue engineering to more closely mimic the size scale and architecture of the native extracellular matrix [83]. Many biodegradable polymers including PLGA [83], PCL [87], and natural materials such as collagen [2, 88, 89] or engineered elastin proteins [39, 40] have been electrospun for study in various tissue engineering applications including cardiovascular and nervous tissue. Electrospun scaffolds are currently under investigation for cardiovascular applications such as cardiac and vessel grafts. Shin et al. have shown that cardiomyocytes can attach, proliferate and spontaneously beat on electrospun PCL meshes suspended across wire meshes [87]. Also, smooth muscle cells were found to align themselves on scaffolds of poly(L-lactide-*co*-$\varepsilon$-caprolactone) with aligned nanofibers for application in blood vessel tissue engineering [90]. Non-biodegradable medical grade polyurethane was electrospun for vascular graft applications [91]. Another group investigated the effects of various processing variables on electrospinning non-biodegradable polyurethane [92]. Furthermore, non-biodegradable medical grade polyurethane was electrospun by Kidoaki et al. using a multilayering process [93]. However, to date there of few reports on electrospinning of an elastomeric biodegradable polyurethane suitable for biomedical applications.

## 1.4 SPECIFIC AIMS

Ideal soft tissue replacements should mimic the mechanical and bioactive properties of the native tissue. However, to date truly functional engineered soft tissue such as myocardium or a tissue engineered blood vessel has not been created. Many limitations can be attributed to the absence of a suitable scaffold that possesses compliant properties necessary for function in a load bearing environment. While most reports in the literature focused on using a series of non-compliant biodegradable polyesters, here it was proposed that by utilizing a biodegradable elastomeric scaffold processed by innovative fabrication techniques, functional tissue could be developed.

Cytocompatible, biodegradable poly(ester urethane)ureas (PEUUs) based on polycaprolactone diol (PCL), 1,4-diisocyanatobutane, and putrescine were utilized as the base materials for scaffold fabrication. These polyurethanes were processed along with bioactive extracellular matrix proteins such as collagen or urinary bladder matrix by an electrospinning technique to produce scaffolds consisting of sub-micron scale fibers that resembled in size and scale the native extracellular matrix. The following dissertation set forth to complete the following specific aims.

1) **Biodegradable, elastomeric scaffolds were fabricated with biomimetic anisotropy and incorporated bioactive compounds.**

Ideal tissue engineering matrices would mimic the structure and properties of the tissue they seek to repair. Tissue biomimetic anisotropy could be introduced into scaffolds through fiber alignment from high speed target rotation. Further, these biomimetic matrices were achieved by combining biodegradable PEUU with extracellular matrix proteins such as structural proteins (collagen, gelatin, and urinary bladder matrix) or growth factors such as basic fibroblast growth factor (bFGF) by blending with the polymer spinning solution or co-spinning from

separate nozzles. These elastomeric matrices possessed bioactive cell signaling capabilities and enzyme sensitivity for remodeling to impact current approaches to soft tissue replacement.

2) **A method to microintegrate cells into nanofiber matrices was developed to allow for high density cellular in-growth.**

In order to develop working tissue *in vitro* or *in vivo* it was necessary to achieve high density cell in-growth. Due to the small size scale of the electrospinning scaffold fibers and pores, cell culture times can be long before in-growth occurs. Therefore, to overcome this disadvantage, we hypothesized that it may be possible to incorporate cells into the nanofiber matrix concurrent with the electrospinning process. This dynamic seeding method termed "cellular microintegration", was employed by electrospraying cells directly into the scaffold during the fabrication process. It was hypothesized that this method could achieve high cell density in the constructs immediately after fabrication and would greatly facilitate the process of tissue development.

3) **Electrospun scaffolds developed in previous aims were utilized to create a controlled release vehicle for growth factor or antibiotic delivery for improved fasciotomy management and wound healing.**

Electrospun sheets of PEUU were loaded with growth factors and / or antibiotics and studied for applications in fasciotomy management and repair. As stated previously, significant means of nutrient diffusion is necessary in creating viable tissue. It is well known that for scaffolds thicker than 100 μm, transport by diffusion alone is insufficient. Many believe that for adequate cellular infiltration of thicker three-dimensional scaffolds, vascularization is necessary. Therefore, by loading scaffolds with an angiogenic growth factors such as bFGF, it could be possible to induce vascularization. However, because some electrospinning solvents are rather

harsh to proteins, the effects of this process on growth factor bioactivity were examined. Furthermore, the release profile was assessed in an attempt to elucidate the effect of the large surface area of electrospun nanofibers on drug delivery. An obvious concern with many treatments both in the hospital and on the battlefield is infection. It was hypothesized that electrospun biodegradable polyurethane scaffolds would be ideally suited for the application of antibiotic release to reduce bacterial activity at a wound site. An ideal outcome of this aim was to illustrate that these biodegradable elastomerics possess the capability to be loaded with either growth factors or drugs and then release active forms of protein or drug in a controlled manner.

4) **Electrospun tubular scaffolds fabricated with technology developed in previous aims will be utilized to create a functional tissue engineered blood vessel.**

As an extension of the work completed in the previous aims, the matrices developed were directly studied in engineering biomechanically robust vessel replacements. The elastomeric and anisotropic properties of the scaffolds provided sufficient support to allow for development of functional tissue in the mechanically demanding environment to which vessel grafts were exposed. Electrospun PEUU small diameter tubular conduits were seeded or micro-integrated with appropriate cells such as smooth muscle cells, endothelial cells, or stem cells and examined under *in vitro* pulsatile flow conditions or *in vivo* small animal models.

Successful completion of the proposed aims made available novel processing techniques that result in mechanically and biologically biomimetic scaffolds to facilitate the development of functional tissue. The technology developed could beneficially impact engineering approaches to soft tissue replacement.

# 2.0 SYNTHESIS AND ELECTROSPINNING OF BIODEGRADABLE POLYURETHANES

## 2.1 INTRODUCTION

Biodegradable elastomers offer attractive mechanical properties for many soft-tissue engineering applications where non-elastomeric biodegradable polymers are currently used. In order to develop functionally compliant and mechanically robust tissue, evidence suggests that scaffolds should be designed to effectively transmit mechanical signals to the developing tissue in the dynamic *in vitro* or *in vivo* environment [9-14]. To date, the majority of tissue engineering reports in the literature have focused on a narrow series of biodegradable polyesters that are stiff with limited or no elastomeric properties. Therefore, several groups are actively pursuing the development of degradable and cytocompatible elastomeric materials that could find application in engineering soft tissues [15-21]. Our laboratory has developed a family of biodegradable polyurethanes since this material class allows for great latitude in design through the choice of hard and soft segments and also due to its potential to serve as a processable thermoplastic elastomer [15, 16].

Several types of biodegradable elastomers have been reported in the literature, however, there are fewer reports wherein these materials are fabricated into three-dimensional scaffolds compatible with cell growth. Techniques to fabricate porous structures for tissue engineering include particulate leaching, melt molding, fiber casting, thermally induced phase separation,

ink-jet printing, fused deposition modeling, and others [43, 77, 94]. Another technique, electrospinning, offers a means to process a polymer into sub-micron diameter fibers [95]. While this method was originally studied in 1914 and patented in the 1930's [85, 86], recent interest exists in its application towards development of tissue engineering scaffolds in order to more closely mimic the size and scale of the natural extracellular matrix [83, 96]. Briefly, electrospinning occurs when a polymer solution or melt is charged with a high voltage generating an electrical force that can overcome the surface tension of a pendant drop of the solution by first forming a conical shape called the Taylor cone and then ejecting a polymer jet [84]. The ejected jet experiences a complicated bending and whipping instability combined with fiber splaying and rapid solvent evaporation to yield fibers of very narrow diameters which can be collected on a grounded or charged collection surface. The processing variables of electrospinning can greatly influence the resulting morphology and size of the fibers. These variables include voltage magnitude, polymer feed rate, pendant drop-collector distance, solution viscosity, solution concentration, and polymer molecular weight.

The objective of this study was to synthesize and process biodegradable, elastomeric scaffolds with sub-micron scale fibrillar morphologies using an electrospinning technique. Two families of biodegradable polyurethanes were synthesized. The first and most extensively studied material was a poly(ester urethane)urea based on a soft segment diol of poly(ε-caprolactone) reacted with 1,4-butanediisocyanate and chain extended with putrescine. To incorporate greater "tunability" in biodegradation rates, a second family of polymers was synthesized that utilized a polyester-polyether-polyester triblock copolymer diol as the soft segment. By altering the ratio of polyether to polyester lengths in the soft segment, the polymer hydrophilicity and biodegradation rate can be altered. These materials were electrospun into

nanofibrillar, porous scaffolds for tissue engineering applications. The impact of polymer concentration in the spinning solution on scaffold morphology was investigated. Scaffold tensile mechanical properties were measured as well.

## 2.2 METHODS

### 2.2.1 Synthesis of biodegradable poly(ester urethane)urea (PEUU)

Stannous octoate (Sigma) and hexafluorisopropanol (HFIP) (Oakwood Products) were used as received. 1,4-diisocyanatobutane (BDI) (Fluka) and putrescine (Fluka) were distilled under vacuum. Polycaprolactone diol (*MW* = 2000, Aldrich) (PCL) was dried under vacuum for 48 h to remove residual water. Solvents dimethyl sulfoxide (DMSO) and N,N-dimethylformamide (DMF) were dried over 4-Å molecular sieves.

PEUU was synthesized as reported previously as shown in **Figure 2-1** [15]**.** The reaction occurred as a two step solution polymerization in a 250-mL three-neck round bottom flask under argon purge. A 2:1:1 molar ratio of BDI:PCL:putrescine was used. First, a 5 wt% solution of BDI in DMSO was reacted with a 15 wt% solution of PCL in DMSO with stannous octoate as catalyst for 3 h with continuous stirring at 75°C. The prepolymer solution was allowed to cool to room temperature and then putrescine was added dropwise while stirring. After 18 h of reaction at room temperature, the polymer solution was precipitated in distilled water and then wet polymer was incubated in 2-propanol for 48 h to remove unreacted monomer. The polymer was then dried under vacuum at 50°C for 48 h.

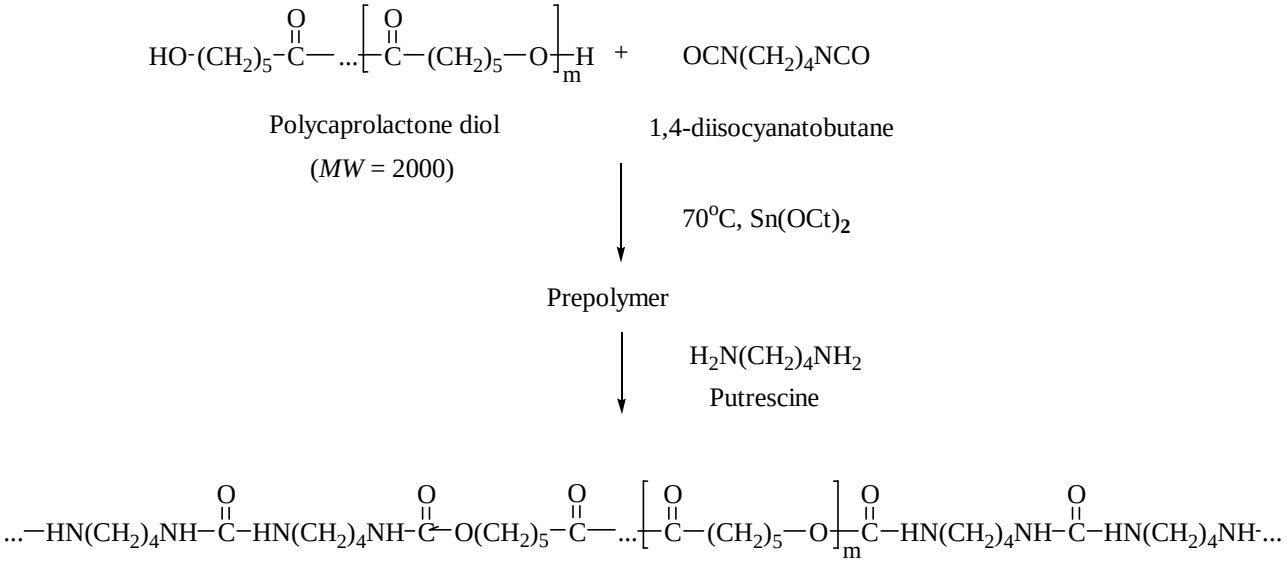


**Figure 2-1.** Poly(ester urethane)urea (PEUU) synthesis.

PEUU transparent films were prepared from a 3 wt% PEUU solution in DMF. If the presence of insoluble crosslinked PEUU was observed, PEUU solution was centrifuged at 3000 rpm to remove the gel. Hot polymer solution was cast onto polytetrafluoroethylene dishes and solvent was allowed to evaporate at room temperature. Films were subsequently dried under vacuum for 48 h. Transparent PEUU films obtained were approximately 50 μm thick and were utilized in further characterization experiments.

### 2.2.2 Synthesis of biodegradable poly(ether ester urethane)urea

Stannous octoate (Sigma) was used as received. 1,4-diisocyanatobutane (BDI) (Fluka) and putrescine (Fluka) were distilled under vacuum. Poly(ethylene glycol) (*MW* = 600, Aldrich) was dried under vacuum for 48 h to remove residual water. ε-caprolactone (Aldrich) was dried over

$CaH_2$. Solvents dimethyl sulfoxide (DMSO) and N,N-dimethylformamide (DMF) were dried over 4-Å molecular sieves.

PCL-PEG-PCL triblock copolymers were synthesized with PEG initiating polymerization of ε-caprolactone with a molar ratio of PCL:PEG of 18.0. The reaction occurred for 24 h at 120°C under argon gas. Prepolymer was then washed with ethyl ether and hexane and dried under vacuum.

PEEUU was synthesized as reported previously as shown in **Figure 2-2** [16]**.** The reaction occurred as a solution polymerization in a 250-mL three-neck round bottom flask under argon purge. A 2:1:1 molar ratio of BDI:triblock PCL-PEG-PCL:putrescine was used. First, a 15 wt% solution of BDI in DMSO was reacted with a 25 wt% solution of triblock prepolymer in DMSO with stannous octoate as catalyst for 3 h with continuous stirring at 75°C. The prepolymer solution was allowed to cool to room temperature and then putrescine was added dropwise while stirring. After 18 h of reaction at room temperature, the polymer solution was precipitated in distilled water and then wet polymer was incubated in 2-propanol for 48 h to remove unreacted monomer. The polymer was then dried under vacuum at 50°C for 48 h. PEEUU cast films were prepared with the same procedure used for PEUU cast films.

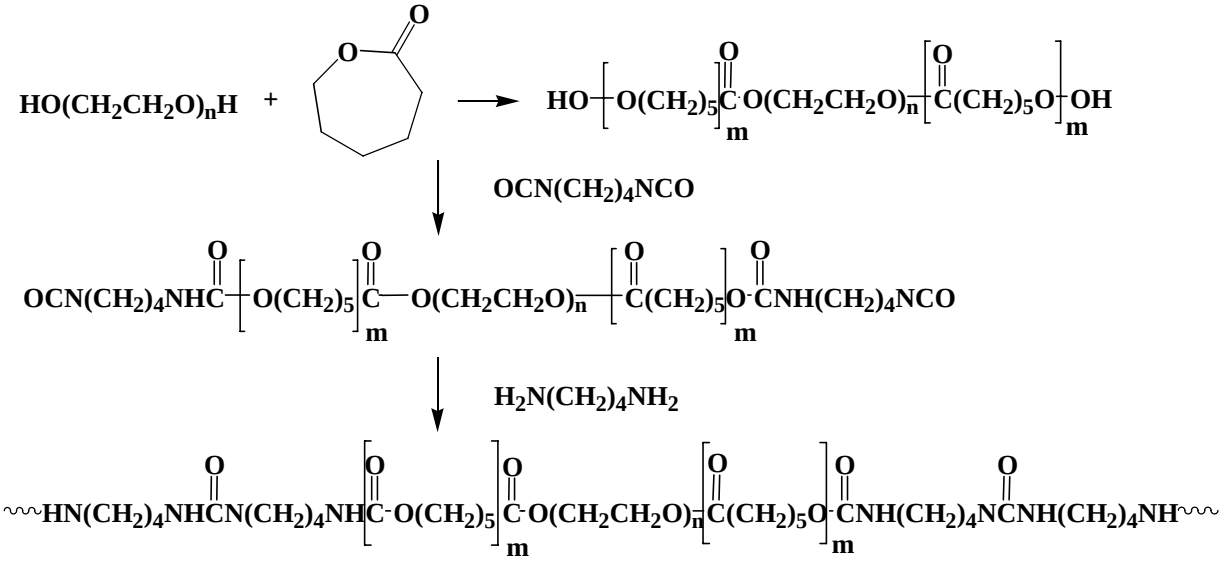


**Figure 2-2.** Poly(ether-ester urethane)urea (PEEUU) synthesis.

### 2.2.3 Polymer characterization

Polymer molecular weight was determined by gel permeation chromatography (GPC, Waters Breeze V3.2, Waters 1515 isocratic HPLC pump, Waters 2414 refractive index detector) using monodisperse polystyrene standards for calibration. Measurements were made at 35°C with 1-methyl-2-pyrrolidione (NMP) as solvent. Injection volume was 100 μL and PEUU concentration was 10 mg/mL.

Fourier transform infrared spectra (FTIR) were measured using a Genesis II FTIR spectrometer at room temperature. For FTIR, a 5 wt% PEUU solution in DMF was cast onto NaCl crystals. After evaporation of DMF under vacuum at 50°C for 4 h, spectra were measured.

Differential scanning calorimetry (DSC) was performed on a differential scanning calorimeter (Shimadzu; DSC 60) under helium and nitrogen purge. Scanning rates of 20°C/min

were used over a temperature range of -100°C to 250°C. Tensile properties were measured on an MTS Tytron™ 250 MicroForce Testing Workstation (10 mm/min crosshead speed) according to ASTM D638-98. Five samples were tested at each condition studied.

### 2.2.4 Surface modification

To modify the PEUU surface for attachment of cell adhesion peptides, it was first treated with radiofrequency glow discharge (RFGD) under an ammonia atmosphere as demonstrated previously **(Figure 2-3)** [15]. More specifically, PEUU cast film was inserted into a reaction vessel (PLASMOD) at 100 W and 13.6 MHz for 2 min under a vacuum of $3 \times 10^{-3}$ Torr. RGDS (Sigma) was attached to the modified PEUU surface, PEUU-$NH_2$, via a BDI spacer. Briefly, PEUU-$NH_2$ was incubated in BDI for 10 min followed by toluene and acetone rinses, and then placed in RGDS in PBS (20 μg/mL) for 10 h. PEUU with RGDS was then rinsed multiple times with PBS.

PEUU surface modification was quantified using the ninhydrin reaction [97, 98]. To first hydrolyze the spacer, PEUU-RGDS films were placed in vials with 0.93 mL 4*N* HCl and 1.57 mL deionized water at 120°C for 30 min. Next, 1.0 mL of 3.75 *N* NaOH neutralized the reaction followed by adding 1 mL of ninhydrin solution. The vial was heated to 120°C for 10 min, cooled in an ice bath, and optical density measured at 570 nm. Optical density was calibrated by known concentrations of soluble RGDS. The quantity of RGDS attached to PEUU was calculated by subtraction of the value for PEUU-$NH_2$ modified by BDI spacer alone.

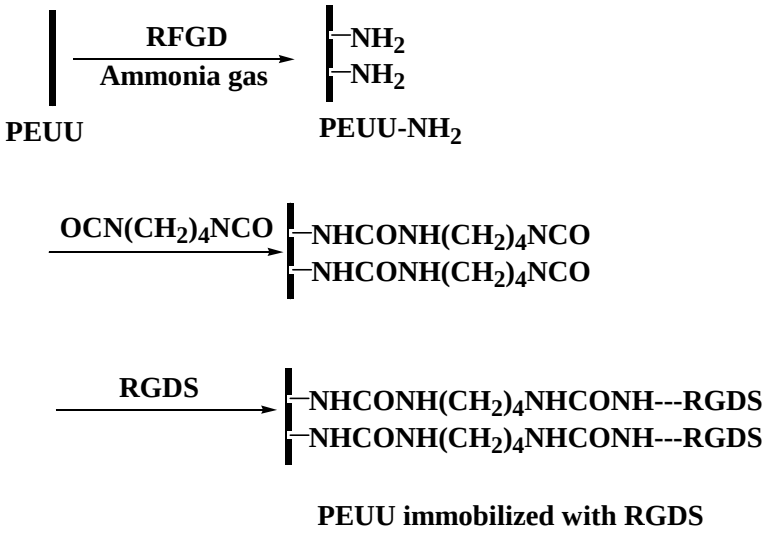


**Figure 2-3.** Radio frequency glow discharge with ammonia gas, followed by RGDS attachment with a BDI spacer.

### 2.2.5 Electrospinning

PEUU was dissolved in hexafluoroisopropanol (HFIP) at various concentrations (1, 2, 3, 4, 5, 8, and 10 wt %) under mechanical stirring at room temperature. PEEUU was dissolved at 8 wt% for electrospinning. The polymer solution was fed by syringe pump (Harvard Apparatus) into a steel capillary (I.D. = 0.047″) suspended vertically over the center of a cylindrical steel mesh focusing screen and aluminum collector plate (**Figure 2-4**). A combination of three high voltage generators (Gamma High Voltage Research) was employed with a high positive voltage (12 kV) to charge the steel capillary containing the polymer solution, a negative voltage (–7 kV) to charge the aluminum collector plate, and a slightly lower positive voltage (3 kV) to charge a steel mesh screen. The screen acted to control the area of fiber deposition onto the aluminum plate. Preliminary investigations without the control mesh found evidence of unwanted fiber deposition on the outer surfaces of the fume hood containing the apparatus. This set-up was

similar to the multiple field electrospinning apparatus constructed by Deitzel et al [99]. By adjusting the voltage magnitude charged to the control mesh, it was possible to minimize outside electrical disturbances as well as to electrospin thicker scaffolds more rapidly. The component spacing and applied voltages were optimized to provide controlled deposition of scaffolds up to 500 μm thick. PEUU was electrospun at various concentrations to assess the effect of polymer concentration on scaffold morphology. Deposited scaffolds were allowed to dry overnight at room temperature and then placed under vacuum for 48 h at 30°C.

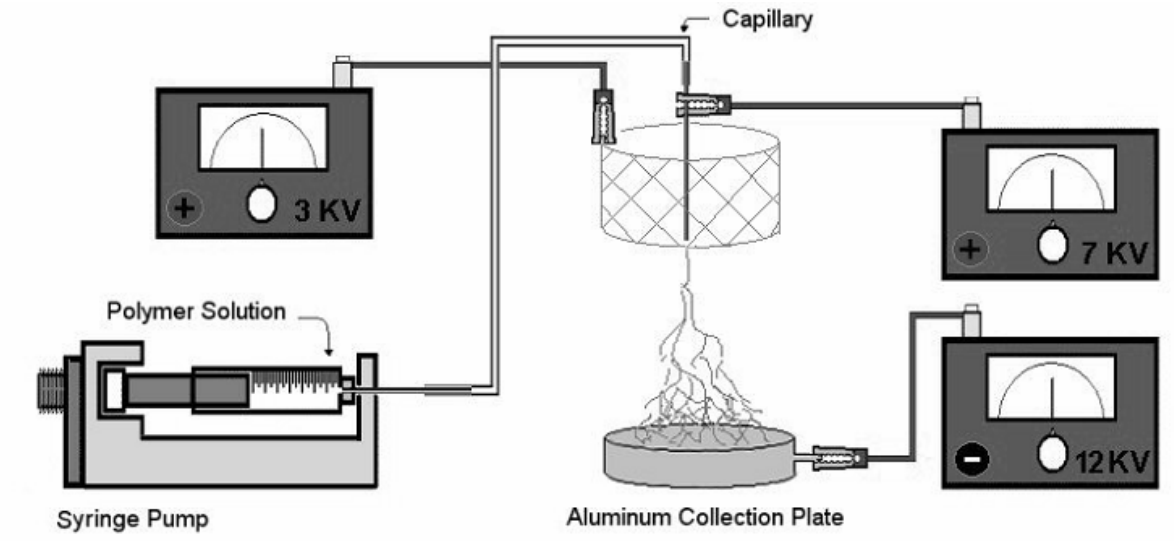


**Figure 2-4.** Electrospinning setup consisting of a syringe pump to feed polymer solution along with a combination of 3 high-voltage generators and a steel mesh screen to control the area of fiber deposition.

### 2.2.6 Scaffold characterization

Samples were sputter coated with Pd/Au and imaged with scanning electron microscopy (JEOL JSM6330F). Fiber diameter as a function of PEUU wt % in HFIP was quantified using digital image processing. Scaffold tensile mechanical properties were measured similar to those of the cast polymer films described above with an MTS Tytron™ 250 MicroForce Testing Workstation (10 mm/min crosshead speed) according to ASTM D638-98. Five samples were again tested at each condition studied.

### 2.2.7 Endothelial cell adhesion and growth

PEUU films were evaluated for their ability to support human umbilical vein endothelial cell (HUVEC, Cambrex, passage 5) adhesion and growth. Samples tested include PEUU, PEUU-$NH_2$ + BDI spacer, and PEUU with RGDS. PEUU 6-mm discs were punched and sterilized by 70% ethanol for 6 h followed by multiple PBS rinses, and exposure to ultraviolet (UV) light for 16h. PEUU discs were placed in wells of a 96-well TCPS plate. HUVECs were subcultured and seeded at a density of 20 x $10^4$ cells/mL in culture medium (Cambrex EGM-2). Cellular adhesion 1 day after cell seeding was evaluated using the MTT mitochondrial activity assay (n = 5 per sample studied) [100]. Data were normalized to tissue culture polystyrene (TCPS). HUVEC proliferation was evaluated over at 1, 3, and 5 days after seeding by MTT assay. Samples seeded were PEUU cast film, RGDS modified PEUU film, electrospun PEUU, and TCPS control.

### 2.2.8 Statistics

Results are displayed as the mean ± standard deviation. Pearson's correlation was used to evaluate the linearity of the fiber diameter versus concentration plot. One-way ANOVA testing was carried out for quantification of surface modification by RGDS, cell adhesion, and mechanical properties and using the Neuman-Keuls test for *post hoc* assessments of the differences between samples

## 2.3 RESULTS

### 2.3.1 Polymer characterization

#### 2.3.1.1 PEUU characterization

PEUU weight average molecular weight and number average molecular weight as determined by GPC were 228700 and 87600 respectively yielding a polydispersity index of 2.61. DSC results indicated a glass transition temperature of –54.6°C and soft segment melt temperature of 41.0°C. These results along with mechanical properties are summarized in **Table 2-1**. FTIR spectra of PEUU indicated urethane, urea and ester groups as well as the absence of any unreacted isocyanate peaks (at approximately 2267 $cm^{-1}$) or residual solvent **(Figure 2-5)**. PEUU was flexible and found to have a tensile strength of 27 ± 4 MPa and a breaking strain of 820 ± 70 % **(Figure 2-9)**.

#### 2.3.1.2 PEEUU characterization

NMR results for the PCL-*b*-PEG-*b*-PCL prepolymer indicated peaks characteristic of the four PEG protons nearest the PCL segment at 4.2 ppm (integration = 1). A value was found for the two PCL protons representative of each PCL segment of 1.6 ppm (integration = 8.7). Since the molecular weight of PEG was known to be 600, the ratio of the integration values for PCL to PEG for these peaks multiplied by two times the molecular weight of a PCL segment (*MW* = 114) yielded the PCL-*b*-PEG-*b*-PCL block lengths of 1000-600-1000 respectively.

PEEUU weight average molecular weight and number average molecular weight as determined by GPC were 119700 and 52000 respectively yielding a polydispersity index of 2.30. FTIR spectra of PEEUU indicated urethane, urea and ester groups as well as the absence of any unreacted isocyanate peaks (at approximately 2275 $cm^{-1}$) or residual solvent. DSC results indicated a glass transition temperature of –47.1°C and soft segment melt temperature of 41.0°C. PEEUU was flexible and found to have a tensile strength of 16 ± 1 MPa and a breaking strain of 580 ± 40 %. A summary of PEEUU properties is also displayed in **Table 2-1.**

**Table 2-1.** Physical property summary of PEUU and PEEUU.

| Polymer | Mw | Mn | Mw/Mn | Tg (C) | Tm (C) | Tensile Strength (MPa) | Breaking strain (%) |
|---|---|---|---|---|---|---|---|
| PEUU film | 228700 | 87600 | 2.61 | -54.6 | 41.0 | 27 ± 4 | 820 ± 70 |
| PEEUU film | 119,700 | 52000 | 2.3 | -47.1 | 41.0 | 16 ± 1 | 580 ± 40 |
| electrospun PEUU | - | - | - | - | - | 13 ± 4 | 220 ± 80 |
| electrospun PEEUU | - | - | - | - | - | 6.9 ± 2 | 190 ± 40 |
| TIPS PEUU | - | - | - | - | - | 1.5 ± 0.2 | 200 ± 60 |

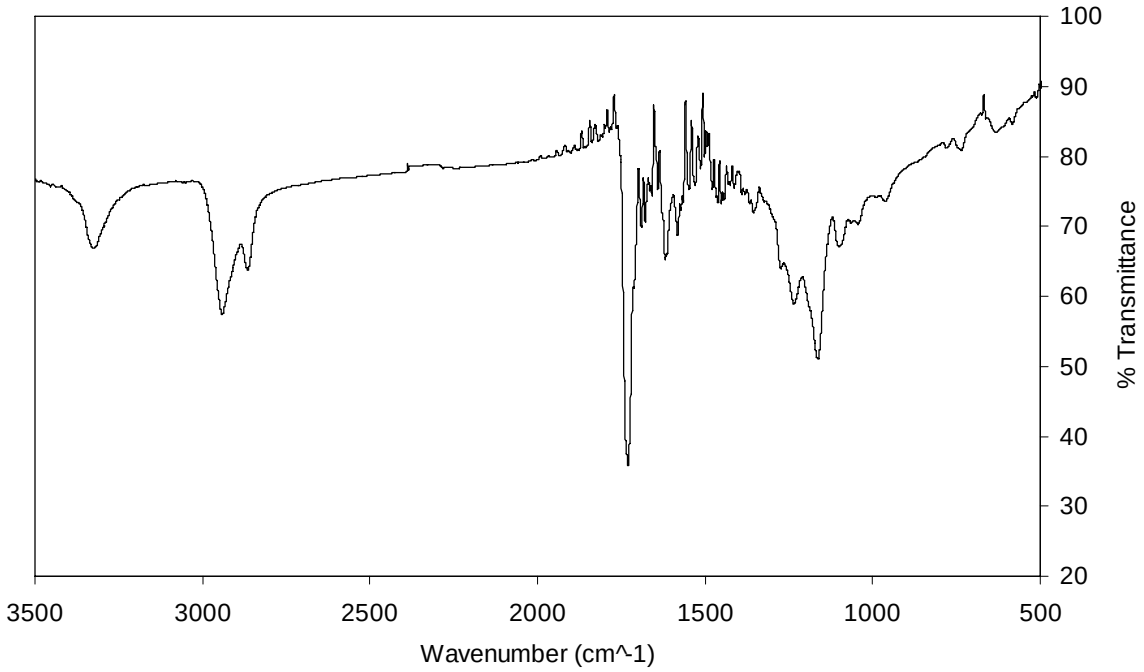


**Figure 2-5.** FTIR spectrum of PEUU. The spectrum for PEEUU exhibited similar functionalities.

### 2.3.2 Electrospinning and scaffold characterization

In order to fabricate scaffolds with continuous fibers of sub-micron dimensions, the feed polymer concentration was varied and electrospun PEUU morphology was investigated by SEM (**Figure 2-6**). At concentrations below 2%, a "beads on a string" morphology was observed. At polymer concentrations greater than 2%, continuous fibers were spun with diameters in the hundreds of nanometers. A trend of increasing fiber diameter with increasing polymer concentration was observed (**Figure 2-7**). Pearson's correlation for linearity revealed $r = 0.90$ at $p < 0.05$. Scaffolds possessed fiber diameters ranging from 100 nm to 2000 nm as a function of polymer concentration ranging from 1% to 10%.

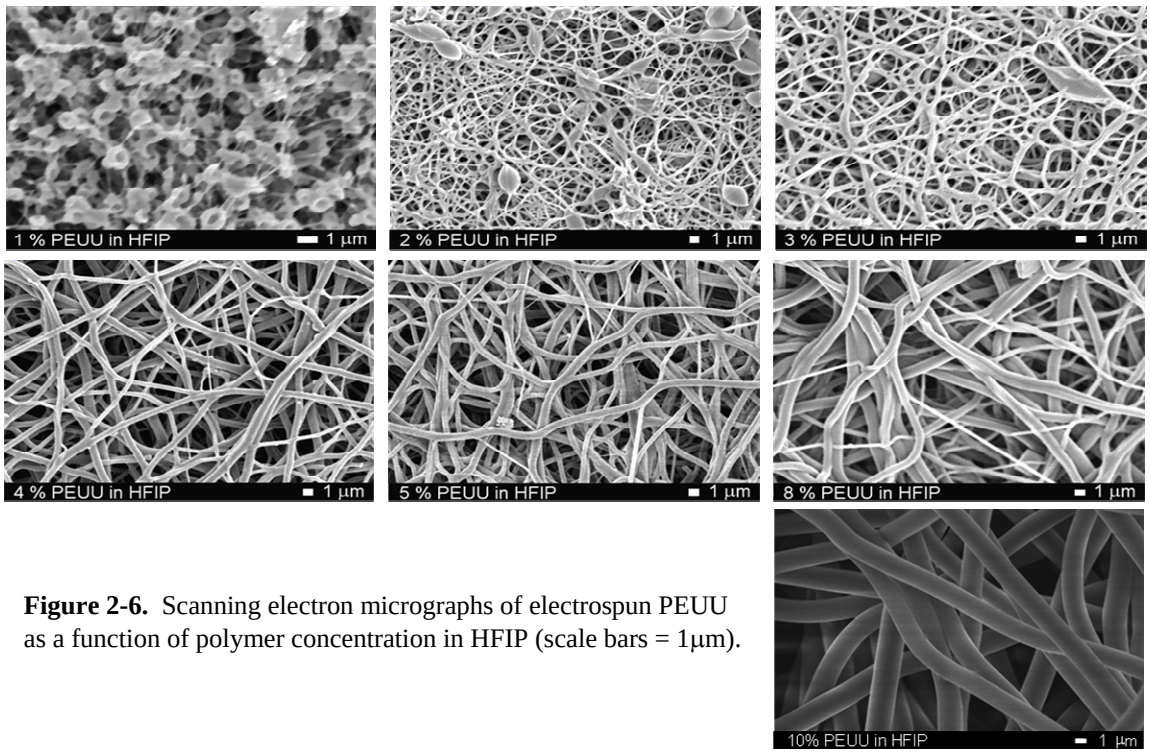


**Figure 2-6.** Scanning electron micrographs of electrospun PEUU as a function of polymer concentration in HFIP (scale bars = 1µm).

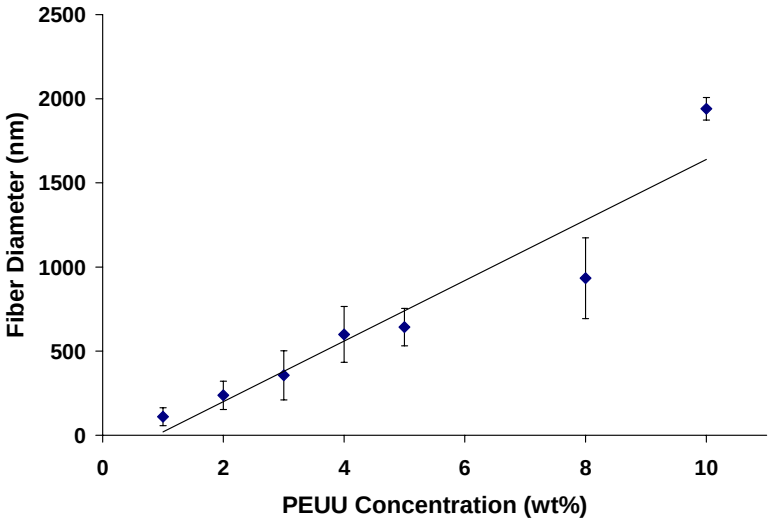


**Figure 2-7.** Electrospun fiber diameter as a function of PEUU concentration in the feed solution ($r$ = 0.90; $p$ < 0.05).

PEEUU was processed at 8 wt% in HFIP to produce continuous electrospun fibers. The presence of sparse beads was observed in lower magnification SEMs **(Figure 2-8 (a))**. More tendency for bead formation can result from the lower molecular weight PEEUU relative to PEUU. Fibers displayed a more gelled and tortuous appearance under qualitative investigation. One can observe SEMs of electrospun PEEUU in **Figure 2-8**.

Mechanical properties of electrospun scaffolds are summarized in **Table 2-1.** Electrospun PEUU had a tensile strength of 13 ± 4 MPa and a breaking strain of 220 ± 80%. Electrospun PEUU had a tensile strength of 6.9 ± 2 MPa and a breaking strain of 190 ± 40%. **Figure 2-9** displays typical stress-strain curves for PEUU film along with electrospun PEUU and thermally induced phase separation (TIPS) PEUU.

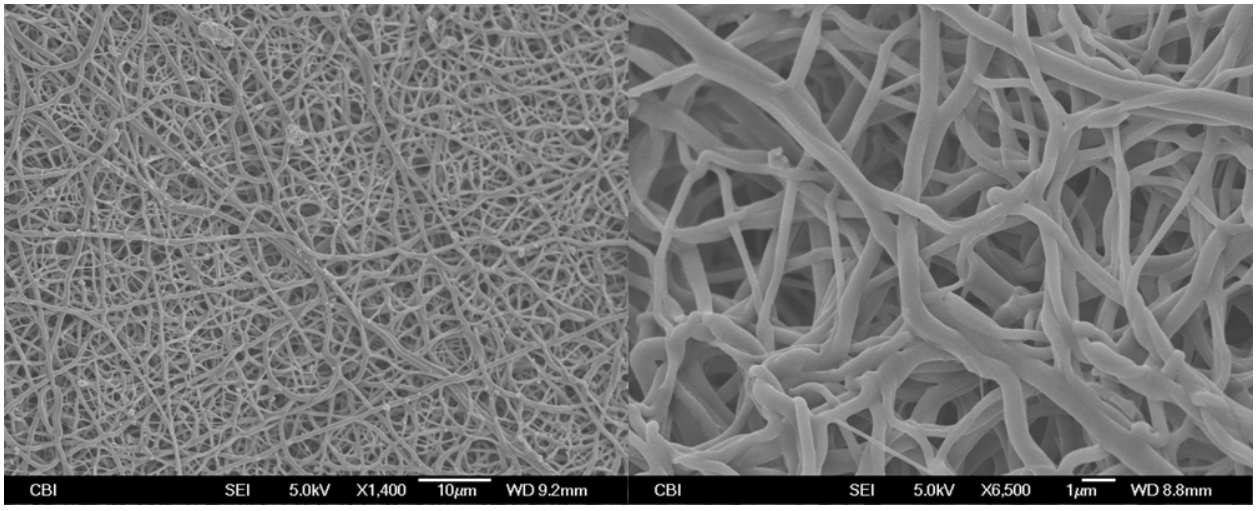


**Figure 2-8.** SEMs demonstrating fibrous scaffold morphology of electrospun PEEUU.

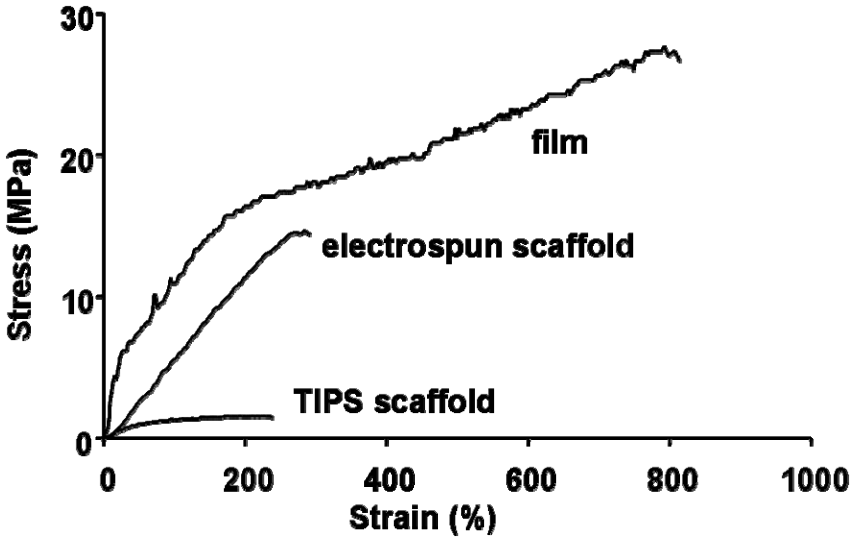


**Figure 2-9.** Typical stress-strain curves of PEUU cast film, electrospun PEUU scaffold, and TIPS PEUU scaffold.

### 2.3.3 Endothelial cell adhesion and proliferation

HUVEC adhesion 1 d after seeding onto cast PEUU films, PEUU films after RFGD and BDI treatment, and RGDS modified PEUU was evaluated and normalized to TCPS as illustrated in **Figure 2-10**. PEUU cast film was found to exhibit an adhesion of 73 ± 2 % TCPS. A significantly higher adhesion value of 124 ± 4% was observed for RGDS modified PEUU in comparison with all other samples ($p < 0.05$).

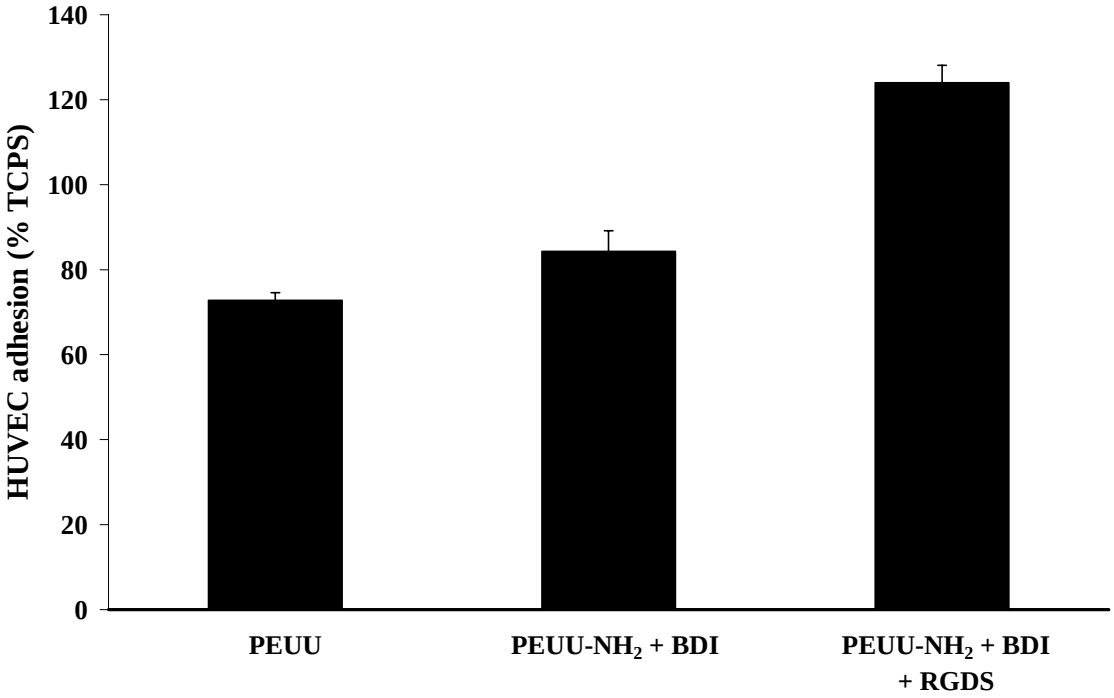


**Figure 2-10.** 24 h HUVEC adhesion to PEUU and RGDS modified PEUU relative to TCPS.

HUVEC proliferation on PEUU, RGDS modified PEUU, electrospun PEUU and TCPS was evaluated over 5 days **(Figure 2-11)**. No significant difference was observed between cell numbers on TCPS or PEUU at day 5 of culture. RGDS modified PEUU demonstrated significantly higher cell numbers than TCPS or PEUU at each timepoint ($p < 0.05$). For electrospun PEUU scaffolds, significantly higher cell numbers were observed at day 5 relative to cast PEUU films ($p < 0.05$). The nanofibrous scaffolds also exhibited similar values to RGDS modified surfaces.

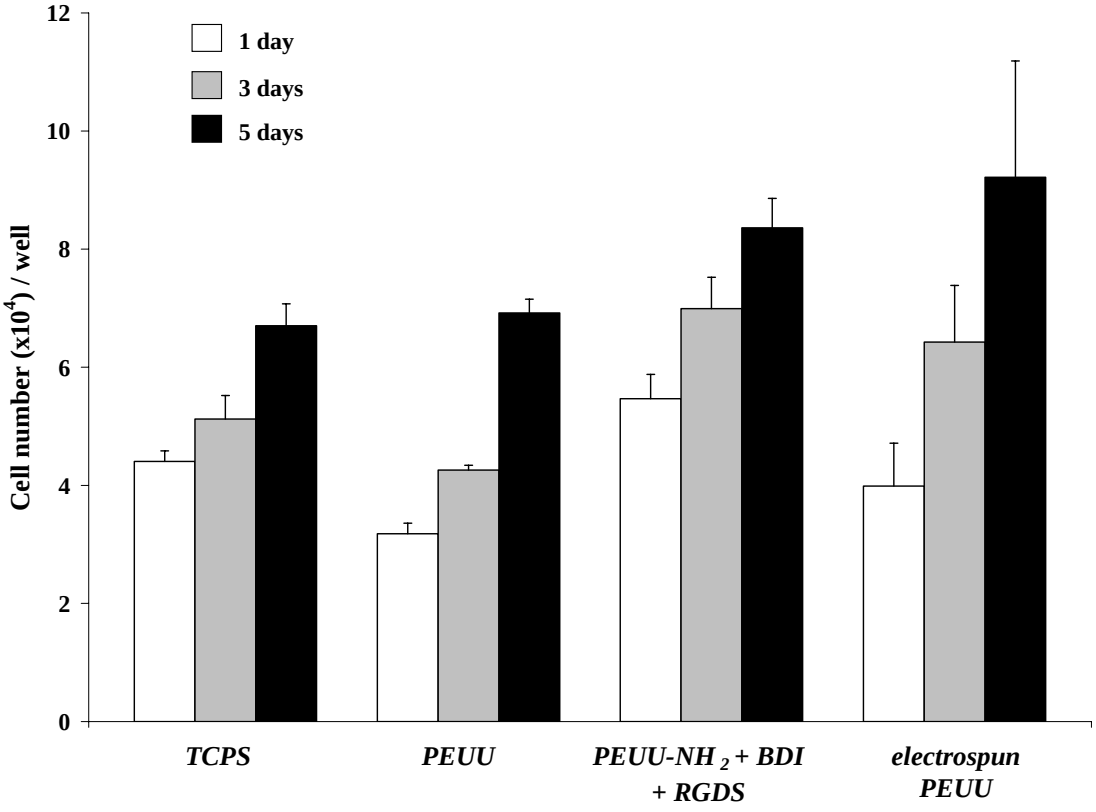


**Figure 2-11.** HUVEC growth on TCPS, PEUU cast film, RGDS modified cast PEUU film and electrospun PEUU.

## 2.4 DISCUSSION

Biodegradable polyesters have been the most commonly investigated materials in developing tissue engineering scaffolds. For example, poly(glycolic acid) (PGA), poly(lactic acid) (PLA), and their copolymers (PLGA), are relatively stiff, non-elastic materials and are not ideally suited for engineering of soft flexible tissues under a mechanically demanding environment such as cardiovascular tissue, urological, and gastrointestinal tissue. Mechanical signals are thought necessary to develop cell alignment leading to tissue structure exhibiting correct biomechanical properties and function [10, 11]. Kim et al. showed that cyclic straining upregulated extracellular matrix production in developing smooth muscle tissue resulting in increased mechanical properties of the tissue constructs [12]. They also demonstrated that for longer culture periods under cyclic strain, a more elastic scaffold than PLLA-bonded PGA fibers would be necessary [13]. Reports have also shown that mechanical stimulation can lead to increased matrix production and mechanical strength in tissue engineered cardiac muscle grafts [101]. In addition, tissue engineered blood vessels cultured under pulsatile flow were found to more closely resemble native vessels in both histological appearance and function than vessels cultured under non-pulsed conditions [9].

Electrospinning offers a means to generate polymeric fibers with diameters in the 100-1000 nm range. This technique, first patented in the 1930's by Formhals [86], has seen recent interest in the tissue engineering community and for other applications. Several groups have reported on the electrospinning of PLGA [83, 96]. Annis et al. have electrospun non-biodegradable polyurethane for vascular graft applications [91] and Demir et al. investigated the results of various solution properties on electrospinning non-biodegradable polyurethane [92]. Furthermore, investigators have demonstrated spinning of natural materials such as collagen [88,

89, 102] or engineered proteins such as elastin [39, 40]. However, to date no groups have reported on the electrospinning of an elastomeric biodegradable polyurethane that might be suitable for biomedical applications.

Electrospinning is influenced by a multitude of process variables. In general, these variables can affect the resulting size and morphology of electrospun fibers [96, 99]. The most notable effect is the transition from electrospraying (i.e. spraying droplets of polymer in contrast to continuous nanofibers) to electrospinning. We observed a trend of increasing fiber diameter with increasing PEUU concentration. This trend was consistent with reports in the literature for other electrospun polymers such as poly(ethylene-co-vinyl alcohol) [103]. Preliminary investigations into the effect of capillary-to-collector distance on electrospun PEUU revealed lower fiber density at distances greater than 30 cm. Varying polymer feedrate did not appear to have a significant effect on fiber diameter or density. HFIP was found to be an ideal electrospinning solvent for PEUU because it evaporates rapidly, is non-flammable, and is applicable for solubilization of polyesters or proteins such as collagen. At PEUU concentrations less than 2 wt% and holding the voltage magnitudes constant (+12 kV to polymer solution, +3 kV to steel cage, and –7 kV to Al collector plate) more of a “beads on a string” morphology [104] was observed than continuous fibers. As the polymer concentration was increased above 2%, almost entirely continuous fibers were observed. This trend was thought to be due to the increasing polymer concentration resulting in increased solution viscosity and surface tension more appropriate for spinning continuous fibers.

While most porous scaffold processing techniques greatly reduce the mechanical properties relative to the bulk polymer, electrospinning retains a great deal of the strength and distensibility of the bulk PEUU. This trend is evident when comparing the stress-strain curves of

PEUU film and electrospun PEUU in **Figure 2-8**. The fibrillar microstructure of the electrospun scaffolds may be responsible for the robust mechanical properties observed. A single electrospun PEUU fiber would be expected to possess a higher tensile strength and lower breaking strain compared with the cast PEUU film due to potential molecular alignment. However, because the network of fibers is porous, the overall scaffold tensile strength would be expected to decrease in comparison to the PEUU film. The attractive distension observed in the scaffolds may result from randomly orientated fibers aligning themselves in the direction of stress. Distension would be expected to approximate the breaking strains measured once fibers are aligned.

Cell adhesion was only slightly less on PEUU cast film compared with TCPS. As a result of attachment of RGDS to the PEUU surface, higher cell adhesion could be achieved. Ninhydrin results further confirmed the presence of RGDS peptide with a 65% higher absorbance value observed for RGDS modified PEUU compared with PEUU treated with RFGD and BDI. Electrospun scaffolds also resulted in increased cell proliferation at 5 days. This result may be due to both the increased surface area of the nanofibrillar scaffold and a more favorable interaction of HUVECs on the surface that mimics actual ECM structure. These results indicate that electrospun PEUU warrants further investigation as a scaffold material for soft tissue engineering applications.

# 3.0 ELECTROSPINNING OF COLLAGEN BASED ELASTOMERIC SCAFFOLDS

## 3.1 INTRODUCTION

Since polymers can be electrospun from solution, the potential exists to blend biodegradable elastomers with proteins to introduce biomacromolecules into the resulting scaffold. Elastic scaffolds might be modified to incorporate biological activity from proteins found in the extracellular matrix such as growth factors, adhesive proteins, and structural proteins as well as to introduce enzyme sensitivity for remodeling. Collagen is an obvious candidate given its support of cell adhesion, relatively resilient conformation, and sensitivity to collagenase [25]. However, fabrication of scaffolds composed of collagen alone can lead to poor mechanical strength and the absence of the appropriate flexibility to undergo cyclic mechanical loading [43, 105]. By blending with a polyurethane, the combined biofunctionality of collagen with the mechanical properties of the polyurethane might result in an elastic matrix with potential to impact tissue engineering approaches to soft tissue replacement.

The objective was to process and characterize biodegradable, elastomeric scaffolds with sub-micron scale fibrillar morphologies using an electrospinning technique. A previously reported biodegradable and cytocompatible poly(ester urethane)urea (PEUU) from our laboratory based on polycaprolactone diol (PCL) and 1,4-diisocyanatobutane (BDI) was used as the base material [15]. Biofunctionality was introduced into scaffolds by blending the

polyurethane with type I collagen prior to electrospinning. The impact of polymer concentration in the spinning solution on scaffold morphology as well as scaffold collagen content and collagen structure preservation was determined using contact angle, FTIR, picrosirius red staining, and circular dichroism (CD) spectroscopy. Tensile mechanical properties were measured of both the cast polymer film and the scaffolds. Furthermore, human umbilical vein endothelial cell adhesion and smooth muscle cell adhesion were evaluated on the electrospun PEUU / collagen scaffolds.

## 3.2 METHODS

### 3.2.1 PEUU / collagen scaffold fabrication

PEUU was synthesized as reported previously (**Figure 2-1)** and cast into transparent films [15]. PEUU and type I acid soluble bovine collagen (Sigma) (at 0, 2.5, 5, 10, 20, 50, 60, 70, 80, and 90 final wt% of collagen) were blended in HFIP at 6 wt.% under mechanical stirring at 25°C. The polymer / protein solution was electrospun as described previously and illustrated in **Figure 2-4**. Briefly, solution was fed by syringe pump at 1.0 mL/hr and electrospun over a distance of 13 cm with voltages of +12 kV, +3kV, and -7kV applied to the nozzle, screen, and target respectively. The component spacing and applied voltages were optimized to provide controlled deposition of scaffolds up to 500 μm thick. Deposited scaffolds were allowed to dry overnight at room temperature and then placed under vacuum for 24 h.

### 3.2.2 Scaffold characterization

Samples were sputter coated with Pd/Au and imaged with SEM. Water contact angles (n = 5) were measured by the sessile drop technique using a VCA2000 device (AST Products). For picrosirius red staining [106], samples were cryosectioned and fixed on glass slides with 2% formaldehyde for 20 min. Samples were rinsed with water and then picrosirius red solution (0.3 g Sirius red F3B and 500 mL saturated aqueous picric acid) was added for 1 h. Next, the samples were washed twice with acetic acid solution, dehydrated with ethanol (50%, 70%, 90%, and 100%) and mounted. To quantify absorbance, 6 mm diameter scaffold discs were weighed and stained with picrosirius red as above. Next, stained scaffolds were incubated in 0.1 N NaOH at 37°C for 30 min to transfer the stain from the scaffold to solution. The absorbance of the solutions was read at 540 nm and normalized by dividing by scaffold mass.

CD spectroscopy was performed to evaluate the preservation of collagen secondary structure in the electrospun biohybrid scaffolds. Collagen was removed from the scaffolds by incubation in 0.1M acetic acid for 48 h at 25°C and then lyophilizing the resulting solutions. CD spectra were run on an Aviv 62A DS Circular Dichroism Spectrometer using 1 mg/mL collagen solutions in 0.1M acetic acid at 25°C. Wavelength scans (n = 3) were performed from 280-185 nm sampling every 1 nm with a 1 s averaging time. Scaffold uniaxial mechanical properties were measured similar to those of the cast polymer films described previously.

In order to quantify PEUU / collagen scaffold degradation, dry films and scaffolds were weighed and immersed in 15 mL of PBS (pH = 7.4) with or without collagenase (Clostridiopeptidase A, Sigma, 10 units/mL) and incubated at 37°C. Samples were removed at

the time points studied and vacuumed dried for 48 hours before weighing. Mass remaining was calculated as

$$\text{Mass remaining (\%)} = m_3/m_1 \times 100 \qquad (3\text{-}1)$$

where $m_1$ and $m_3$ are the masses of films before and after degradation, respectively.

### 3.2.3 Cell adhesion on PEUU/collagen scaffolds

PEUU/collagen samples were punched into 6-mm diameter discs and sterilized by immersion in 90% alcohol for 7 h, rinsed multiple times with PBS, and then placed in media in an incubator overnight. PEUU/collagen discs were placed in wells of a 96-well TCPS plate and human umbilical vein endothelial cells (HUVECs) were subcultured and seeded at a density of 20 x $10^4$ cells/mL in culture medium (Cambrex EGM-2). Cellular adhesion 1 day after cell seeding was evaluated using the MTT mitochondrial activity assay (n = 5 per sample studied) [100]. Data were normalized to tissue culture polystyrene (TCPS).

For smooth muscle culture, media consisted of Dulbecco's Modified Eagle Medium supplemented with 10% fetal bovine serum and 1% penicillin-streptomycin. Vascular smooth muscle cells isolated from a rat aorta [107] (SMCs, $8^{th}$ passage) were statically seeded on scaffolds at a density of 2 x $10^6$ cells/mL. Cellular adhesion 1 day after cell seeding was evaluated using the MTT mitochondrial activity assay (n = 5 per sample studied). Data were normalized to tissue culture polystyrene (TCPS). Samples were also rinsed with PBS, fixed with 2.5% glutaraldehyde and 1% osmium tetraoxide in PBS and subjected to graded ethanol dehydrations before being critical point dried, sputter-coated and then imaged by SEM to observe cellular morphology.

### 3.2.4 Statistics

Results are displayed as the mean ± standard deviation. Pearson's correlation was used to evaluate the linearity of the fiber diameter versus concentration plot. One-way ANOVA testing was carried out on contact angle results, picrosirius absorbance, mechanical properties and SMC adhesion using the Neuman-Keuls test for *post hoc* assessments of the differences between samples.

## 3.3 RESULTS

### 3.3.1 Scaffold characterization

Scanning electron micrographs revealed continuous fiber morphologies spun at all concentrations (0, 2.5, 5, 10, 20, 50, 60, 70, 80, 90% type I collagen) examined (**Figure 3-1**). Different diameters and morphologies were observed at the various PEUU/collagen ratios studied. Water in air contact angles were found to decrease as a function of % collagen blended with PEUU to give values ranging from 75° for PEUU alone to less than 40° with 50% collagen blended ($p < 0.05$) (**Figure 3-2**). FTIR of PEUU/collagen samples revealed peaks characteristic of type I collagen. For example, **Figure 3-3** shows the FTIR spectrum of PEUU alone subtracted from the spectrum for a 50/50 PEUU/collagen blend to yield a N-H stretch at 3310 $cm^{-1}$, an amide I band at 1650 $cm^{-1}$, and an amide II band at 1560 $cm^{-1}$. Picrosirius red stained PEUU/collagen electrospun scaffolds positive and polarization microscopy revealed the presence

of birefringence in the electrospun scaffolds containing collagen. In general, more prominent staining and birefringence were observed in samples containing at least 20% electrospun collagen. **Figure 3-4a** shows picrosirius staining of electrospun PEUU/collagen (50/50) and also compares birefringence in pre-processed acid soluble type I collagen (**Figure 3-4b**), an electrospun blend of 50/50 PEUU/collagen (**Figure 3-4c**), and electrospun collagen (**Figure 3-4d**). Stain leached from scaffolds after the picrosirius staining procedure displayed a trend of increasing absorbance with % type I collagen (**Figure 3-5**).

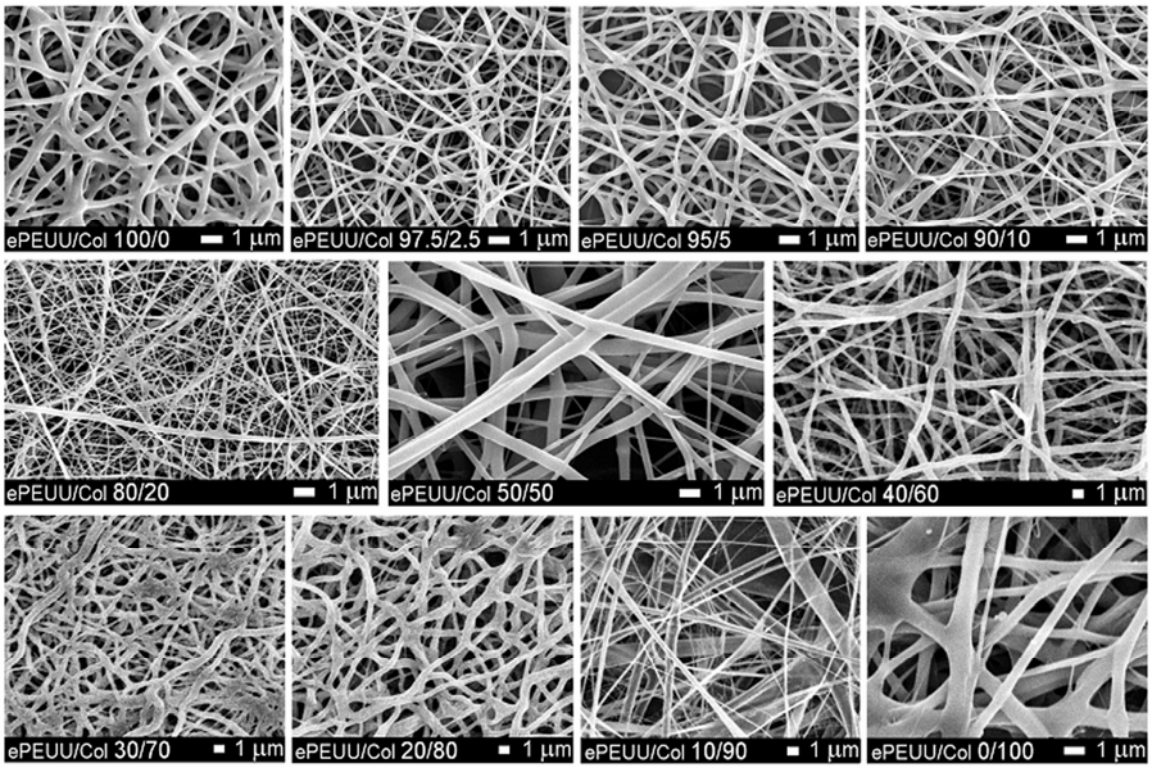


**Figure 3-1.** Scanning electron micrographs of electrospun scaffolds composed of varying ratios of PEUU and type I collagen.

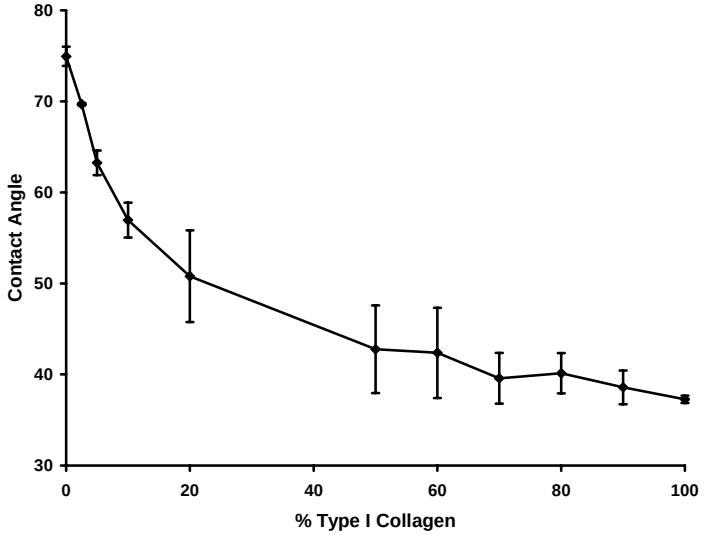


**Figure 3-2.** Water-in-air contact angle of PEUU/collagen blends as a function of collagen concentration.

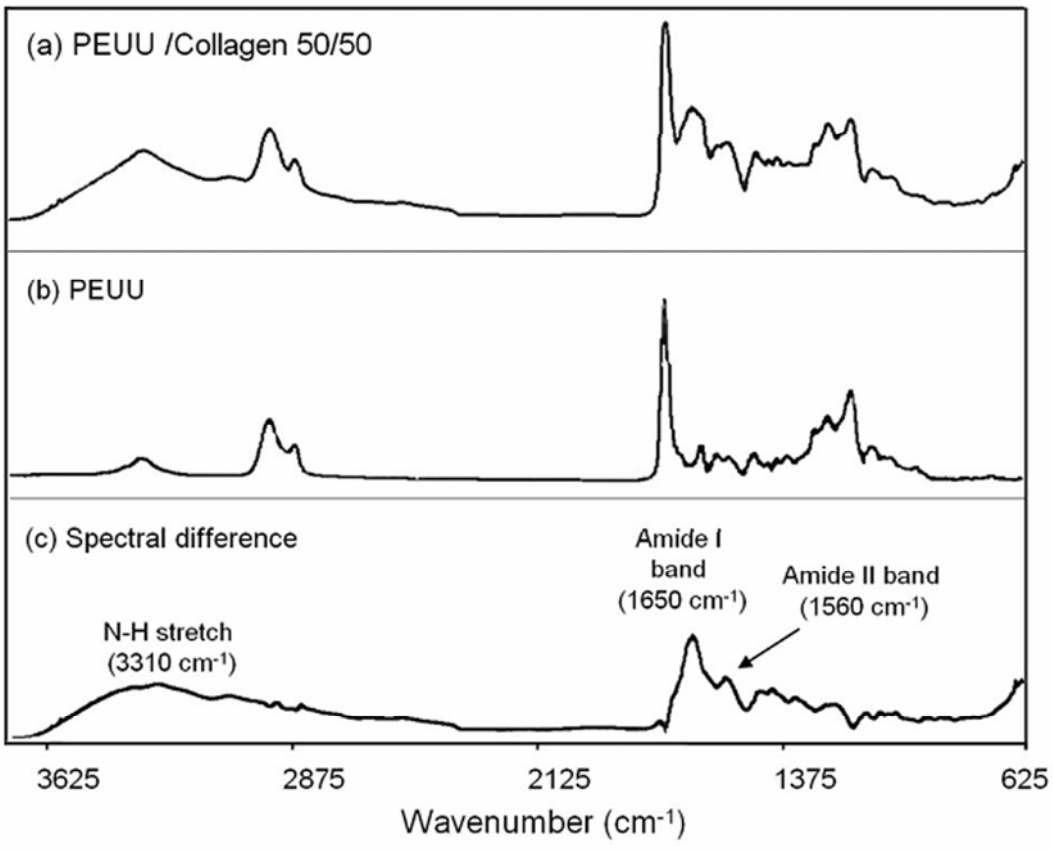


**Figure 3-3.** FTIR spectra of (a) blend of 50/50 PEUU/collagen, (b) PEUU, and (c) difference spectrum resulting from subtraction of (b) from (a). Peaks attributable to collagen are noted in the difference spectrum.

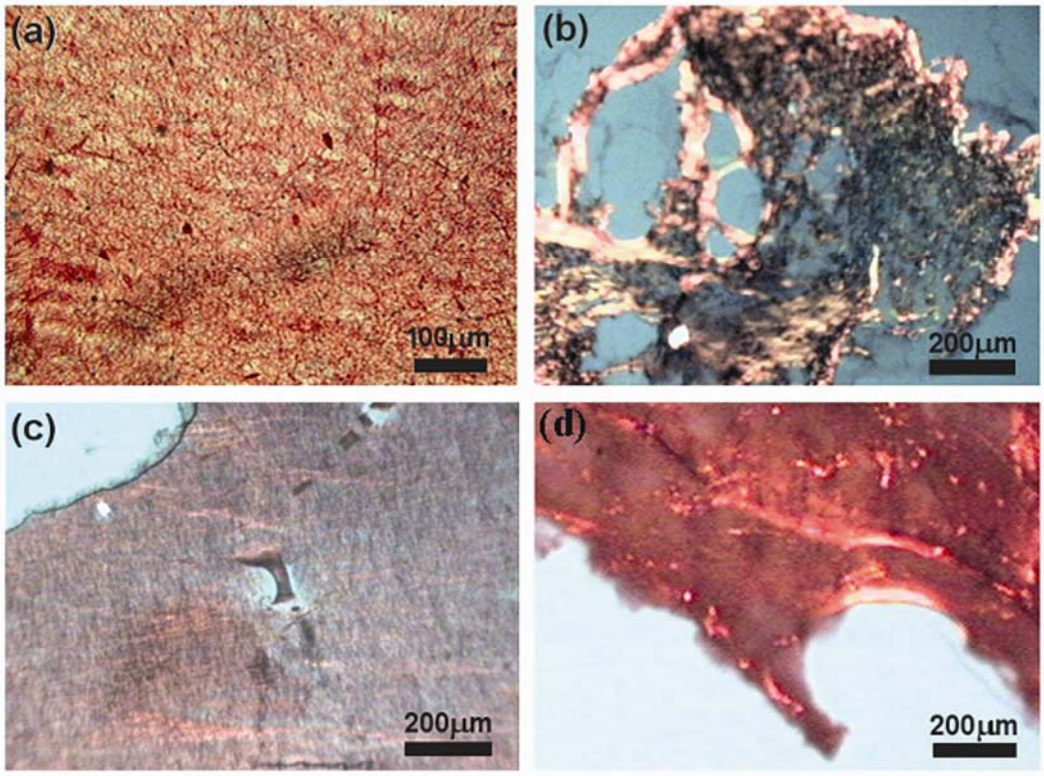


**Figure 3-4.** Picrosirius red staining of electrospun PEUU/collagen blends: (a) optical micrograph of 50/50 PEUU/collagen, polarized light micrographs of (b) collagen (c) 50/50 electrospun PEUU/collagen, and (d) 0/100 electrospun PEUU/collagen.

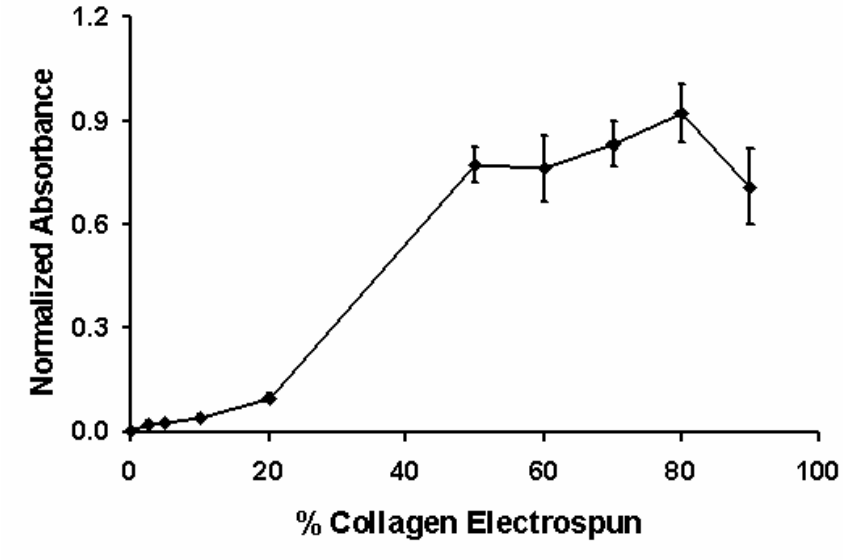


**Figure 3-5.** Absorbance normalized to scaffold mass as a function of collagen concentration for picrosirius red stain removed by NaOH.

### 3.3.2 Circular dichroism spectroscopy

CD spectra of collagen removed from the electrospun scaffolds into 0.1M acetic acid were compared with spectra of type I collagen before processing and also type I collagen that was thermally denatured at 50°C. Representative spectra of electrospun PEUU/collagen samples studied are displayed in **Figure 3-6**. **Table 3-1** shows the difference in ellipticities between electrospun collagen samples relative to the collagen control at different blending ratios. The spectrum of the collagen control exhibits a maxima peak at 221 nm and a minima peak of 197 nm. Upon thermal denaturation at 50°C, the collagen spectrum exhibited loss of the peak at 221 nm along with a difference in ellipticity of 54.36 mdeg from the non-denatured collagen. In general, a trend of decreasing difference in ellipticity between the collagen control was exhibited at increasing collagen ratios. This trend indicated more triple helix retention in electrospun samples containing 50% or more collagen. Electrospun samples containing 2.5%, 5%, 10%, and 20% collagen did not show a peak at 221 nm and had differences in minima ellipticity greater than 66 mdeg. Samples containing 50% and 60% collagen gave small or no peaks at 221 nm with minima ellipticity differences from the collagen control at 45.23 mdeg and 33.26 mdeg respectively. Electrospun samples containing 70-100% collagen exhibited peaks at 221 nm and minima ellipticity differences at 10.33 mdeg or less indicating greater collagen helix retention. All electrospun samples including electrospun collagen alone possessed some secondary structure modification as a result of the electrospinning process and exposure to the HFIP solvent. CD signal error consisted of a few hundredths of a mdeg for all samples except near 185 nm and is not shown for sake of clarity.

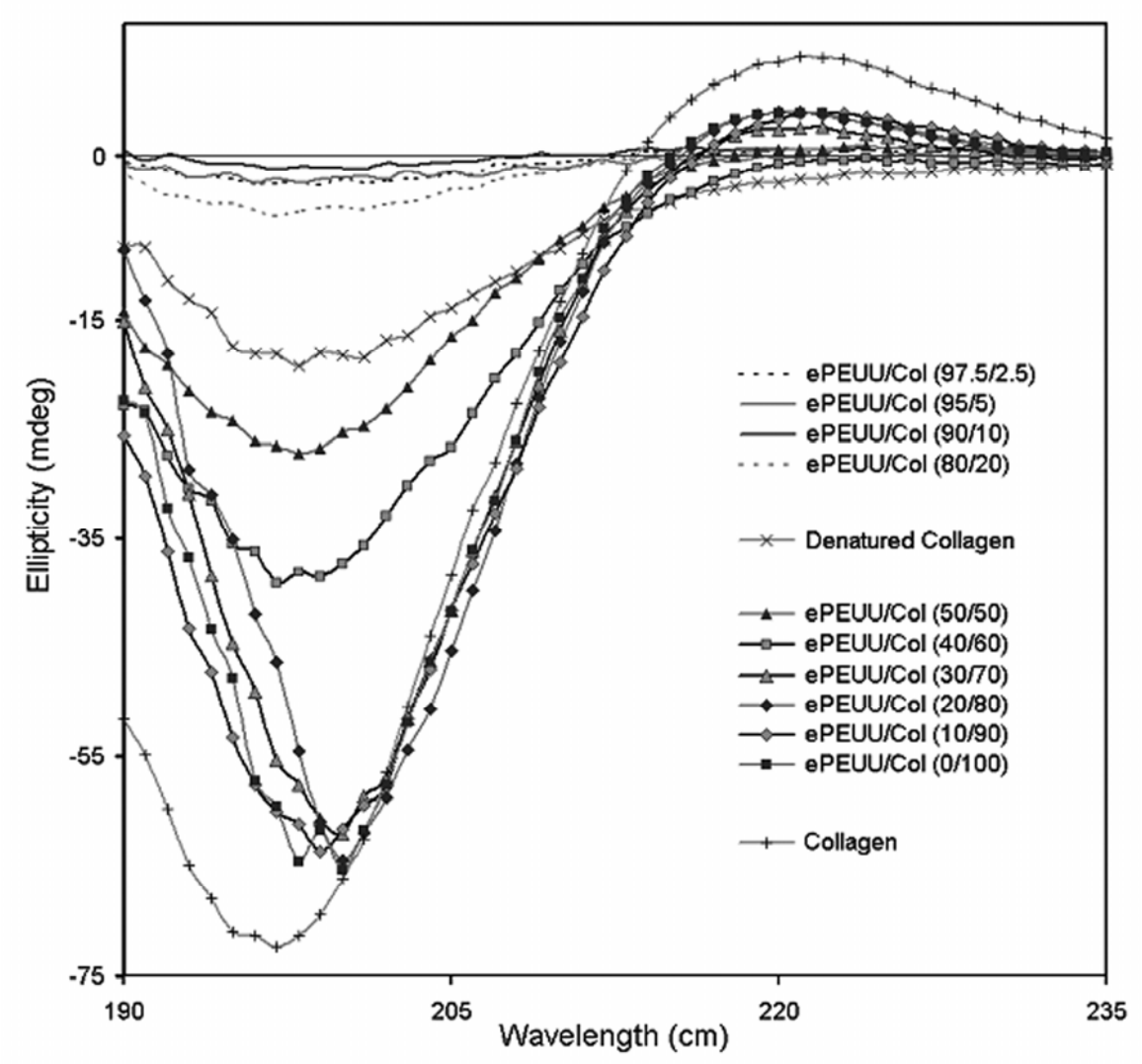


**Figure 3-6.** CD spectra of 1mg/mL collagen removed from scaffolds in 0.1*M* acetic acid compared with spectra of type I collagen control and thermally denatured type I collagen.

**Table 3-1.** Comparison of ellipticities of ππ* (minima) and nπ* (maxima) transitions between type I collagen control and collagen processed into ePEUU/Col scaffolds.

| Sample | Ellipticity (mdeg) ππ* | Collagen Ellipticity Difference (mdeg) ππ* | Ellipticity (mdeg) nπ* | Collagen Ellipticity Difference (mdeg) nπ* |
|---|---|---|---|---|
| Collagen | -72.43 | - | 9.02 | - |
| Denatured Collagen | -18.07 | 54.36 | -2.18 | 11.20 |
| ePEUU/Col (0/100) | -65.29 | 7.14 | 3.90 | 5.12 |
| ePEUU/Col (10/90) | -63.62 | 8.81 | 3.82 | 5.20 |
| ePEUU/Col (20/80) | -64.46 | 7.97 | 3.96 | 5.06 |
| ePEUU/Col (30/70) | -62.10 | 10.33 | 2.54 | 6.48 |
| ePEUU/Col (40/60) | -39.17 | 33.26 | -0.55 | 9.57 |
| ePEUU/Col (50/50) | -27.20 | 45.23 | 0.91 | 8.11 |
| ePEUU/Col (80/20) | -5.62 | 66.81 | 0.80 | 8.22 |
| ePEUU/Col (90/10) | -1.32 | 71.11 | 0.60 | 8.42 |
| ePEUU/Col (95/5) | -2.54 | 69.89 | -0.54 | 9.56 |
| ePEUU/Col (97.5/2.5) | -2.75 | 69.68 | 0.48 | 8.54 |
| ePEUU/Col (100/0) | - | - | - | - |

e = electrospun scaffold; Col = collagen

### 3.3.3 Mechanical properties

Mechanical properties of electrospun biohybrid scaffolds are summarized in **Table 3-2**. Tensile strengths ranged from 2 MPa to 13 MPa and breaking strains from 160% to 280%. Electrospun PEUU had a tensile strength of 13 ± 4 MPa and a breaking strain of 220 ± 80%. **Figure 3-7** displays typical stress-strain curves for PEUU film along with electrospun PEUU and electrospun PEUU/collagen (50/50) scaffolds. Incorporation of collagen lead to a significant decrease in tensile strength for samples containing 2.5%, 10%, 50%, 60%, 70%, 80%, and 90% collagen ($p < 0.05$) as well as reductions in initial and 100% modulus for samples containing 5%,

10%, 20%, 50%, 60%, 70%, 80%, and 90% collagen ($p < 0.05$). No significant correlation between increasing collagen content and breaking strain were observed for electrospun scaffolds.

**Table 3-2.** Tensile Properties of Electrospun Scaffolds Compared with Cast PEUU Film.

| Sample | Initial Modulus (MPa) | 100% Modulus (MPa) | Tensile Strength (MPa) | Breaking Strain (%) |
|---|---|---|---|---|
| PEUU(film) | 60 ± 10 | 2 ± 0.4 | 27 ± 4 | 820 ± 70 |
| e-PEUU | 8 ± 2 | 8 ± 2 | 13 ± 4 | 220 ± 80 |
| e-PEUU/Col (97.5/2.5) | 7 ± 1 | 7 ± 1 | 8 ± 2 | 160 ± 40 |
| e-PEUU/Col (95/5) | 6 ± 2 | 6 ± 2 | 10 ± 4 | 210 ± 70 |
| e-PEUU/Col (90/10) | 6 ± 2 | 4 ± 2 | 7 ± 3 | 160 ± 60 |
| e-PEUU/Col (80/20) | 9 ± 2 | 6 ± 3 | 11 ± 2 | 170 ± 40 |
| e-PEUU/Col (50/50) | 3 ± 1 | 3 ± 1 | 6 ± 1 | 240 ± 40 |
| e-PEUU/Col (40/60) | 1 ± 0.1 | 2 ± 0.3 | 3 ± 1 | 280 ± 10 |
| e-PEUU/Col (30/70) | 1 ± 0.3 | 1 ± 0.2 | 2 ± 1 | 240 ± 30 |
| e-PEUU/Col (20/80) | 1 ± 0.3 | 1 ± 0.1 | 3 ± 0.4 | 250 ± 30 |
| e-PEUU/Col (10/90) | 2 ± 0.3 | 1 ± 0.1 | 2 ± 0.1 | 270 ± 50 |

e = electrospun scaffold; Col = collagen

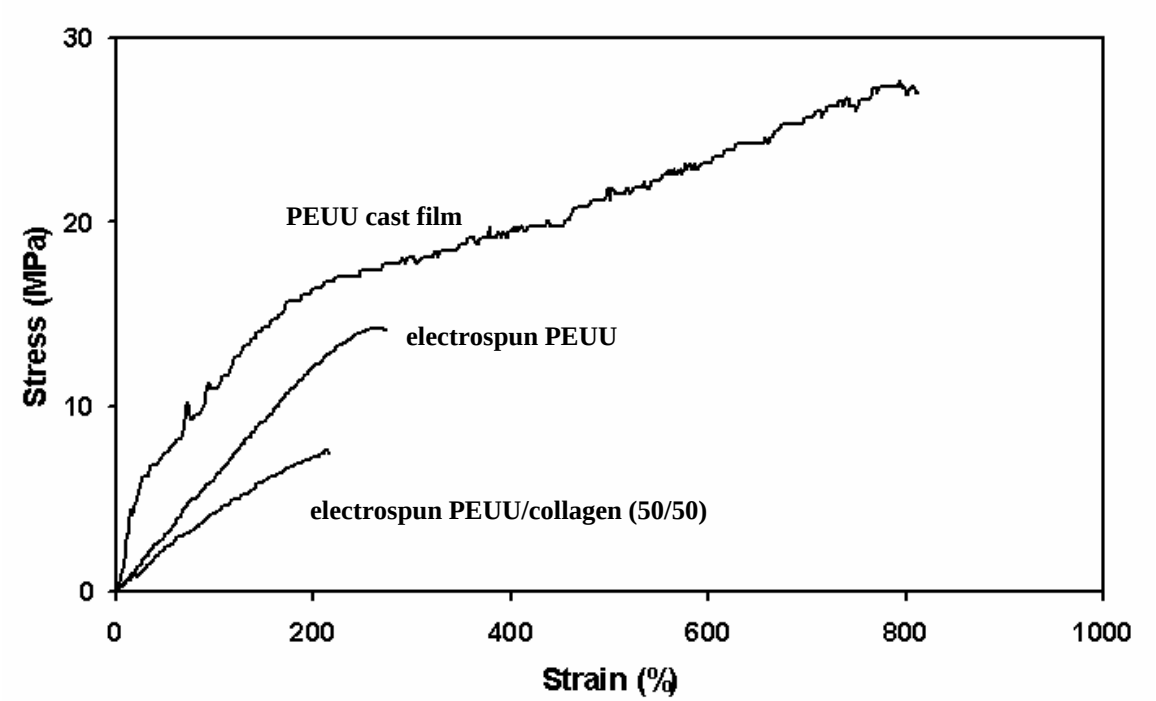


**Figure 3-7.** Typical stress-strain curves of PEUU cast film, electrospun PEUU scaffold, and electrospun PEUU/collagen (50/50).

### 3.3.4 Degradation

Results from *in vitro* degradation studies with electrospun biohybrid scaffolds in PBS with and without collagenase are presented in **Figure 3-8**. For electrospun PEUU, no significant difference was observed in the weight remaining between samples incubated with or without the enzyme collagenase at 8 wks and the mass remaining at that time for electrospun PEUU was not significantly different from that of the PEUU cast film (results not shown). For electrospun scaffolds containing type I collagen, there was decreased mass remaining at all concentrations as a result of incubation with collagenase ($p < 0.05$) with increasing sensitivity at higher collagen content. Furthermore, enzymatic degradation tended to increase with collagen content ($p < 0.05$ except in comparing 2.5% and 5%; or 5%, 10%, and 20% collagen samples). Electrospun PEUU exhibited mass loss of 5% without and 10% with collagenase. For samples containing 2.5, 5%, 10%, and 20% collagen relative to PEUU there was 94%, 94%, 92%, and 90% mass remaining after 8 weeks in PBS respectively. Addition of collagenase, reduced these values to 85%, 82%, 81%, and 75% respectively. Further, with samples containing 50% collagen relative to PEUU there was 44% mass remaining after collagenase incubation versus 57% mass remaining without enzyme. Results with 60% and higher collagen relative to PEUU demonstrated even lower mass remaining down to 6% and 3% for 90% collagen without or with collagenase. Results at 8 wks for all samples are summarized in **Table 3-3**.

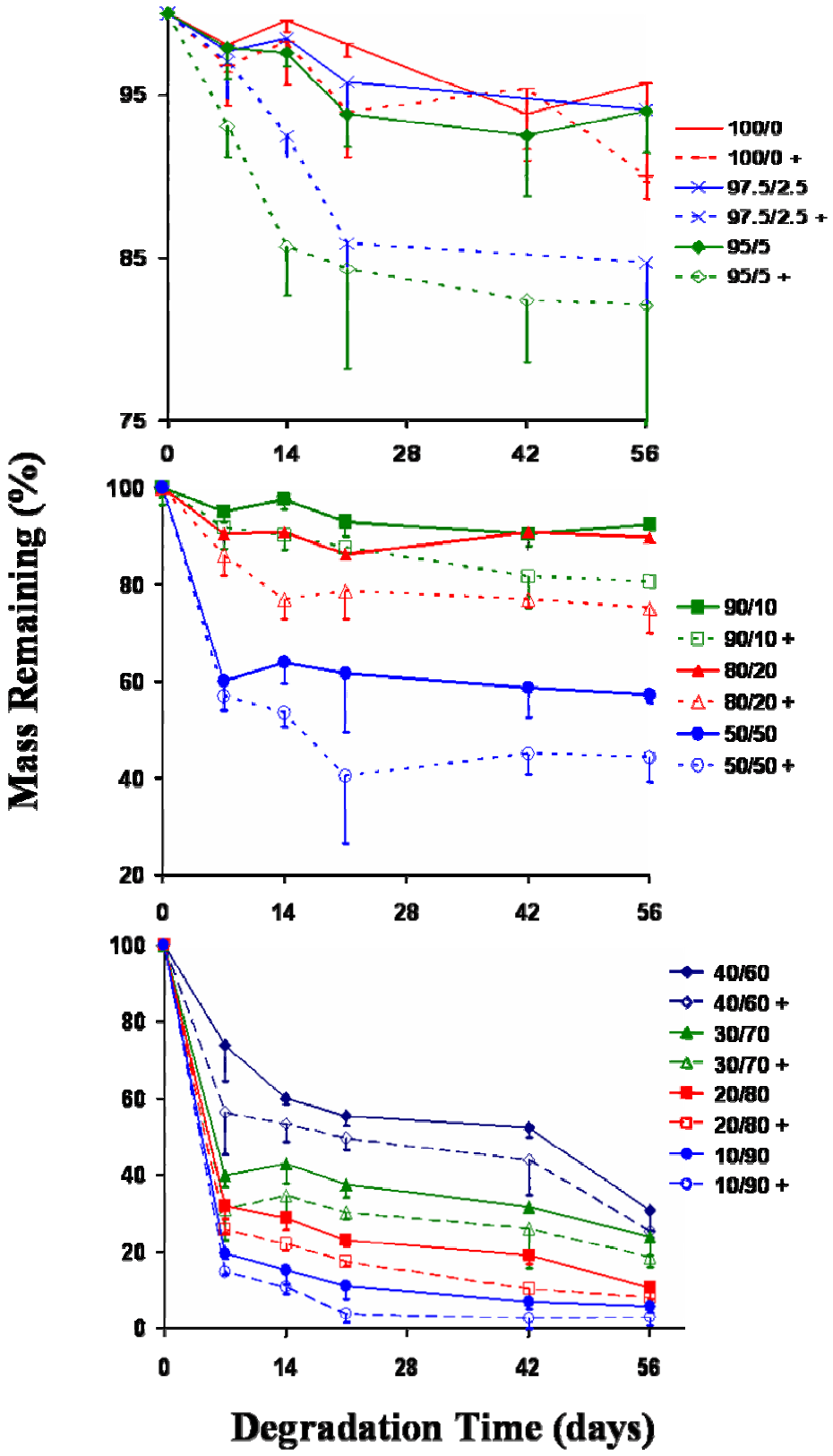


**Figure 3-8.** Mass remaining of electrospun biohybrid scaffolds as result of incubation time in buffer with or without collagenase. (% PEUU / % collagen; + indicates with collagenase)

**Table 3-3.** Summary of 8 wks *in vitro* degradation for electrospun PEUU/collagen.

| Sample | Mass Remaining at 8 wks (%) | Mass Remaining at 8 wks w/ collagenase (%) |
|---|---|---|
| e-PEUU | 94 ± 3 | 90 ± 2 |
| e-PEUU/Col (97.5/2.5) | 94 ± 3 | 85 ± 7 |
| e-PEUU/Col (95/5) | 94 ± 3 | 82 ± 8 |
| e-PEUU/Col (90/10) | 92 ± 3 | 81 ± 7 |
| e-PEUU/Col (80/20) | 90 ± 2 | 75 ± 5 |
| e-PEUU/Col (50/50) | 57 ± 2 | 44 ± 5 |
| e-PEUU/Col (40/60) | 31 ± 5 | 25 ± 2 |
| e-PEUU/Col (30/70) | 24 ± 5 | 19 ± 3 |
| e-PEUU/Col (20/80) | 11 ± 3 | 8 ± 1 |
| e-PEUU/Col (10/90) | 6 ± 1 | 3 ± 2 |

e = electrospun scaffold; Col = collagen

### 3.3.5 Cell adhesion on PEUU/collagen scaffolds

HUVECs cultured on PEUU electrospun scaffolds demonstrated cell adhesion at 122 ± 11 % of tissue culture polystyrene (TCPS). The presence of blended collagen demonstrated increased cell adhesion relative to TCPS for ($p < .05$) (**Figure 3-9)**. For 2.5% collagen added, cell adhesion was similar to electrospun PEUU at 120 ± 8 %. For 10% collagen added relative to PEUU, cell adhesion was significantly larger compared with both TCPS, cast PEUU films and electrospun PEUU alone ($p < 0.05$). HUVECs appeared attached and spread on electrospun PEUU surfaces with apparent nuclei visible as imaged by SEM in **Figure 3-10.**

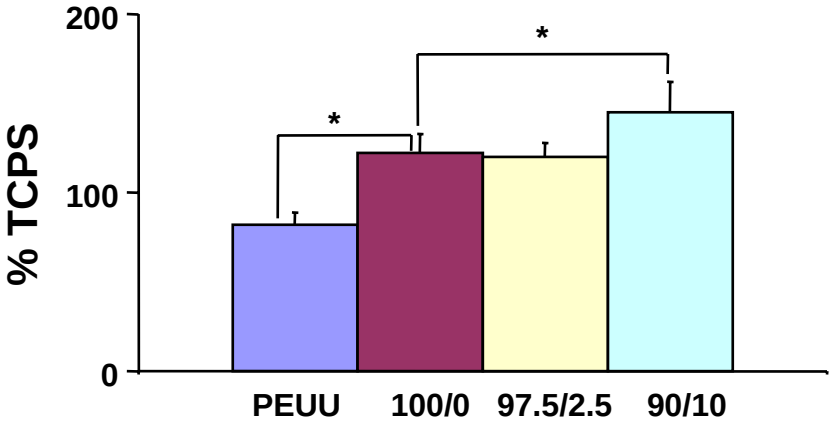


**Figure 3-9.** HUVEC adhesion on electrospun PEUU/collagen scaffolds compared with cast PEUU film. Data are normalized to TCPS. ($p < 0.05$)

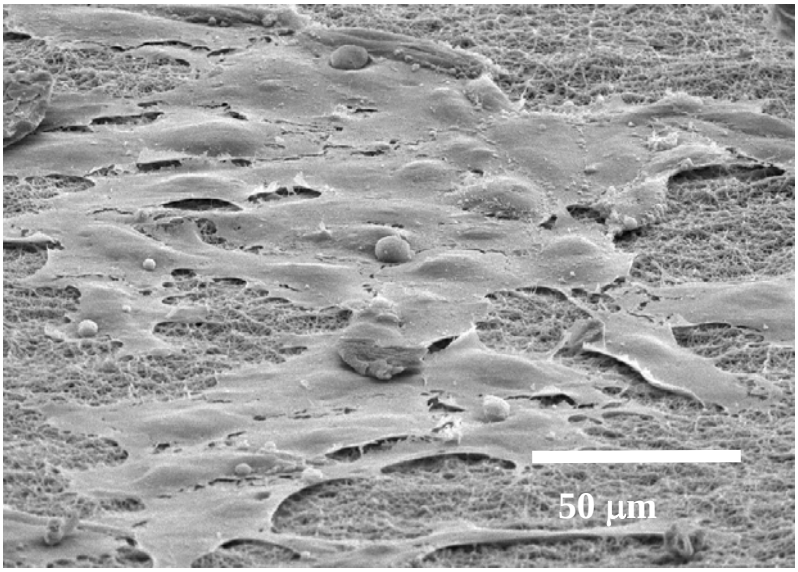


**Figure 3-10.** Representative HUVEC morphology on electrospun PEUU.

**Table 3-4** summarizes rat smooth muscle cell adhesion relative to TCPS after 1 day in culture on electrospun PEUU and electrospun PEUU/collagen scaffolds. Electrospun PEUU exhibited increased SMC adhesion as reflected by an MTT absorbance value 118% of TCPS. Collagen or gelatin presence led to significant increases in SMC adhesion onto electrospun PEUU/collagen for samples containing 5%, 10%, 20%, 50%, and 70% collagen relative to both electrospun PEUU alone and TCPS with values ranging 160-200% of TCPS ($p < 0.05$). Electron micrographs (not shown) qualitatively supported this result showing surfaces more confluent and with more spread cells for samples containing collagen versus PEUU alone. A typical image representing SMC morphology 1 day after cell seeding onto electrospun PEUU is shown in Figure 10. The cells appeared spread and attached to the electrospun scaffolds. No differences were observed in the cell morphologies between electrospun PEUU and the various electrospun PEUU/collagen samples aside from the relative amount of adherent cells. It is of note that SMC adhesion was greater even on samples containing primarily gelatin as indicated by CD results.

**Table 3-4**. SMC adhesion on biohybrid scaffolds.

| Sample | % TCPS |
|---|---|
| e-PEUU | 117.9 ± 12.8 |
| e-PEUU/Col (95/5)* | 174.3 ± 16.4 |
| e-PEUU/Col (90/10)* | 158.6 ± 8.8 |
| e-PEUU/Col (80/20)* | 175.5 ± 16.9 |
| e-PEUU/Col (50/50)* | 196.9 ± 63.0 |
| e-PEUU/Col (40/60) | 140.7 ± 18.2 |
| e-PEUU/Col (30/70)* | 161.0 ± 20.7 |
| e-PEUU/Col (20/80) | 123.5 ± 8.5 |
| e-PEUU/Col (10/90) | 107.2 ± 16.2 |

e = electrospun scaffold; Col = collagen; * ($p < 0.05$)

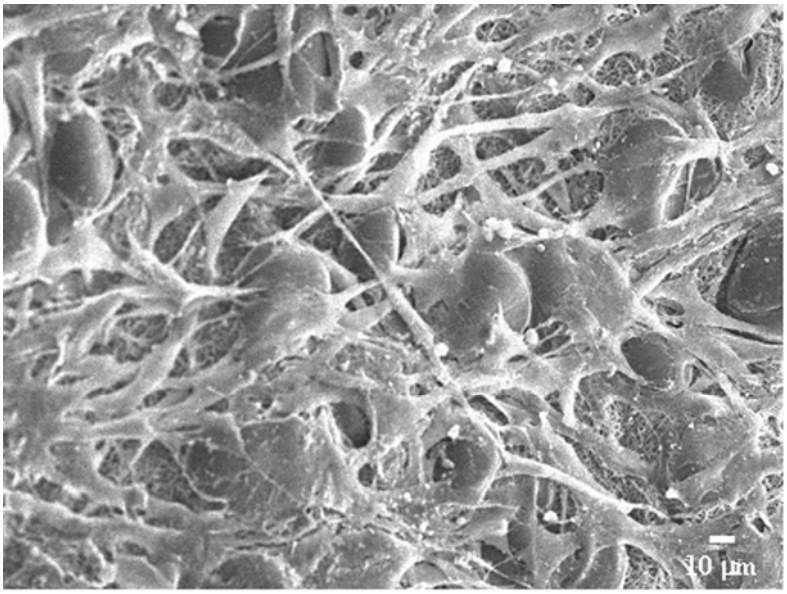


**Figure 3-11.** Representative SMC morphology on electrospun PEUU.

## 3.4 DISCUSSION

It was desired to incorporate bioactivity to develop scaffolds capable of increased cellular interactions as well as enzyme sensitive degradation. By incorporating these properties into polymer scaffolds, scaffolds that degrade at least in part, due to cellular infiltration and enzyme secretion might be produced. To accomplish this design we blended PEUU with type I bovine collagen in HFIP. It was previously shown by Matthews et al. that this type of collagen can be electrospun in HFIP and still retain its characteristic banding [89]. Continuous fibers of PEUU/collagen blends were spun at all of the polymer / protein ratios examined. To achieve this it was necessary to modify some electrospinning process variables to attain continuous fibers and avoid transitioning to electrospraying. The most common modification was a slight increase in voltage magnitude charged to the polymer solutions. For some of the higher collagen concentrations studied, it was necessary to increase the solution feedrate. This increase in feedrate may have contributed to the changes in fiber diameter qualitatively observed in **Figure 3-1** at these concentrations.

Water in air contact angles were found to decrease as a function of the amount of collagen blended with PEUU to give values ranging from 75° for PEUU alone to less than 40° with 50% collagen blended. To illustrate that collagen was present after treatment with HFIP, the FTIR spectrum of PEUU was subtracted from the spectrum for a PEUU/collagen (50/50) blend. The resulting spectrum yielded peaks characteristic of collagen as reported previously by other groups [108, 109]. The presence of collagen in the electrospun scaffolds was visualized by staining with picrosirius red. This stain, specific for collagen, reacts through its sulphonic acid groups with the basic groups of collagen. The extended dye molecule aligns parallel with

structurally intact collagen fibers resulting in increased birefringence under polarized light [106]. The scaffolds containing blended type I collagen stained positive for picrosirius red with increased absorbance as a function of increased collagen content ($p < 0.05$ for 20%, 50%, and 80%). The slight decrease of the 90% collagen sample may have been a result of the lower mechanical stability and slight shrinkage of the high collagen sample after staining and NaOH treatment. The picrosirius absorbance trend provides some insight into the morphology of the blends indicating the presence of collagen at the fiber surface. Samples at lower collagen contents such as 2.5%, 5%, and 10% collagen may have more PEUU present on the fiber surface compared with 20% and greater collagen samples. In addition to the trend of total picrosirius red binding, increased birefringence under polarized light was observed with samples containing at least 20% collagen, further suggesting the presence of non-denatured collagen in the scaffolds.

In processing a triple helical biomacromolecule such as collagen in solution it is important to characterize its structure retention in the resulting scaffold. Structure retention is important in providing maximal bioactivity to the scaffold in terms of its ability to influence cell adhesion or enzymatic degradation. Structural information may also provide insight into the mechanical property contribution from the electrospun collagen. Circular dichroism spectroscopy is a technique used to compare protein structure upon some pertubation. When circularly polarized light passes through a chiral protein solution it becomes elliptically polarized light. Ellipticity is measured versus wavelength and the various transitions observed give valuable information regarding the secondary structure of proteins. For example, CD can give a relative measure of collagen triple-helical content through comparison of the minima ($\pi\pi^*$ amide transition) at 197 nm and maxima ($n\pi^*$ transition) at 221 nm of the collagen spectrum [110]. From the CD results on collagen released from electrospun PEUU/collagen blends, all samples,

including electrospun collagen alone, showed signs of some secondary structure modification. This slight modification likely resulted from exposure to the HFIP solvent. These results are consistent with those reported by Doillon et al. that HFIP modified the secondary structure of collagen [111]. This report also found that cell growth was not impaired on post-HFIP treated collagen [111]. Samples with less than 50% collagen appeared to consist mostly of denatured collagen or gelatin and PEUU. This greater loss of triple helix structure was perhaps due to the presence of larger amounts of PEUU disrupting the collagen hydrogen bonding. In general, samples with higher collagen content (collagen > 50%) possessed greater evidence of triple helical retention with ellipticity difference values lower than that of denatured collagen, indicating at least partial collagen structure retention at these concentrations.

While most porous scaffold processing techniques greatly reduce the mechanical properties relative to the bulk polymer, electrospinning retains a great deal of the strength and distensibility of the bulk PEUU. In general, the incorporation of collagen led to slight decreases in mechanical properties such as tensile strength in the samples containing 2.5%, 10% and 50% collagen. Larger decreases in tensile strength were observed in samples containing 60% and greater collagen. The collagen molecules may act to reduce hydrogen bonding interactions between the polyurethane molecules thus eliminating some of the physical crosslinking that give polyurethanes their impressive mechanical properties. It was unexpected that the high collagen content samples would still be distensible with elongations of at least 240% since the electrospun collagen sample (without PEUU) was extremely brittle and could not be removed from the collection plate for testing.

In order to develop scaffolds that mimic the function of the native extracellular matrix, the incorporation of a biomacromolecule such as collagen would be ideal to guide and support

cell adhesion. The data show increased smooth muscle cell adhesion to samples containing collagen and gelatin. High adhesion values resulted even from samples containing primarily gelatin This trend may result simply from increased fibronectin from the culture medium binding to gelatin. It is well known that denatured collagen possesses greater binding affinity for fibronectin than structurally intact collagen because the binding sites on the interior of the triple-helical collagen may be inaccessible [25]. Further, another factor that may contribute to larger cell adhesion may be the greater mechanical stability of the samples with 50% or less collagen incorporated. Samples containing at least 50% collagen experienced some slight contraction with time after cell seeding. This effect was most prominent in the samples with 80% and 90% collagen.

The electrospun PEUU / collagen scaffolds degraded at rates that could be attractive for soft tissue engineering applications. By adjusting the collagen concentration relative to PEUU, it was possible to [in the presence of collagenase] accelerate the mass loss. Slowing of degradation rates after 2-3 weeks for most of the collagen blended scaffolds was observed. This may be explained by the loss of the exposed hydrophilic protein on the fiber surfaces, followed by the exposure of less rapidly degrading components (PEUU) at time points greater than 3 weeks. Of note, most scaffolds still retained greater than 100% elongation (results not shown) after the 8 week degradation period. Furthermore, this degradation study may not accurately portray the complex degradation process involved *in vivo*. The presence of complex enzyme systems along with the potential inflammatory response of a wound bed could lead to even faster degradation rates *in vivo*. Finally, these materials are designed to be cultured under cyclic loading, which would also be expected to result in increased degradation.

# 4.0 ELECTROSPINNING OF URINARY BLADDER MATRIX BASED ELASTOMERIC SCAFFOLDS

## 4.1 INTRODUCTION

There exists a need for biodegradable materials that possess bioactive components and also exhibit elastomeric mechanical properties similar to native tissue. These materials may be utilized in a large number of applications involving wound healing and tissue regeneration. Scaffolds derived from the extracellular matrix (ECM) of tissues have been successfully studied in a broad array of clinical arenas. These applications include constructive remodeling of the urinary tract, skin, vascular tissue and musculotendinous structures [41, 112-114]. However, they remain limited for some applications by their inherent mechanical properties. Synthetic scaffolds can be molecularly designed for desired mechanical properties, biodegradability, and processability, but are limited in terms of the breadth of bioactivity that can be prescribed. The objective was to create a hybrid matrix that imparted the mechanical properties of a biodegradable elastomer to ECM and that could be processed into a microporous scaffold format. Specifically, we combined a biodegradable poly(ester urethane) urea (PEUU) with porcine urinary bladder matrix (UBM) and utilized electrospinning to create elastomeric hybrid scaffolds that were characterized for their morphologies, tensile properties, biodegradation rates, and cytocompatibility.

## 4.2 METHODS

### 4.2.1 Electrospinning UBM/PEUU scaffolds

PEUU was synthesized from polycaprolactone diol and 1,4-diisocyanatobutane with chain extension by putrescine as previously reported [15]. PEUU transparent films were cast from a 3 wt% solution in DMF and dried under vacuum for 48 h. Urinary bladder matrix was obtained through collaboration with the laboratory of Professor S.F. Badylak of the University of Pittsburgh.

Briefly, porcine urinary bladders were harvested from pigs immediately following euthanasia. Connective tissue and adipose tissue were removed from the serosal surface and any residual urine was removed by multiple water rinses. The tunica serosa, tunica muscularis externa, the tunica submucosa, and most of the tunica muscularis interna were mechanically removed and the luminal urothelial cells of the basement membrane were dissociated by soaking in 1.0 N saline solution. After this step, all that remained was the basement membrane plus the subjacent tunica propria. This bi-laminate material was referred to as urinary bladder matrix (UBM). UBM sheets were disinfected for two hours on a shaker in a solution containing 0.1% (v/v) peracetic acid, 4% (v/v) ethanol, and 95.9% (v/v) sterile water. Peracetic acid residue was removed by washing twice with sterile PBS (pH=7.4) and twice with sterile water for 15 min each time. UBM sheets were subsequently lyophilized and powdered. One gram of lyophilized UBM powder and 100 mg pepsin were added to 100 mL of 0.01 M HCl under mechanical stirring for 48 h at room temperature. After pepsin digestion, the digest was aliquotted and

stored at -20°C until use or at 4°C after initial thawing. UBM digest was subsequently lyophilized before re-dissolving for electrospinning.

For electrospinning UBM was dissolved in hexafluoroisopropanol at various concentrations (6, 9, 10, 12, and 15 wt%). UBM and PEUU were also blended in hexafluoroisopropanol at 6 wt% (0, 25, 50, 75 solute wt% UBM) and then electrospun prior to electrospinning. A similar method to that described previously was utilized for electrospinning [115]. The electrospinning process consisted of feeding polymer solution at 1.0 mL/min through Teflon tubing to a stainless steel capillary located 15 cm from an aluminum disc. Samples were electrospun by charging the solution at 10 kV and the aluminum target at -10kV. The target was also attached to an x-y stage translating in a square pattern of 5 cm step distances to produce scaffolds of uniform thickness.

### 4.2.2 Electrospun UBM/PEUU scaffold characterization

Samples were sputter coated with Pd/Au and imaged with SEM to characterize scaffold fiber morphologies. Uniaxial tensile testing was completed according to ASTM D638-98. Rat vascular smooth muscle cells (SMCs) were seeded onto scaffolds at a density of 20 x $10^4$ cells/mL and cell adhesion was quantified 1 day after seeding using the MTT mitochondrial activity assay. For confocal microscopy, cell/scaffold constructs were fixed with 2% paraformaldehyde for 2h, permeabilized with 0.1% Triton x-100 for 45 min, and stained with draq-5 nuclear stain (Biostatus Ltd) and rhodamine phalloidin (Molecular Probes) for 30min. Imaging was done on a Leica TCS-SL laser scanning confocal microscope. Representative images were taken as individual scans or as a series of stacked images.

*In vitro s*caffold mass loss was measured in PBS at 37°C over 2 wks. Dry scaffolds were weighed and immersed in 15 mL of PBS (pH = 7.4) and incubated at 37°C. Samples were removed at the time points studied and lyophilized for 48 hours before weighing. Mass remaining was calculated as

$$\text{Mass remaining (\%)} = m_3/m_1 \times 100 \quad (4\text{-}1)$$

where $m_1$ and $m_3$ are the masses of films before and after degradation, respectively.

## 4.3 RESULTS AND DISCUSSION

### 4.3.1 Electrospun UBM scaffolds

The process of electrospinning occurs when a polymer solution is charged with a high voltage that generates an electrical force that can extrude a polymer jet. This jet then breaks down to sub-micron scale fibers through a complicated bending and whipping process. During the process, solvent is evaporated and the dry fibers can be collected on a grounded or oppositely charged conductive surface in the form of a non-woven fiber scaffold. The resulting nano-fibrous scaffold morphology mimics actual native ECM architecture.

In this study, it was first evaluated whether it was possible to electrospin urinary bladder matrix digest alone using an appropriate electrospinning solvent such as HFIP. Solution concentration is an important variable when electrospinning so that we first investigated the effect of UBM concentration on resulting scaffold morphologies. UBM was dissolved in HFIP at various concentrations (6, 9, 10, 12, 15 wt%) and electrospun. At a concentration of 6 wt%,

electrospinning of continuous fibers was not achieved and instead electrospraying of UBM droplets occurred. Electrospinning of fibers was possible at concentrations of 9wt% and greater but UBM agglomerates were present at all concentrations. Electron micrographs demonstrating the UBM electrospun scaffold microstructure are shown in **Figure 4-1**. In addition, electrospun UBM was very water soluble and a fragile, brittle material not ideally suited for use as a load bearing scaffold.

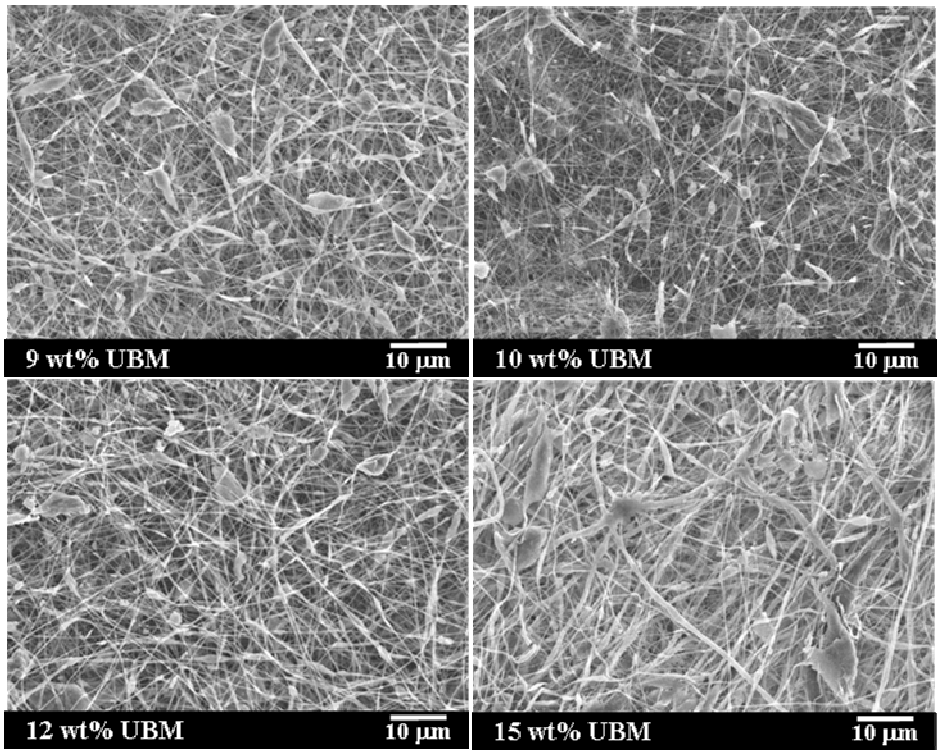


**Figure 4-1.** Morphologies of electrospun UBM at 9 wt% (a), 10 wt% (b), 12 wt% (c), and 15 wt% (d) by SEM.

### 4.3.2 Electrospun UBM/PEUU scaffolds

To improve on the limited mechanical properties of electrospun UBM alone, PEUU was blended into the spinning solution. With UBM/PEUU blends, continuous fibers could be fabricated at concentrations as low as 6 wt%. Continuous artifact free fibers were observed as UBM/PEUU ratios of 25/75, 50/50, and 75/25 as can be observed in **Figure 4-2.**

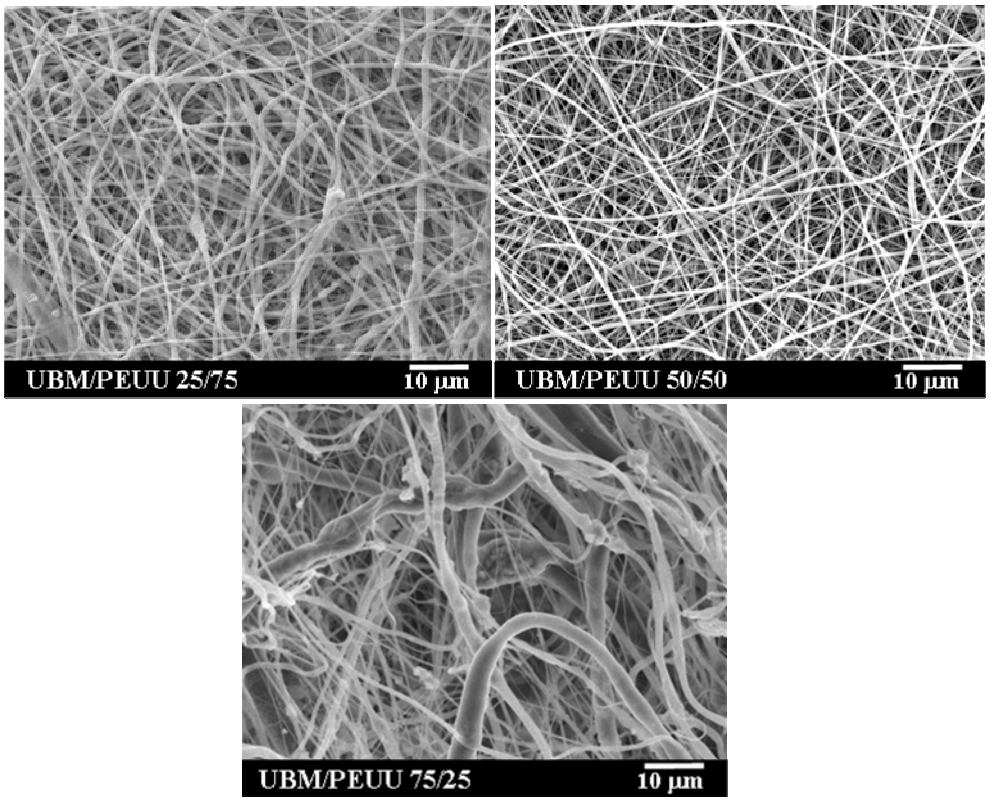


**Figure 4-2.** SEMs of continuous fiber morphologies of electrospun UBM/PEUU at 25, 50, and 75% UBM.

### 4.3.3 Electrospun UBM/PEUU scaffold characterization and cytocompatibility

In contrast to electrospun UBM, electrospun UBM/PEUU blends were both strong and distensible with tensile strengths ranging from 2-13 MPa and breaking strains from 38-220% with values decreasing with higher UBM content (**Table 4-1**). In addition, the scaffold was more resistant to degradation compared with electrospun UBM alone.

Electrospun PEUU/UBM scaffolds at all concentrations supported cell attachment. A fluorescent image of smooth muscle cells cultured on electrospun PEUU/UBM after 1 wk is shown in **Figure 4-3**. The cells appear spread and healthy near the scaffold surface. Cell adhesion was similar to tissue culture polystyrene for all samples except those containing 75% UBM, which had significantly higher adhesion (151% of TCPS, $p<0.05$). **(Table 4-1)**. Mass loss increased at higher UBM content with values ranging from 18% to 66% at 2wks for UBM based electrospun samples.

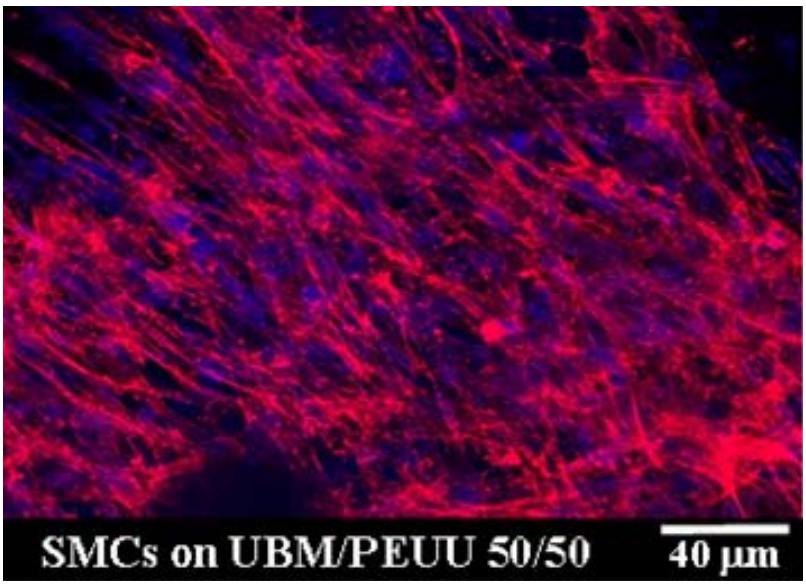


**Figure 4-3**. Confocal micrograph of SMCs cultured on electrospun UBM / PEUU (50/50) for 10 days. (red = f-actin, blue = nuclei)

**Table 4-1. Electrospun UBM/PEUU scaffold properties.**

| % UBM / % PEUU | Tensile Strength (MPa) | Breaking Strain (%) | SMC Adhesion (% TCPS) | Mass Loss 2wks (%) |
|---|---|---|---|---|
| 0/100 | 13 ± 4 | 220 ± 80 | 111 ± 14 | 5 ± 3 |
| 25/75 | 12 ± 1 | 141 ± 11 | 104 ± 14 | 18 ± 2 |
| 50/50 | 5 ± 2 | 85 ± 28 | 127 ± 25 | 42 ± 1 |
| 75/25 | 2 ± 0.1 | 38 ± 1 | 151 ± 20 | 66 ± 1 |

Further efforts to characterize the bioactivity of electrospun PEUU/UBM matrices are ongoing. SMC growth will be evaluated over 1 week of static culture on electrospun PEUU/UBM. Circular dichroism spectroscopy will be used to study the retention of secondary structure of the proteins in these materials. Lastly, subcutaneous implantation of these biohybrid scaffolds will occur to better evaluate their ability to generate a healing response.

This method of combining synthetic and biological materials into nanoscale fibers can be applied to a broad variety of material combinations provided that appropriate solvents are available for the electrospinning process. Materials can be blended into one electrospinning stream as performed here or also electrospun from multiple nozzles to produce a composite scaffold. Multiple nozzles can be utilized when a common benign processing solvent can not be found for multiple materials. Some other ECM extracts that may be utilized as the biological component include but are not limited to small intestinal submucosa or liver extract.

Urinary bladder matrix extract was combined with a biodegradable and cytocompatible polyurethane through electrospinning to create elastomeric nanofiber scaffolds. This hybrid material combination resulted in increased mechanical robustness and flexibility from the synthetic component and increased cell adhesion and degradation rates from the natural component. These hybrid scaffolds have potential to be utilized in soft tissue engineering applications were increased strength and elasticity may be required.

# 5.0 FABRICATION OF BIOMIMETIC ALIGNED NANOFIBER MATRICES

## 5.1 INTRODUCTION

Scaffolds for engineering mechanically robust tissue such as cardiovascular tissue would ideally be mechanically compliant and anisotropic to imitate the complex mechanical behavior of the native tissue. Anisotropy is of interest in creating oriented cellular structures and to control stress translation during tissue mechanical conditioning. Most load bearing soft tissues exhibit an exponential-like stress-strain response, "the J-curve", with the initial compliance as a result of stretching of coiled and flexible elastin fibers followed by a stiffening response from the high tensile strength collagen fiber component [116]. This type of mechanical response would be ideal to mimic in biodegradable, porous scaffolding for functional tissue engineering.

Biodegradable elastomers, like the cytocompatible polyurethanes developed in our laboratory, represent attractive alternatives to the more common stiff biodegradable polyesters utilized in tissue engineering. These materials can be processed into scaffolds suitable for *in vivo* placement or for support of *in vitro* cellular adhesion and growth by various processing techniques. These materials can also be exposed to cyclic straining with little plastic deformation.

Engineered tissues should ideally mimic the actual mechanical behavior of the original healthy tissue sought to replace. Actual tissues can be considered sophisticated nanofibrous composites with varying degrees of mechanical anisotropy. Therefore, a method to fabricate

nanofibrous scaffolds will controlled levels of anisotropy is warranted. This type of process would allow fabrication based control of mechanical properties appropriate for each specific tissue type.

One process, electrospinning, where an electric field overcomes surface tension to generate and draw nanoscale fibers, can produce scaffolds with extracellular matrix-like morphologies that retain mechanical strength and flexibility while also permitting protein incorporation into spun fibers to impart bioactivity [83, 115, 117]. Furthermore, electrospun scaffolds of random or aligned fiber morphologies can be fabricated by utilization of high speed rotating targets. This method suggests that varying degrees of fiber alignment may be achieved by modifying the rotational speed of the target [118]. Another attractive facet of this type of nanoscale fiber alignment is that it has been shown to influence cell growth, morphology, and extracellular matrix production. For example, smooth muscle cells have been demonstrated to align themselves on aligned PLCL electrospun fibers [90].

The objective was to fabricate biodegradable elastomeric scaffolds that approximate soft tissue mechanical anisotropy. This objective was achieved by electrospinning biodegradable polyurethanes onto a high speed rotating target. The scaffold morphologies, mechanical properties and smooth muscle cell response have been characterized as a function of target rotation velocity.

## 5.2 METHODS

### 5.2.1 Aligned scaffold fabrication

Cytocompatible poly (ester urethane) urea (PEUU) was synthesized from polycaprolactone diol and 1,4-diisocyanatobutane with subsequent chain extension by putrescine as described previously [15]. PEUU transparent films were cast from a 3 wt% solution in DMF and dried under vacuum for 48 h. 5 wt% PEUU in hexafluoroisopropanol (HFIP) was fed at 1.0 ml/hr by syringe pump into a Type 316 stainless steel capillary (Small Parts) suspended 13 cm vertically over a 4.5″ diameter aluminum mandrel **(Figure 5-1)**. PEUU was charged with +12 kV and the aluminum target with -7 kV using high voltage generators (Gamma High Voltage Research). Aligned PEUU fibers were formed by electrospinning onto the target rotating at speeds of 0 to 2300 rpm or linear velocities from 0.0 to 13.8 m/s. Scaffolds were allowed to dry overnight at room temperature and then placed under vacuum for 48 h at 30°C.

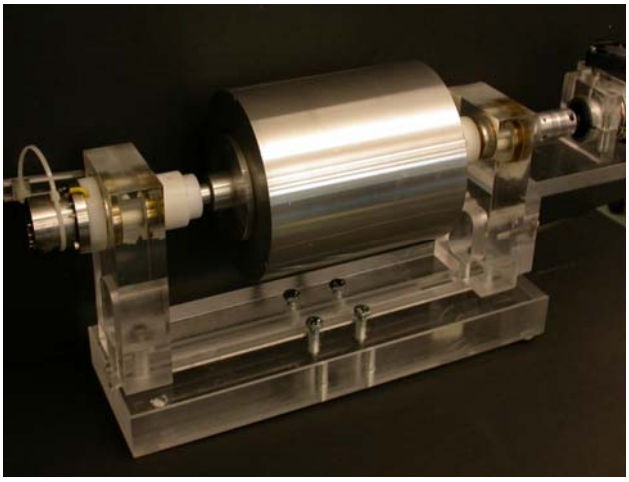

**Figure 5-1.** Rotating aluminum barrel target (4.5″ diameter) utilized to produce anisotropic electrospun PEUU scaffolds at speeds from 0 to 2300 rpm.

### 5.2.2 Aligned scaffold characterization

For scaffold morphology, electrospun samples were sputter coated with Pd/Au and imaged with scanning electron microscopy (SEM, JEOL JSM6330F) to characterize fiber morphologies. These samples were cut while keeping the known preferred axis of fiber alignment parallel to the y-axis of the SEM. Six images were taken from random locations of each sample to minimize local orientation effects.

To quantify fiber orientation from SEM images, custom image analysis software was designed in collaboration with the Biomechanics Laboratory of Professor M.S. Sacks of the University of Pittsburgh. Briefly, fiber alignment was measured using an algorithm developed by Chaudhuri [119], modified by Karlon [120] and coded in MATLAB software (MathWorks) [121]. The data acquired from each image were then placed into a histogram. The histograms were then averaged to result in the orientation data.

For X-ray diffraction (XRD) to characterize scaffold crystallinity, samples were mounted onto a standard XRD specimen holder for analysis so that the fiber orientation was parallel to the X-ray beam. Samples were analyzed on a PANalytical X'Pert Pro diffractometer utilizing copper radiation. Porosity was measured by comparing the densities of electrospun scaffolds and cast PEUU films in the following equation,

$$Porosity = (1 - \rho_e / \rho_f) \times 100 \quad (5\text{-}1)$$

where $\rho_e$ is the density of the electrospun scaffold and $\rho_f$ is the density of the cast PEUU film.

In further collaboration with Professor M.S. Sacks, biaxial mechanical properties were characterized under cyclic loading in perpendicular axes. This method has been described previously [2]. Briefly, square 2-cm by 2-cm samples are attached to the carriages of the device

using surgical staples at the end of two sutures. Samples were marked in four spots (1-mm diameter) in the central 4-mm by 4-mm area of the sample using tissue dye (Cancer Diagnostics). These spots were employed to calculate local strains using established methods established by Sacks [2]. Load is measured in perpendicular directions by utilizing two load cells. Diagrams of the biaxial testing device and testing sample are shown in **Figure 5-2**.

Stress along the longitudinal and circumferential axes was measured as force divided by unloaded cross-sectional area. All testing was performed in phosphate buffered saline at room temperature. Elongation was determined from the displacement of 4 marks on the surface of the specimen. The axial stretches $\lambda_{PD}=F_{11}$ and $\lambda_{XD}=F_{22}$ were measured, from the deformation gradient tensor where PD and XD refer to the preferred (more aligned) and cross-preferred (less aligned) fiber directions, respectively. For all tests, the maximum membrane tension was chosen as 90 N/m. This value was chosen to compare with previous studies on valve tissues [122]. All test protocols maintained a constant ratio of membrane tension of PD:XD during cycling. Runs started with tensions of each axis equal to 90 N/m. The next 7 runs used ratios of tension PD:XD of 9:90, 45:90, 67.5:90, 90:90, 90:67.5, 90:45, and 90:9 N/m, respectively. Data were presented as mean ± standard deviation and group differences.

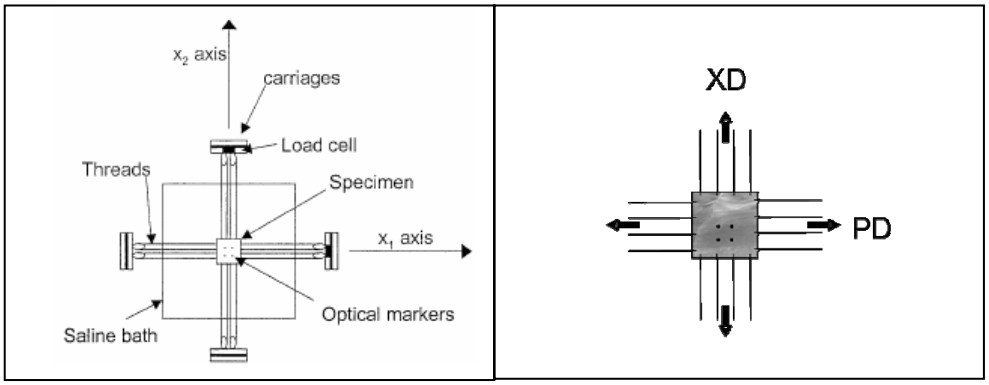


**Figure 5-2.** Schematic of biaxial mechanical testing device (left panel) and sample preparation (right panel). Reproduced from Sacks et al. [2]

### 5.2.3 Smooth muscle cell growth and morphology

PEUU scaffolds of random (target linear velocity = 0 m/s) or aligned (target linear velocity = 13.8 m/s) morphologies were evaluated for their ability to support smooth muscle cell (SMC) growth. Samples were punched into 6-mm discs and sterilized by 70% ethanol for 6h, rinsed multiple times with PBS, placed under UV light for 16 h and placed in SMC media overnight in an incubator. PEUU discs were then placed in wells of a 96-well TCPS plate for cell seeding.

For smooth muscle culture, media consisted of DMEM supplemented with 10% fetal bovine serum and 1% penicillin-streptomycin. Vascular smooth muscle cells isolated from a rat aorta [107] (SMCs, $8^{th}$ passage) were statically seeded on scaffolds at a density of 20 x $10^4$ cells/mL. SMC proliferation was evaluated at days 1, 3, 5, and 7 using the MTT assay (n = 5 per sample studied). Samples were also rinsed with PBS, fixed with 2.5% glutaraldehyde and 1% osmium tetraoxide in PBS and subjected to graded ethanol dehydrations before being critical point dried, sputter-coated and then imaged by SEM to observe cellular morphology.

## 5.3 RESULTS

### 5.3.1 Aligned scaffold fabrication and analysis

Continuous electrospun fibers were fabricated and various degrees of fiber alignment were made possible by adjusting the rotation speed of the mandrel. Fiber alignments ranged from random (target linear velocity 0.0 m/s) to highly aligned (13.8 m/s) as shown in **Figure 5-3**. No obvious

degrees of alignment were obvious at mandrel velocities of 1.5 m/s or less and the fiber matrices could be considered isotropic. At linear velocities of 3.0 m/s or greater, various degrees of fiber alignment were obtained. This alignment became increasingly visible up to 13.8 m/s (**Figure 5-3)**.

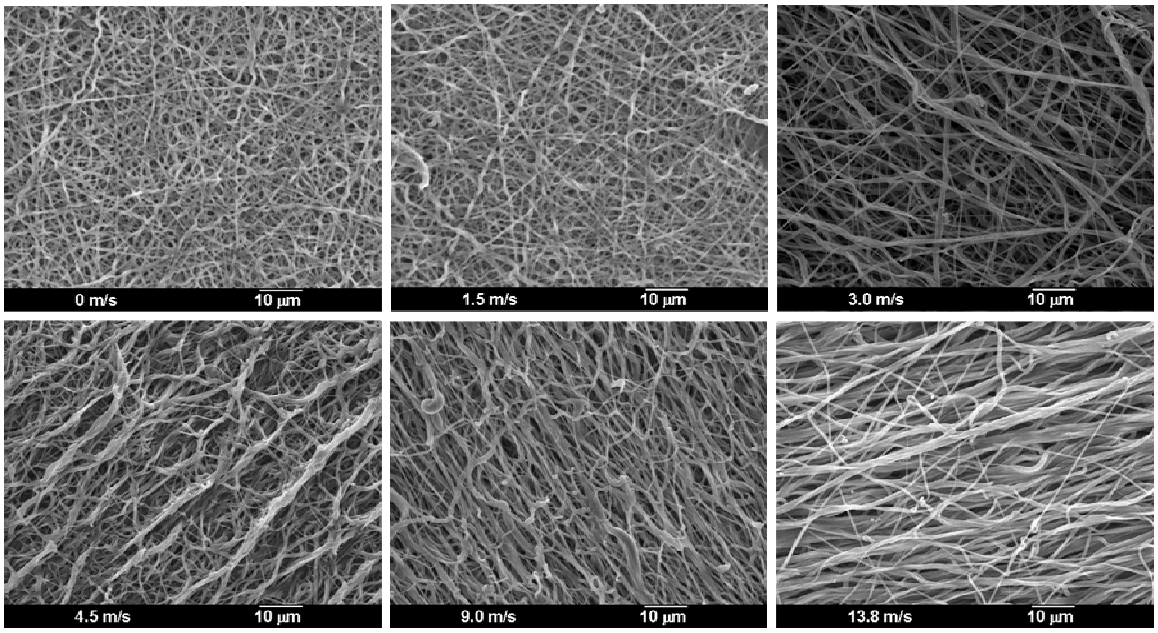


**Figure 5-3.** Fiber morphologies of PEUU electrospun onto a mandrel rotating at 0 to 2300 rpm (linear velocities of 0 to 13.8 m/s) as imaged by SEM.

The custom image analysis software enabled accurate quantification and characterization of fiber alignment from SEMs of electrospun PEUU samples **(Figure 5-4)**. Alignment histograms mimicked what could be observed qualitatively by exhibiting increased fiber alignment at target velocities of 3.0 m/s or greater. Values shown in **Figure 5-4** further illustrate that by holding all electrospinning process variables constant except target mandrel velocity, aligned and anisotropic matrices may be fabricated.

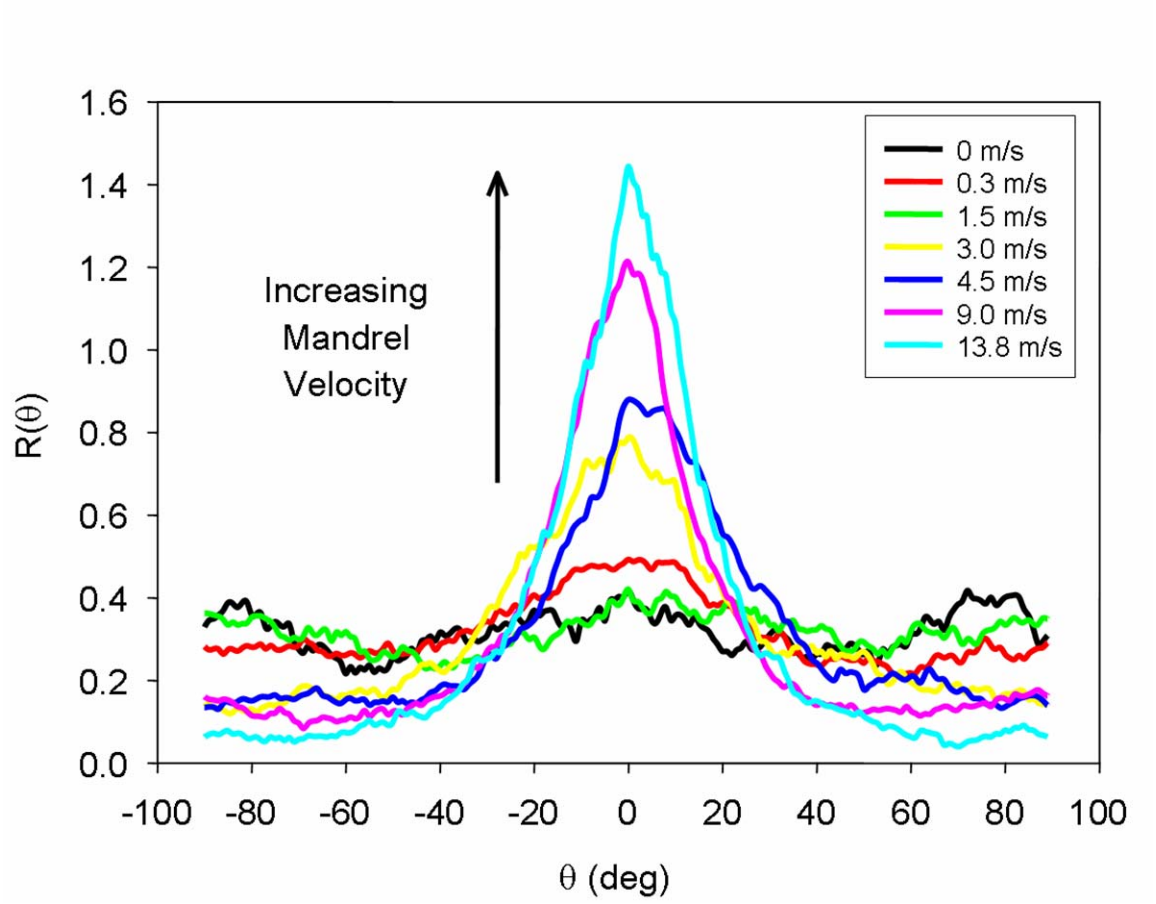


**Figure 5-4.** Fiber alignment as a function of mandrel linear velocity from 0 to 13.8 m/s using custom analysis program. (Data courtesy of T.Courtney)

XRD was utilized to measure crystallinity of PEUU samples electrospun at 0, 250, 750, and 2300 rpm, which correspond to linear velocities of 0.0, 1.5, 4.5, and 13.8 m/s **(Figure 5-5)**. Percent crystallinity values were relative and the 2500 rpm sample exhibited the largest intensity maxima peak so was assumed 100% crystalline. Percent crystallinity of samples from other speeds was measured as a percentage of the 2500 rpm sample. As evidenced in **Figure 5-5** and summarized in **Table 5-1**, crystallinity increased as a function of mandrel velocity. In contrast, scaffold porosity, decreased with mandrel velocity (**Table 5-1**) from values of 82% to 72% at speeds ranging from 0.0 m/s to 13.8 m/s.

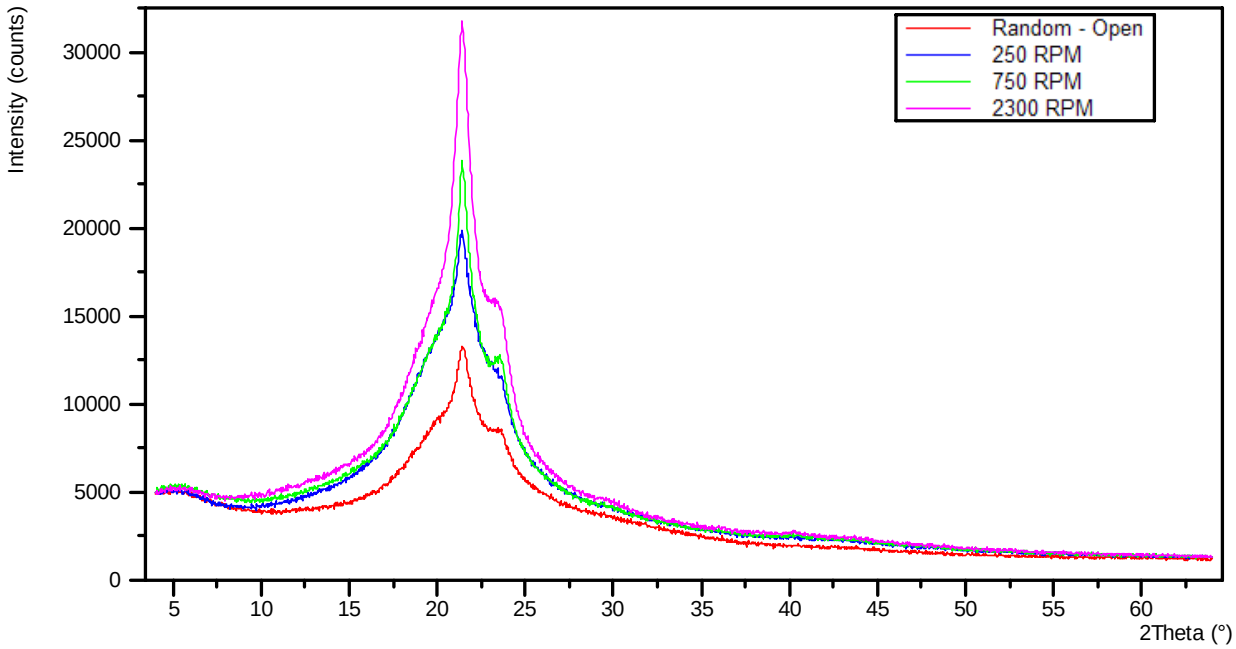


**Figure 5-5.** XRD spectra of PEUU electrospun at various rpm speeds.

**Table 5-1.** Summary of aligned scaffold properties and morphologies.

| Mandrel rpm | Mandrel Linear Velocity (m/s) | Porosity (%) | Crystallinity (%) | Fiber Morphology |
|---|---|---|---|---|
| 0 | 0.0 | 82 ± 5 | 37 | Random |
| 50 | 0.3 | - | - | Random |
| 250 | 1.5 | 78 ± 4 | 58 | Random |
| 500 | 3.0 | - | - | Aligned |
| 750 | 4.5 | 72 ± 4 | 72 | Aligned |
| 1500 | 9.0 | - | - | Aligned |
| 2300 | 13.8 | 72 ± 2 | 100 | Aligned |

### 5.3.2 Biaxial mechanical properties

Biaxial mechanical testing of PEUU electrospun at all mandrel velocities was conducted in the preferred and cross-preferred scaffold directions and results are displayed in **Figure 5-6**. For PEUU samples electrospun at 1.5 m/s and lower speeds, there was no apparent difference between the stress-strain curves of either the preferred or cross-preferred directions (maximum stretch, $\lambda \cong 1.2$). At mandrel velocities greater than 1.5 m/s, the scaffolds became increasingly anisotropic. Highly aligned scaffolds like that fabricated at 13.8 m/s exhibited a stiff fiber-like mechanical behavior for the preferred axis and a more flexible, compliant behavior along the cross-preferred axis. Upon comparing this sample to previously reported planar biaxial mechanical property results from the native pulmonary heart valve, a strong similarity was observed in mechanical behavior [123]. One can notice the similar stiff behavior of both the preferred direction of PEUU and the circumferential (circ) direction of the pulmonary valve (PV). The cross-preferred direction also mimics the mechanical response of the radial direction of the PV. This initial compliant response followed by a later stiffening effect, "the J-curve," as seen in the XD direction is difficult to achieve with synthetic materials [124].

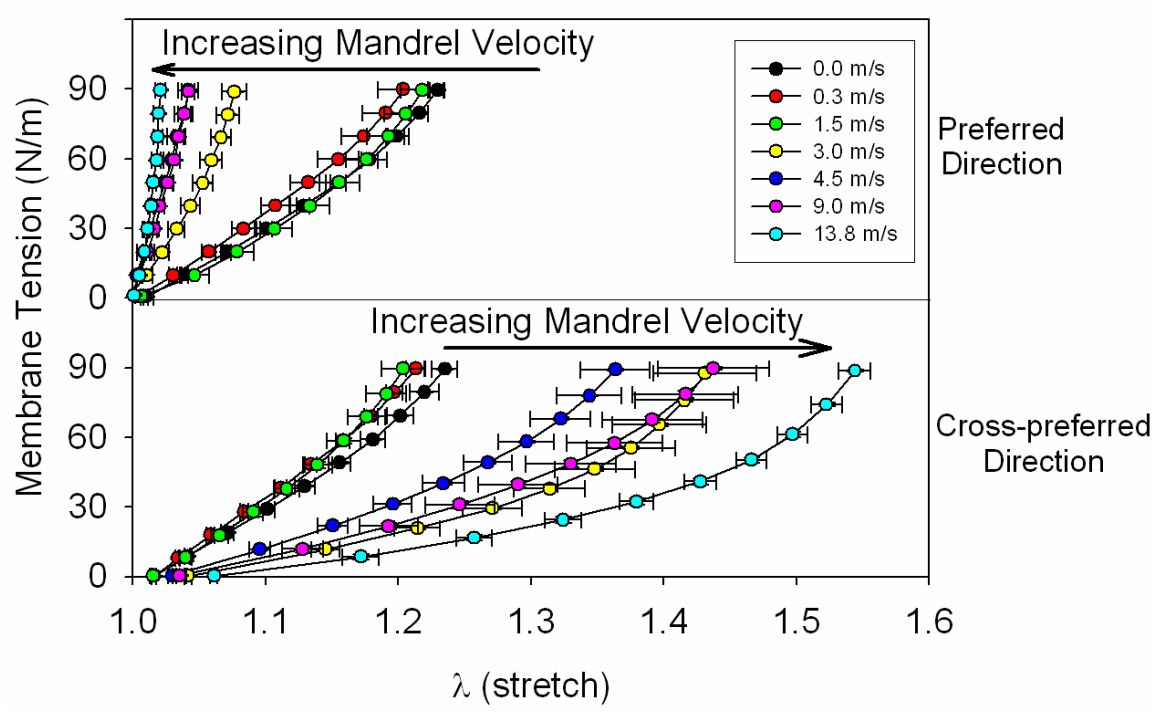


**Figure 5-6.** Biaxial mechanical properties of electrospun PEUU scaffolds as a function of fiber direction and mandrel velocity. (Data courtesy of T. Courtney)

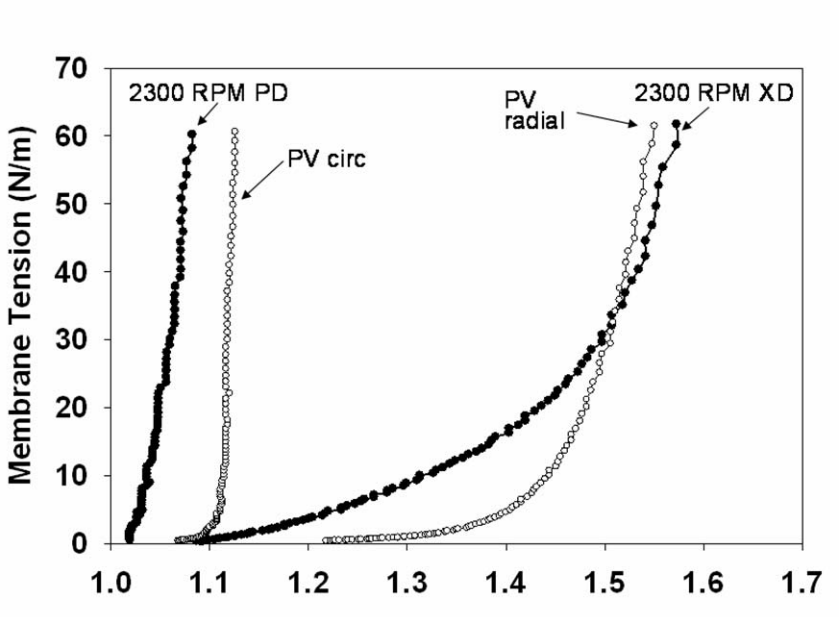


**Figure 5-7.** Comparison of biaxial tensile properties of PD and XD of aligned electrospun PEUU (2300 rpm) versus the circ and radial axes of a bioprosthetic heart valve. (Data courtesy of T. Courtney)

### 5.3.3 Smooth muscle cell growth and morphology

Smooth muscle proliferation was measured on random or highly aligned electrospun PEUU at 1, 3, 5, and 7 days **(Figure 5-8)**. At either 1 day or 7 days of culture no significant difference was observed between cell numbers on TCPS, random, or aligned PEUU. However, when examining SMC morphology on these materials, it was observed that SMCs cultured on random scaffolds exhibited random spread morphologies while those on the aligned scaffolds exhibited high degrees of alignment parallel to the fiber direction (**Figure 5-9**).

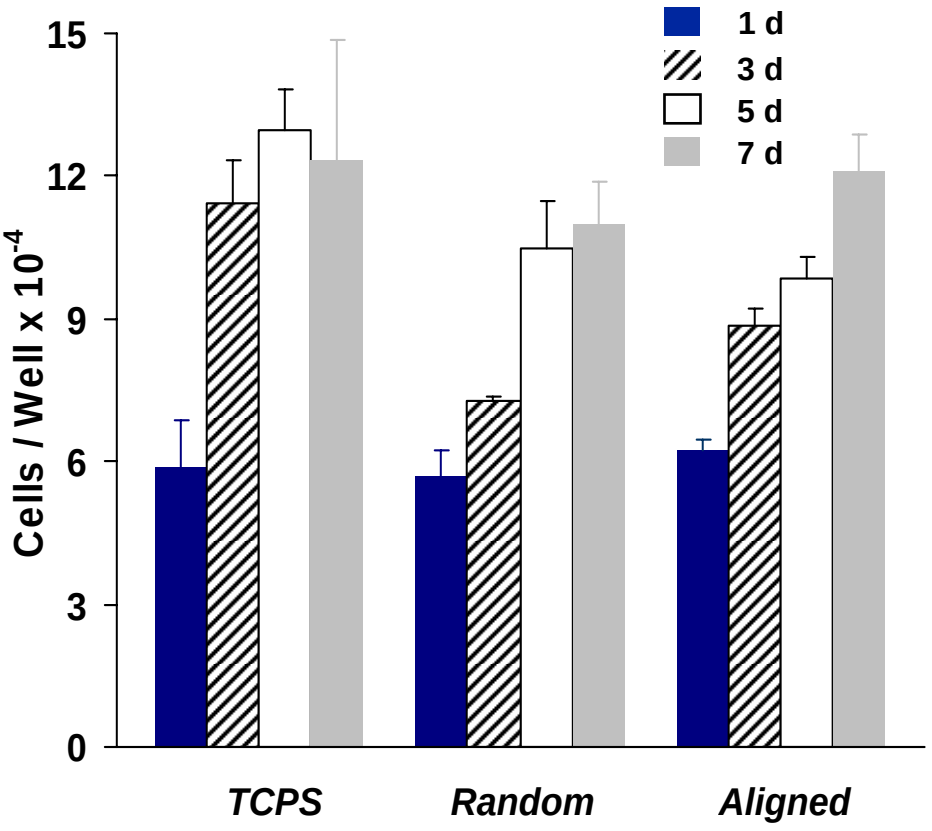


**Figure 5-8.** Smooth muscle cell growth on random and aligned electrospun PEUU compared with TCPS.

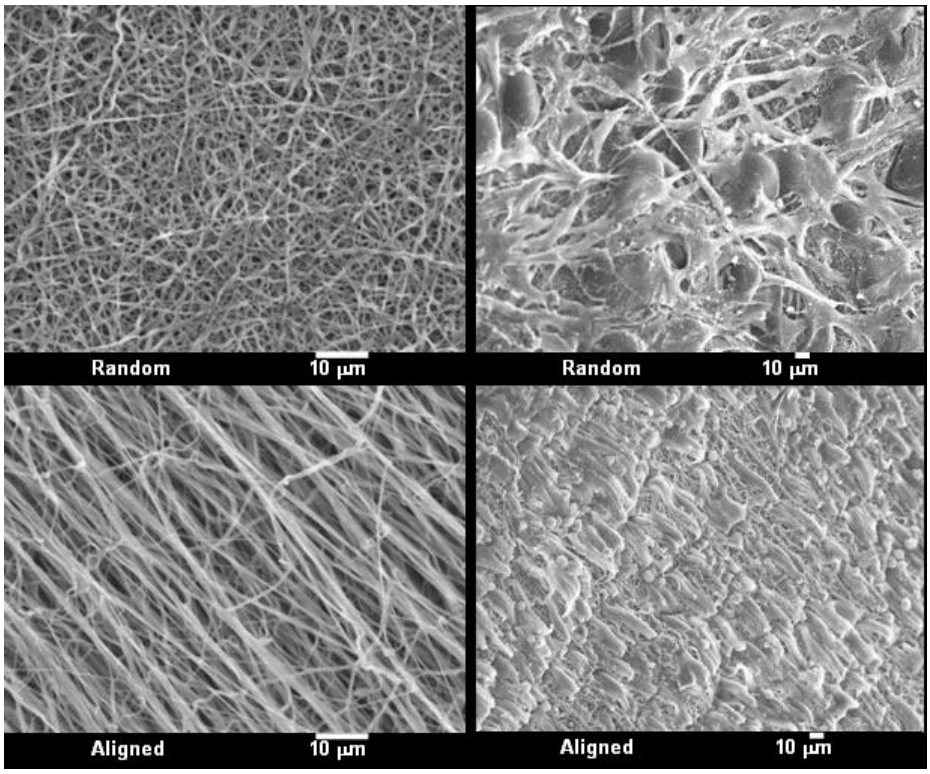


**Figure 5-9.** Morphologies of random (top) and aligned (bottom) electrospun PEUU before (left panels) and after (right panels) cell culture.

## 5.4 DISCUSSION

Due to its ability to mimic the scale and architecture of the native extracellular matrix, electrospinning has become more frequently employed by the tissue engineering community [93, 113, 117, 125, 126]. However, there are fewer examples in the literature describing methods to fabricate highly aligned electrospun scaffolds. Matsuda et al. fabricated tubular constructs onto mandrels at low or high rotation and quantified the different uniaxial mechanical response [127]. Here, we have developed a method to fabricate scaffolds of controlled fiber alignment, characterized the mechanical response with more physiologically relevant biaxial testing, and produced biodegradable elastomeric scaffolds more appropriate for functional engineering of soft tissue.

From results seen here and other results obtained by Professor M.S. Sacks, fiber orientation seems to begin with step-function behavior at a target linear velocities of 2 m/s [121]. This phenomenon may be explained when considering the fabrication process in more detail. In the electrospinning process, the fiber is first “electrically extruded” as a straight polymer jet that approaches the mandrel but at some point becomes curved and more complicated. This curved path results from an electrically-driven bending instability within the charged jet. The trajectory of a typical segment can move in and out towards the direction of the applied electric field between the nozzle and mandrel. This segment may also be influenced from distant segments of the jet. The curved segment is bent and elongated by self-repulsion of electrical charges within that segment. When utilizing a moving mandrel as the target, the surface velocity of the mandrel would be expected to exceed fiber delivery rate in order for mandrel rotations to induce fiber orientation.

For example, using a flow rate of the 5% PEUU solution of 1.0 mL/hr through a 1.19 mm inner diameter capillary, the velocity of the feed solution at the nozzle would be $9.4x10^{-6}$ m/s. Assuming a single fabricated fiber being delivered at 0.05 mL / hr (5% of 1 mL/hr for 5% PEUU in HFIP), the fiber diameter would have to be approximately 940 nm in diameter so that fiber velocity would approximate 2 m/s. Thus, it appears there can be 3 to 5 fibers depositing concurrently to achieve a 2 m/s velocity. Random scaffolds electrospun onto target linear velocities below 2m/s could then result from the solution flow rate exceeding the 2m/s threshold.

In the scaffold approach to tissue engineering, it is the role of the scaffold to provide mechanical and structural support for cells until they develop into tissue that can bear the mechanical load. The structural and mechanical features of the scaffold can also interact with cells to influence cell morphology and ECM production. For example, Xu et al. have demonstrated smooth muscle cell alignment on aligned fiber scaffold [90]. Others have shown that aligned nanofiber scaffolds are appropriate for mechanical stimulation and can result in increased ECM production by fibroblasts [128]. The aligned elastomeric scaffolds developed here possess properties that mimic actual tissue mechanical anisotropy as well as directly influence cell morphology. These materials would be expected to be ideal candidates for cyclic mechanical straining during culture in future studies aimed at developing functional tissue such as a tissue engineered heart valve.

# 6.0 CELLULAR MICROINTEGRATION

## 6.1 INTRODUCTION

Highly cellularized and mechanically functional engineered tissue constructs are desired to repair or replace diseased cardiovascular and other soft tissues. A typical method to create such constructs involves fabricating biodegradable porous scaffolds that are subsequently seeded with cells, cultured *in vitro,* and then implanted. While synthetic or processed natural material scaffolds can provide some mechanical support, the use of load bearing scaffolds often is coupled with long cell seeding and culture times to achieve high cellular densities in the scaffold and adequate mechanical properties for *in vivo* transplantation [3, 9]. Mechanically robust, contractile muscle or cardiovascular tissues consist of high densities of aligned cell morphologies. To fabricate functional tissue, it is also desired that scaffolds are designed to both support cell-cell interactions as well as to direct cell alignment in mimicking this tissue structure.

The method of electrospinning, originally patented in the 1930's, has recently experienced renewed interest for tissue engineering applications [74, 83, 86, 87]. Electrospinning is attractive to the tissue engineering community in that it permits fabrication of scaffolds that resemble the scale and fibrous nature of the native extracellular matrix (ECM). The ECM is composed of fibers, pores, and other surface features at the sub-micron and nanometer size scale. Many believe that such nanoscale features directly impact cellular

interactions with synthetic materials such as migration and orientation [129, 130]. Electrospinning also permits fabrication of oriented fibers to result in scaffolds with inherent anisotropy. These aligned scaffolds can influence cellular growth, morphology and ECM production. For example, Xu et al. found smooth muscle cell (SMC) alignment with poly(L-lactide-*co*-ε-caprolactone) fibers [90] and Lee et al. submitted aligned non-biodegradable polyurethane to mechanical stimulation and found cells cultured on aligned scaffolds produced more ECM than those on randomly organized scaffolds [128].

While electrospinning can fabricate scaffolds that possess an ECM-like fibrous structure, this morphology also results in pore sizes that are generally smaller (< 50 μm) and more tortuous than those produced by other scaffold methods such as salt leaching and thermally induced phase separation [81] . Therefore, methods to seed high densities of cells into scaffolds such as vacuum filtration [131] are not effective in achieving a uniform distribution throughout a thick construct. It has been suggested that cells statically seeded on electrospun matrices can migrate into the interior by displacing or enzymatically degrading individual fibers in the process [83]. While this may be possible, an extended culture period and appropriate signals for cell migration into thick construct interiors might also be required. To overcome this problem and achieve a highly cellularized tissue engineered construct while also providing elastomeric mechanical support, we have developed a microintegration approach wherein a meshwork of sub-micron elastomeric fibers is electrospun concurrent with cellular placement. The constructs fabricated by this method were characterized for fiber and cell morphologies, mechanical properties, and cell viability and proliferation.

After seeding scaffolds with high cell densities it is important to provide sufficient nutrient and waste transfer to preserve cell viability and support proliferation. Reports have

shown that nutrient transport is often limited to diffusion alone [132]. Diffusion usually proves sufficient for relatively thin scaffolds of 100-200 μm. However, with thicker scaffolds (> 200 μm) tissue development can be limited. Transmural perfusion has been shown to result in increased cell density and uniformity within cultured scaffolds [133]. Therefore, we have employed a perfusion bioreactor similar in design to that reported by Radisic et al. [133] to provide significant media convection for high density SMC growth in our microintegrated constructs.

The process of SMC microintegration into electrospun poly(ester urethane)urea (PEUU) or PEUU and type I bovine collagen blends was investigated. Biodegradable and cytocompatible PEUU based on polycaprolactone diol, 1,4-diisocyanatobutane, and putrescine was utilized as the elastomeric fiber material. Cellular viability as a function of the cellular incorporation method was studied using trypan blue staining. An electrospinning apparatus previously described was modified to produce mechanically robust cell microintegrated scaffolds that were cultured statically or in a trans-mural perfusion bioreactor. Cell growth and morphology within the elastomeric fiber matrices were evaluated. Tensile mechanical properties were measured following the microintegration process. More recently, we have extended and reproduced this process to illustrate the validity of producing muscle derived stem cell (MSDC) and endothelial progenitor cell (EPC) microintegrated constructs

## 6.2 MATERIALS AND METHODS

### 6.2.1 Polymer synthesis and characterization

1,4-diisocyanatobutane (BDI, Fluka) and putrescine (Sigma) were distilled under vacuum. Polycaprolactone diol (PCL, *MW* = 2000, Aldrich) was vacuum dried for 48 h. Dimethyl sulfoxide (DMSO) and N,N–dimethylformamide (DMF) were dried over 4-A molecular sieves. Stannous octoate (Sigma) and hexafluoroisopropanol (HFIP, Oakwood Products) were used as obtained.

Cytocompatible and biodegradable PEUU was synthesized from PCL and BDI with subsequent chain extension by putrescine as reported previously [15]. The reaction consisted of a two-step solution polymerization in DMSO using a 2:1:1 BDI: PCL: putrescine mole ratio. PEUU cast films were prepared from a 3-wt% solution in DMF and dried under vacuum for 48 h. PEUU was characterized for molecular weight, thermal transitions and uniaxial tensile properties as described previously [115].

### 6.2.2 Electrospinning

PEUU was electrospun using a technique similar to that previously described. In brief, PEUU was dissolved in HFIP under mechanical stirring at 12-wt%. For PEUU/collagen electrospinning, PEUU and type I bovine collagen (Sigma) were dissolved in HFIP under mechanical stirring at a ratio of PEUU/collagen of 75/25 by mass. The polymer solution was fed at 1.5 mL/hr using a syringe pump (Harvard Apparatus PhD) through Teflon tubing and then into a stainless steel capillary (I.D. = 0.047″) located 23-cm from a conductive target. High voltage

generators (Gamma High Voltage Research) were utilized to charge the polymer solution at 10 kV and the respective target at -10 kV.

### 6.2.3 SMC spraying / electrospraying

Vascular smooth muscle cells (SMCs) isolated from rat aorta were expanded on tissue culture polystyrene (TCPS) culture plates under Dulbecco's Modified Eagle Medium (DMEM) supplemented with 10% fetal bovine serum and 1% penicillin-streptomycin [107]. SMCs were sprayed from a sterile air pressurized polypropylene bottle with an attached spray nozzle (Fisher) or electrosprayed from a sterile stainless steel capillary (I.D. = 0.047″) at 10 kV over a distance of 20 cm onto glass slides placed on an aluminum plate charged at -15 kV. To shield cells from processing effects and in an effort to maximize viability, some cell suspensions were supplemented with 3-wt% bovine skin gelatin (Sigma) before spraying or electrospraying. For assessment of cell viability, 50 μL of sprayed or electrosprayed SMCs in culture medium were added to 50 μL of 0.4% trypan blue (Gibco). After 5 min incubation, viability was calculated as:

$$\% \text{ cell viability} = [\#\text{ unstained cells (living)} / \#\text{ total cells (dead + living)}] \times 100\%.$$

### 6.2.4 SMC Microintegration

The first microintegration technique evaluated consisted of simultaneously electrospraying cells and electrospinning polymer with a side-by-side capillary configuration located 23-cm from the target as depicted in **Figure 6-1 (a)**. $5 \times 10^6$ SMCs/mL in media were fed at 0.25 mL/min with a syringe pump (Harvard Apparatus) through sterile tubing into a sterile capillary charged at 5 kV. 5-wt.% PEUU or PEUU/collagen (75/25) was fed at 1.5 mL/hr into a capillary charged at 10 kV.

The target was a sterile aluminum plate charged at -10 kV located on an x-y stage (Velmex) translating 8-cm along each axis at a speed of 8 cm/s.

In order to fabricate thicker constructs with more uniform cell incorporation, a subsequent microintegration technique was utilized as shown in **Figure 6-1 (b)**. In this case, SMCs were electrosprayed concurrently with polymer electrospinning using a perpendicular nozzle configuration. 7.5 x $10^6$ SMCs/mL were fed at 0.25 mL/min into a sterile capillary charged at 8 kV and located 5-cm from the target. 12 wt% PEUU was fed at 1.5 mL/hr into a capillary charged at 10 kV and located 23-cm from the target. The target consisted of a sterile stainless steel rod (3/4″ diameter) charged at -10 kV and rotating at 200 rpm while translating 8-cm along its axis at 8 cm/s. 5-cm by 5-cm constructs were filleted off the mandrel using a sterile blade by first trimming 1.5-cm off each end before removal. A fabrication time of 45 min was used with both microintegration techniques.

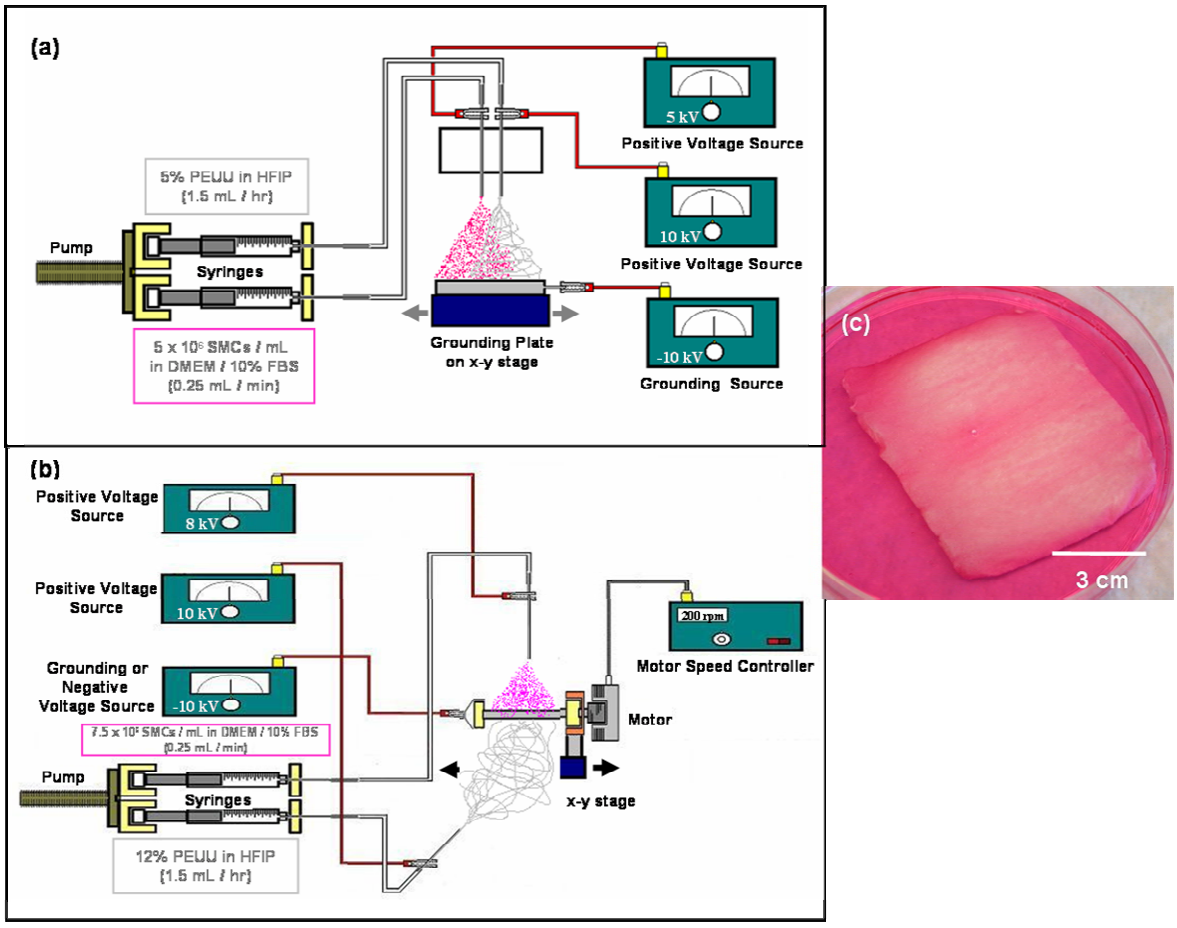


**Figure 6-1.** Approaches to cellular microintegration. (a) Microintegration using a side-by-side capillary configuration for electrospinning polymer and electrospraying cells onto a flat target moving on an x-y stage. (b) Microintegration using a perpendicular capillary configuration for electrospinning polymer and electrospraying cells onto a rotating mandrel moving on a linear stage to result in the construct shown in (c).

### 6.2.5 Muscle derived stem cell microintegration

Murine muscle derived stem cells (MDSCs) were obtained through collaboration with the laboratory of Professor J. Huard of the University of Pittsburgh. MDSCs were isolated from normal newborn mice through a collagenase based enzymatic digestion method followed by separation based on adhesion characteristics to collagen modified tissue culture flasks (pre-plate method) as described previously [134]. Specifically, MDSCs were clonal colonies of cells that adhered at pre-plate number six. Each pre-plate time consisted of 24 h to allow for cell attachment. These cells have been demonstrated to maintain their phenotype for over thirty subculture periods as well as exhibit the potential to differentiate into muscle, neural, and endothelial cells either *in vitro* or *in vivo*. MSDCs were cultured in media that consisted of DMEM supplemented with 10% FBS, 10% horse serum, and 1% penicillin/streptomycin. MSDCs were expanded and microintegrated using the same process variables as described above for SMCs.

### 6.2.6 Endothelial progenitor cell microintegration

Endothelial progenitor cells (EPCs) were isolated from juvenile ovine peripheral blood by a histopaque gradient / pre-plate method and cultured in EBM-2 medium supplemented with EGM-2 SingleQuots without hydrocortisone and 20% fetal bovine serum on 1% gelatin-coated plates. Following 4 to 6 wks expansion and prior to seeding, EPCs were characterized by indirect immunofluorescence as CD31 and vWF positive and α-SMA negative. EPCs were subcultured and microintegrated using identical processing conditions as described above for SMCs.

### 6.2.7 Scaffold / cell culture

After fabrication, samples were immediately removed from their respective microintegration targets and placed in a sterile polystyrene dish with a minimal amount of culture medium to cover the sample. Areas of the thin SMC microintegrated sheets fabricated on the flat target that appeared to possess uniform cell integration with electrospun PEUU were punched into 6-mm discs. These discs were cultured statically in poly-2-hydroxyethyl methacrylate (poly-HEMA) coated TCPS 96-well plates with 200 μL of media in each well. As a control, TCPS wells were seeded with SMCs. Media was changed every day.

The thicker constructs fabricated using the mandrel target were characterized initially for uniformity of cellular integration. Samples for subsequent study were first cultured with a minimal amount of media to cover the sample for 4 h to encourage cell adhesion. At this point, cells were considered adherent and an additional 15 mL of media was added to support the cells for 16 h of static culture. Next, samples were either cultured statically as 6-mm discs in poly-HEMA coated TCPS 96-well plates or under transmural perfusion in a custom designed bioreactor. For perfusion culture, samples were cut into 13-mm discs and placed into polypropylene in-line filter holders (VWR) between silicone and Teflon o-rings and a support screen. A schematic of the bioreactor as adapted from a previously reported design is shown in **Figure 6-2** [133]. Each sample was placed in its own flow loop containing a 32-mL media bag (American Fluoroseal Corp), a 2.5-m length of platinum silicone tubing (Cole Parmer, 1/16″ I.D.) to serve as a gas exchanger, and two syringes for adding or removing media or bubbles. A multi-channel peristaltic pump (Harvard Apparatus) was utilized to perfuse the loops at 0.5 mL / min. 50% of the media was changed every 2 days.

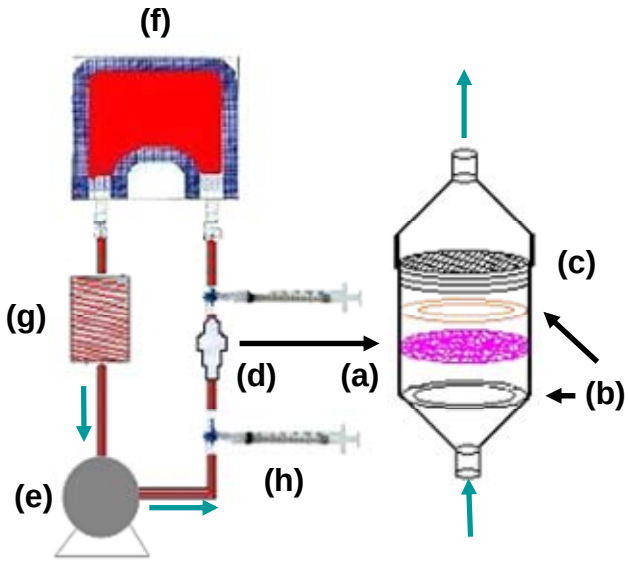


**Figure 6-2.** Schematic of the perfusion bioreactor employed with microintegrated constructs. 13-mm diameter construct discs (a) were placed between O-rings (b) and a support screen (c) of in-line filter holders (d) followed by perfusion at 0.5 mL/min with a multi-channel peristaltic pump (e). Each construct was placed in its own loop consisting of a 32 mL media bag (f), silicone tubing gas exchanger (g) and syringes for media exchange.

### 6.2.8 Characterization

Quantification of cell viability was achieved using the MTT mitochondrial activity assay (n = 5 per sample studied) [100]. Regions exposed to flow from samples removed from the bioreactor were punched into 6-mm discs for MTT. For scanning electron microscopy (SEM) to observe cellular and construct morphologies, samples were rinsed with PBS, fixed with 2.5% glutaraldehyde and 1% osmium tetraoxide in PBS and subjected to graded ethanol dehydrations before being critical point dried, sputter-coated and imaged.

Thin SMC microintegrated samples immediately and 1 day after fabrication, were stained with TUNEL to identify apoptotic cells as follows. Samples were rinsed with PBS, fixed in 2% paraformaldehyde for 30 min then placed in PBS overnight. Samples were then permeabilized

with 0.1% Triton x-100 for 45 min, and then incubated in TUNEL solution for 1 h at 37°C. TUNEL solution (terminal transferase, Roche) consisted of 45 μL deionized water, 20 μL cobalt, 32 μL buffer, 2 μL biotin, and 1 μL TdT buffer (25 *mM* Tris-HCl, pH = 6.6, 0.2 *M* potassium cacodylate, 0.25 mg/mL BSA,). Samples were then rinsed multiple times in PBS and then placed in rhodamine phalloidin (1:250, Molecular Probes) and draq5 (1:1000, Biostatus) and streptavidin Alexa 488 (1:200) for 1 h at room temperature. Samples were placed on slides with coverslips mounted with gelvatol 1 h before imaging.

Samples at later timepoints were rinsed with PBS, fixed with 2% paraformaldehyde, permeabilized with 0.1% Triton x-100 and stained with rhodamine phalloidin (1:250, Molecular Probes) for f-actin and draq-5 (1:1000, Biostatus Ltd) for nuclei. Imaging was done on a Leica TCS-SL laser scanning confocal microscope. Representative images were taken as individual scans or as a series of stacked images.

For sectional histology, samples were fixed in 10% neutral buffered formalin, embedded in paraffin, cross sectioned at 10 μm and stained with Hematoxylin and Eosin or Masson's Trichrome. Construct tensile mechanical properties immediately after fabrication using the method shown in **Figure 6-1 (b)** were measured on an ATS 1101 Universal Testing Machine (10 mm/min crosshead speed) according to ASTM D638-98 while wetted with media and immediately after removal from a 37°C incubator.

### 6.2.9 Statistics

Results are displayed as the mean ± standard deviation. One-factor analysis of variance (ANOVA) was utilized to evaluate cell viability, cell growth and mechanical properties using the Neuman-Keuls test for *post hoc* assessments of the differences between samples.

## 6.3 RESULTS AND DISCUSSION

### 6.3.1 Polymer characterization

PEUU number average molecular weight was 88000 and weight average molecular weight was 230000 as determined by GPC to give a polydispersity of 2.6. DSC values reported a glass transition temperature of –55.0°C and soft segment melt temperature of 41.0°C. Cast PEUU film was strong and distensible with a tensile strength of 27 ± 4 MPa and a breaking strain of 820 ± 70 %.

### 6.3.2 SMC spraying / electrospraying

Electrospinning occurs when a polymer solution is charged to high voltage that generates an electrical force that can extrude out a polymer jet, which then breaks down to sub-micron scale fibers through a complicated bending and whipping process [87]. As stated in an earlier chapter, when solution parameters such as polymer molecular weight, concentration and viscosity are not

appropriate to fabricate continuous fibers, electrospraying occurs whereby polymer droplets are deposited on the target [135]. This phenomenon has been investigated for some drug delivery applications [136, 137] and some researchers have even electrosprayed cells encapsulated within hydrogels and reported no viability loss after exposure to high electrostatic potentials [138].

To evaluate the potential cytotoxic effect of different methods to incorporate cells into electrospun matrices, SMCs were either sprayed from a nozzle under pressure or electrosprayed and SMC viability was assessed as a function of each processing variable as shown in **Figure 6-3**. These variables included spraying alone, spraying onto a target charged at -15 kV, spraying onto a target charged at -15 kV with PEUU electrospinning, electrospraying at 10 kV onto a target charged at -15 kV, and electrospraying at 10 kV onto a target charged at -15 kV with PEUU electrospinning. A significant reduction in SMC viability resulted from spraying cells through the nozzle. The physical forces of the pressurized spray in combination with exposure of cells to processing solvents may have caused this result since viability was lost both from spraying alone and even more so by spraying during e-PEUU fabrication. Decreased viability from cell aerosol spraying has been reported by others and found to depend largely on nozzle diameter, spray pressure, and solution viscosity [139]. Therefore, cells were also sprayed from media supplemented with gelatin to increase viscosity and help protect the cells from mechanical and chemical stresses. Viability was recovered yet the mechanical integrity of the PEUU matrices was disrupted because of gelation within the fiber network.

In contrast to pressurized spraying, electrospraying cells did not affect cell viability or proliferation. This result was significant since it was expected that the high voltage would cause some disruption or permeabilization of the cell membrane similar to electroporation. With electroporation, when an electric field external to the cell surpasses the cell membrane

capacitance, a reversible membrane permeabilization occurs [140]. This technique is exploited as a means to deliver drugs and genes to cells. Initial viability reports with trypan blue and propidium iodide staining indicated intact cell membranes after electrospraying. Therefore, the cell membranes do not appear to be permanently comprised as an effect of electrospraying. In fact, these results were consistent with reports by others that cells can survive exposure to the high voltage electric fields of electrospraying [138, 141]. Even in the presence of PEUU electrospinning, SMC electrospraying viability was not reduced, perhaps because the positively charged electrospinning and electrospraying streams repelled each other and avoided exposing cells to solvent prior to deposition. Also, due to the relatively large electrospinning distance of 23-cm, PEUU fibers were likely free of solvent by the time they were deposited. Electrospraying from media supplemented with gelatin resulted in reduced construct mechanical properties such that electrospraying from media alone was the preferred cellular incorporation method.

### 6.3.3 Microintegration

Initial attempts to microintegrate SMCs into electrospun PEUU consisted of side-by-side electrospraying and electrospinning capillaries and a flat conductive target moving on an x-y stage **(Figure 6-1 (a))**. This technique yielded an approximately 100 μm thick construct after 45 min of fabrication. However, the area of electrospraying and electrospinning stream convergence was relatively small such that non-uniformity of cellular integration was an issue. This effect was most likely due to a stream repulsion effect from Coulombic forces [118].

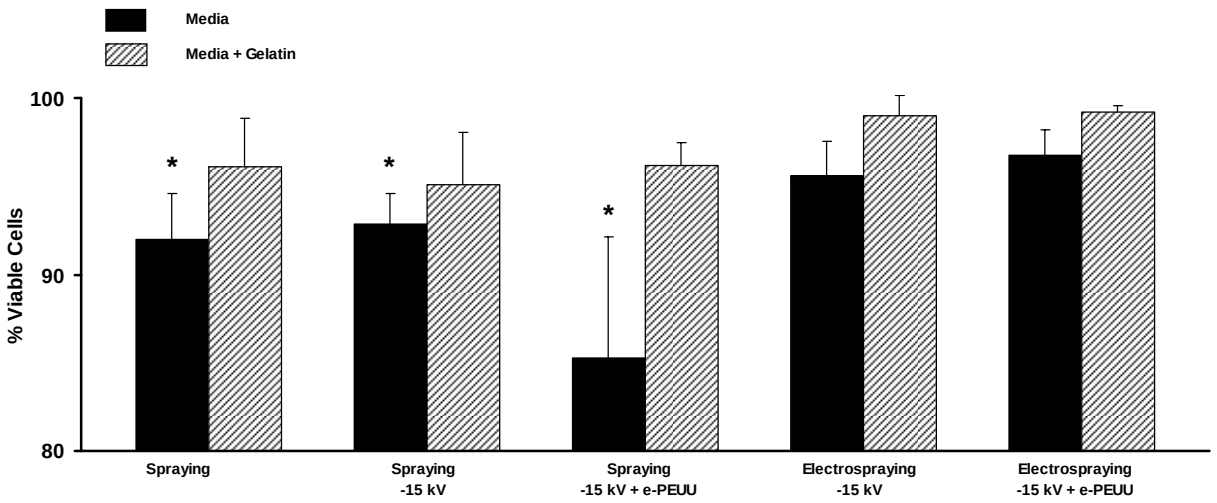


**Figure 6-3.** Trypan blue staining results for SMC viability after various processing treatments. (Spraying = SMCs sprayed from spray nozzle, Spraying -15 kV = SMCs sprayed from spray nozzle onto -15 kV charged target, Spraying -15 kV + e-PEUU = SMCs sprayed from spray nozzle onto -15 kV charged target during PEUU electrospinning, Electrospraying -15kV = SMCs electrosprayed at 10kV onto -15 kV charged target, Electrospraying -15 kV + e-PEUU = SMCs electrosprayed SMCs electrosprayed at 10kV onto -15kV charged target during PEUU electrospinning.

To limit charged stream interactions the apparatus was modified such that the nozzles were located perpendicular to one another and the target was a rotating mandrel translating on its axis **(Figure 6-1 (b))**. Since the electrospun polymer and electrosprayed SMC streams were arriving from different directions stream repulsion was minimized and the combination of rotation and translation of the mandrel target induced component mixing even further. This electrospinning nozzle and target configuration may find other applications as a means to fabricate more uniform composite scaffolds by electrospinning multiple materials or introducing drug laden microspheres between fibers. SMC microintegration using this configuration allowed fabrication of approximately 5-cm by 5-cm construct sheets of thickness ranging from 300-500 μm as shown in **Figure 6-1(c)**. Scaffold thickness could be controlled by adjusting polymer feedrate or fabrication time. In addition, a more uniform cellular integration was qualitatively visible by observing the overlap of the electrosprayed media and electrospun fibers.

### 6.3.4 SMC growth and morphology

SMC growth in thin constructs fabricated as in **Figure 6-1 (a)** is summarized in **Figure. 6-4 (a)**. Cell numbers for both sample types increased significantly from 1 day until 1 week in static culture ($p < 0.05$). SMCs on TCPS increased approximately 40% from 1 day until 1 week while those integrated in electrospun PEUU increased by 122% during this period. Fluorescent imaging of SMC microintegrated PEUU indicated that cells remained spherical in shape at 1 h but exhibited a spread morphology after 1 day of static culture with little or no presence of apoptotic cells **(Figure 6-5).** SEM micrographs of fixed samples at 1 week exhibited confluent cellular layers present beneath sub-micron diameter PEUU fibers as shown in **Figure 6-6.**

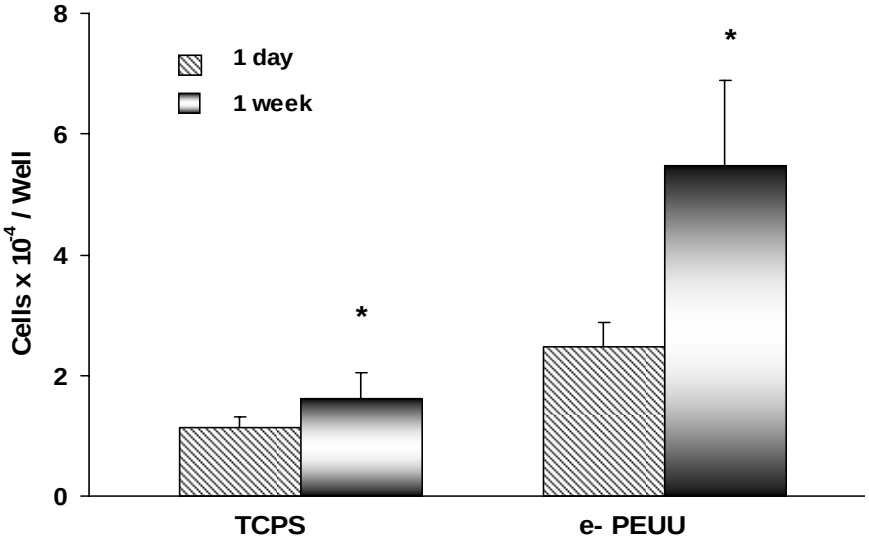


**Figure 6-4.** Cell growth in thin SMC microintegrated e-PEUU constructs fabricated on a flat target versus TCPS over 1 week in static culture. (* $p < 0.05$ increase from 1 day to 1 week)

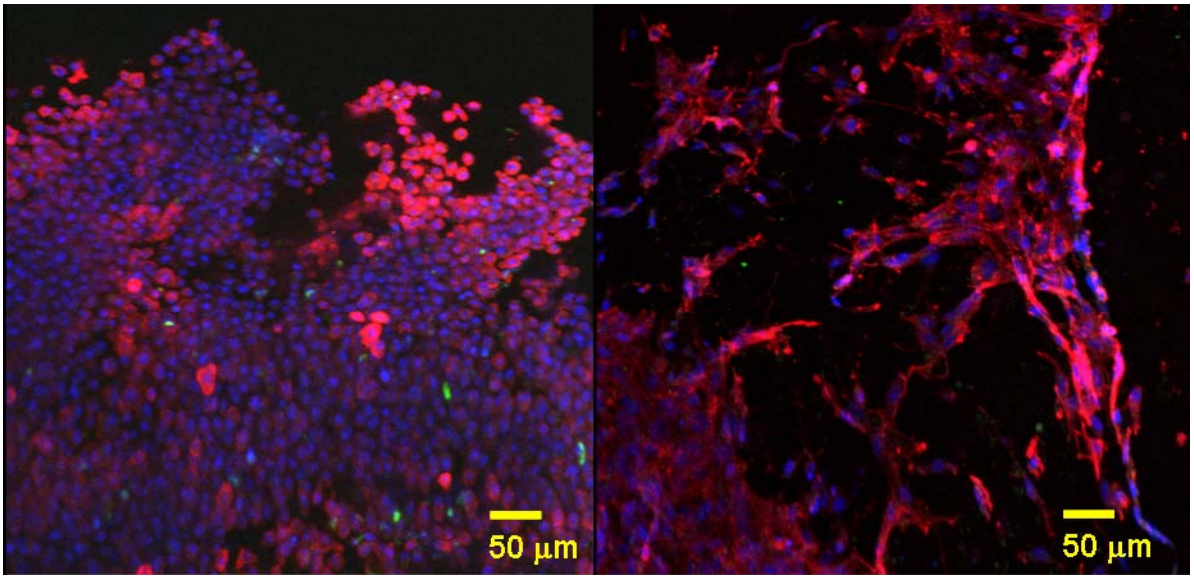


**Figure 6-5.** Confocal imaging of SMC integrated thin PEUU constructs immediately after fabrication (left panel) and 1 day after static culture (right panel). (red = f-actin, blue = nuclei, and green = apoptotic cells)

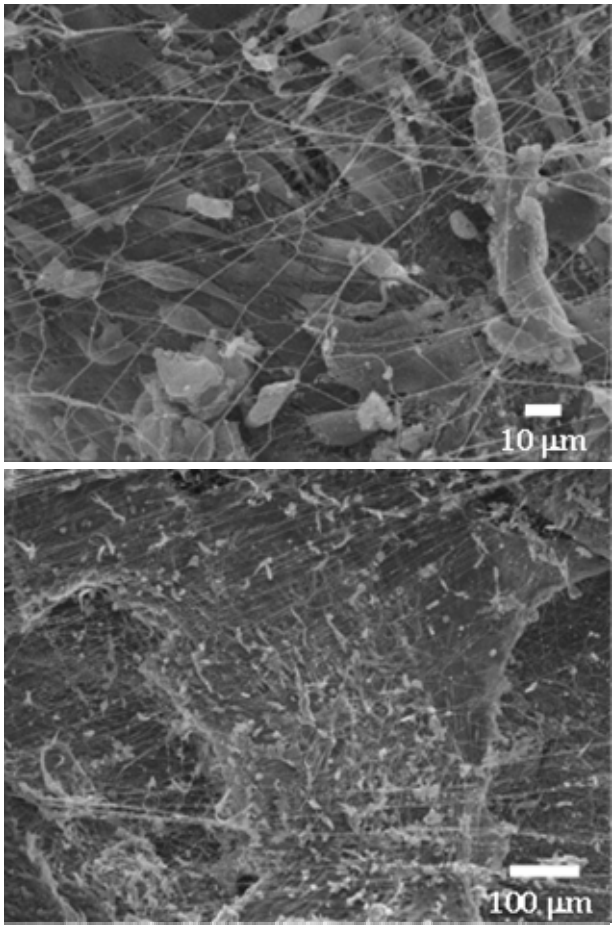


**Figure 6-6.** Representative electron micrographs of thin flat sheet SMC microintegrated samples after 1 wk of static culture.

When thicker SMC microintegrated PEUU scaffolds were submitted to this same static culture method, cells did not proliferate within the construct interior. This effect was attributed to poor exchange of nutrients, waste, and oxygen due to diffusional limitations. Also, cells that followed apoptotic or necrotic pathways remaining in the matrix could detrimentally affect the viability of neighboring healthy cells. Thus, a transmural perfusion bioreactor was constructed to allow for increased convective and diffusive transport. This bioreactor was adapted from a report by Radisic et al. who engineered contractile cardiac tissue by exposing neonatal cardiomyocytes seeded into collagen sponges to perfusion culture [133]. We hypothesized that this type of culture system would encourage SMC proliferation in our microintegrated constructs and the elastomeric fibers would help retain adherent cells during flow.

Initial SMC densities in thicker microintegrated PEUU constructs fabricated as in **Figure 6-1 (b)** and **(c)** are presented in **Figure 6-7 (a).** Cell numbers as measured by MTT immediately after construct fabrication ranged from $8.9 \times 10^4$ to $1.6 \times 10^5$ cells / well as a function of position. Although no statistically significant difference was found in cell number with position, constructs were trimmed of 1.5-cm from each edge of the mandrel axis prior to further study. Cellular growth over one week with static or perfusion culture is summarized in **Figure 6-7 (b)**. No significant differences in SMC number was found between days 1, 4 or 7 in static culture. However, for samples cultured under transmural perfusion, significantly higher SMC numbers were measured at day 4 and day 7 relative to day 1 ($p < 0.05$). These results translate to a 131% and 98% increase in cellular density for perfusion culture versus static culture at day 4 and day 7 respectively.

A representative confocal fluorescent image of cellular morphology within the thicker PEUU fabricated constructs after 1 day of static culture is shown in **Figure 6-8 (a)**. SMCs

appeared spread and healthy as well as uniformly distributed within the scaffold. In addition, constructs cultured under perfusion exhibited high numbers of spread, healthy appearing cells uniformly located throughout the samples as demonstrated in representative images of **Figure 6-8 (b, c, d)**. With perfusion, SMCs were found distributed in greater abundance throughout the fiber matrix as well as deeper beneath the fibers. However, at days 4 and 7 of static culture, as displayed representatively in **Figure 6-8 (e) and (g)**, the SMCs appeared less abundant as well as exhibited less f-actin staining. Patches of higher cell densities were found at both days 4 and 7 of static culture near the construct surface and not deeper in the fiber network as shown in **Figure 6-8 (f) and (h)**. The morphology of SMCs at day 7 of static culture did improve slightly in appearance in comparison with day 4.

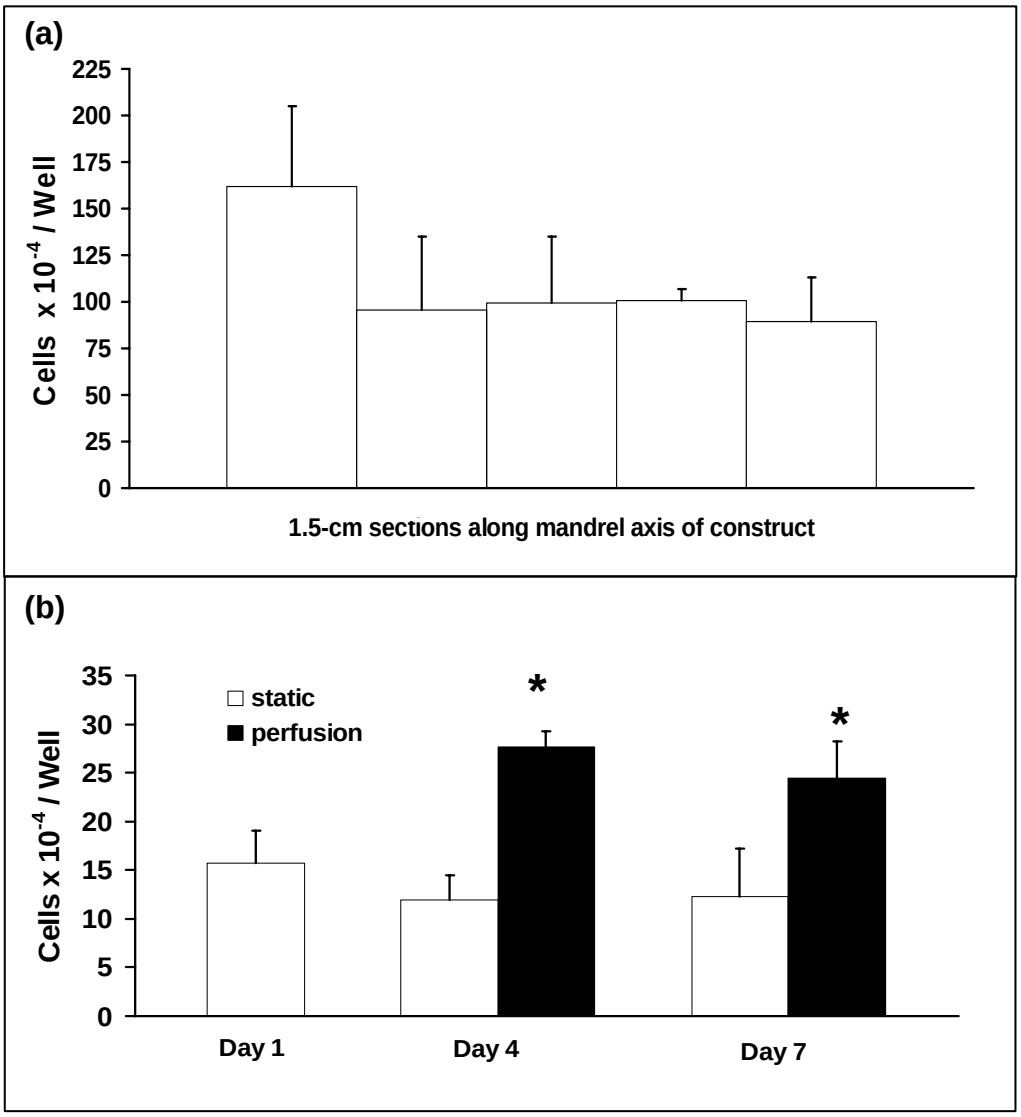


**Figure 6-7**. (a) Initial cellular uniformity in SMC microintegrated e-PEUU fabricated on a mandrel target. (b) Cell growth in thick SMC microintegrated e-PEUU constructs with static versus perfusion culture. Perfusion was initiated after 1 day in static culture. (* $p < 0.05$ increase with perfusion versus static culture)

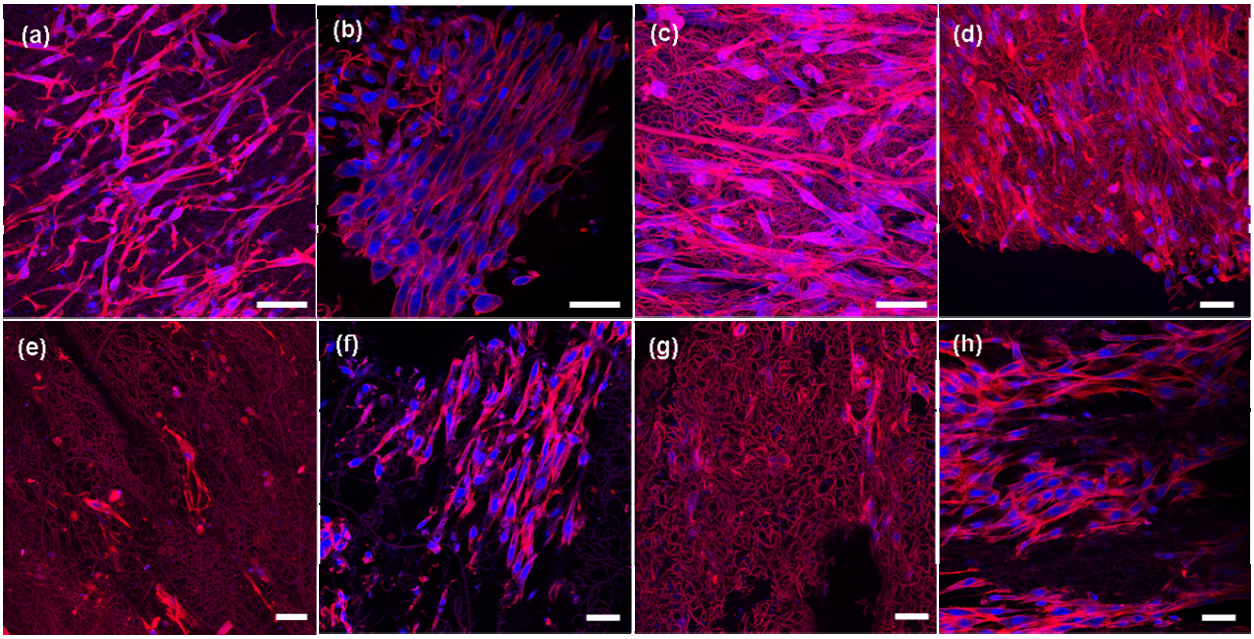


**Figure 6-8.** Fluorescent micrographs of SMC microintegrated e-PEUU constructs after one day of static culture (a), day 4 of perfusion culture (b), day 4 of perfusion culture (c), day 7 of perfusion culture (d), day 4 of static culture (e), high cell number surface image of day 4 of static culture (f), day 7 of static culture (g), and day 7 of static culture (h). (scale bar = 40 μm, red = f-actin and e-PEUU, blue = nuclei).

Hematoxylin and eosin stains of PEUU construct cross-sections in **Figure 6-9** further illustrated the trend of higher cellular density achieved with perfusion culture. One can observe high numbers of layered cells after 1 day of static culture in **Figure 6-9 (a, d)**. Yet, after 4 days of static culture, the cells appear less spread and healthy in **Figure 6-9 (b, e)**. High densities of SMCs microintegrated within the elastomeric fiber network can be observed in **Figure 6-9 (c, f)** after 4 days of perfusion culture**.**

As a result of the electrospinning set-up that we employed it was possible to induce fiber orientation to influence the cells to organize themselves in an aligned manner. SMCs within the PEUU elastomeric fiber matrices qualitatively exhibited an aligned morphology, as seen in **Figure 6-8 (b)** for instance**.** The estimated shear stress to which the SMCs integrated into e-PEUU matrices (at approximately 80% porosity) were exposed in perfusion culture was on the

order of 1 dyne/cm$^2$ [142]. This shear stress is relatively low and would not be expected to significantly influence cell morphology or decrease viability [143]. We observed SMC orientation to be parallel to the direction of scaffold fiber orientation instead of aligned with the perfusion flow direction.

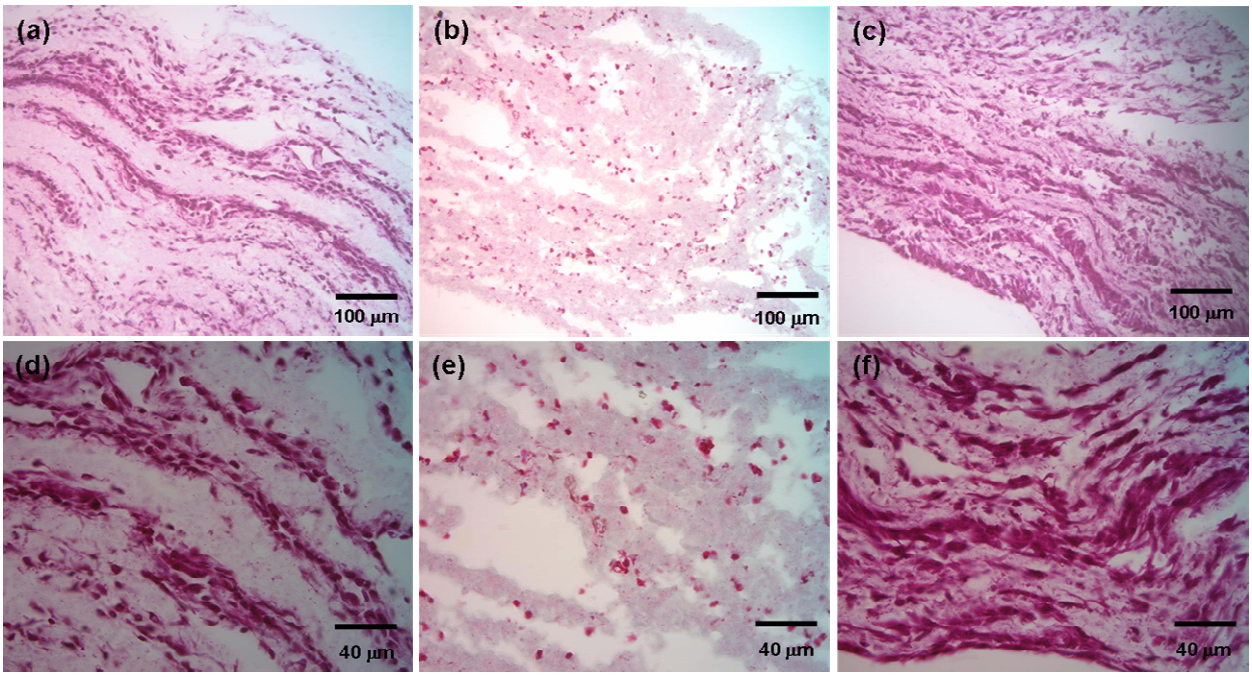


**Figure 6-9.** Hematoxylin and eosin stained sections of SMC microintegrated e-PEUU constructs after one day of static culture (a, c), day 4 of static culture (b, e), and day 4 of perfusion culture (c, f).

Cell alignment seemed even more qualitatively pronounced in the SMC microintegrated PEUU/collagen (75/25) samples. One can observe the high numbers of microintegrated cells after 1 days of static culture in **Figure 6-10 (a)**. The cells are in high density but do not appear very spread or elongated. This may be due to cells aligning themselves into the plane of the image. For example, when observing the SMCs integrated into electrospun PEUU/collagen after

13 days of perfusion culture (0.5 mL/min) one can observe the same cell morphology in **Figure 6-10 (c)**. However, whenever the sample is sectioned along its other axis (preferred direction of fiber alignment), one can observe high numbers of elongated SMCs aligned with this material axis in **Figure 6-10 (d)**. Also, near the surface of the SMC microintegrated PEUU/collagen are aligned at 14 days after fabrication as well **(Figure 6-10 (b))**.

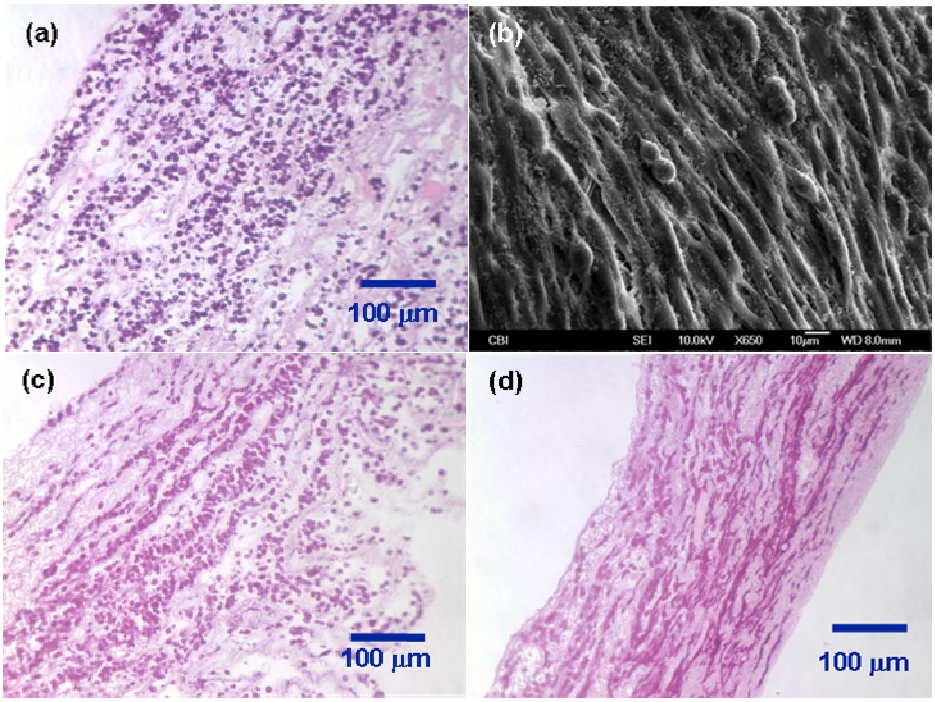


**Figure 6-10.** H&E staining or SEM of SMC microintegrated PEUU/collagen (75/25). (a) SMCs are aligned into the plane of the sample after 1 day of static culture. (b) SEM illustrates SMC alignment near the surface of PEUU/collagen after 13 days of perfusion culture (scale bar = 10 µm). (c) H&E stain after 13 days of perfusion culture indicating cells aligned into the plane of the image. (d) H&E stain after 13 days of perfusion culture indicating high density cell alignment. Note that perfusion was initiated at 0.5 mL/min after 1 day of static culture.

### 6.3.5 Mechanical Properties

Tensile mechanical properties of SMC microintegrated PEUU and PEUU/collagen (75/25) measured immediately after fabrication are summarized in **Table 6-1** and compared with electrospun PEUU. Electrospun PEUU (e-PEUU) was found to retain much of the mechanical strength and flexibility of the cast film (reported in Chapter 2.0). SMC microintegrated PEUU was found to retain a portion of the mechanical strength and distensibility of e-PEUU, with lower tensile strengths and higher breaking strains. SMC microintegrated PEUU/collagen possessed even lower values for these parameters. These results may be due to microintegrated SMCs and media disrupting the PEUU fiber network and replacing elastic fiber volume with cellular volume. Yet, the measured properties are still more than sufficient for the SMC microintegrated PEUU or PEUU/collagen to serve as support structures for soft tissue growth and mechanical training.

As a result of the fabrication process, SMC microintegrated PEUU and PEUU/collagen were found to have tensile properties that differed as a function of the material axis. The axis orientated with the mandrel axis (preferred axis) possessed a significantly higher tensile strength and 100% modulus and a lower breaking strain than the axis orientated with the circumference of the mandrel (cross-preferred axis) ($p < 0.05$). Some degree of fiber alignment in the matrices was induced by a combination of the stage translation speed of 8 cm/s and the mandrel length to diameter ratio of 8. It was believed that this ratio provided more opportunity for the fibers to deposit parallel to the mandrel axis. Since the mandrel rotation velocity was less (3 cm/s at 200 rpm) than the translation speed, it was not expected to greatly influence fiber alignment. As would be expected, the preferred fiber axis possessed a higher tensile strength and lower breaking strain from a more direct influence on the stretching of the fibrous microstructure of the

PEUU. The cross-preferred material axis would be expected to allow more elongation at lower stresses since the mechanical properties would be more influenced by PEUU fiber bending than stretching. By manipulating mandrel rotation and translation rates it should be possible to alter the direction and degree of construct anisotropy. This inherent construct anisotropy and fiber orientation appeared to induce the previously mentioned SMC alignment within the matrices.

**Table 6-1.** Tensile properties of SMC microintegrated PEUU and PEUU/collagen blends.

| Sample | Initial Modulus (MPa) | 100% Modulus (MPa) | Tensile Strength (MPa) | Breaking Strain (%) |
|---|---|---|---|---|
| e-PEUU (random) | 2.5 ± 1.2 | 2.8 ± 1.1 | 7.8 ± 2.3 | 280 ± 40 |
| μSMC-e-PEUU (preferred) | 1.7 ± 0.2 | 1.4 ± 0.2 | 6.5 ± 1.6 | 850 ± 200 |
| μSMC-e-PEUU (cross-preferred) | - | 0.3 ± 0.1 | 2.0 ± 0.5 | 1700 ± 100 |
| μSMC-e-PEUU/collagen (75/25) (preferred) | - | - | 3.9 ± 0.9 | 160 ± 40 |
| μSMC-e-PEUU/collagen (75/25) (cross-prefer) | - | - | 0.7 ± 0.1 | 170 ± 40 |

e = electrospun scaffold; μSMC = SMC microintegrated

### 6.3.6 MDSC microintegration, culture and characterization

Using identical processing conditions as described above for SMC microintegration, MDSCs were microintegrated into electrospun PEUU at high density. These constructs were also mechanically thick and robust with an almost identical appearance to SMC integrated constructs. These MDSC samples were also subjected to one day of static culture and then 5 days of perfusion culture. MTT data indicated viable cells present 1 day after fabrication **(Figure 6-11)**. Significantly higher cell numbers were present at day 3 and day 6 after fabrication with both static and perfusion samples compared with day 1 ($p < 0.05$). These values were different from

the trend seen with static culture of SMC microintegrated constructs that did not increase in cell number after 1 day. These results may have been due to the more highly proliferative nature of the MDSCs. In addition, significantly higher cell numbers were observed with perfusion culture in comparison to static culture. This trend was consistent with that observed with SMC culture under perfusion. MTT results were summarized in **Figure 6-11**.

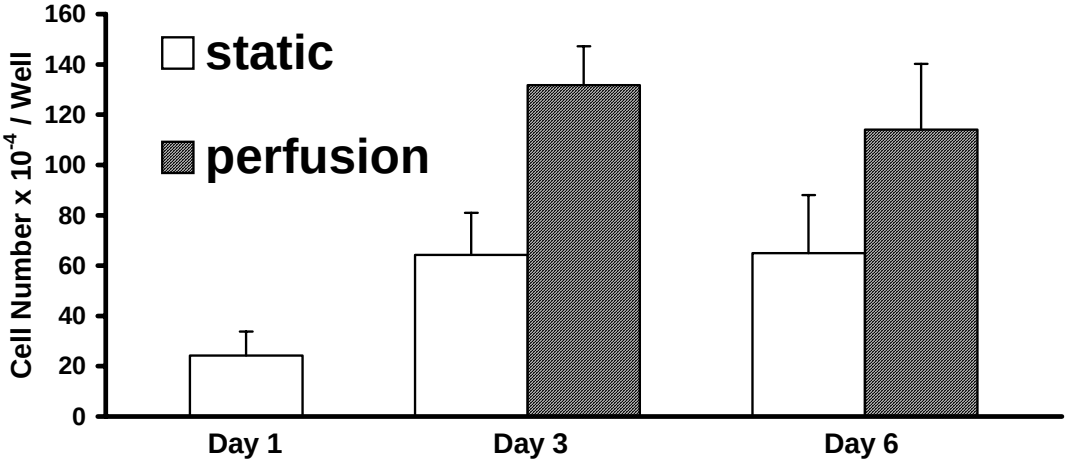


**Figure 6-11.** MTT data for MDSC microintegrated PEUU after 6 days of culture. Samples were cultured statically for 1 day and then subjected to either perfusion (0.5 mL/min) or static culture for an additional 5 days.

Confocal micrographs taken after 5 days of perfusion culture indicated a high density of aligned cells within the MDSC microintegrated construct **(Figure 6-12 (a))**. These samples appeared even higher in cell density than the SMC microintegrated confocal micrographs after 6 days of perfusion culture. This image together with the relative values for cell numbers from the MTT data for both MDSC and SMC microintegrated constructs **(Figures 6-7** and **6-11)** generally

indicated a higher proliferative capacity for the MDSCs. Masson's Trichrome stained samples from 5 days of MDSC perfusion culture indicated production within the elastomeric PEUU fiber network **(Figure 6-12 (b))**.

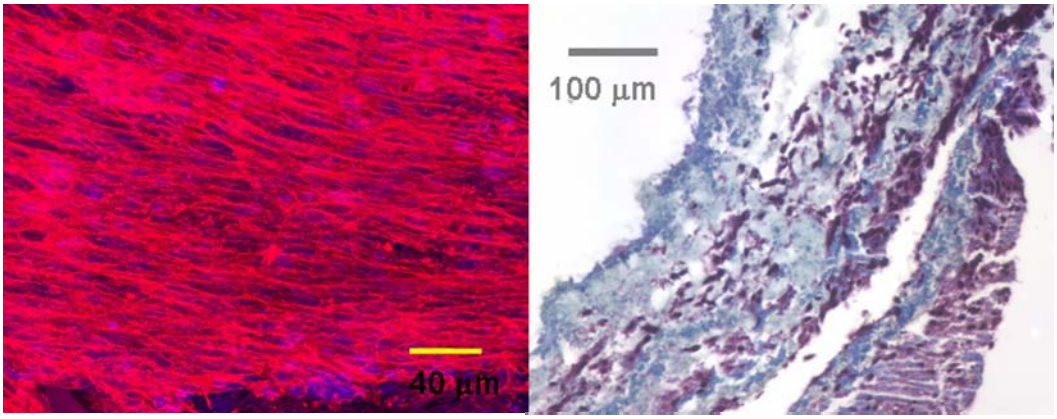


**Figure 6-12.** (Left panel) Confocal micrograph of MDSC microintegrated PEUU demonstrating high density of aligned cells (red = f-actin, blue = nuclei, scale bar = 40 µm). (Right panel) Masson's Trichrome stained MDSC sample indicating collagen production. Both samples are after 5 days of perfusion culture at 0.5 mL/min.

### 6.3.7 EPC microintegration, culture and characterization

Using identical processing conditions as described above for SMC microintegration, EPCs were microintegrated into electrospun PEUU. These constructs were also mechanically robust and possessed a similar appearance to SMC integrated constructs. These EPC samples were subjected to one day of static culture and then 3 days of perfusion culture at 0.5 mL/min. MTT data indicated viable cells present for both static and perfusion culture 4 days after fabrication

**(Figure 6-13 (a))**. Spread EPCs were observed in confocal micrographs after 4 days of static culture and perfusion culture **(Figure 6-13 (b, c))**. However, **Figure 6-13 (c)** is representative of higher numbers of cells located deeper within the EPC microintegrated fiber networks after perfusion.

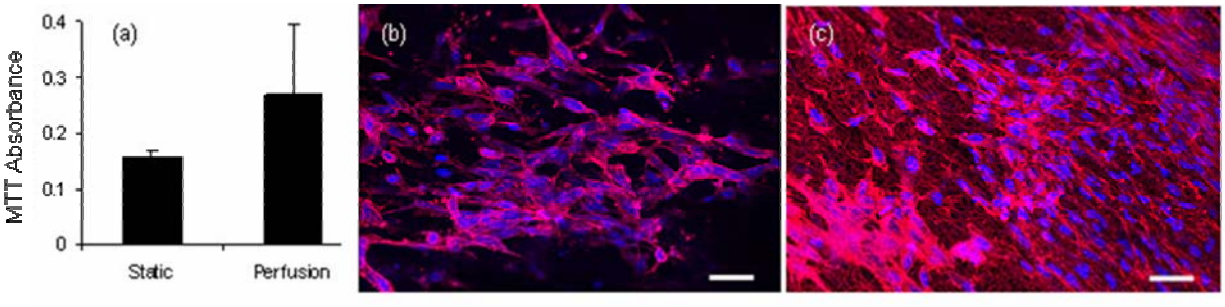


**Figure 6-13.** Microintegrated EPC viability. (a) MTT results after 3 days of static or perfusion culture. (b) Confocal micrograph of day 4 static culture sample. (c) Confocal micrograph of day 4 perfusion sample.

The relatively rapid creation of a hybrid tissue engineered construct that is primarily cellular and reinforced with an elastomeric fiber matrix, may offer a meaningful advancement over current tissue engineering approaches. The advantage of high cell densities achieved over short time periods could facilitate the development of functional connections between cells and provide a construct with appropriate cellularity and mechanical properties for soft tissue replacement. The ability to incorporate anisotropy to direct cell morphology is important in both forming functional tissue and mimicking the biomechanics of native aligned tissue structures. This technique might find future application in the engineering of tubular structures, such as a tissue engineered blood vessel, and sheets of elastic tissues for other soft tissue replacement needs.

# 7.0 CONTROLLED RELEASE NANOFIBER MATRICES FOR FASCIA AND ABDOMINAL REPAIR

## 7.1 INTRODUCTION

Trauma to the extremities, including fracture, crush injury, and vascular damage can lead to the morbidity and mortality associated with compartment syndrome. Compartment syndrome results when rising interstitial pressure in a compartment overwhelms capillary perfusion pressure. The result is tissue hypoxia, which can lead to further increases in vascular wall permeability, and thus a cycle of further elevations in compartmental pressure and vascular stasis. Untreated, compartment syndrome can lead to tissue necrosis and permanent loss of function, and, in severe cases, can trigger multi-organ failure and death. The preferred treatment method for compartment syndrome of the extremities is fasciotomy, wherein the compartmental pressure is "released", at the expense of an open injury. In a field setting, fasciotomy may be done prophylactically when careful monitoring and management of the patient may not be practical. However, an obvious concern with fasciotomy, particularly in a setting where the surgical field may readily become contaminated or where there are other wounds, is infection. In considering the temporary closure fasciotomy procedure for compartment syndrome and a follow-up treatment that would be both desirable and practical, it is the central hypothesis of this study that

there would exist value in developing a scaffold patch for abdominal wall repair fasciotomy coverage that would:

- serve as a selective barrier to the external environment, while still allowing adequate gas transfer,
- possess superior surgical handling characteristics compatible with rapid sizing and placement,
- be flexible, to allow distension of the patch over the field, thus allowing for further expansion of the field without transferring this complete force to the surrounding fascia, and while maintaining the barrier function,
- be capable of being loaded with antibiotics, for controlled release to the wound bed to control the infection risk,
- be capable of being loaded with drugs and/or growth factors, for controlled release to the wound bed to facilitate tissue healing and angiogenesis,
- be biodegradable, so that no permanent foreign body exists and so that subsequent barrier removal is not required and it could avoid enteric fistula and persistent infection frequently caused by using non-biodegradable materials.

In an effort to meet such requirements, the development of a thin, microporous elastic sheet with high tensile strength and distensibility made from a biodegradable poly(ester urethane)urea (PEUU) loaded with the angiogenic basic fibroblast growth factor (bFGF) or the antibiotic, tetracycline, and processed with electrospinning is reported. bFGF loaded scaffolds were evaluated for their morphology, tensile properties, bFGF release and bioactivity, cell

adhesiveness, and preliminary subcutaneous implantation response. Tetracycline loaded scaffolds were characterized for their morphology, drug release, antimicrobial ability, and tensile properties.

## 7.2 BASIC FIBROBLAST GROWTH FACTOR DELIVERY FROM NANOFIBER MATRICES

### 7.2.1 Methods

#### 7.2.1.1 bFGF loading and scaffold fabrication

PEUU was synthesized from polycaprolactone diol and 1,4-diisocyanatobutane with chain extension by putrescine as previously reported [15]. bFGF with 100:1 bovine serum albumin (BSA, Sigma) to bFGF (human, Peprotech) was dissolved in PBS, frozen and subsequently lyophilized. For radiolabeled release studies, a small quantity of I-125 labeled bFGF (Perkin Elmer) was also added to this solution with the ratio of BSA:bFGF remaining 100:1. PEUU was then dissolved with BSA:bFGF under mechanical stirring to make a 6 wt% PEUU solution in hexafluoroisopropanol (HFIP) at 1000 ng bFGF / mg PEUU. After solubilization the solution was loaded into a 10mL polypropylene syringe and electrospun over a 15-cm distance using a 1.0 mL/min solution flowrate and by charging the polymer/BSA/bFGF solution at 10kV and an aluminum disc target at -10kV in a manner similar to that previously reported [1]. The target was also attached to an x-y stage translating in a square pattern of 5 cm step distances to produce scaffolds of uniform thickness. Scanning electron microscopy (SEM) was utilized to characterize fiber morphologies and tensile testing was used to characterize mechanical properties as described previously.

#### 7.2.1.2 bFGF release and mitogenicity

Pre-weighed strips of bFGF loaded electrospun PEUU were incubated in DMEM with 0.5% fetal bovine serum and 1% penicillin /streptomycin at 37°C for bFGF release studies. Radiolabelled release over time was quantified with a gamma counter by measuring the scaffold activity at each timepoint. Release medium at various timepoints over 4 wks was removed and frozen until analyzed. A bFGF immunoassay (R&D Systems) was used to quantify bFGF concentration in the release medium. This ELISA procedure was performed as follows:

Frozen bFGF release media was thawed in a water batch and then 100 μL of medium added to 100 μL of a protein buffered blue dye (diluent RD1-43) in each well of a 96-well custom assay plate. This plate was covered with an adhesive strip and incubated for 2 h at room temperature. After 2 h, sample wells were aspirated and rinsed four times with wash buffer, blotted dry and then 200 μL of mouse monoclonal antibody against FGF basic conjugated to horseradish peroxidase (FGF basic Conjugate) was added to each well. The plate was again covered with an adhesive strip and incubated for 2 h at room temperature. After 2h, sample wells were again aspirated, washed four times with wash buffer, and blotted dry. Equal volumes of stabilized hydrogen peroxide (Color Reagent A) and chromogen (tetramethylbenzidine, Color Reagent B) were mixed and 200 μL added to each well in the dark. After 30 min, 50 μL of 2 *N* sulfuric acid was added as a stop solution. Optical density was measured on a plate reader at 450 nm with a 570 nm reference filter. Calibration of absorbance to bFGF concentration was performed with known standards.

Released bFGF bioactivity was measured by mitogenic assay. Briefly, rat vascular smooth muscle cells (SMCs) were seeded at 200 μL of 1.5 x $10^5$ cells/mL in each well of a 96-well plate. Medium was replaced at 4 h with the appropriate bFGF containing degradation

medium and cell number was measured 48 h later using the MTT mitochondrial activity assay. For cell adhesion studies, SMCs were seeded onto sheets at a density of 2.0 x $10^5$ cells/mL and cell adhesion was quantified 1 day after seeding using MTT.

#### 7.2.1.3 Rat hindlimb implantation

As a preliminary investigation into the *in vivo* behavior of electrospun PEUU and bFGF loaded electrospun PEUU, samples were implanted in the rat hindlimb in 10 wk old female Lewis rats. All animals were treated humanely according to an approved IUCAC protocol. Rats were anesthetized with an intramuscular injection of ketamine hydrochloride (22 mg/kg), followed by an intraperitoneal injection of sodium pentobarbital (30 mg/kg). The rats were then endotracheally intubated and mechanically ventilated with a small animal respirator (Harvard) at a frequency of 60-70 breaths/min. Tidal volume was set at 0.6 to 2.0 mL depending on the body weight of the rat. The rat was placed on a warming pad (37°C) in the supine position. The hair on the hind limb was trimmed with an electrical clipper. The skin leads for electrocardiography were attached to both fore-limbs on the left hind limb and the electrocardiogram was monitored. Before skin incision, one dose of cefuroxime antibiotic (100 mg/kg) was administered intramuscularly for prophylaxis of surgical infection.

The skin of the left hindlimb was then sterilized with providone-iodine solution. All surgeries were performed using aseptic techniques with sterile instruments. 6-mm diameter electrospun PEUU or bFGF loaded PEUU patches were placed underneath the skin and sutured to the exposed gastrocnemius muscle of the hindlimb using a non-absorbable suture. The skin was then closed with 4-0 Vicryl suture and the rats were observed in the surgical suite until fully recovered from the anesthesia. The first 3 days after surgery, buprenorpine (1 mg/kg) as

analgesic and cefuroxime (100 mg/kg) as antibiotic was administered intramuscularly twice daily.

Rats were sacrificed with an overdose of pentobarbital (100 mg/kg) at 4 wks and 12 wks after implantation and the patches explanted. Samples were fixed in 2% paraformaldehyde for 2 h, 30% sucrose overnight, and then frozen at -80°C in 2-methylpentane prior to histology. The healing response was evaluated by standard cellular and matrix staining (Hematoxylin and Eosin, Masson's Trichrome) and immunofluorescent labeling of endothelial markers (anti-CD31, anti-vWF) and smooth muscle α-actin for assessment of vascularity. Blood vessels were quantified by the number per field. The inflammatory response was scored in a blinded manner.

### 7.2.2 Results

#### 7.2.2.1 Scaffold characterization

Electrospun sheets of PEUU and PEUU with bFGF consisted of continuous, bead-free sub-micron diameter fibers as observed by SEM in **Figure 7-1**. Furthermore, no significant difference in tensile properties was found between PEUU and PEUU loaded with growth factor. Electrospun PEUU possessed a tensile strength of 11.4 ± 2.1 MPa and a breaking strain of 230 ± 40 %. bFGF loaded electrospun PEUU had a tensile strength of 12.1 ± 1.7 MPa and a breaking strain of 210 ± 30 %.

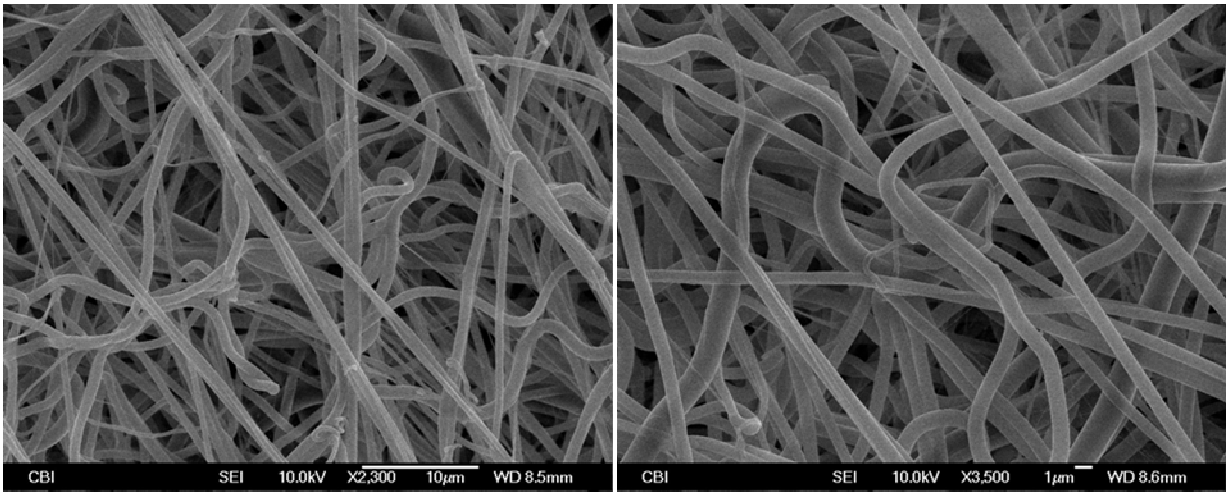


**Figure 7-1.** SEMs of bFGF loaded electrospun. No beads visible as a result of protein incorporation. (left scale bar = 10 μm, right scale bar = 1 μm)

### 7.2.2.2 bFGF release and mitogenicity

bFGF radiolabelled release from electrospun PEUU consisted of an initial 25% burst followed by slower release up to 50% by 3 wks **(Figure 7-2)**. These values were based on the total initial measurement of radiolabelled bFGF in the scaffolds. In contrast, ELISA demonstrated a higher initial burst release of approximately 75% of the 3 wk value of 200 ng bFGF **(Figure 7-3)**. When the ELISA values are converted to a percentage of total bFGF incorporated the total release by 4 wks was less than 10% of initial bFGF loaded. These values indicated that radiolabelled bFGF release was more indicative of either active or inactive (denatured) bFGF release. ELISA results, on the other hand, suggested that a substantial amount of growth factor may have lost bioactivity after scaffold processing.

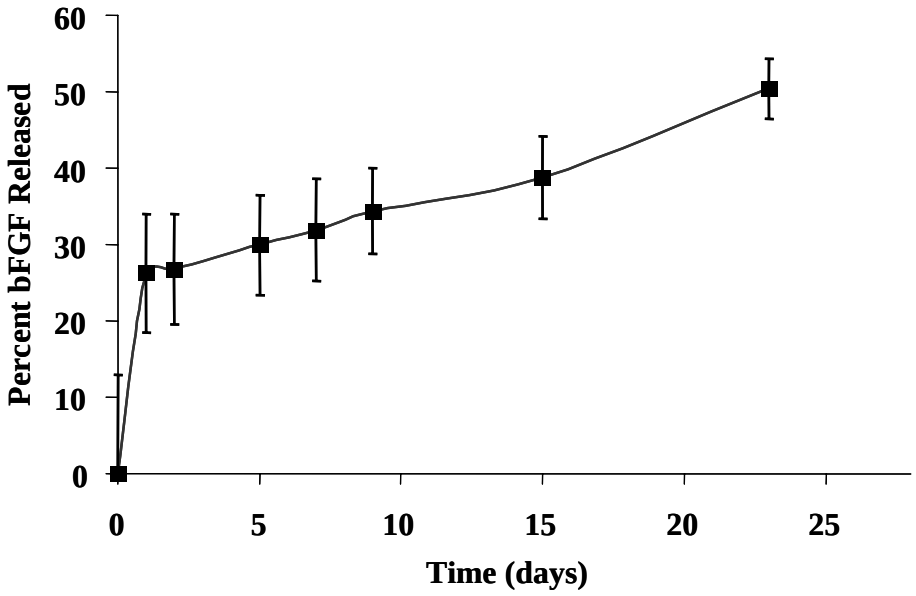


**Figure 7-2.** Release profile of I-125 radiolabelled bFGF from electrospun PEUU.

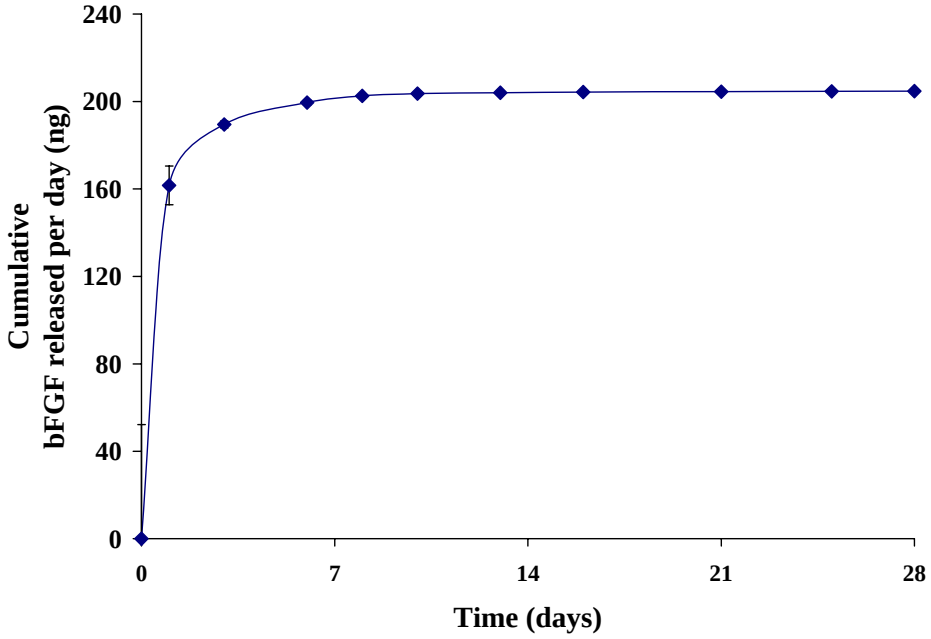


**Figure 7-3.** bFGF release profile for bFGF loaded electrospun PEUU scaffold degradation media as measured by ELISA.

Mitogenic SMC bioactivity assay was performed on bFGF release media from 2 wks of release and compared with that of controls consisting of electrospun PEUU, medium, and 1 ng/mg bFGF in medium. Results indicated a statistically similar SMC number or mitogenic effect between bFGF loaded PEUU release media from the 1st week and bFGF control **(Figure 7-4)**. Both values were significantly higher in relative cell number than either media control or electrospun PEUU control with values of 162 ± 17% medium for bFGF released from PEUU and 173 ± 30 for control bFGF ($p < 0.05$). At 2 wks of release, only the bFGF control was significantly larger than the relative cell number for the medium control. Also, a lower cell number was observed for the PEUU control relative to the medium control at 1 wk with no difference noted at 2 wks of release ($p < 0.05$) Cell adhesion values one day after seeding were evaluated by MTT assay to be 148 ± 5% of tissue culture polystyrene (TCPS) for PEUU loaded with bFGF. This value was significantly higher relative to adhesion on both TCPS and electrospun PEUU alone ($p<0.05$).

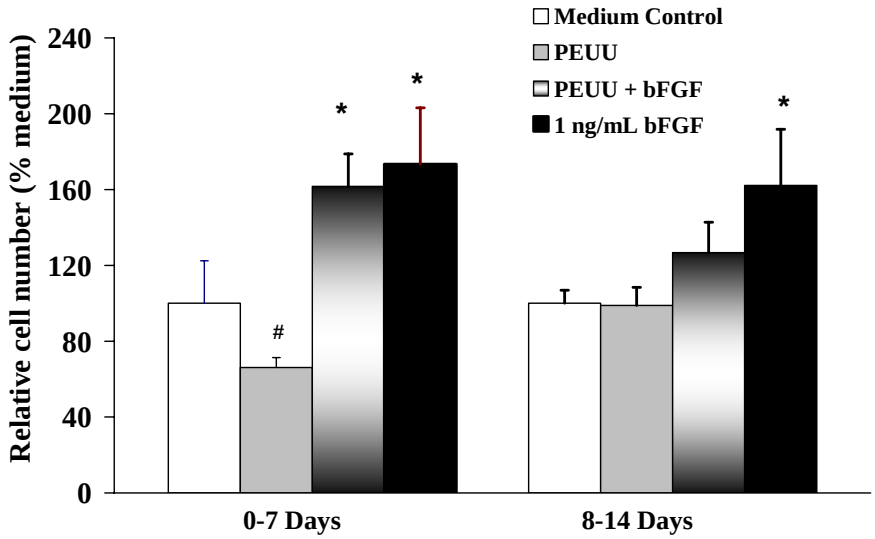


**Figure 7-4**. Released bFGF bioactivity at 1 and 2 wks using a SMC mitogenic assay with comparison to a 1 ng/mL bFGF control . (*$p < 0.05$ greater than medium control, #$p < 0.05$ less than medium control).

#### 7.2.2.3 Scaffold explantation and histology

A preliminary investigation into the *in vivo* response of bFGF loaded PEUU was conducted in a rat hindlimb model. Of particular interest was the ability of released growth factor to encourage cell proliferation and capillary formation. For this investigation, scaffold discs were sutured to the hindlimb muscle of the rat and explanted at 4 or 12 wks. The explants appearances at 12 wks are illustrated in **Figure 7-5**. Electrospun PEUU controls appeared to have a slightly yellow tint with some capillaries clearly visible across the scaffold surface **(Figure 7-5, left panels)**. In contrast, bFGF releasing PEUU were much redder in color possibly due to increased vascularization. These growth factor loaded patches also qualitatively were more adhered to the underlying muscle layer compared with electrospun PEUU controls. At explantation, degradation of both sample types did not seem to be substantial at either timepoint.

Histological analysis was utilized to qualitatively and quantitatively assess differences in capillary numbers present near the patch periphery. Representative images of 12 wk explants are shown in **Figure 7-6**. H&E stains of the electrospun PEUU control indicated an inflammatory response with the presence of macrophages, fibrous encapsulation and slow PEUU degradation at 12 wks (**Figure 7-6 (a)**). H&E staining of 12 wk explants of bFGF loaded PEUU showed slighter more degradation with PEUU fragments visible (**Figure 7-6 (b)**). Immunostaining of SMC α-actin and the endothelial marker, CD31, was also utilized to evaluate 12 wk explants. The electrospun PEUU control demonstrated little or sparse CD31 or SMC α-actin staining indicating little capillary formation (**Figure 7-6 (c)**). In contrast, bFGF releasing PEUU demonstrated rich capillary formation from the significantly higher number of CD31 and SMC α-actin visible (**Figure 7-6 (d)**). These capillaries were primarily located in the loose connective tissue near the patch but not in the muscle tissue.

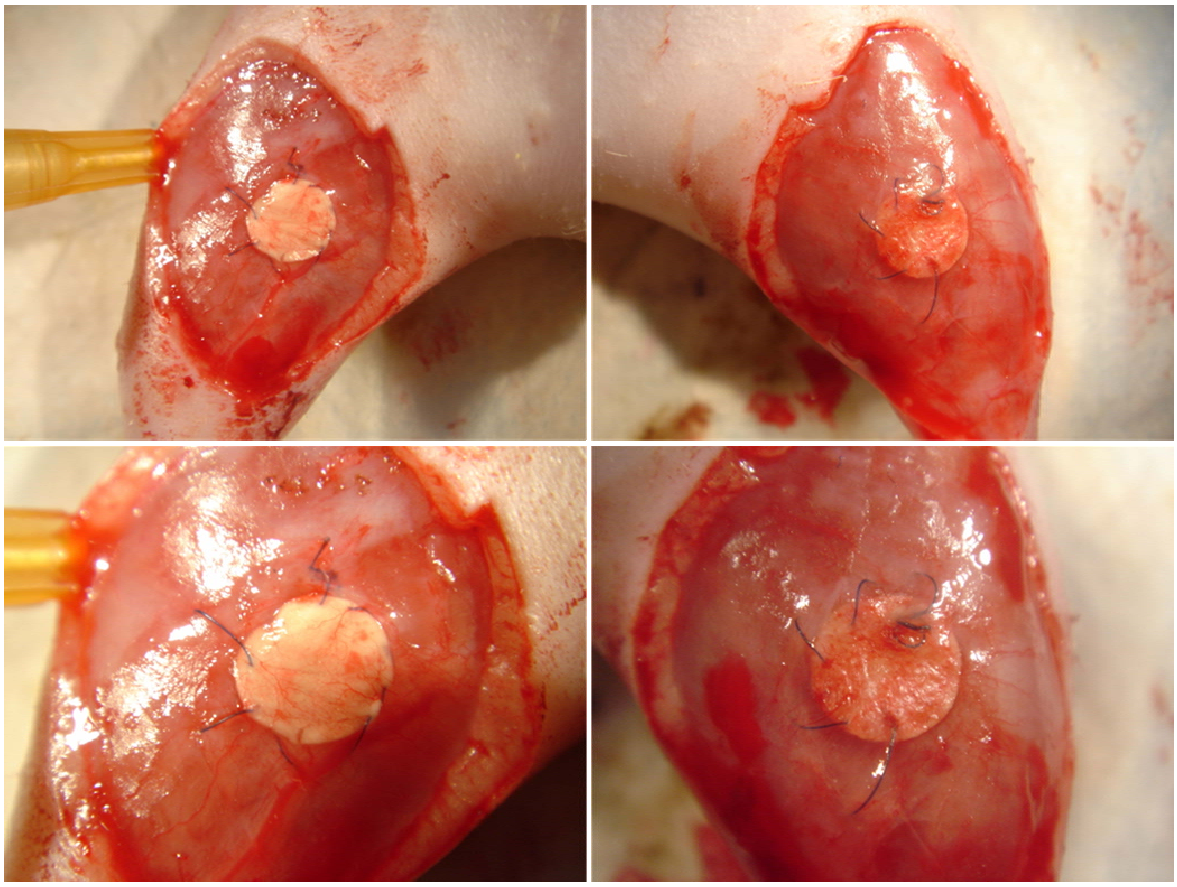

**Figure 7-5.** Appearance of electrospun patch explants at 12 wks. (left panels = PEUU control, right panels = bFGF loaded specimen)

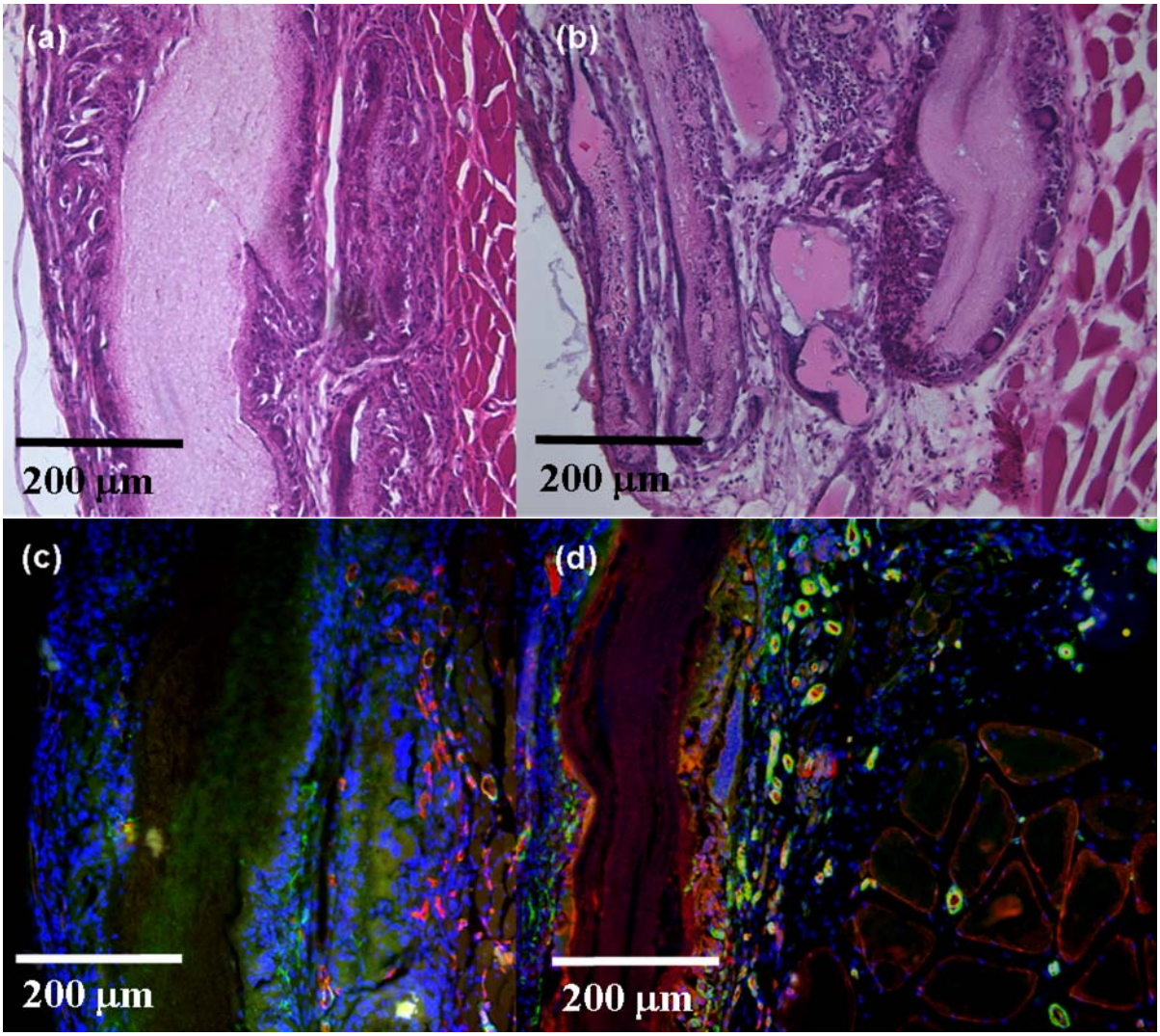


**Figure 7-6.** Representative histology of electrospun patch explants at 12 wks. (a) H&E stain of electrospun PEUU control exhibiting fibrous encapsulation. (b) H&E stain showing more apparent degradation and patch fragmentation of bFGF loaded PEUU. (c) Immunostaining of PEUU control indicating sparse capillary development. (d) Immunostaining of bFGF loaded PEUU with evidence of several capillaries in patch periphery. (green = SMC α-actin, blue = nuclei, and red = CD31, data courtesy of K.Fujimoto)

### 7.2.3 Discussion

For wound healing applications in which the underlying traumatized tissue will experience substantial volumetric changes due to edema, it would be attractive to have a barrier dressing that could be sutured to the healthy wound periphery, but readily distend and contract to meet the mechanical demands imposed by the underlying tissue. Controlled release of a growth factor to facilitate wound healing from this material could provide added benefit. In an effort to meet such requirements we report here on the development of a thin, microporous elastic sheet with high tensile strength made from a biodegradable poly(ester urethane)urea loaded with the angiogenic basic fibroblast growth factor and processed with electrospinning.

With the electrospinning technique it is possible to introduce proteins into the scaffold in several ways. The most straightforward technique is to electrospin a blended protein and polymer solution using a single-nozzle technique from a single syringe, as performed in this work. We have previously used this technique by combining collagen and poly(ester urethane)urea and have verified the retention of the secondary helical structure in collagen (Chapter 3.0) [115]. It was also demonstrated in Chapter 4.0 that UBM could be combined with PEUU and electrospun. When spinning these protein/polymer scaffolds we have found that the elastomeric mechanical properties reflect that of the synthetic PEUU even at low (20%) mass fractions of polymer [115].

Through the previous examples mentioned above bioactivity was introduced into a synthetic scaffold. However these methods incorporated large proteins or protein extracts that may perform a variety of functions. The objective of this work was to evaluate the ability to incorporate specific bioactive elements such as purified growth factors into the synthetic scaffold to induce a specific biological response. Therefore, basic fibroblast growth factor, bFGF, was examined since this factor has been demonstrated in numerous reports to induce angiogenesis in

a variety of tissue beds [144, 145]. We also possessed previous expertise in loading this factor in PEUU by a different processing method, thermally induced phase separation [146]. The release of this growth factor was shown to be well characterized by protein radiolabelling or ELISA and the resulting activity by a mitogenic cell growth assay.

The results of this work illustrated that bioactive bFGF could be released from electrospun PEUU for up to one week in medium. This bioactivity did result at the cost of some bFGF loss of activity. While this result was not ideal, it was also not entirely unexpected as the electrospinning processing solvent, HFIP, is known to be a strong hydrogen bond promoter and has been demonstrated to modify the secondary structures of proteins. In Chapter 3.0, it was discovered that by increasing protein load, some retention of protein secondary structure was evident [115]. Therefore, we utilized a relatively high bFGF load of 1000 ng bFGF to 1 mg PEUU. Furthermore, after subcutaneous implantation of the electrospun patches in a rat model, at 12 wks significantly higher numbers of rich capillaries were observed near the bFGF patch periphery in contrast to the PEUU control. This result further indicated retention of bFGF bioactivity after electrospraying.

As the single-nozzle electrospinning technique resulted in a scaffold with some loss of released bFGF bioactivity, a core-shell electrospinning technique is under development wherein the core material would be a carrier polymer loaded with growth factor in a mild solvent and the shell would be the elastomeric polymer and its preferred solvent (likely HFIP). This technique is possible by keeping each solution separate until introducing one inside the other at the outlet of a co-axial syringe. By preventing extensive interaction between the different solvent systems of the core and shell material, growth factor activity may be preserved.

## 7.3 TETRACYCLINE DELIVERY FROM NANOFIBER MATRICES

### 7.3.1 Methods

#### 7.3.1.1 Tetracycline loading and scaffold fabrication

PEUU was synthesized from polycaprolactone diol and 1,4-diisocyanatobutane with chain extension by putrescine as previously reported [15]. Tetracycline hydrochloride (tet, Fisher) was dissolved in HFIP and loaded at 1, 5, and 10% PEUU by weight to yield a transparent, viscous solution of yellow tint. The chemical structure of tetracycline is displayed in **Figure 7-7**. PEUU concentration in the electrospinning solutions were 6 wt%. These PEUU/tet solutions were then electrospun from a 10 mL polypropylene syringe over a 15-cm distance using a 1.0 mL/min solution flowrate and by charging the polymer/tet solution at 10 kV and an aluminum disc target at -10 kV in a manner similar to that previously reported [1]. The target was also attached to an x-y stage translating in a square pattern of 5 cm step distances to produce scaffolds of uniform thickness. Scanning electron microscopy (SEM) was utilized to characterize fiber morphologies and tensile testing was used to characterize mechanical properties as described previously.

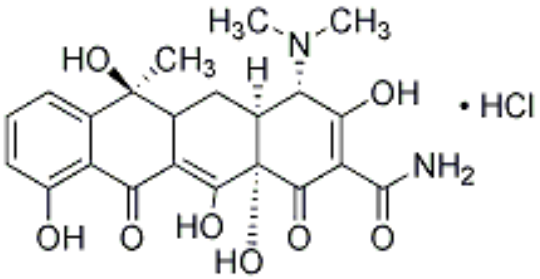


**Figure 7-7.** Chemical structure of tetracycline hydrochloride.

#### 7.3.1.2 Tetracycline release measurement

Preweighed samples of electrospun PEUU/tet were placed in PBS buffer at 37°C in order to characterize the drug release profile. At timepoints of 1 h, 1 day, 3 days, and 1 wk, release buffer was changed and samples frozen until analysis. Tetracycline concentration in the degradation buffers was then quantified by measuring UV absorbance at 350 nm minus buffer absorbance and comparing values with those of known tetracycline concentrations.

#### 7.3.1.3 Bacteria culture and antimicrobial activity assays

Activity of released tetracycline in the degradation medium was quantified using an antimicrobial activity assay utilizing *E.coli* (clinical isolate, ATCC 25922) and *S.aureus* (wound isolate, ATCC 29213) similar to a previously described method [147]. Bacteria culture was initiated as follows. First tryptic soy broth liquid medium was prepared by adding 30 g of tryptic soy broth (BD) to 1 L of deionized water in a 1000 mL beaker under mixing. This medium was autoclaved at 121°C for 20 min and subsequently stored at 4°C until use. For either *E.coli* or *S.aureus* growth and expansion, the bacteria pellet was rehydrated with 0.5 mL of tryptic soy broth and transferred to a conical tube containing 4.5 mL tryptic soy broth and mixed well. 5mL additional volume of tryptic soy broth was added to make a total volume of 10 mL. Tubes containing *E.coli* or *S.aureus* were then incubated overnight at 37°C with vigorous shaking.

For the antimicrobial assay, all degradation medium samples were then thawed at 37°C. Overnight bacteria cultures were then diluted to approximately 5 x $10^5$ CFU/mL in tryptic soy broth medium. More specifically, 10 μL of overnight culture suspension was diluted to 36 mL in order to measure an optical density of 0.1 at 570 nm. Diluted bacteria were then dispensed at 100 μL into each well of a 96 well microplate. To this suspension was added 11 μL of the

appropriate degradation buffer or sample control. Samples included the following: (1) soy broth liquid medium (negative control) (2) tetracycline antibiotic (final concentration = 8 μg/mL),(3) electrospun PEUU/tetracycline (ePEUU/tet) 10% 1 hr release, (4) ePEUU/tet 10% 1 d release, (5) ePEUU/tet 10% 2 d release, (6) electrospun PEUU/UBM (50/50) 1 d release, (7) electrospun PEUU/collagen (50/50) 1 d release, (8) electrospun PEUU control 1 d release, and (9) tetracycline control solution at 80 μg/mL in PBS. Immediately after adding samples to the wells, plates were gently mixed and optical density read at 570 nm for a zero hour reading. Subsequent readings were then recorded at timepoints of 2, 4, 6, 8, 12, 20, and 24 h.

In order to further characterize the microbial resistance of antibiotic loaded electrospun PEUU, scaffold discs were assessed for their inhibitory zone diameters. Briefly, Brain Heart Infusion agar plates (Difco Laboratories) were streaked with either *E.coli* or *S.aureus* using sterile inoculation loops. 6-mm scaffold samples or 6-mm tetracycline disc controls were then plated on the agar and allowed to incubate for 24 h at 37°C. Samples studied were ePEUU/tet 10%, ePEUU/tet 5%, ePEUU/tet 1%, electrospun PEUU/UBM, electrospun PEUU/collagen, and electrospun PEUU. Zone diameters were measured after 24 h with a micrometer.

### 7.3.2 Results

#### 7.3.2.1 Tetracycline loaded scaffold characterization

Tetracycline was dissolved in HFIP and loaded at 1%, 5%, and 10% PEUU by weight. These solutions were then electrospun into fibrous scaffolds. As can be observed in **Figure 7-8**, scaffolds contained continuous fibers with no polymer beads or drug crystals present. As similar to bFGF loading, no significant difference was observed in tensile properties with or without

tetracycline loading. For example, electrospun PEUU possessed a tensile strength of 11.4 ± 2.1 MPa and a breaking strain of 230 ± 40 %. Tetracycline loaded electrospun PEUU had a tensile strength of 13.4 ± 2.4 MPa and a breaking strain of 210 ± 40 %.

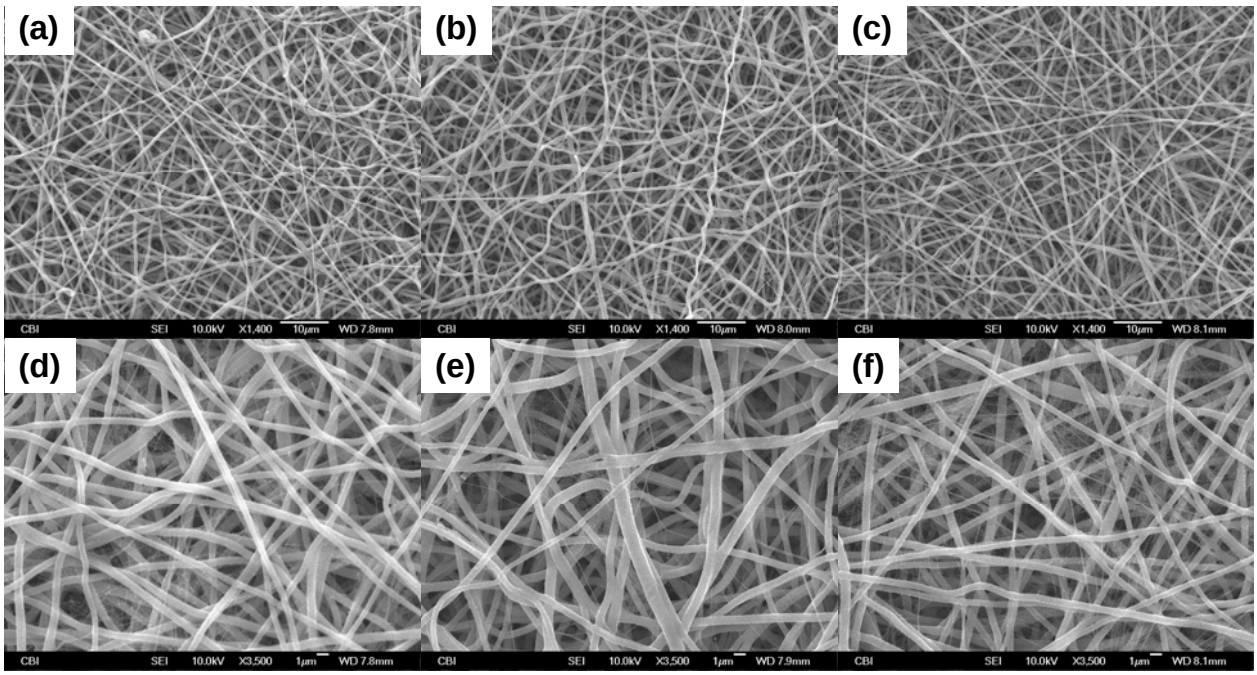


**Figure 7-8.** Scaffold morphologies of tetracycline loaded scaffolds at 1% (a, d), 5% (b, e) and 10% (c, f) of PEUU by weight as imaged with SEM. (scale bars = 10 μm (a, b, c) or 1 μm (d, e, f))

Tetracycline release from the scaffolds was quantified over 1 wk by measuring the UV absorbance of the degradation solution at 350 nm and comparing with known standards. These results are summarized in **Figure 7-9**. For all concentrations a rapid release of the hydrophilic antibiotic occurred initially followed by a more sustained release over time. Approximate 1h burst releases of 37 ± 4 %, 58 ± 2 %, and 64 ± 18 % for Tet loading of 1%, 5%, and 10% of PEUU mass respectively. After 24 h, drug release seemed was negligible.

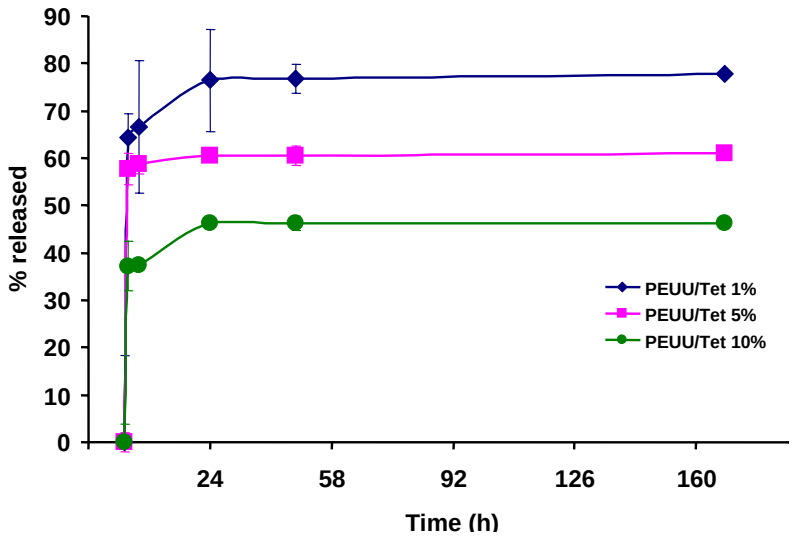


**Figure 7-9.** Tetracycline release from electrospun PEUU scaffolds into buffer as measured at 350 nm.

### 7.3.2.2 Bacteria culture and antimicrobial activity assays

Antibiotic bioactivity in degradation buffer was assessed using an antimicrobial activity assay [147]. Degradation solution in buffer was added to *E.coli* or *S.aureus* cultures in 96-well plates and absorbance at 570 nm was measured as a function of time. The results of this assay over 24 h are displayed in **Figure 7-10**. While no antimicrobial activity was found from degradation buffer from PEUU alone, inhibition of both *E.coli* and *S.aureus* growth occurred from 1 hr and 1 day degradation solutions from 10% tetracycline loaded scaffolds along with the tetracycline controls. Degradation buffer from 2 d release buffer from ePEUU/tet 10% did not inhibit bacteria growth. Furthermore, degradation buffer from either UBM or collagen blended scaffolds resulted in no measurable antimicrobial activity.

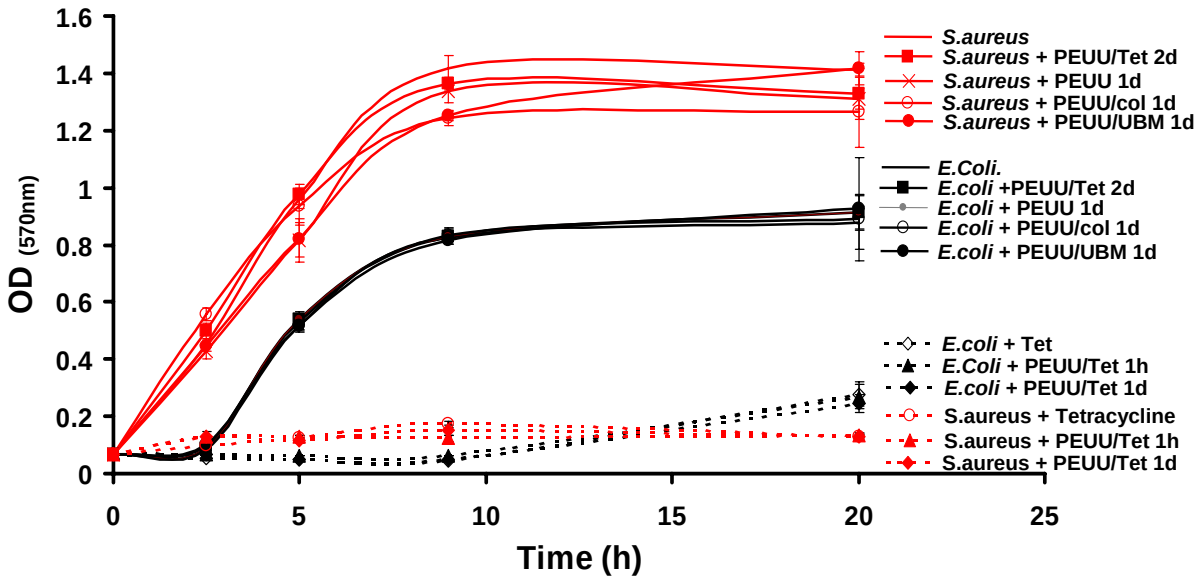


**Figure 7-10.** Antibacterial activity of degradation solutions from 10% tetracycline loaded electrospun PEUU (PEUU/Tet) and controls of PEUU alone and tetracycline.

The antimicrobial activity of the scaffold structure itself was assessed by measuring its inhibition zone diameter. 6-mm scaffold discs were plated on agar cultures of *E.coli* and *S.aureus*. Bacterial growth was significantly inhibited at 24 h for electrospun PEUU discs containing 1%, 5%, and 10% tetracycline as well as for tetracycline control discs. Respective inhibition zone diameters were 20.7 ± 0.2 mm, 21.1 ± 0.7 mm, 14.0 ± 1.1 mm, and 11.2 ± 0.2 for *E.coli* and 23.0 ± 0.1 mm, 22.1 ± 1.2 mm, 17.5 ± 1.0 mm, and 14.0 ± 1.4 mm for *S.aureus.* Therefore, scaffolds were effective in inhibiting either *E.coli* or *S.aureus*. Similar to results found from degradation buffer, bacteria growth was not inhibited by electrospun PEUU alone or PEUU samples blended with UBM or collagen. Results of inhibition zone diameter are summarized in **Figure 7-11**.

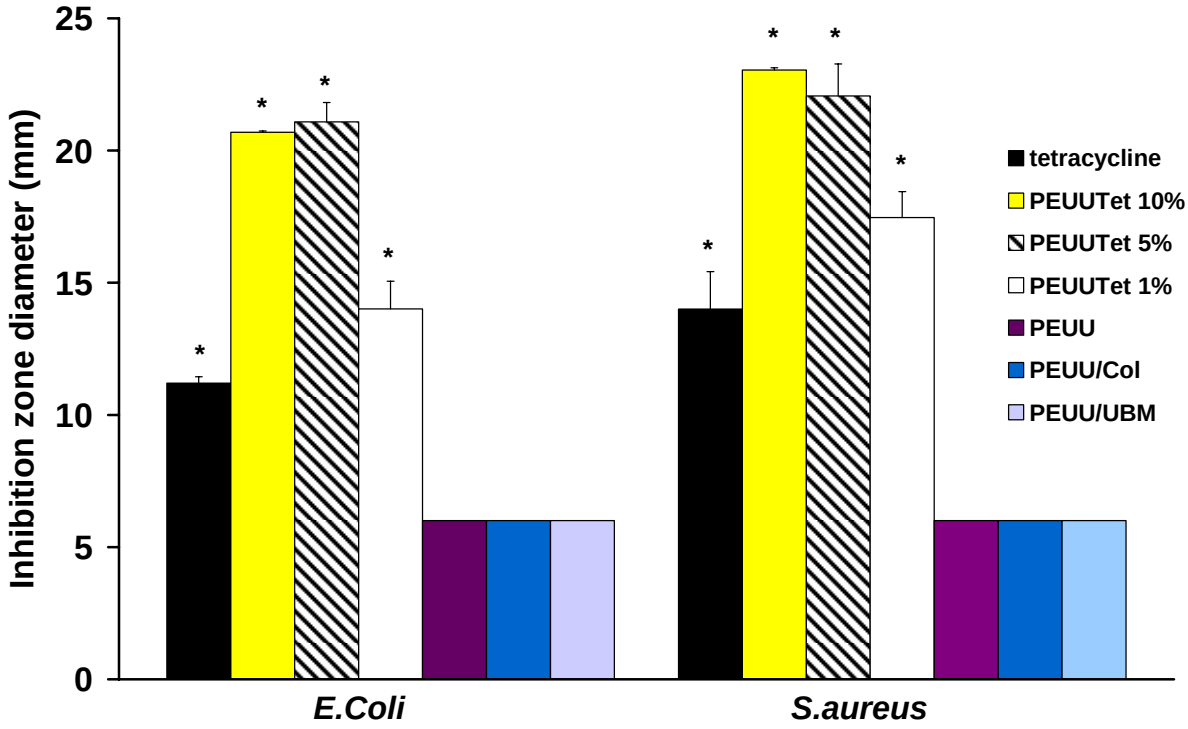


**Figure 7-11.** Inhibition zone diameters for 6-mm electrospun scaffold discs plated on agar growths of *E.coli* and *S.aureus* as measured at 24 h. (* $p < 0.05$)

### 7.3.3 Discussion

Abdominal trauma accounts for approximately 20% of all combat wounds (varying from 5% to 22% during the Vietnam conflict [148], up to 30% during the Iran–Iraq war [149]. Battlefield trauma can commonly lead to compartment syndrome. Further, since it may not be feasible to promptly remove or monitor injured personnel, prophylactic fasciotomy may be employed. The patterns of abdominal injury are also altered by the mechanisms of injury and the personal protection measures used. Military wounds can be caused by crush injuries (e.g. armored vehicle accidents), blast injuries (e.g. rocket propelled grenades, mortar injuries) or, most commonly, by projectile penetration. The military use of body armour has been shown to result in a lower

percentage of bullet injuries to the chest, paradoxically increasing the number of casualties that survive with abdominal wounds.

The aims of initial damage control laparotomy (DCL) are to obtain haemorrhage control, perform a rapid exploration, control any contamination, pack the abdomen and perform a temporary abdominal closure. Temporary abdominal closure prevents the development of intra-abdominal compartment syndrome and facilitates the planned re-operation. The intraperitoneal cavity has high risk of bacterial contamination from injured intestine and also the field setting or the injured person may have concurrent wounds that are infection risks.

Given this situation it would be of military significance to develop an elastomeric scaffold that could serve as a barrier and patch over the abdominal wall fasciotomy to facilitate healing, minimize infection risk, provide the capacity for further compartmental expansion, and be readily placed with minimal surgical expertise.

We believe that electrospun biodegradable elastomeric scaffolds could be ideally suited for the use of an abdominal wall fasciotomy patch in that they are exceptionally strong and elastic, while having a low profile. In this study, these scaffolds were processed to incorporate the broad spectrum antibiotic, tetracycline. Tetracycline acts as a bacteriostatic agent by inhibiting bacterial protein synthesis at the ribosomal level. By halting bacterial growth, tetracycline allows the immune system more time to destroy the bacteria.

It can be observed in **Figure 7-9** that the initial percent of tetracycline released is lower for higher concentrations of drug loaded in the polymer (10% versus 5% and 1% tet loaded relative to PEUU). This effect may be explained by rapid loss drug loss at or near the fiber surface and a greater amount of drug being trapped inside the fibers for the higher loaded samples. Therefore a higher ratio of surface tetracycline to bulk tetracycline can occur at lower

tetracycline loading concentrations. After the initial burst from tetracycline near the fiber surface, the semi-crystalline nature of the PEUU may cause a slower release of the trapped drug farther inside the fibers.

In general, a burst release is observed with release of the hydrophilic antibiotic, tetracycline. This trend is consistent with other reports in the literature for drug release from electrospun matrices [150, 151]. The high surface to volume ratio of the nanofibrous scaffolds allows rapid surface loss and diffusion of loaded drugs. Future work with more advanced encapsulation methods such as core-shell processing or covalent drug to polymer attachment could lead to more sustained release profiles.

# 8.0 ELECTROSPUN TUBULAR CONSTRUCTS FOR BLOOD VESSEL TISSUE ENGINEERING

## 8.1 INTRODUCTION

Given the incidence of coronary and peripheral arterial disease and the complications associated with treating this condition the need for engineered tissue replacements for small diameter blood vessels is clear. A wide variety of groups are pursuing research aimed at creating a blood vessel tissue equivalent based upon cells alone (cultured into sheets and rolled) [3, 27], cells combined with natural matrices (e.g. fibrin and collagen) [152, 153], and cells combined with synthetic matrices (e.g. hydrolytically labile polyesters) [9, 154]. Common to many of these approaches, particularly those that possess higher cell densities, are inadequate vessel mechanical properties. Although a synthetic or processed natural matrix can provide mechanical support, this usually comes at the expense of long culture times which can be on the order of months [3, 9].

A critical requirement of blood vessel replacements is accurate replication of the original vessel compliance. Compliance mismatch is a complex phenomenon because it involves the host artery, anastomosis, and the graft itself [5]. Blood flow can be traumatized causing turbulence and low shear stress that favors platelet deposition. These complications can further lead to myointimal hyperplasia and graft failure. Therefore, in developing an ideal blood vessel replacement, it is necessary to not only create a non-thrombogenic luminal surface but to also

closely replicate the elastic properties of the vessel wall. To maintain a highly cellularized blood vessel construct, but to also provide substantial elastomeric mechanical support, we have developed a micro-integrated approach wherein a meshwork of submicron elastomeric fibers is built into a vessel wall with or without the cellular placement process. Cellularity can be developed through *in vitro* culture methods or *in vivo.* We have developed a method to luminally surface seed small diameter electrospun polyurethane conduits and also studied their behavior as rat aorta replacements *in vivo*. We have also extended the electrospinning technology to incorporate cells during scaffold fabrication to better encourage tissue development. These constructs were characterized for their cellularity and mechanical properties.

## 8.2 ELECTROSPUN POLYURETHANE TUBULAR CONDUITS

### 8.2.1 Methods

#### 8.2.1.1 Tubular electrospinning and scaffold characterization

Poly(ester urethane)urea was synthesized from poly(ε-caprolactone)diol and 1,4-diisocyanatobutane with putrescine chain extension as described previously [15]. PEUU was dissolved at 6 wt% in hexafluoroisopropanol and electrospun [115]. Electrospinning conditions included a solution volumetric flowrate of 1.0 mL/hr, a distance between nozzle and target of 13.5 cm, and voltages of +12 kV to the nozzle and -3 kV to the target. The target used for fabrication of small diameter tubes for implantation was a Type 316 stainless steel mandrel of

1.3 mm diameter that was rotating at 250 rpm. An image of this custom designed and constructed target is displayed in **Figure 8-1**. This mandrel was also translating along its axis 8 cm on a linear stage at a speed of approximately 8 cm/s to produce a more uniform conduit thickness. Samples were electrospun for 15 min to produce porous tubular constructs with wall thicknesses on the order of 150 to 200 μm. For endothelialization studies a 4.7 mm stainless mandrel was instead utilized with the same process conditions.

After fabrication, the mandrel was dipped in 70% ethanol in order to more easily remove it from the steel mandrel. The conduit is then rinsed in deionized water multiple times, blotted dry and then dried under vacuum at room temperature 24 to 48h. Conduits were then examined for their gross structure with a dissecting microscope or their fibrous morphologies with scanning electron microscopy. In order to view an uninterrupted fibrous cross-section, samples were dipped in liquid $N_2$ for 1 min and then fractured before sputtercoating for SEM.

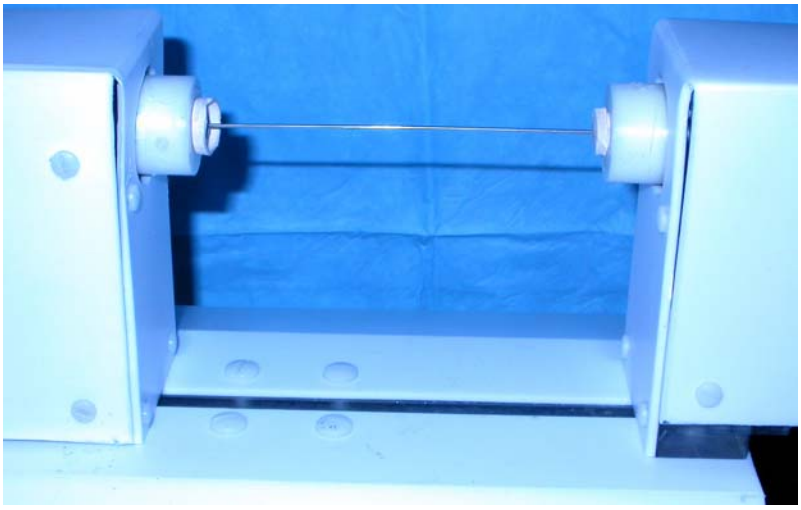

**Figure 8-1.** Target used to electrospin 1.3 mm inner diameter porous conduits for blood vessel tissue engineering. The mandrel is rotated at 250 rpm and charged at -3kV.

#### 8.2.1.2 Surface seeding of conduit lumen

PEUU conduits (4.7 mm) were positioned inside a custom designed rotational vacuum seeding device in collaboration with Prof. D.Vorp and L.Soletti of the University of Pittsburgh and seeded with 20 x $10^6$ muscle derived stem cells (MDSCs). More specifically, the electrospun conduit was placed on metal stubs and a light vacuum was applied to the exterior of the conduit. Subcultured MSDCs were then perfused through the lumen of the conduit and forced into the fibrous lumen side wall of the tube by vacuum. Constructs were cultured under static conditions in Petri dishes for 24 h. Samples were then fixed in 2% paraformaldehyde before permeabilization with 0.1% triton-x 100 and staining with DAPI or draq 5 nuclear stain and rhodamine phallodin for f-actin and imaged with fluorescence microscopy.

#### 8.2.1.3 In vivo implantation as a rat aorta replacement

Porous 1.3 mm inner diameter tubular electrospun scaffolds were implanted as interposition grafts in the abdominal aorta of rats with collaboration from Prof. D.Vorp and A. Nieponice. Lewis female rats weighing 250-300 g were anesthetized with 1% isofluorane and 2.5 mg/100 g ketamine. A mid-abdominal incision was performed and the retroperitoneal cavity exposed. The descending aorta below renal level was dissected, clamped proximally and distally sectioned to make a 1 cm gap. The electrospun conduit was then implanted in an end-to-end manner using prolene 10.0 sutures. Intravenous heparin was administered before clamping with 200 Units/kg. The abdominal wall was closed in two layers with Vycril 2.0 sutures. Rats were sacrificed at 2 wks and sample explants fixed in 10% neutral buffered formalin at room temperature. Samples were then embedded in paraffin and sectioned before staining with Hematoxylin and Eosin or Masson's Trichrome.

### 8.2.2 Results

#### 8.2.2.1 Scaffold morphology and mechanical characterization

PEUU at 6 wt% in HFIP was electrospun onto a negatively charged rotating mandrel at 250 rpm to produce a tubular construct. **Figure 8-2** demonstrates the gross appearance of the conduit. The electrospun tubes possessed 1.3 mm inner diameters, lengths up to 8 cm and wall thicknesses of 150-200 μm. The fibrous structures of the scaffold tubes are shown by SEM in **Figure 8-3**. One can observe fiber sizes approximately in the range of 1000 m. In addition, these constructs were suturable and retained their lumens.

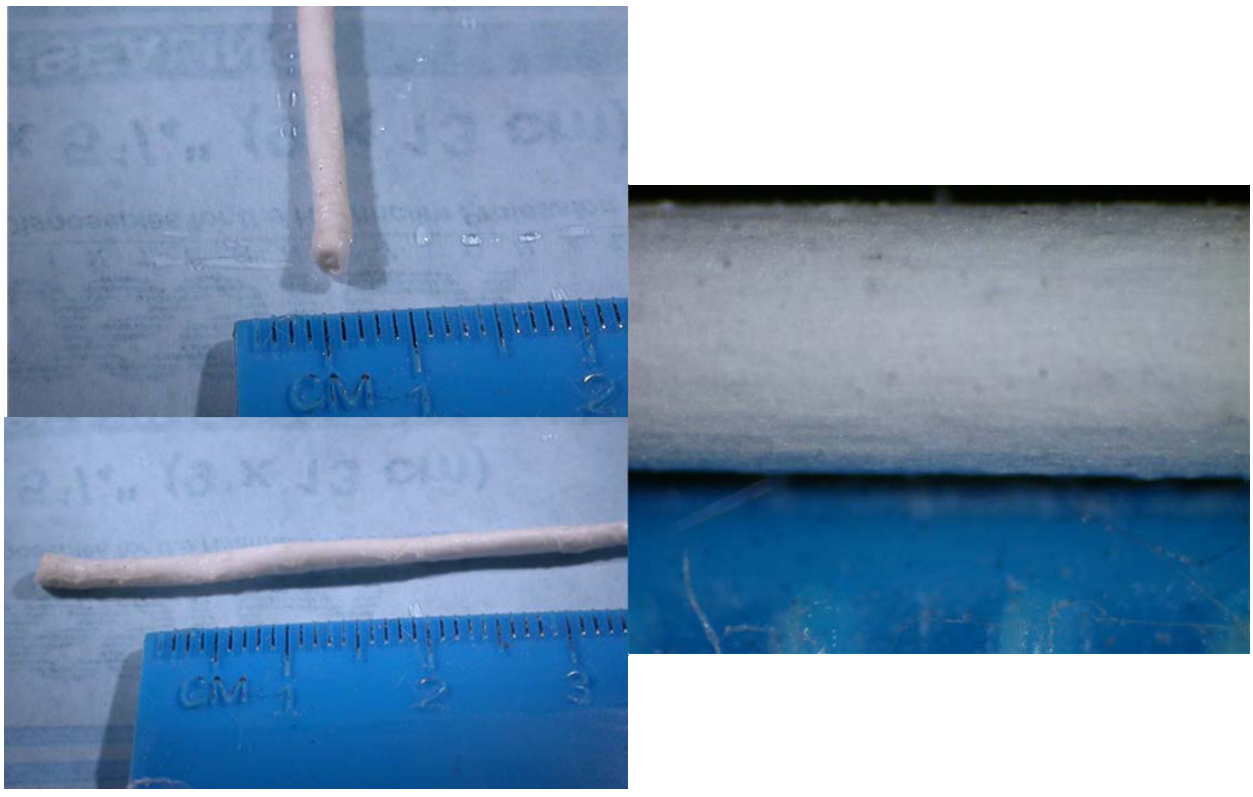

**Figure 8-2.** Macroscale appearance of electrospun tube. (bottom = higher magnification)

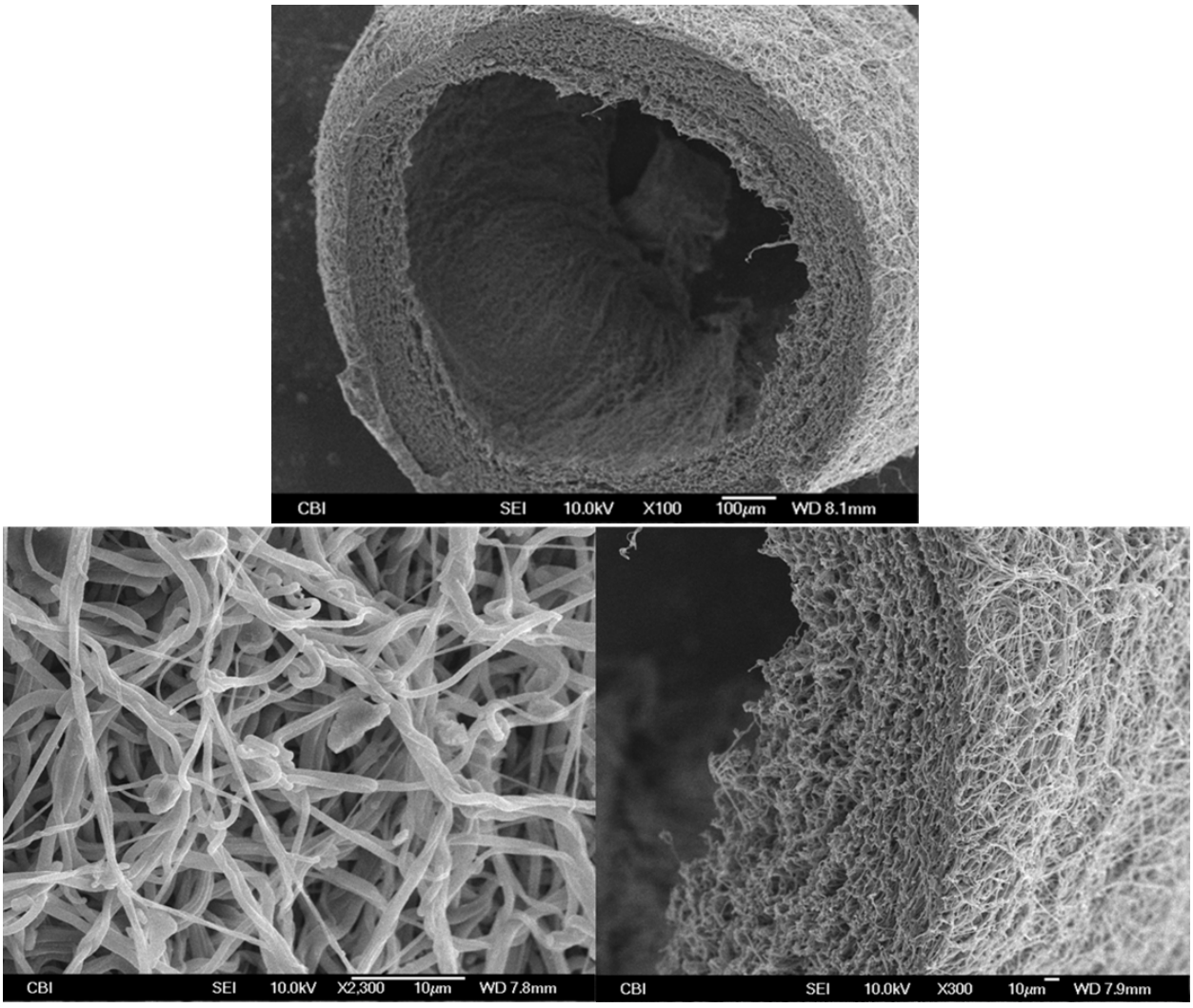


**Figure 8-3.** SEMs of PEUU electrospun conduits. Bottom left image displays conduit exterior and bottom right image displays the conduit cross-section (scale bars = 10 μm).

### 8.2.2.2 Surface seeding of conduit lumen

Porous electrospun PEUU was mounted inside a custom developed vacuum seeding device designed by D. Vorp and L.Soletti. Subcultured MDSCs were then seeded or pulled into the fibrous lumen of these tubes. This seeding device allowed the cells to uniformly cover the conduit lumens immediately after seeding. After 24 h of static culture, cells were viable, adhered to the lumen and formed a monolayer. An image depicting the cells lining the construct interior is shown in **Figure 8-4**. This image was a fluorescent micrograph depicting the cell nuclei and f-actin staining.

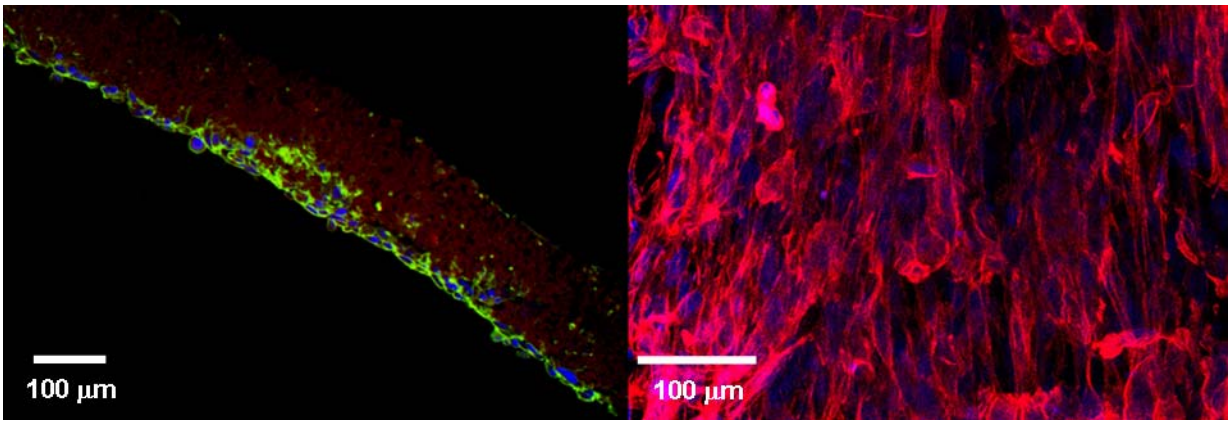


**Figure 8-4.** Fluorescent micrograph of MDSCs lining the interior of an electrospun tubular conduit. (Left panel) Nuclear (blue, Dapi) and f-actin (green, rhodamine phalloidin) staining indicating cell attachment on polymer lumen (red, autofluorescence) after 24 h of static culture. (Right panel) Confocal image stack demonstrating nuclear (blue, draq5) and f-actin (red, rhodamine phalloidin) staining of the PEUU lumen. (data courtesy of L.Soletti)

### 8.2.2.3 Graft function and explant histology in a rat model

Porous electrospun 1.3 mm inner diameter tubular constructs were utilized as vascular grafts to replace the aorta of rats. Constructs were suturable and easily retained their lumens *in vivo*. An image of the graft immediately after implantation is shown in **Figure 8-5**. Rats were able to recover from the surgeries with limb function. At 2 wks after implantation, grafts remained patent and functional. Hematoxylin and eosin staining demonstrated external capsule formation around the explanted grafts. Masson's Trichrome staining indicated the capsule was composed of aligned collagen together with the presence of newly developed capillary vessels. Cell and tissue in-growth was observed throughout the constructs with the presence of collagen development. Cells were also demonstrated to have formed a monolayer in locations around the construct lumens. Images representative of histological examination of the 2 wk explants are displayed in **Figure 8-6**.

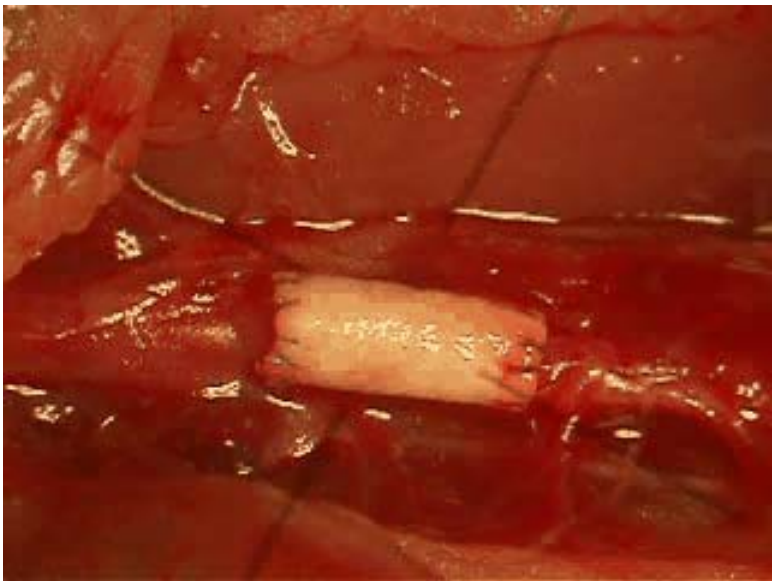

**Figure 8-5.** Image of electrospun vascular graft immediately after implantation to replace a section of the rat aorta. (image courtesy of A. Nieponice)

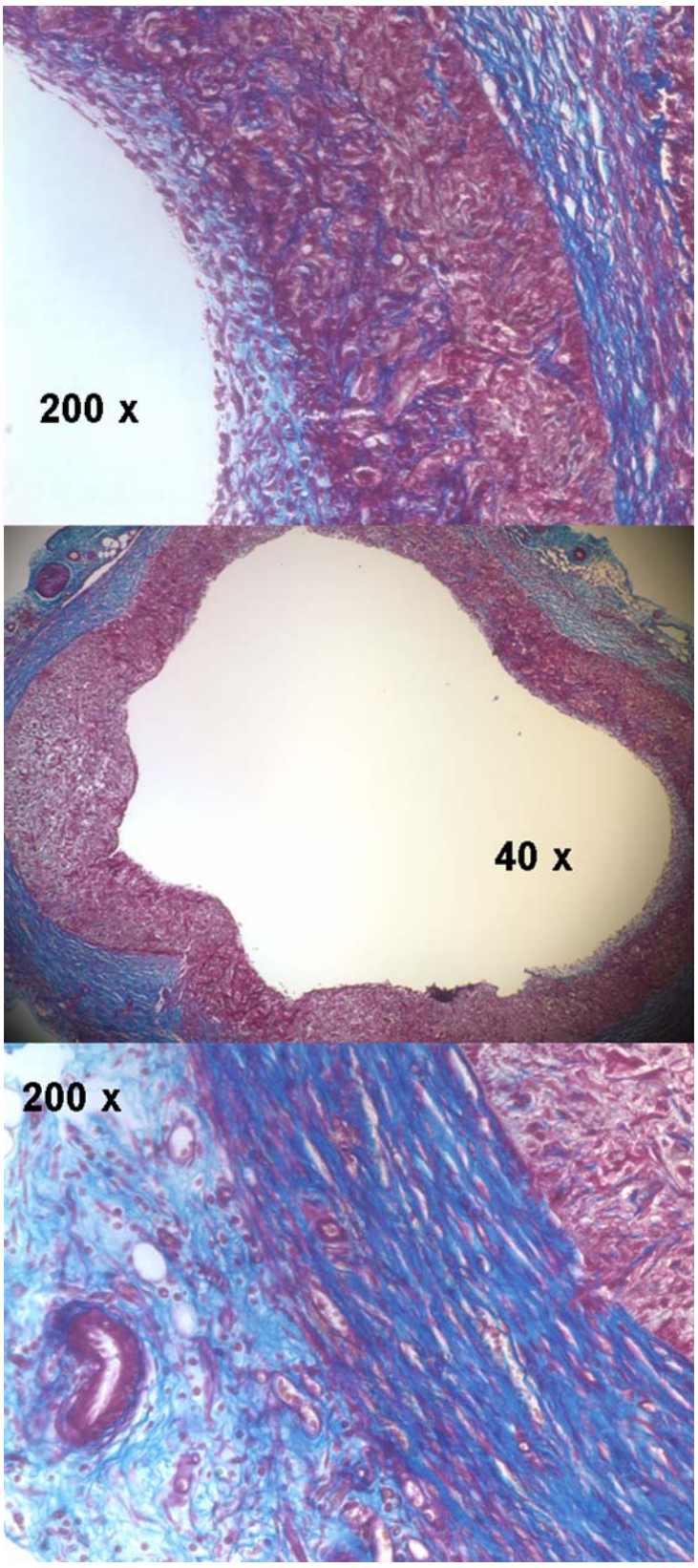


**Figure 8-6.** H&E / Trichrome stains of 2 wk explants of electrospun vascular grafts. Notice the presence of collagenous capsule and neovessels in graft exterior (bottom image) and luminal cell growth (top image).

## 8.3 SMC MICROINTEGRATED POLYURETHANE CONDUITS

### 8.3.1 Methods

#### 8.3.1.1 Conduit microintegration technique

Vascular smooth muscle cells (SMCs) isolated from rat aortas were expanded on tissue culture polystyrene (TCPS) culture plates under Dulbecco's Modified Eagle Medium (DMEM) supplemented with 10% fetal bovine serum and 1% penicillin-streptomycin [107]. Microintegration was performed similar to described previously with some modifications to allow for a smaller diameter electrospraying / electrospinning mandrel [155].

7.5 x $10^6$ SMCs/mL were subcultured in medium and fed at 0.1 mL/min into a sterile Type 316 stainless steel capillary charged at 8.5 kV and located 4.5 cm from the target. 6 wt% PEUU or 6 wt% PEUU/collagen (75/25) in HFIP was fed at 1.5 mL/min into a capillary charged at 12 kV and located 23 cm from the target. The target consisted of a sterile stainless steel mandrel (4.7 mm diameter) charged at -3 kV and rotating at 250 rpm while translating 8-cm along its axis at 1.6 mm/s. A fabrication time of 30 min was used to produce each microintegrated conduit. After fabrication the conduit and mandrel were gently placed with aseptic technique into a roller bottle and cultured statically for 16 h. After 16 h, samples were gently removed from the mandrel for culture. Samples were then cut into 15 mm lengths and sutured to metal stubs and perfused media with pulsatile flow for 3 days. Images depicting the perfusion sample and reactor are shown in **Figure 8-7**.

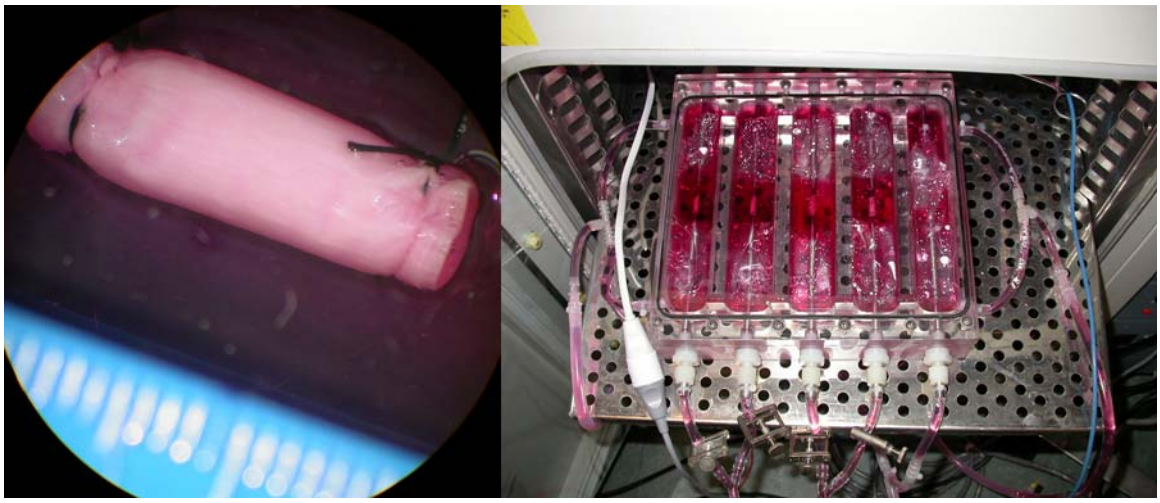

**Figure 8-7.** Images of SMC microintegrated PEUU conduit (left) prepared for insertion into perfusion bioreactor (right).

### 8.3.1.2 Conduit characterization

At timepoints of 1 day and 4 days after fabrication, samples were characterized. The MTT mitochondrial assay was used to measure cell viability. For histological investigation, samples were fixed in 10% neutral buffered formalin at room temperature. Samples were then embedded in paraffin, sectioned and stained with hematoxylin and eosin.

Samples were analyzed for their biomechanical properties immediately after fabrication. Properties measured included ring strength, dynamic compliance, and burst pressure. In order to measure ring strength, stainless steel staples were inserted into 5mm long tubular sections and then into the grips of a uniaxial tensile tester (ATS). An image of this set-up is shown in **Figure 8-8**. Using a 10 lb load cell and a displacement rate of 10.05 mm/min samples were strained until break.

For dynamic compliance and burst strength, 15 mm long tubular samples were mounted in a flow loop driven by a centrifugal pump (Biomedicus) and submerged in PBS at 37°C. The

pressure was monitored and recorded at 30 Hz using a standard in-line strain-gage pressure transducer and a PC acquisition board. The vessel construct was perfused with a pulsatile flow (110-70 mmHg, 1.2 Hz) and the dynamic compliance, C, was measured by recording the external diameter of the sample with a He-Ne laser micrometer (Lasermike). Compliance was calculated as

$$C = \frac{(D_{\max} - D_{\min})}{D_{\min}(P_{\max} - P_{\min})} \tag{8-1}$$

for each pulse (D = maximum or minimum diameter, P = maximum or minimum pressure). A porcine mammary artery was used as a control for comparison with microintegrated PEUU in compliance studies. For measuring burst pressure, the sample outlet was sealed and flow was increased until tube rupture. The maximum pressure before rupture was taken as the burst pressure.

### 8.3.2 Results

#### 8.3.2.1 Scaffold structure

In order to extend the technology of cellular microintegration to small diameter tubes, a 4.7 mm diameter stainless steel mandrel was used in the place of the previously employed 19 mm diameter mandrel for sheet microintegration [155]. In order to microintegrate highly cellular and defect free tubular constructs, it was necessary to slightly decrease electrospraying distance 0.5 cm and lower the mandrel negative charge from -10kV to -3 kV from previous methods. During fabrication, PEUU appeared pink and glistening on the mandrel indicative of uniform cellular electrospray. After removal from the mandrel, samples of either PEUU or PEUU / collagen (75/25) were found to be mechanically robust in that they were suturable and could

retain their lumens after compression. Images depicting the suturability and gross appearance of SMC microintegrated PEUU conduits are illustrated in **Figure 8-8**.

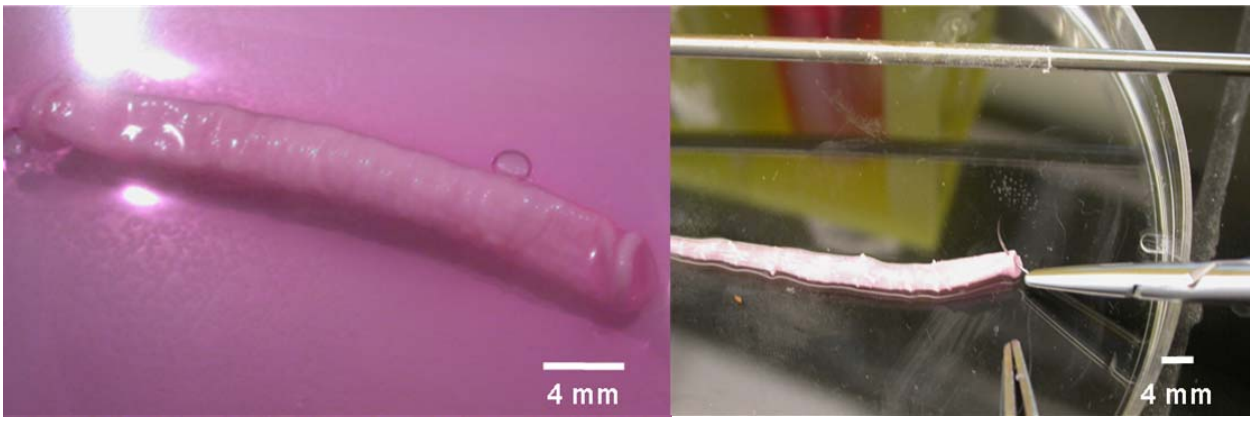


**Figure 8-8.** Gross appearance of SMC microintegrated PEUU tubular constructs after removal from the fabrication mandrel.

### 8.3.2.2 Cell growth and histology

Cell placement and viability in the SMC microintegrated constructs was investigated initially and after 4 days of static or perfusion culture. After perfusion, samples were gently removed and then sectioned into representative slices for MTT and histology. MTT results indicated viable cells 1 day after fabrication. Furthermore, cells remained viable at day 4 with either static or perfusion culture with cell number values reported slightly higher for perfusion culture. MTT data are summarized in **Figure 8-9**. Samples were fixed and stained with hematoxylin and eosin staining. A representative H&E stain of uniform initial cell integration within the tubular construct is shown in **Figure 8-10**. This half-tube image consists of multiple images taken from the tube periphery grouped together to create a representative image.

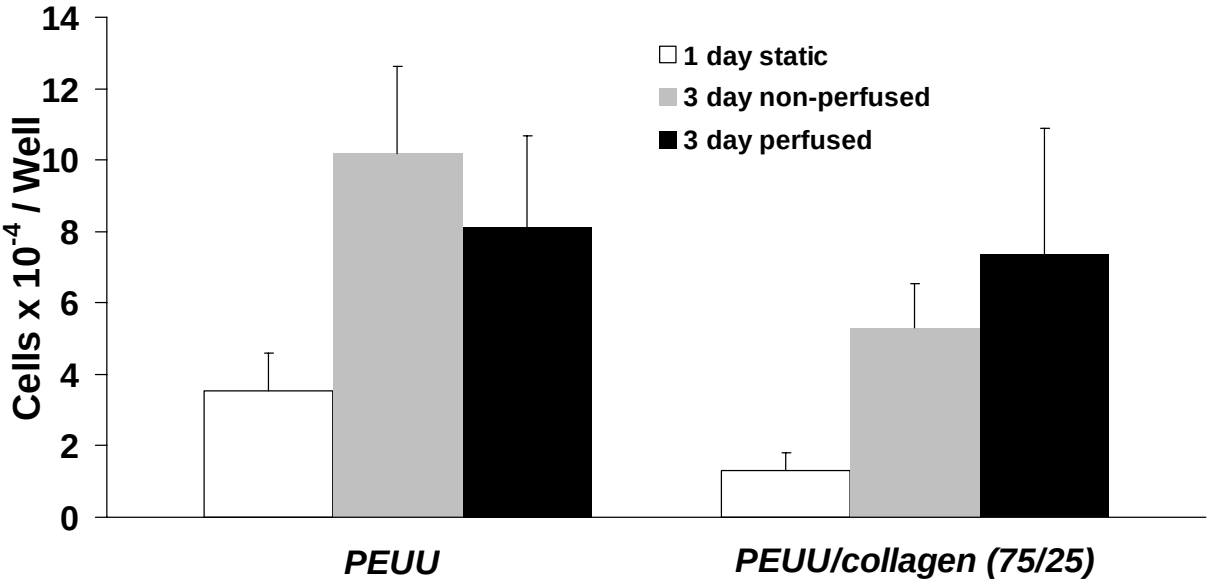


**Figure 8-9.** MTT SMC viability data for microintegrated conduits of either PEUU or PEUU/collagen. Perfusion was initiated after 1 day of static culture for cell attachment.

### 8.3.2.3 Mechanical properties

Ring strength, burst pressure, and suture retention strength were assessed in the microintegrated constructs after fabrication under collaboration with Prof. D.Vorp. The stress-strain response from subjecting a small tube section to uniaxial tensile testing is displayed in **Figure 8-11** below. These rings were mechanically robust and flexible with maximum stress and strain values of 6.3 MPa and 170% respectively. The ring samples did not break cleanly in each case and seemed to pull apart or delaminate past the ultimate stress value.

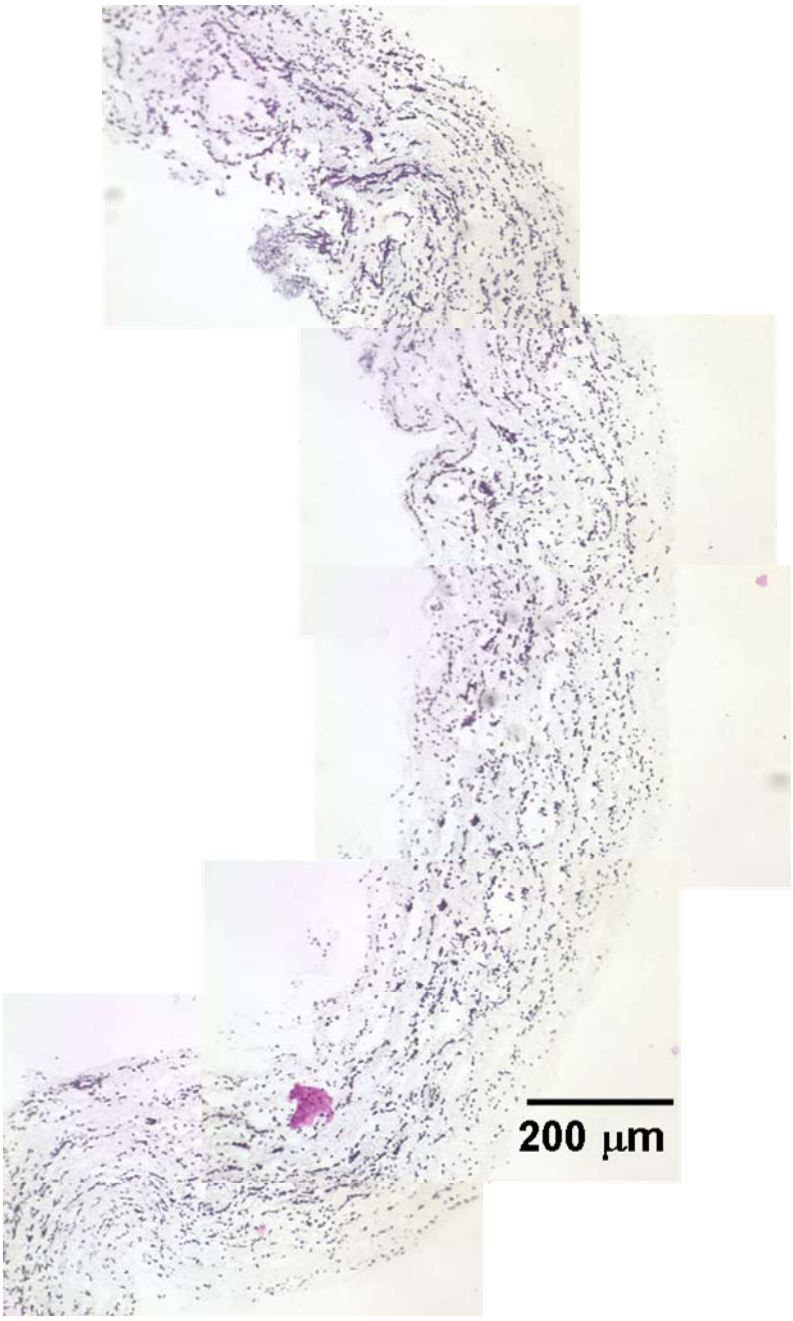


**Figure 8-10.** Uniform SMC placement after 1 day of static culture for microintegrated PEUU conduit.

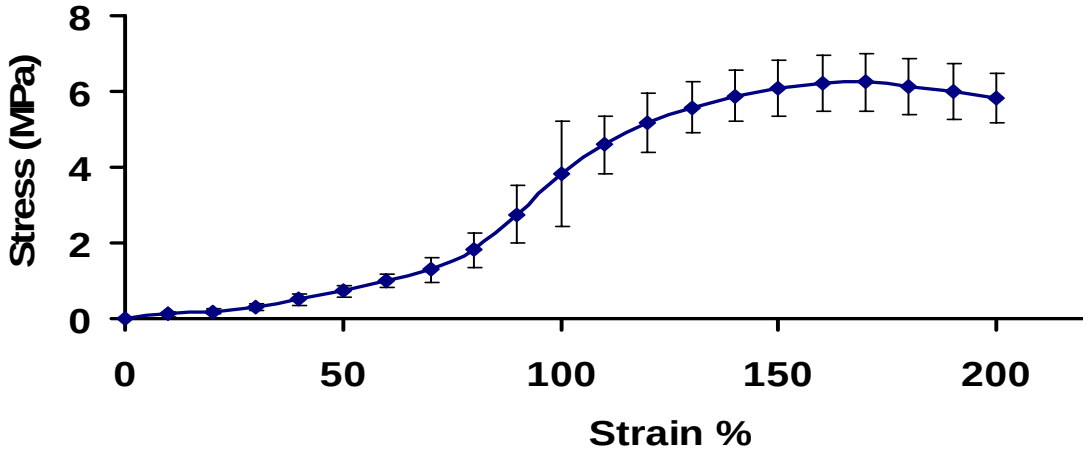


**Figure 8-11.** Averaged stress-strain curve for ring test of SMC microintegrated 4.7 mm electrospun PEUU tube. (Data courtesy of L.Soletti)

In order to calculate the dynamic compliance of the microintegrated constructs, samples were exposed to pulsatile flow and the pressure / diameter relationship was evaluated. This relationship was compared with a porcine mammary artery (pMA) exposed to the same pulsatile flow. As one can observe in **Figure 8-12**, the mechanical response of both the pMA and microintegrated PEUU was very similar with values falling for both samples falling between one another. Compliance values were $1.02 \pm 0.33 \times 10^{-3}$ $mmHg^{-1}$ for pMA and $0.71 \pm 0.13 \times 10^{-3}$ $mmHg^{-1}$ for SMC microintegrated PEUU. Burst pressure values for all samples were greater than 1500 mmHg. It must be noted that burst pressure values were approximations due to the porous nature of the microintegrated tubes.

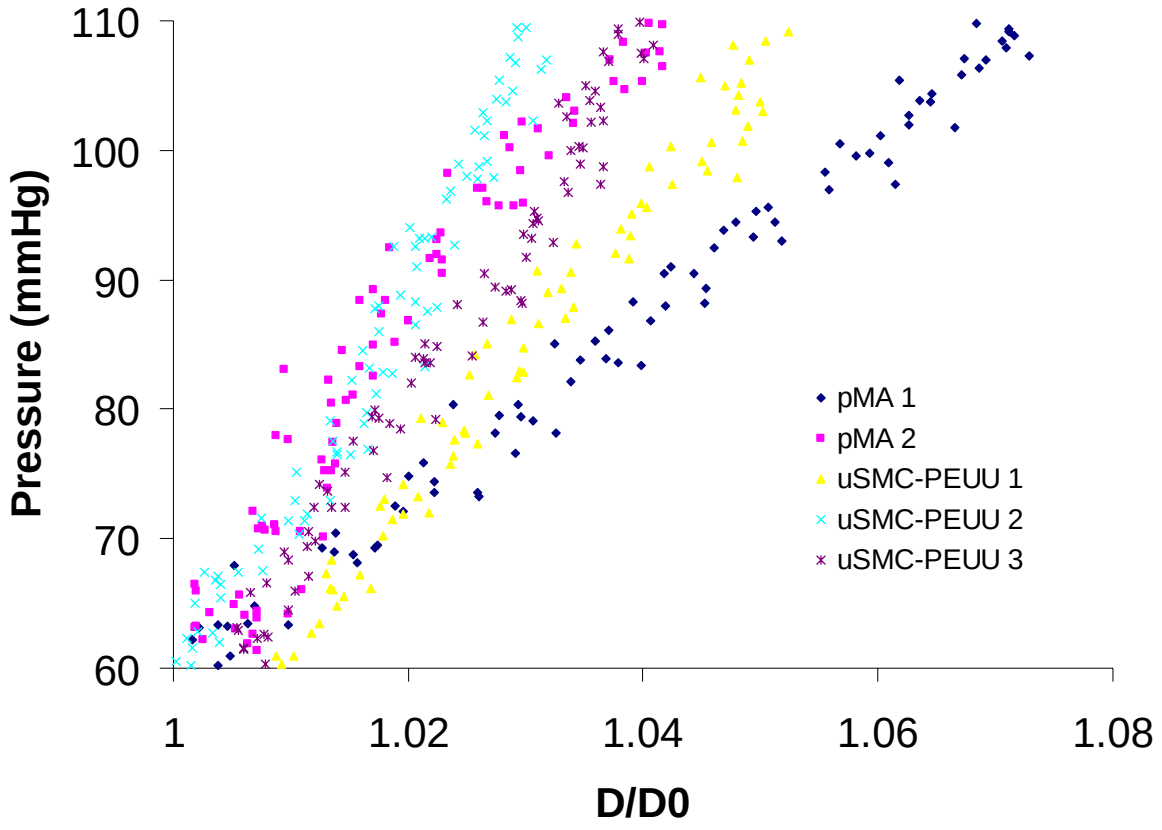


**Figure 8-12.** Pressure / diameter relationship comparison between porcine mammary artery (pMA) and SMC microintegrated PEUU tubular constructs (μSMC-PEUU). (Data courtesy of L.Soletti)

### 8.3.3 Discussion

Efforts have been extensive in the tissue engineering community for development of a highly cellular and functional blood vessel replacement [91, 152]. Central to this theme of functionality is development of grafts that have adequate burst strength and compliance to function in an *in vivo* environment. Electrospinning technology in particular has been studied for its ability to fabricate small diameter tubular constructs with fibers sizes and architectures that mimic the extracellular matrix. For example, Inoguchi et al. demonstrated the electrospinning of tubular and elastic poly(L-lactide-co-caprolactone) (PLCL) conduits [156]. The mechanical properties of these conduits were investigated in depth and they were shown to pulsate under pulsatile flow *in vitro*. Also, work by Vaz et al. demonstrated a multi-layering electrospinning technique to fabricate PCL and PLA composite scaffold conduits [157]. They also seeded fibroblasts on the surface of these materials. However, to date there have been no reports of a method to produce highly cellularized electrospun conduits that possess compliance values similar to native vessels.

The objective of this work was to successfully fabricate a highly cellularized blood vessel construct that also provides substantial elastomeric mechanical support. Two methods were pursued for this goal, an i*n vivo* approach or *in vitro* approach. For the *in vivo* approach, a biodegradable and cytocompatible, elastomeric poly(ester urethane)urea was electrospun into small diameter tubes appropriate for implantation in a rat model. For the *in vitro* approach, SMCs were seeded into electrospun nanofibers concurrently with scaffold fabrication using a microintegration technique [155].

Previous results in achieving cellular infiltration in electrospun synthetics have been time difficult [158]. While some believe cells can slowly migrate and “push” their way through fibers *in vitro* this has not been adequately demonstrated in the literature. Furthermore, there is not

much incentive for cells to migrate into regions of synthetic materials *in vitro* that would make diffusion of cell nutrients and waste more difficult. However, it would be expected that when implanted *in vivo* electrospun scaffolds would be more quickly infiltrated with cells as a result of the highly dynamic environment including potential inflammatory responses. To assess this concept, Telemeco et al. subcutaneous implanted synthetic electrospun materials and compared with electrospun collagen and gelatin [158]. The most rapid cellular infiltration was observed for electrospun collagen. Slow infiltration and some fibrous encapsulation occurred on the synthetic PGA and PLA electrospun materials. While the study by Telemeco et al. was only for 1 wk, it does demonstrate that cellular infiltration is relatively slow *in vivo* as well for electrospun synthetics. We have also demonstrated a slow cell infiltration with subcutaneous implantation of electrospun PEUU after 12 wks in rats in Chapter 7.0.

However, in this chapter we have discovered rapid and high density cellular infiltration into electrospun PEUU constructs when implanted as interposition grafts in the aorta of rats. At 2 wks after implantation constructs were patent. After explant, H&E staining indicted approximately 80% tissue infiltration and the presence of collagen deposition throughout the constructs. Small capillaries were also forming on the construct periphery. This significant result may be attributed to the placement of the construct in a highly functional environment with blood flow and mechanical stimulation. Results are on-going in improving construct properties and characterizing the tissue development at longer timepoints

Since the ability to seed cells into electrospun synthetics *in vitro* is limited by the small pore sizes we have previously developed a microintegrated approach wherein cells are seeded into the submicron fibers concurrent with the electrospinning process [155]. This method produced highly cellularized elastomeric scaffolds. Cells were viable after fabrication and

proliferated under perfusion culture. In order to extend this technology to microintegrate cells into small diameter tubular constructs as a blood vessel prototype, we had to slightly modify some process variables.

For example, in order to adequately target and electrospray cells onto the smaller diameter mandrel it was necessary to decrease the distance between electrospray nozzle and mandrel. Also, using a high negative charge to the rotating mandrel target resulted in polymer protrusion defects, or "spikes," in the tube which could disrupt conduit integrity and cell viability. Therefore, we decreased mandrel charge to result in homogenously cellular and fibrous tubular conduits. These constructs were then cultured under a perfusion bioreactor to encourage better exchange of nutrients, waste, and oxygen to the cells in the tube interior. H&E and MTT results indicated viable cells present within the constructs after fabrication and perfusion culture. Further work is in progress to assess the optimal culture conditions to encourage SMC proliferation and ECM deposition.

The mechanical properties of electrospun tubes fabricated by either method were mechanically assessed and found to have compliances and burst strengths appropriate for vessel replacement and similar to native vessels. These constructs also seem appropriate for function in a mechanically demanding environment. As the next stage for this project, it is possible that mechanical training may be required to better develop ECM production in the blood vessel constructs.

In summary, a significant advance in developing a method to fabricate a hybrid tissue engineered blood vessel construct that is primarily cellular and reinforced with an elastomeric fiber matrix has been developed. These constructs are cytocompatible, suturable and possess compliance values similar to native vessels. Current and future studies consist of investigating

the optimal fiber material composition as well as characterizing cell phenotype and ECM production over longer *in vitro* culture periods. Our expectation is that the results from these studies will provide the motivation to study the fabricated vessel constructs in a larger animal model.

# 9.0 CONCLUSIONS AND FUTURE WORK

## 9.1 CONCLUSIONS

In this dissertation, novel biodegradable elastomers were synthesized and fabricated into scaffolds appropriate for engineering of cardiovascular or other soft tissue. These materials represent attractive alternatives to currently available biodegradable polyesters utilized in tissue engineering. Biodegradable and cytocompatible poly(ester urethane)ureas were synthesized to high molecular weight and processed into scaffolds suitable for *in vivo* placement or for support of cellular adhesion and growth by an electrospinning technique. This process, where an electric field overcomes surface tension to generate and draw nanoscale fibers, produced scaffolds with extracellular matrix-like morphologies that retained mechanical strength and flexibility while also permitting protein incorporation into spun fibers to impart bioactivity.

PEUU was processed with electrospinning to create scaffolds using a novel method of physically blending collagen or urinary bladder matrix as bioactive components. The incorporation of collagen was useful as a means to increase cell adhesion and scaffold degradation rates. While at low concentrations of collagen the protein appeared to lose its helical structure, it still imparted increased cell adhesion. Urinary bladder matrix was also blended with PEUU and electrospun to produce scaffolds with even more potential bioactive character as UBM is known to possess bioactive peptide components in addition to collagen. These hybrid

material combinations resulted in increased mechanical robustness and flexibility from the synthetic component and increased cell recognition and degradation from the natural components.

Scaffolds with mechanical anisotropy were of interest in creating oriented cellular structures and to control stress translation during tissue mechanical conditioning. Therefore a method was developed to fabricate nanofibrous scaffolds of controlled fiber orientation and mechanical anisotropy by electrospinning onto a high speed rotating mandrel. These scaffolds were demonstrated to direct oriented smooth muscle cell growth. In addition, these materials were shown to possess mechanical properties and exhibit stress-strain curves that mimic those of the native pulmonary valve.

These elastomeric matrices could provide mechanical support, but typically required long seeding and culture times to achieve high density cellular in-growth. Therefore, we developed a microintegrated method during which a mesh of submicron elastomeric fibers was built into the scaffold wall during the cellular placement process. Cells such as smooth muscle cells, muscle derived stem cells, and endothelial progenitor cells were electrosprayed during the electrospinning of a synthetic elastomer, which expedited the time required for scaffold construction and cell seeding. *In vitro* culture of these microintegrated constructs under transmural perfusion resulted in a tissue engineered construct that was largely cellular and supported with an elastomeric fiber net. Such a construct could be appropriate for soft tissue replacement including the engineering of conduit structures such as a tissue engineered blood vessel.

Electrospun PEUU was also studied as a means to develop porous and elastomeric scaffolds for controlled release of growth factors or antibiotics to encourage wound healing and

repair during fasciotomy management. PEUU was loaded with bFGF and processed into microporous sheets comprised of sub-micron scale fibers. These elastomeric sheets were capable of bioactive bFGF release for at least 1 week and facilitated increased SMC adhesion. In addition, PEUU was loaded with the antibiotic, tetracycline, and electrospun. These scaffolds were capable of inhibiting the growth of *E.coli* and *S.aureus*. In wound healing applications where material flexibility and growth factor or drug release from a barrier would be desirable, these growth factor or antibiotic loaded sheets may provide attractive functionality.

In order to develop a more mechanically appropriate tissue engineered blood vessel, PEUU was electrospun into small diameter tubular conduits. Two approaches for achieving cellularity and functionality were pursued, an *in vivo* approach and an *in vitro* approach. More specifically, the *in vivo* approach involved implanting an electrospun, elastomeric PEUU conduit as an interposition graft in a rat aorta. The graft was patent at 2 wks and exhibited cell infiltration. Produced extracellular matrix was present throughout the constructs. The *in vitro* approach involved the extending of cellular microintegration technology towards the construction of highly cellularized small diameter tubular conduits. By modifying some process variables, microintegrated small diameter tubes were fabricated with uniform cell placement and mechanical properties including a compliance and burst pressure similar to native vessels.

The research conducted in this dissertation was foremost directed toward the objective of fabricating more biomimetic scaffolding for use in development of functional engineered cardiovascular tissue replacements. As ischemic heart disease is a leading cause of death in this country, it is the hope of this author that some outcome of this work may be further expanded and utilized in the near or future to ultimately improve patient care and suffering regarding this terrible disease.

## 9.2 FUTURE WORK

### 9.2.1 Multi-nozzle electrospinning for elastomeric synthetic ECM development

In order to develop materials that more closely mimic the actual extracellular matrix, a combination of polymer synthesis and processing may be pursued. Biodegradable polyurethanes with enzyme specific degradable sequences have been previously developed [159]. By utilizing a multi-nozzle electrospinning technique, a composite scaffold can be constructed with fiber components consisting of individual enzyme sensitive degradable polymers. It will be necessary to develop a method to overcome the inherent limitation of stream repulsion of multiple electrospinning streams. Preliminary investigation in this work has demonstrated the usefulness of target rotational motion and perpendicular nozzle placement. More specifically, the experimental set-up utilized in microintegration may be successfully translated or modified to minimize multi-nozzle stream repulsion. These biomimetics will further take advantage of the mechanical robustness of synthetic elastomers together with the bioactivity of natural components to result in constructs that act as synthetic versions of the extracellular matrix.

### 9.2.2 Coaxial electrospinning for controlled drug release

A more advanced electrospinning technique that can be beneficial for single or multiple drug delivery is coaxial electrospinning [160, 161]. This technology consists of electrospinning one or more materials inside the core of an outer electrospun fiber using a specialized feed device as shown in **Figure 9-1**. The coaxial electrospinning process occurs at a fast enough rate that mixing of the core and shell material is minimal. This process provides greater flexibility than

what is possible with traditional single solution electrospinning. For example, some biomacromolecules that cannot be electrospun alone from appropriate solvents may be stabilized within the core of more spinnable components such as biodegradable polyurethanes. Specific growth factors can be loaded into each material with the faster degrading component yielding an increased release rate. Furthermore, growth factor activity can be better preserved by loading in a benign core solvent that would not be possible to electrospin as stable fibers in the shell layer. Processing variables such as feed rate and electrostatic potential may also be modulated to control the thickness of the shell and core layer to influence release kinetics.

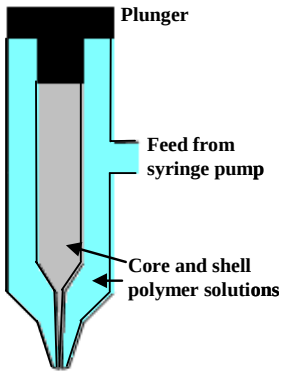


**Figure 9-1**. Coaxial electrospinning feed chamber consisting of concentric polymer solution chambers.

### 9.2.3 Co-microintegration for development of functional vascularized tissue

Previously developed cellular microintegration technology can be extended for integration of multiple cell types either concurrently or sequentially. For example, a functional small-diameter tissue engineered blood vessel may be developed by utilizing advanced cell co-culture methods in fabricating biodegradable tubular conduits. These conduits can be fabricated by electrospraying sequential cell streams of first endothelial cells (ECs) and then smooth muscle cells (SMCs) onto a rotating small diameter mandrel while concurrently electrospinning of synthetic extracellular matrix to create a mechanically robust vessel conduit as illustrated in **Figure 9-2**. The polymer and cellular deposition rates can be altered to created specific lamina, such as one separating an EC rich region and SMC region. It is expected that high cell densities will facilitate the development of functional connections between cells and provide a construct that has mechanical properties appropriate for arterial placement. This technology can also be studied as a means to generate and study vascularized tissue development *in vitro* through simultaneously microintegrated ECs and SMCs [162].

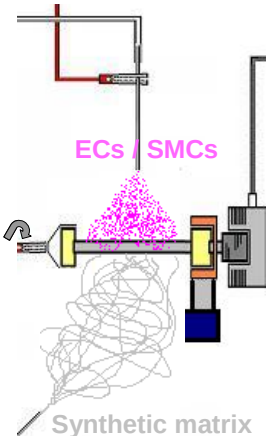


**Figure 9-2**. Sequential EC and SMC integration with electrospinning of a synthetic extracellular matrix conduit.

# APPENDIX A

## REPRESENTATIVE DIFFERENTIAL SCANNING CALORIMETRY SPECTRUM FOR CAST PEUU FILM

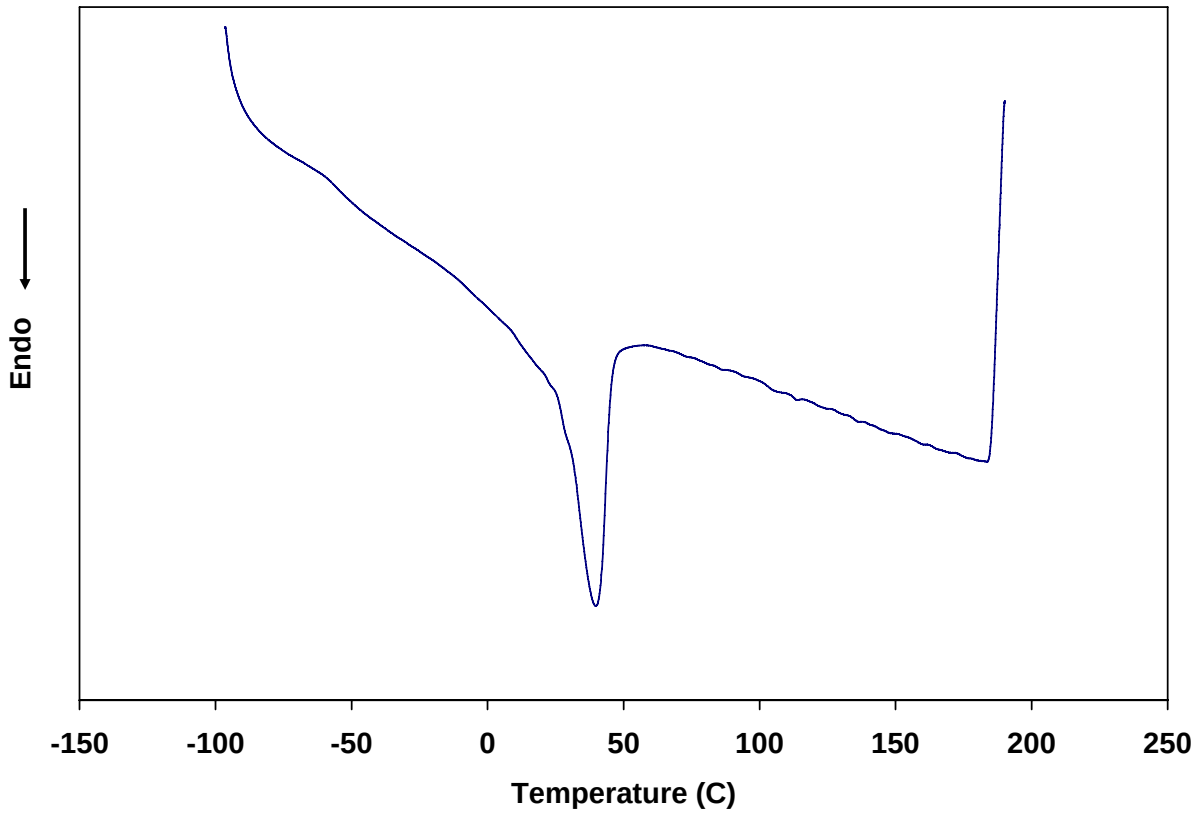

# APPENDIX B

## HUVEC SUBCULTURING METHOD

Materials:

25 mL serological pipettes
175 $cm^2$ TCPS flasks
50 mL conical tubes
Endothelial Basal Medium-2 (EBM-2, Cambrex)
Hepes-buffered saline solution (HBSS)
Trypsin/EDTA (T-E)
Trypsin neutralizing solution (TNS)

1. Warm all reagents to 37°C in water bath.
2. In a sterile biologic hood, remove old medium from each culture flask.
3. Add 10 mL HBSS to each flask, rinse the cell surface, then remove.
4. Add 10 mL T-E to each flask and place in 37°C incubator for 10 min.
5. Add 10 mL TNS to each flask and wash off cells from flask surface.
6. Transfer 20 mL of cell solution to 50 mL conical tube.
7. Centrifuge tube for 5 min at 1000 rpm.
8. Remove and discard supernatant.
9. Resuspend HUVEC pellet in desired volume EBM-2.
10. Seed cells onto scaffolds or new plates typically at 1:3 or 1:4 ratio.

# APPENDIX C

## SMC SUBCULTURING METHOD

Materials:

25 mL serological pipettes
175 $cm^2$ TCPS flasks
50 mL conical tubes
DMEM with 10% fetal bovine serum and 1% penicillin/streptomycin
Trypsin/EDTA (T-E)

1. Warm all reagents to 37°C in water bath.
2. In a sterile biologic hood, remove old medium from each culture flask.
3. Add 4 mL T-E to each flask, rinse the cell surface, then remove.
4. Add 6 mL T-E to each flask and place in 37°C incubator for 10 min.
5. Add 14 mL medium to each flask and wash off cells from flask surface.
6. Transfer 20 mL of cell solution to 50 mL conical tube.
7. Centrifuge tube for 5 min at 125 x g.
8. Remove and discard supernatant.
9. Resuspend SMC pellet in desired volume medium.
10. Seed cells onto scaffolds or new plates typically at 1:3 or 1:4 ratio.

# APPENDIX D

## MTT MITOCHONDRIAL ACTIVITY ASSAY

Materials:

MTT (thiazoyl blue, Sigma)
PBS
2-propanol
10 M HCl
96 well TCPS plate
200 μL pipettor

1. Place samples in wells of a 96 well plate.
2. Add 200 μL medium.
3. Add 20 μL of a 5 mg/mL solution of MTT in PBS.
4. Place at 37°C in an incubator for 3-5 h.
5. Remove media and MTT solution.
6. Add 200 μL of 0.04 *N* HCl in 2-propanol.
7. Cover plate, seal with tape and place at 0°C for 24-48 h.
8. Measure solution optical density at 570 nm with a 650 nm reference.
9. Convert optical density to cell number using calibration curve from known cell densities.

# APPENDIX E

## SEM FIXATION AND DEHYDRATION FOR CELL SEEDED SAMPLES

Materials:

2.5% glutaraldehyde in PBS
PBS
1% osmium tetraoxide ($OsO_4$)
Ethanol

1. Fix samples in 2.5% glutaraldehyde in PBS for 1 h to overnight.
2. Wash with PBS for 10 min (repeat 3 times).
3. Fix samples in 1% osmium tetraoxide for 1 h at 4 °C.
4. Wash with PBS for 10 min (repeat 3 times).
5. Immerse in 30% ethanol for 10 min.
6. Immerse in 50% ethanol for 10 min.
7. Immerse in 70% ethanol for 10 min.
8. Immerse in 90% ethanol for 10 min.
9. Immerse in 100% ethanol for 15 min (repeat 4 times).

# APPENDIX F

## HEMATOXYLIN AND EOSIN STAINING

Materials:

Xylene
Harris' acidified Hematoxylin (Thermo Electron Corp)
Alcoholic Eosin Y (Thermo Electron Corp)
Ammonia water

1. Immerse in xylene for 3 min (repeat 3 times).
2. Immerse in 100% ethanol for 1 min.
3. Immerse in 95% ethanol for 1 min.
4. Wash with water for 2 min.
5. Stain with Harris' acidified Hematoxylin for 7 min.
6. Wash with water for 2 min then repeat for 1 min.
7. Immerse in ammonia water for 30 s.
8. Wash with water for 1 min.
9. Immerse in 95% ethanol for 30 s.
10. Stain with alcoholic Eosin for 30 s.
11. Immerse in 95% ethanol for 30 s (repeat twice).
12. Immerse in 100% ethanol for 30 s (repeat 3 times).
13. Immerse in xylene for 30 s (repeat 3 times)
14. Coverslip samples.

# APPENDIX G

## TRICHROME STAINING

Materials:

Xylene
Weigert's Hematoxylin
Beibrich Scarlet
Phosphotungstic/phosphomolbdic acid solution
Aniline Blue
Alcoholic Eosin Y (Thermo Electron Corp)
Ammonia water and acid water
Acid water

1. Wash with water for 10 min.
2. Stain with Weigert's Hematoxylin for 10 min.
3. Wash with water for 10 min.
4. Stain with Biebrich for 2 min.
5. Wash with water for 30 s.
6. Immerse in phosphotungstic/phosphomolbdic acid solution for 15 min.
7. Stain with aniline blue for 5 min.
8. Wash with water for 30 s.
9. Immerse in acid water for 1 min.
10. Wash with water for 30 s.
11. Immerse in 95% ethanol for 30 s.

12. Immerse in 100% ethanol for 30 s (repeat twice).

13. Immerse in xylene for 30 s (repeat 3 times).

14. Coverslip samples.

## BIBLIOGRAPHY


1. Stankus, J.J., J. Guan, and W.R. Wagner, *Elastomers, biodegradable,* in *Encyclopedia of Biomaterials and Biomedical Engineering*. 2004, Marcel Dekker: New York. p. 484-494.

2. Sacks, M.S., *Biaxial mechanical evaluation of planar biological materials.* J Elasticity, 2000. **61**: p. 199-246.

3. L'Heurex, N., et al., *A completely biological tissue-engineered human blood vessel.* Faseb J, 1998. **12**: p. 47-56.

4. Langer, R. and J.P. Vacanti, *Tissue engineering.* Science, 1993. **260**: p. 920-926.

5. Greisler, H. and P. Zilla, *Tissue Engineering of Vascular Prosthetic Grafts*. 1999, Austin: Landes.

6. Fuchs, J.R., B.A. Nasseri, and J.P. Vacanti, *Tissue engineering: A 21st century solution to surgical reconstruction.* Ann Thorac Surg, 2001. **72**(2): p. 577-591.

7. Cundiff, D.K., *Coronary artery bypass grafting (CABG): reassessing efficacy, safety, and cost.* Medscape Gen Med, 2002. **2**: p. 1-12.

8. Atkins, R.E., *Can tissue engineering mend broken hearts?* Circ Res, 2002. **90**: p. 120-122.

9. Niklason, L.E., et al., *Functional arteries grown in vitro.* Science, 1999. **284**(5413): p. 489-493.

10. Butler, D.L., S.A. Goldstein, and F. Guilak, *Functional tissue engineering: the role of biomechanics.* J Biomech Eng-T ASME, 2000. **122**: p. 570-575.

11. Simpson, D.G., et al., *Role of mechanical stimulation in the establishment and maintenance of muscle cell differentiation.* Int Rev Cytol, 1994. **150**: p. 69-92.

12. Kim, B.S., et al., *Cyclic mechanical strain regulates the development of engineered smooth muscle tissue.* Nat Biotechnol, 1999. **17**: p. 979-983.

13. Kim, B.S. and D.J. Mooney, *Scaffolds for engineering smooth muscle under cyclic mechanical strain conditions.* J Biomech Eng, 2000. **122**: p. 210-215.

14. Akhyari, P., et al., *Mechanical stretch regimen enhances the formation of bioengineered autologous cardiac muscle grafts.* . Circulation, 2002. **106**: p. I337-I342.

15. Guan, J., et al., *Synthesis, characterization, and cytocompatibility of elastomeric, biodegradable poly(ester-urethane)ureas based on poly(caprolactone) and putrescine.* J Biomed Mater Res, 2002. **61**: p. 493-503.

16. Guan, J., et al., *Biodegradable poly(ether ester urethane)urea elastomers based on poly(ether ester) triblock copolymers and putrescine: synthesis, characterization, and cytocompatibility.* Biomaterials, 2004. **25**: p. 85-96.

17. Kylma, J. and J.V. Seppala, *Synthesis and characterization of a biodegradable thermoplastic poly(ester-urethane) elastomer.* Macromolecules, 1997. **30**: p. 2876-2882.

18. Saad, B., et al., *Development of degradable polyesterurethanes for medical applications.* J Biomed Mater Res, 1997. **36**: p. 65-74.

19. Skarja, G.A. and K.A. Woodhouse, *Synthesis and characterization of degradable polyurethane elastomers containing an amino-acid based chain extender.* J Biomater Sci Polym Edn, 1998. **9**: p. 271-295.

20. Skarja, G.A. and K.A. Woodhouse, *Structure-property relationships of degradable polyurethane elastomers containing an amino acid-based chain extender.* J Appl Polym Sci, 2000. **75**: p. 1522-1534.

21. Spaans, C.J., et al., *High molecular weight polyurethane urea based on 1,4-diisocyanatobutane.* Polym Bull, 1998. **41**: p. 131-138.

22. Lee, C.H., A. Singla, and Y. Lee, *Biomedical applications of collagen.* Int J Pharm, 2001. **221**: p. 1-22.

23. Beckman, M.J., K.J. Shields, and R.F. Diegelmann, *Collagen*, in *Encyclopedia of Biomaterials and Biomedical Engineering*. 2004, Marcel Dekker: New York.

24. Fujioka, K., et al., *Protein release from collagen matrices.* Adv Drug Deliv Rev, 1998. **31**: p. 247-266.

25. Kleinman, H.K., R.J. Klebe, and G.R. Martin, *Role of collageneous matrices in the adhesion and growth of cells.* J Cell Biol, 1981. **88**: p. 473-485.

26. Koob, T.J., *Collagen Fixation*, in *Encyclopedia of Biomaterials and Biomedical Engineering*. 2004, Marcel Dekker: New York.

27. L'Heurex, N., *In vitro construction of a human blood vessel from cultured vascular cells: a morphologic study.* J Vasc Surg, 1993. **17**: p. 499-509.

28. Ecschenhagen, T., *Three-dimensional reoconstitution of embryonic cardiomyocytes in a collagen matrix: a new heart muscle model system.* Faseb J, 1997. **11**: p. 683-694.

29. Kofidis, T., *In vitro engineering of heart muscle: artificial myocardial tissue.* J Thorac Cardiovasc Surg, 2002. **124**: p. 63-69.

30. Gosline, J., et al., *Elastic proteins: biological roles and mechanical properties.* Phil Trans R Soc Lond, 2002. **357**: p. 121-132.

31. Martino, M., T. Perri, and A.M. Tamburro, *Elastin-based biopolymers: chemical synthesis and structural characterization of linear and cross-linked poly(OrnGlyGlyOrnGly)* Biomacromolecules, 2002. **3**: p. 297-304.

32. McMillan, R.A. and R.P. Conticello, *Synthesis and characterization of elastin-mimetic protein gels derived from a well-defined polypeptide precursor.* Macromolecules, 2000. **33**: p. 4809-4821.

33. McPherson, D.T., et al., *Production and purification of a recombinant elastomeric polypeptide, G-(VPGVG)$_{19}$-VPGV, from Escherichia coli.* Biotechnol Prog, 1992. **8**: p. 347-352.

34. McPherson, D.T., J. Xu, and D.W. Urry, *Product purification by reversible phase transition following Escherichia coli expression of genes encoding up to 251 repeats of the elastomeric pentapeptide GVGVP.* Protein Expres Purif, 1996. **7**: p. 51-57.

35. Panitch, A., et al., *Design and biosynthesis of elastin-like artificial extracellular matrix proteins containing periodically spaced fibronectin CS5 domains.* Macromolecules, 1999. **32**: p. 1701-1703.

36. Urry, D.W., et al., *Elastin protein-based polymers in soft tissue augmentation and generation*. Polymers for Tissue Engineering, ed. M.S. Shoichet and J.A. Hubbell. 1998, Utrecht, The Netherlands: VSP. 19-52.

37. Welsh, E.R. and D.A. Tirrell, *Engineering the extracellular matrix: a novel approach to polymeric biomaterials. I. Control of the physical properties of artificial protein matrices designed to support adhesion of vascular endothelial cells.* Biomacromolecules, 2000. **1**: p. 23-30.

38. Abbott, W.M., *Biologic and synthetic vascular prostheses*. 1982, New York: Gurne & Stratton.

39. Huang, L., et al., *Generation of synthetic elastin-mimetic small diameter fibers and fiber networks.* Macromolecules, 2000. **33**: p. 2989-2997.

40. Nagapudi, K., et al., *Photomediated solid-state cross-linking of an elastin-mimetic recombinant protein polymer.* Macromolecules, 2002. **35**: p. 1730-1737.

41. Badylak, S.F., *The extracellular matrix as a scaffold for tissue reconstruction.* Cell Dev Biol, 2002. **13**: p. 377-383.

42. Badylak, S.F., *Extracellular matrix scaffolds*, in *Encyclopedia of Biomaterials and Biomedical Engineering*. 2004, Marcel Dekker: New York.

43. Yang, S., et al., *The design of scaffolds for use in tissue engineering. Part I. Traditional Factors.* Tiss Eng, 2001. **7**: p. 679-689.

44. Lee, S.H., et al., *Elastic biodegradable poly(glycolide-co-caprolactone) scaffold for tissue engineering.* J Biomed Mater Res, 2003. **66A**: p. 29-37.

45. Jeong, S.I., et al., *Morphology of elastic poly(L-lactide-co-ε-caprolactone) copolymers and in vitro and in vivo degradation behavior of their scaffolds.* Biomacromolecules, 2004. **5**: p. 1303-1309.

46. Zhu, Y., et al., *Protein bonding on biodegradable poly(L-lactide-co-caprolactone) membrane for esophageal tissue engineering.* Biomaterials, 2006. **27**: p. 68-78.

47. Pego, A.P., et al., *Preparation of degradable porous structures based on 1,3-trimethylene carbonate and D,L-lactide (co)polymers for heart tissue engineering.* Tiss Eng, 2003. **9**: p. 981-994.

48. Pego, A.P., et al., *Copolymers of trimethylene carbonate and epsilon-caprolactone for porous nerve guides: synthesis and properties.* J Biomater Sci Polym Edn, 2001. **12**: p. 35-53.

49. Wang, Y., *Biorubber/poly(glycerol sebacate)*, in *Encyclopedia of Biomaterials and Biomedical Engineering*. 2004, Marcel Dekker: New York. p. 121-128.

50. Wang, Y., et al., *A tough biodegradable elastomer.* Nat Biotechnol, 2002. **20**: p. 602-606.

51. Gorna, K., S. Polowinski, and S. Gogolewski, *Synthesis and characterization of biodegradable poly(ε-caprolactone urethane)s. I. Effect of the polyol molecular weight, catalyst, and chain extender on the molecular and physical characteristics.* J Polym Sci Polym Chem, 2002. **40**: p. 156-170.

52. Agrawal, C. and R. Ray, *Biodegradable polymeric scaffolds for musculoskeletal tissue engineering.* J Biomed Mater Res, 2001. **55**: p. 141-150.

53. Dobrzynski, P., *Synthesis of biodegradable copolymers with low-toxicity zirconium compounds. II. Copolymerization of glycolide with ε-caprolactone initiated by zirconium (IV) acetylacetonate and zirconium (IV) chloride.* J Polym Sci Polym Chem, 2002. **40**: p. 1379-1394.

54. Jeong, S.I., et al., *Manufacture of elastic biodegradable PLCL scaffolds for mechano-active vascular tissue-engineering.* J Biomater Sci Polym Edn, 2003. **15**: p. 645-660.

55. Jeong, S.I., et al., *Mechano-active tissue engineering of vascular smooth muscle using pulsatile perfusion bioreactors and elastic PLCL scaffolds.* Biomaterials, 2005. **26**: p. 1405-1411.

56. Pego, A.P., et al., *In vitro degradation of trimethylene carbonate based (co)polymers.* Macromol Biosci, 2002. **2**: p. 411-419.

57. Fabre, T., et al., *Study of a (trimethylenecarbonate-co-ℓ-caprolactone) polymer – part 2: in vitro cytocompatibility analysis and in vivo ED1 cell response of a new nerve guide.* Biomaterials, 2001. **22**: p. 2951-2958.

58. Bruin, P., J. Smedinga, and A.J. Pennings, *Biodegradable lysine diisocyanate-based poly(glycolide-co-ε-caprolactone)-urethane network in artificial skin.* Biomaterials, 1990. **11**: p. 291-295.

59. Bruin, P., et al., *Design and synthesis of biodegradable poly(ester-urethane) elastomer networks composed of non-toxic building blocks.* Makromol Chem Rapid Commun, 1988. **9**: p. 589-594.

60. Storey, R.F., J.S. Wiggins, and A.D. Puckett, *Hydrolyzable poly(ester-urethane) networks from L-lysine diisocyanate and D,L-lactide / ε-caprolactone homo- and copolyester triols.* J Polym Sci Polym Chem, 1994. **32**: p. 2345-2363.

61. Spaans, C.J., et al., *A new biomedical polyurethane with a high modulus based on 1,4-butanediisocyanate and ε-caprolactone.* J Mater Sci Mater Med, 1998. **9**: p. 675-678.

62. Lendlein, A., P. Neuenschwander, and U.W. Suter, *Tissue-compatible multiblock copolymers for medical applications, controllable in degradation rate and mechanical properties.* Macromol Chem Phy, 1998. **199**: p. 2785-2796.

63. Gorna, K. and S. Gogolewski, *Biodegradable polyurethanes for implants. II. In vitro degradation and calcification of materials from poly(ε-caprolactone)-poly(ethylene oxide) diols and various chain extenders.* J Biomed Mater Res, 2002. **60**: p. 592-606.

64. Cohn, D. and A. Hotovely-Salomon, *Biodegradable multi-block PEO/PLA thermoplastic elastomers: molecular design and properties.* Polymer, 2005. **46**: p. 2068-2075.

65. Saad, G.R., Y.J. Lee, and H. Seliger, *Synthesis and characterization of biodegradable poly(ester-urethanes) based on bacterial poly(R-3-hydroxybutyrate.* J Appl Polym Sci, 2002. **83**: p. 703-718.

66. Guelcher, S.A., et al., *Synthesis of biocompatible segmented polyurethanes from aliphatic diisocyanates and diurea diol chain extenders.* Acta Biomat, 2005. **1**: p. 471-484.

67. de Groot, J.H., et al., *New biomedical polyurethane ureas with high tear strengths.* Polym Bull, 1997. **38**: p. 211-218.

68. Lendlein, A. and R. Langer, *Biodegradable, elastic shape-memory polymers for potential biomedical applications.* Science, 2002. **296**: p. 1673-1676.

69. *National Toxicology Program Technical Report on the Carcinogenesis Bioassay of 4,4'-methylenedianiline dihydrochloride, NTP-81-143*. 1982, National Institutes of Health: Bethesda, MD.

70. Lamba, N.M.K., K.A. Woodhouse, and S.L. Cooper, *Polyurethanes in Biomedical Application*. 1998, New York: CRC Press.

71. Schoental, R., *Carcinogenic and chronic effects of 4,4-diamino-diphenyl methane, an epoxy resin hardener.* Nature, 1968. **219**: p. 219.

72. Cohn, D., et al., *Biodegradable poly(ethylene oxide)/poly(ε-caprolactone) multiblock copolymers.* 2002. **59**: p. 273-281.

73. de Groot, J.H., et al., *On the role of aminolysis and transesterification in the synthesis of ε-caprolactone and L-lactide based polyurethanes.* Polym Bull, 1998. **41**: p. 299-306.

74. Lendlein, A., et al., *Hydrolytic degradation of phase-segregated multiblock copoly(ester urethane)s containing weak links.* Macromol Chem Phy, 2001. **202**: p. 2702-2711.

75. Skarja, G.A. and K.A. Woodhouse, *In vitro degradation and erosion of degradable, segmented polyurethanes containing an amino acid-based chain extender.* J Biomater Sci Polym Edn, 2001. **12**: p. 851-873.

76. Borkenhagen, M., et al., *In vivo performance of a new biodegradable polyester urethane system used as a nerve guidance channel.* Biomaterials, 1998. **19**: p. 2155-2165.

77. Hutmacher, D.W., *Scaffolds in tissue engineering bone and cartilage.* Biomaterials, 2000. **21**: p. 2529-2543.

78. Ma, Z., et al., *Potential of nanofiber matrix as tissue-engineering scaffolds.* Tiss Eng, 2005. **11**: p. 101-109.

79. Mikos, A.G., *Preparation and characterization of poly(L-lactic acid) foams.* Polymer, 1994. **35**: p. 1068.

80. Whang, K., C.H. Thomas, and K.E. Healy, *A novel method to fabricate bioabsorbable scaffolds.* Polymer, 1999. **36**: p. 837-842.

81. Guan, J., et al., *Preparation and characterization of highly porous, biodegradable polyurethane scaffolds for soft tissue applications.* Biomaterials, 2005. **26**: p. 3961-3971.

82. Zein, I., et al., *Fused deposition modeling of novel scaffold architectures for tissue engineering applications.* Biomaterials, 2002. **23**: p. 1169-1185.

83. Li, W.J., et al., *Electrospun nanofibrous structure: a novel scaffold for tissue engineering.* J Biomed Mater Res, 2002. **60**: p. 613-621.

84. Taylor, G.I., *Disintegration of water drops in an electric field.* Proc Roy Soc Lond, 1964. **280**: p. 383-397.

85. Zeleny, J., *The electrical discharge from liquid points, and a hydrostatic method of measuring the electric intensity at their surfaces.* J Phys Rev, 1914. **3**: p. 69-91.

86. Formhals, A., *Apparatus for producing artificial filaments from material such as cellulose acetate*. 1934; US Patent 1975504.

87. Shin, M., et al., *Contractile cardiac grafts using a novel nanofibrous mesh.* Biomaterials, 2004. **25**: p. 3717-3723.

88. Huang, L., et al., *Engineered collagen-PEO nanofibers and fabrics.* J Biomater Sci Polym Edn, 2001. **12**: p. 979-993.

89. Matthews, J.A., et al., *Electrospinning of collagen nanofibers.* Biomacromolecules, 2002. **3**: p. 232-238.

90. Xu, C.Y., et al., *Aligned biodegradable nanofibrous structure: a potential scaffold for blood vessel engineering.* Biomaterials, 2004. **25**: p. 877-886.

91. Annis, D., et al., *An elastomeric vascular prosthesis.* Am Soc Art Int Org, 1978. **24**: p. 209-214.

92. Demir, M.M., et al., *Electrospinning of polyurethane fibers.* Polymer, 2002. **43**: p. 3303-3309.

93. Kidoaki, S., I.K. Kwon, and T. Matsuda, *Mesoscopic spatial designs of nano- and microfiber meshes for tissue-engineering matrix and scaffold based on newly devised multilayering and mixing electrospinning techniques.* Biomaterials, 2005. **26**: p. 37-46.

94. Yang, S., et al., *The design of scaffolds for use in tissue engineering. Part II. Rapid prototyping techniques.* Tiss Eng, 2002. **8**: p. 1-11.

95. Reneker, D. and I. Chun, *Nanometre diameter fibres of polymer, produced by electrospinning.* Nanotechnology, 1996. **7**: p. 216-223.

96. Zong, X., et al., *Structure and process relationship of electrospun bioabsorbable nanofiber membranes.* Polymer, 2002. **43**: p. 4403-4412.

97. Ito, Y., M. Kajihara, and Y. Imanishi, *Materials for enhancing cell adhesion by immobilization of cell adhesive peptide.* J Biomed Mater Res, 1991. **25**: p. 1325-1337.

98. Ito, Y., L.S. Liu, and Y. Imanishi, *In vitro nonthrombogenicity of a thrombin-substrate-immobilized polymer membrane by the inhibition of thrombin activity.* . J Biomater Sci Polym Edn, 1991. **2**: p. 123-128.

99. Deitzel, J.M., et al., *Controlled deposition of electrospun poly(ethylene oxide) fibers.* Polymer, 2001. **42**: p. 8163-8170.

100. Ohno, M. and T. Abe, *Rapid colorimetric assay for the quantification of leukemia inhibitory factor (LIF) and interleukin-6 (IL-6).* J Immunol Methods, 1991. **145**: p. 199-203.

101. Al-Khaldi, A., et al., *Therapeutic angiogenesis using autologous bone marrow stromal cells: improved blood flow in a chronic limb ischemia model.* Ann Thorac Surg, 2003. **75**: p. 204-209.

102. Ding, B., et al., *Fabrication of blend biodegradable nanofibrous nonwoven mats via multi-jet electrospinning.* Polymer, 2004. **45**: p. 1895-1902

103. Kenawy, E.R., et al., *Electrospinning of poly(ethylene-co-vinyl alcohol) fibers.* Biomaterials, 2003. **24**: p. 907-913.

104. Fong, H., I. Chun, and D.H. Reneker, *Beaded nanofibers formed during electrospinning.* Polymer, 1999. **40**: p. 4585-4592.

105. Chen, G., T. Ushida, and T. Tateishi, *Development of biodegradable porous scaffolds for tissue engineering.* Mater Sci Eng, 2001. **17**: p. 63-69.

106. Junqueira, L.C.U., G. Bignolas, and R.R. Brentani, *Picrosirius staining plus polarization microscopy, a specific method for collagen detection in tissue sections.* Histochem J, 1979. **11**: p. 447-455.

107. Ray, J.L., et al., *Isolation of vascular smooth muscle cells from a single murine aorta.* Methods Cell Sci, 2002. **23**: p. 185-188.

108. Camacho, N.P., et al., *FTIR spectroscopic imaging of collagen and proteoglycan in bovine cartilage.* Biopolymers, 2001. **62**: p. 1-8.

109. Sachlos, E., et al., *Novel collagen scaffolds with predefined internal morphology made by solid freeform fabrication.* Biomaterials, 2003. **24**: p. 1487-1497.

110. Bhatnagar, R.S. and C.A. Gough, *Circular dichroism of collagen and related polypeptides*, in *Circular dichroism and the conformational analysis of biomacromolecules*, G.D. Fasman, Editor. 1996, Plenum: New York. p. 183-189.

111. Doillon, C.J., et al., *Chemical inactivators as sterilization agents for bovine collagen materials.* J Biomed Mater Res, 1997. **37**: p. 212-221.

112. Badylak, S., et al., *Extracellular matrix for myocardial repair.* Heart Surg Forum, 2003. **6**: p. E20.

113. Badylak, S.F., *Xenogeneic extracellular matrix as a scaffold for tissue reconstruction.* Transpl. Immunol., 2004. **12**: p. 367-377.

114. Badylak, S.F., et al., *Small intestinal submucosa as a large diameter vascular graft in the dog.* J Surg Res, 1989. **47**: p. 74-80.

115. Stankus, J., J. Guan, and W.R. Wagner, *Fabrication of biodegradable elastomeric scaffolds with sub-micron morphologies.* J Biomed Mater Res, 2004. **70A**: p. 603-614.

116. Fung, Y.C., *Biomechanics: Mechanical Properties of Living Tissues*. 2nd ed. 1993, New York: Springer Verlag.

117. Xu, C., et al., *Electrospun nanofiber fabrication as synthetic extracellular matrix and its potential for vascular tissue engineering.* Tiss Eng, 2004. **10**: p. 1160-1168.

118. Theron, A., E. Zussman, and A.L. Yarin, *Electrostatic field-assisted alignment of electrospun nanofibres.* Nanotechnology, 2001. **12**: p. 384.

119. Chaudhuri, B.B., P. Kundu, and N. Sarkar, *Detection and graduation of oriented texture.* Pattern Recogn Lett, 1993. **14**(2): p. 147-153.

120. Karlon, W.J., et al., *Automated measurement of myofiber disarray in transgenic mice with ventricular expression of ras.* Anat Rec, 1998. **252**: p. 612-625.

121. Courtney, T., et al., *Analysis and design of tissue engineered scaffolds that mimic soft tissue mechanical anisotropy.* Biomaterials, 2006. **27**: p. 3631-3638.

122. Billiar, K.L. and M.S. Sacks, *Biaxial mechanical properties of the natural and glutaraldehyde treated aortic valve cusp--Part I: Experimental results.* J Biomech Eng, 2000. **122**: p. 23-30.

123. Sacks, M.S. and W. Sun, *Multiaxial mechanical behavior of biological materials.* Annu Rev Biomed Eng, 2003.

124. Sonoda, H., et al., *Small-diameter compliant arterial graft prosthesis: Design concept of coaxial double tubular graft and its fabrication.* J Biomed Mater Res, 2001. **55**: p. 266-276.

125. Keun, K.I., S. Kidoaki, and T. Matsuda, *Electrospun nano- to microfiber fabrics made of biodegradable copolyesters: structural characteristics, mechanical properties and cell adhesion potential.* Biomaterials, 2005. **26**: p. 3929-3939.

126. Khil, M.S., et al., *Novel fabricated matrix via electrospinning for tissue engineering.* J Biomed Mater Res, 2005. **72B**: p. 117-124.

127. Matsuda, T., et al., *Mechano-active scaffold design of small-diameter artificial graft made of electrospun segmented polyurethane fabrics.* J Biomed Mater Res, 2005. **73A**: p. 125-131.

128. Lee, C.H., et al., *Nanofiber alignment and direction of mechanical strain affect the ECM production of human ACL fibroblast.* Biomaterials, 2005. **26**: p. 1261-1270.

129. Flemming, R.G., et al., *Effects of synthetic micro- and nano-structured surfaces on cell behavior.* Biomaterials, 1999. **20**: p. 573-578.

130. Thapa, A., T.J. Webster, and K.M. Haberstroh, *Nano-structured polymers enhance bladder smooth muscle cell function.* Biomaterials, 2003. **24**: p. 2915-2926.

131. Li, Y., et al., *Effects of filtration seeding on cell density, spatial distribution, and proliferation in nonwoven fibrous matrices.* Biotechnol Prog, 2001. **17**: p. 935-944.

132. Bursac, N., et al., *Cardiac muscle tissue engineering: towards an in vitro model for electrophysiological studies.* Am J Physiol Heart Circ Physiol, 1999. **277**: p. H433-H444.

133. Radisic, M., et al., *Medium perfusion enables engineering of compact and contractile cardiac tissue.* Am J Physiol Heart Circ Physiol, 2004. **286**: p. H507-H516.

134. Qu-Peterson, Z., et al., *Identification of a novel population of muscle stem cells in mice: potential for muscle regeneration.* J Cell Biol, 2002. **157**: p. 851-864.

135. Grace, J.M. and J.C.M. Marijinissen, *A review of liquid atomization by electrical means.* J Aerosol Sci, 1994. **25**: p. 1005-1019.

136. Ijsebaert, J.C., et al., *Electro-hydrodynamic atomization of drug solutions for inhalation purposes.* J Apply Physiol, 2001. **91**: p. 2735-2741.

137. Reyderman, L. and S. Stavchansky, *Electrostatic spraying and its use in drug delivery from cholesterol microspheres.* Int J Pharm, 1995. **124**: p. 75-85.

138. Nedovic, V.A., et al., *Cell immobilization by electrostatic droplet generation.* Landbauforsch Volk, 2002. **241**: p. 11-17.

139. van Tienen, T.G., et al., *Tissue ingrowth and degradation of two biodegradable porous polymers with different porosities and pore sizes.* Biomaterials, 2002. **23**: p. 1731-1738.

140. Gehl, J., *Electroporation: theory and methods, perspectives for drug delivery, gene therapy and research.* Acta Physiol Scand, 2003. **177**: p. 437-447.

141. Temple, M.D., et al. *Electrostatic transportation of living cells through air.* in *223rd ACS National Meeting*. 2002. Orlando, FL.

142. Carrier, R.L., et al., *Perfusion improves tissue architecture of engineered cardiac muscle.* Tiss Eng, 2002. **8**: p. 175-188.

143. Stathopoulos, N.A. and J.D. Lellums, *Shear stress effects on human embryonic kidney cells in vitro.* Biotechnol Bioeng, 1985. **27**: p. 1021-1026.

144. Baird, A. and P. Bohlen, *Fibroblast Growth Factors*, in *Peptide Growth Factors and Their Receptors I*, M.B. Sporn and A.B. Roberts, Editors. 1990, Springer-Verlag: New York. p. 369.

145. Burgess, W.H. and T. Maciag, Annu Rev Biochem, 1989. **58**: p. 575.

146. Guan, J., J.J. Stankus, and W.R. Wagner, *Development of composite porous scaffolds based on collagen and biodegradable poly(ester urethane)urea.* Cell Transplant, In press.

147. Sarikaya, A., et al., *Antimicrobial activity associated with extracellular matrices.* Tiss Eng, 2002. **8**: p. 63-71.

148. Rignault, D.P., *Abdominal trauma in war.* World J Surg, 1992. **16**: p. 940-946.

149. Heidapour, A. and M.R. Jahani, *Surgical interventions at field hospitals during the Iran and Iraq war.* Military Med, 1999. **164**: p. 136-137.

150. Kenawy, E.R., et al., *Release of tetracycline hydrochloride from electrospun poly(ethylene-co-vinylacetate), poly(lactic acid), and a blend.* J Control Rel, 2002. **81**: p. 57-64.

151. Kim, K., et al., *Incorporation and controlled release of a hydrophilic antibiotic using poly(lactide-co-glycolide)-based electrospun nanofibrous scaffolds.* J Control Release, 2004. **98**: p. 47-56.

152. Ratcliffe, A., *Tissue engineering of vascular grafts.* Matrix Biol, 2000. **19**: p. 353-357.

153. Cummings, C.L., et al., *Properties of engineered vascular constructs made from collagen, fibrin, and collagen-fibrin mixtures.* Biomaterials, 2004. **25**: p. 3699-3706.

154. Hoerstrup, S.P., et al., *Tissue engineering of small caliber vascular grafts.* Eur J Card Thor Surg, 2001. **20**: p. 164-169.

155. Stankus, J.J., et al., *Microintegrating smooth muscle cells into a biodegradable, elastomeric fiber matrix.* Biomaterials, 2006. **27**: p. 735-744.

156. Inoguchi, H., et al., *Mechanical responses of a compliant electrospun poly(L-lactide-co-caprolactone) small-diameter vascular graft.* Biomaterials, 2006. **27**: p. 1470-1478.

157. Vaz, C.M., et al., *Design of scaffolds for blood vessel tissue engineering using a multi-layering electrospinning technique.* Acta Biomat, 2005. **1**: p. 575-582.

158. Telemeco, T.A., et al., *Regulation of cellular infiltration into tissue engineering scaffolds composed of submicron diameter fibrils produced by electrospinning.* Acta Biomat, 2005. **1**: p. 377-385.

159. Guan, J. and W.R. Wagner, *Synthesis, characterization and cytocompatibility of polyurethaneurea elastomers with designed elastase sensitivity.* Biomacromolecules, 2005. **6**: p. 2833-2842.

160. Sun, Z., et al., *Compound core-shell polymer nanofibers by co-electrospinning.* Adv Mater, 2003. **15**: p. 1929-1932.

161. Zhang, Y., et al., *Preparation of PCL-r-gelatin bi-component nanofibers by coaxial electrospinning.* Chem Mater, 2004. **16**: p. 3406-3409.

162. Levenberg, S., et al., *Engineering vascularized skeletal muscle tissue.* Nat Biotechnol, 2005. **23**(7): p. 879-884.